Great ape cardiovascular disease: aetiopathogenesis, risk factors and diagnostic tools

Sophie Moittié

Thesis submitted to

The School of Veterinary Medicine and Science

The University of Nottingham

For the degree of

Doctor of Veterinary Medicine

Supervisors:

Professors Kate White, Kerstin Baiker and Malcolm Cobb

School of Veterinary Medicine and Science, University of Nottingham

Mátyás Liptovszky

Twycross Zoo, Burton Road, Atherstone, CV9 3PX

Abstract

Chimpanzees, orangutans, gorillas and bonobos are commonly kept in zoos across the world, and the understanding of their physiology and susceptibility to diseases is critical for the maintenance of healthy captive individuals and the protection of wild populations. Cardiovascular disease (CVD) is known as a major cause of morbidity and mortality in zoo great apes, and the Ape Heart Project has been studying its epidemiology and pathogenesis since 2014. The first chapter of this thesis critically examines the literature available related to great ape CVD and questions the possible aetiologies of this disease process. The three subsequent chapters explore possible diagnostic tools that could help with the investigation of specific risk factors of CVD in great apes, with zoo chimpanzees as models. Oscillometric and invasive blood pressure measurement devices are compared highlighting the inaccuracy of non-invasive devices when measuring blood pressure in anaesthetised chimpanzees. The value of implantable loop recorders (ILR) is also assessed to investigate the occurrence of arrhythmic events in chimpanzees considered at risk of cardiac disease, and this study demonstrates that ILRs are a valid tool for cardiac screening in great apes. The use of dried blood spots (DBS) to measure vitamin D in chimpanzees is explored in Chapter 4 and found that the analytical error is greater in DBS compared with serum samples, thus limiting the use of the DBS technique to field studies when the collection and analysis of serum samples are not achievable. Chapter 5 investigates the vitamin D status of European zoo chimpanzees and found relatively low serum vitamin D concentrations in a large contingent of this population during the low UVB season, supporting the hypothesis that vitamin D insufficiency may be a risk factor for CVD disease in great apes. Chapter 6 describes the findings of the systematic post-mortem examination of 50 great ape hearts and illustrates some differences seen between species. Finally, the last chapter of this thesis depicts the application of microcomputed tomography to formalin-fixed chimpanzee hearts and the discovery of bone formation within the cardiac skeleton of chimpanzees affected by myocardial fibrosis. Further studies investigating risk factors of great ape cardiovascular disease, especially hypertension and hypovitaminosis D, are urgently needed.

Acknowledgements

I would like to thank the University of Nottingham and Twycross Zoo for allowing me to spend these four years working with the Ape Heart Project. I enjoyed every day of it, and I am deeply appreciative of the high level of clinical and research training that was provided, as it will for sure serve as a steppingstone in my professional career.

To Pip and Sam, thank you for making me feel part of your team, and for understanding my French accent and Spanish attitude…

Thanks to Mat for his constant kindness and thoughtfulness while supervising my clinical and research activities and for having me as the first Twycross Zoo ECZM resident!

Thanks to Sharon Redrobe for integrating me within the Ape Heart Project team; this project is a great initiative, and I am sure that it will continue to contribute to the health of zoo great apes in the future.

Thanks to Mike Martin and Malcolm Cobb for introducing me to the world of veterinary cardiology.

Kerstin Baiker, I will forever remember the afternoons spent together examining heart slides… Thank you for your cheerfulness and your excellent teaching of heart histopathology!

Finally, I am infinitely grateful to my supervisor Kate White for her constant support throughout these past years, for boosting my confidence and for helping me deliver the best of myself.

List of publications

1. Moittié, S., Baiker, K., Strong, V., Cousins E, White K, Liptovszky M, Redrobe S, Alibhai A, Sturrock, C.J., Rutland, C.S. Discovery of os cordis in the cardiac skeleton of chimpanzees (Pan troglodytes). *Scientific Reports*, 2020, 10(1), 9417

2. Moittié, S., N Sheppard, M., Thiele, T., Baiker, K. Non-Infectious, Necrotizing and Granulomatous Aortitis in a Female Gorilla. *Journal of Comparative Pathology*, 2020, 181, pp. 7-12

3. Moittié, S., Graham, P.A., Barlow, N., Dobbs P, Liptovszky, Redrobe, S., White, K. Comparison of 25-hydroxyvitamin D concentration in chimpanzee dried blood spots and serum. *Veterinary Clinical Pathology*, 2020, 49(2), pp. 299-306

4. Moittié, S., Dobbs, P., Liptovszky, M., Martin, M., Redrobe, S., White, K. Evaluation of the agreement of two oscillometric blood pressure devices with invasive blood pressure in anaesthetized chimpanzees (Pan troglodytes). *In press* in *Veterinary Anaesthesia and Analgesia*

5. Strong, V., Moittié, S., Sheppard, M.N., Liptovszky, M., White, K., Redrobe, S., Cobb, M., Baiker, K. Idiopathic Myocardial Fibrosis in Captive Chimpanzees (Pan troglodytes). *Veterinary Pathology*, 2020, 57(1), pp. 183-191

Table of Contents

List of figures

List of tables

Abbreviations and acronyms

α-SMA	α-smooth muscle actin protein
AAMI	Advancement of Medical Instrumentation
AAZV	American Association of Zoo Veterinarian
ACE	angiotensin-converting enzyme
ACVIM	American College of Veterinary Internal Medicine
AHP	Ape Heart Project (at Twycross Zoo)
AM	adipose marrow
AMP	aqueous mobile phase
ANP	atrial natriuretic peptide
AV	atrioventricular
AZA	Association of Zoos and Aquariums
BNP	Brain natriuretic peptide
BP	blood pressure
Bpm	beat per minute
CFB	cardiac fibroblast
CHF	congestive heart failure
CI	confidence interval
CKD	chronic kidney disease
cm	centimetre
CNS	central nervous system
CO2	carbon dioxide
CT	computed tomography
CTn	cardiac troponin
CV	coefficient of variation
CVD	cardiovascular disease
CVF	collagen volume fraction
DAP	diastolic arterial pressure
DCM	dilated cardiomyopathy
DBS	dried blood spots
DEQAS	Vitamin D External Quality Assessment Scheme
d.f	degrees of freedom
EAZA	European Association of Zoo and Aquaria
ECG	electrocardiogram
ECM	extracellular matrix
ECV	extracellular volume fraction
ESI	electrospray Ionization

f_R	respiratory rate
GAHP	Great Ape Heart Project (Zoo Atlanta)
GCA	giant cell arteritis
GI	gastrointestinal
HCM	hypertrophic cardiomyopathy
HDL	high-density lipoprotein
HE	hematoxylin and eosin
HR	heart rate
IBP	invasive blood pressure
ICTP	initial carboxyl-terminal telopeptide
ID	identification
ILR	implantable loop recorder
IMF	idiopathic myocardial fibrosis
IU	International Units
IUCN	International Union for Conservation of Nature
Kg	kilogram
kV	kilovolt
L	litre
LC-MS/MS	liquid chromatography-tandem mass spectrometry
LDL	low-density lipoprotein
LGE	late gadolinium enhancement
LOA	limits of agreement
LPa	lipoprotein-associated phospholipase A2
LVH	left ventricular hypertrophy
µA	micro Amper
µl	microlitre
M	mole
MAP	mean arterial pressure
ml	millilitre
µm	micrometre
min	minute
mm	millimetre
mmHg	millimetre of mercury
MMPs	matrix-metalloproteinases
MRI	magnetic resonance imaging
ms	millisecond
Neu5Gc	N-glycolylneuraminic acid
NIBP	Non-invasive blood pressure
ng	nanogram

nmol	nanomol
NT-proBNP	N-terminal pro-brain natriuretic peptide
OMP	organic mobile phase
PCR	polymerase chain reaction
pg	picogram
PICP	carboxy-terminal propeptide of procollagen type I
PINP	procollagen carboxyl-terminal telopeptide
PIIINP	amino-terminal propeptide of procollagen type III
PM	postmortem
RNA	ribonucleic acid
SA	sinoatrial
SAP	systolic arterial pressure
SARS-CoV-2	severe acute respiratory syndrome coronavirus 2
SCD	sudden cardiac death
SD	standard deviation
SSP	Species Survival Plan
TAK	Takayasu arteritis
TGF-β	transforming growth factor
TIMPs	tissue inhibitors of metalloproteinases
TNF-α	tumour necrosis factor alpha
UK	United Kingdom
UKAS	United Kingdom Accreditation Service
USA / US	United States of America
UTE	ultrashort echo time
UV	ultraviolet
VF	ventricular fibrillation
VDR	vitamin D receptor
VDSP	Vitamin D Standardisation Program
VPC	ventricular premature complex
ZIMS	Zoological Information Management System
<	inferior to
25-OHD	25-hydroxyvitamin D

Introduction

Great apes are members of the family Hominidae and include four genera: the orangutans (*Pongo* sp.), the gorillas (*Gorilla* sp.), the chimpanzees and bonobos (*Pan* sp.) and the humans (*Homo* sp). For simplification purposes, the term “great-apes” will be used in this thesis to refer to the seven species of non-human great apes.

Bonobos and chimpanzees are classified as endangered in the wild by the International Union for Conservation of Nature (IUCN) (IUCN 2020), while gorillas and orang-utans are considered critically endangered. Threats in the wild include habitat conversion and fragmentation, poaching for wildlife trade and bushmeat, and infectious diseases mostly due to zoonotic disease outbreaks. Maintaining healthy captive populations is a fundamental part of ex-situ conservation programmes, and the knowledge of epidemiology and pathophysiology of great ape diseases is a crucial tool to enhance animal health and reduce mortality. Cardiovascular disease (CVD) is one of the major causes of mortality of captive great apes and understanding its epidemiology and pathophysiology as well as improving its diagnostic and veterinary management is of utmost importance.

Although great apes share striking genetic and phenotypic similarities with humans, the aetiopathogenesis of cardiac diseases in these species appears to be different. Whereas in humans, coronary artery disease is the most frequent type of heart disease, in captive great apes the most common entity described is interstitial myocardial fibrosis, where cardiac muscle is replaced by connective tissue, leading to impaired cardiac function. Zoo veterinarians and researchers worldwide agree on the need to better understand the epidemiology, aetiology and mechanisms of great ape heart disease. The variability between species and their difficult restraint and handling; the differences in husbandry, environmental conditions and diagnostic capabilities of institutions maintaining great apes; and the lack of homogeneous diagnostic protocols and validated diagnostic tools make the investigation of great ape cardiac diseases highly challenging. The main aim of this thesis is to better characterise the aetiopathogenesis and identify possible risk factors of CVD in zoo great apes.

The present studies have therefore investigated:

1. The accuracy of non-invasive blood-pressure devices in chimpanzees

2. The value of implantable loop recorders to detect arrhythmias in chimpanzees
3. The use of the dried blood spot method to measure vitamin D status in chimpanzees
4. The vitamin D status of the European chimpanzee population
5. Great ape CVD via histopathological examination
6. The use of microcomputed tomography to detect and characterise further the chimpanzee heart

1. Literature review

This first chapter reviews the literature dedicated to the description or investigation of cardiac disease in bonobos, orang-utans, gorillas and chimpanzees. Some advances made in the human cardiology field, especially related to cardiac fibrosis, have also been reviewed for comparison purposes.

1.1. Great ape mortality and morbidity

Most of the data available on diseases and causes of death in great apes are available in the form of individual case reports. Comprehensive reviews and retrospective studies exist only for specific populations during limited time ranges and are based on the available information, thus sometimes not representative of the real significance of each disease.

1.1.1. Captive populations

Retrospectives studies on morbidity and mortality of different ape species housed in American, Canadian and European zoos have been published. In 1975, an examination of cases reported in the literature and at the Aeromedical Research Laboratory in New Mexico over fifteen years relates that conditions involving the gastro-intestinal tract were the most frequent, followed by respiratory and cardiovascular diseases (Schmidt 1975). A review of the medical literature on great apes published in the 1980s found that gonadal tumours and atherosclerosis were frequently reported at the time (Janssen and Bush 1990), however, this review has been criticised by Strong et al. for a lack of methodology and no attempt to quantify the importance of each condition. Strong et al. systematically reviewed the zoological and veterinary literature of great apes from 1990 to 2014 and concluded that the three aetiologies that received most coverage at the time were infectious (especially of the gastrointestinal and respiratory tract), idiopathic (generally associated with cardiovascular disease) and neoplastic (Strong et al. 2016).

The first published review of mortality among the European zoo-housed western lowland gorilla population from 2004 to 2014 found that diseases of the digestive system were responsible for most deaths overall (23%, n=102), although external

causes (especially trauma) were most significant among young gorillas and cardiovascular disease among adult and aged animals (Strong et al. 2017). These results are similar to the mortality survey of the Association of Zoos and Aquariums (AZA) SSP (North American studbook) population of lowland gorillas published in 1994 (n=74), which concluded that 41% of deaths in adults and older adults were due to cardiovascular diseases and that traumatic death represented 60% of infant death. In this survey, gastrointestinal disease was implicated in 36% of the deaths of adult gorillas (Meehan and Lowenstine 1994).

In orang-utans, a survey of the Canadian and American SSP population from 1980 to 2008 found that in 163 animals over 15-year-old, 28.9% of deaths were due to cardiovascular disease, 15.7% to respiratory infections and 15% to chronic renal disease. Other causes of mortality in adults included gastrointestinal (GI) disease, problems during parturition and neoplasia. Approximately one out of six deaths (49/293) were perinatal or neonatal and in these cases, aetiologies involved infections, congenital defects, maternal factors, umbilical strangulation and prematurity. In infants, juveniles and adolescents, parasitism, respiratory infections, gastrointestinal diseases and trauma accounted for most of the deaths (Lowenstine et al. 2008b).

A retrospective review of the mortality of chimpanzees that died at the Southwest Foundation for Biomedical Research between 1967 and 1989 found that the primary causes of death were heart disease, trauma, and respiratory disease. Stillbirths were numerous but were not included in the total. Traumatic deaths were primarily in young chimpanzees and were caused by adults (Hubbard et al. 1991). The latest publication on chimpanzee mortality analysed the cause of death of 137 chimpanzees at the same institution during the last 35 years. Results showed that the most common causes of mortality were cardiomyopathy (40%), stillbirth/abortion, acute myocardial necrosis, trauma, amyloidosis and pneumonia (Hannah et al. 2017). Pathologic lesions were also identified from necropsy or biopsy and the most common findings were cardiomyopathy, followed by haemosiderosis, nematodiasis, oedema and haemorrhage. When lesions were classified by body systems, however, the GI system was the most frequently affected (Kumar et al. 2017). This highlights how results of mortality studies can differ depending on the classification system used. A pathologic review of 94 chimpanzees that died in zoos accredited by the AZA between 1990 and 2003 found that CVD was the most important cause of disease and death (combined)

in adult chimpanzees. However, in young individuals, trauma was the major cause of death followed by infectious pneumonia (in animals between one day and one year old) and premature birth (in neonates). Exhibit-related accidents were implicated in 12% of total deaths and chronic renal disease was the cause of death in 3 out of 24 adult chimpanzees. Both parasitism (especially *Balantidium coli)* and neoplasia were reported in approximately 16% of the cases, but they were identified as the primary cause of death only in rare cases. This study is the only comprehensive report of zoo-housed chimpanzee morbidity and mortality existing to date but is unfortunately only available as a conference proceeding (Gamble 2004).

1.1.2. Wild populations

In the wild, causes of diseases and death vary in different populations studied. Infectious diseases, particularly respiratory infections, are an important cause of morbidity with most deaths occurring during epidemics (Williams et al. 2008). However, many of the respiratory outbreaks reported in chimpanzees and gorillas occurred in human habituated populations and could be attributed to anthropozoonotic disease transmission (Kaur et al. 2008; Köndgen et al. 2008; Palacios et al. 2011). Other infectious diseases such as Ebola or anthrax have caused population declines both in gorillas and chimpanzees (Formenty et al. 1999; Huijbregts et al. 2003; Bermejo et al. 2006; Leendertz et al. 2006). Sporadic polio and mange epidemics have also been described (Lonsdorf et al. 2006). Trauma, particularly intraspecific lethal aggression is a major cause of mortality in wild chimpanzees and it has been reported to be the most common cause of death in chimpanzees from Gombe National Park between 2004 and 2010 (Terio et al. 2011). In this survey, disease was uncommon, and this had been partially attributed to improvements in disease-prevention protocols for tourists and researchers. Other causes of morbidities and mortalities in wild populations include parasitism, effects of simian immunodeficiency virus infections, injuries, maternal death or disability. Although myocardial megalokaryosis was a common finding in Gombe's chimpanzees, only two aged individuals presented with idiopathic myocardial fibrosis (IMF). Reports on diseases of wild bonobos and orang-utans are scarce (Kilbourn et al. 2003; Narat et al. 2015; Yoshida et al. 2016). Two fatal cases of encephalomyocarditis infection in semi-wild bonobos have been described (Jones et al. 2011) and one study showed that a large percentage (31%) of

wild bonobos had antibodies against lymphocryptovirus in their faeces (Yoshida et al. 2016). Infant mortality is less common in bonobos than in chimpanzees (Furuichi et al. 1998). Occasional fatalities in semi-wild orang-utans from tigers and leopards have been reported (Rijksen 1978), as well as traumas from falls or conspecifics (Kanamori et al. 2012). Wild orang-utans have also been observed to be affected by respiratory infections and parasitism, although these issues have not been seen to cause mortalities (Rijksen 1978). One study demonstrated that wild orang-utans were exposed to a variety of viruses such as respiratory syncytial virus, coxsackie virus, dengue virus, zika virus and Epstein-Barr virus, but no link was made with the health status of the animals (Kilbourn et al. 2003). Precise knowledge of morbidity and mortality in wild great apes is made difficult by the lack of comprehensive health monitoring programs for these populations, hence causes of death or diseases are usually deduced based on clinical signs only, as in most cases, no ante-mortem diagnostic procedures nor detailed post-mortem examination are conducted.

1.2. Cardiovascular disease in great apes

CVD is a major cause of death in all great ape species in captivity, representing 20% (orang-utans) to 45% (bonobos) of deaths depending on the species, time interval and specific population studied (Meehan and Lowenstine 1994; Lowenstine et al. 2008b; Strong et al. 2017). The percentage appears to be very high in bonobos, however, although it has been cited in several sources such as SSP data (McManamon and Lowenstine 2012; Lowenstine et al. 2016), no references to published studies have been found to support this number. Gorillas and chimpanzees are the species most extensively studied and recent reviews confirm the significance of CVD in zoos and laboratory settings (Gamble 2004; Hannah et al. 2017; Strong et al. 2017). It has been reported that CVD affected 77% of adult chimpanzees that died in AZA zoos between 1990 and 2003 (Gamble 2004) and was the main cause of death in captive adult Western lowland gorillas (41% of adult deaths in the SSP population and 38% in the European population) (Meehan and Lowenstine 1994; Strong et al. 2017). No review about CVD in captive orang-utans from European zoos exist, and the latest results from the North-American SSP presented in 2008 at the American Association of Zoo Veterinarian (AAZV) conference attributed 29% of adult orang-utan deaths to cardiovascular disease (Lowenstine et al. 2008b).

CVD appears to be more prevalent in males and adult animals (Strong et al. 2017). In wild apes, CVD is infrequently reported and it does not seem to be a primary cause of death when it occurs (Terio et al. 2011; McManamon and Lowenstine 2012). In a study on causes of death in chimpanzees from Gombe National park over 47 years, no evidence of CVD was found (Williams et al. 2008).

Different types of CVD have been identified in apes, including hypertension, cardiomyopathies, atherosclerosis, valvular disease, congenital heart defects, infectious myocarditis, pericarditis and aortic dissections (McManamon and Lowenstine 2012; Strong et al. 2016).

1.2.1. Idiopathic myocardial fibrosis

Idiopathic myocardial fibrosis (IMF), also referred to as fibrosing cardiomyopathy, idiopathic cardiomyopathy, or interstitial myocardial fibrosis, is the most common entity diagnosed in all species. It has been described as myocardial replacement fibrosis with atrophy and hypertrophy of cardiac myocytes, absent to mild myocardial inflammation, with no apparent aetiology or associated disease (Schulman et al. 1995). This entity has been proposed as the major cause of sudden cardiac death commonly observed in great apes (Lammey et al. 2008b).

One of the first cases of myocardial fibrosis was reported in a 26-year-old chimpanzee that died in 1982 at the Texas National Institute of Health Primate Centre. The animal presented in congestive heart failure and was euthanised, and post-mortem and histopathological evaluation revealed cardiomegaly with dilation of both ventricles and hypertrophy of the right ventricle, diffuse myocardial fibrosis and atherosclerotic lesions in several coronary arteries and meningeal vessel. Although the authors suggested that elevated blood pressure due to stress may have aggravated the atherosclerotic lesions in coronary arteries and brain and contributed to the chronic cardiac lesion, they also stated that neither myocardial infarcts nor completely occluded coronary arteries were found (Hansen et al. 1984). In 1984, two male gorillas died at the New York Zoological Society and histopathology revealed cardiac lesions consisting of multifocal areas of fibrosis and adipose tissue within the myocardium with degeneration of myofibres. Although the authors correlated the lesions to a deficiency in vitamin E, these could also represent cases of IMF in gorillas (McNamara et al. 1986).

Four out of ten orang-utans necropsied at the National Zoological Park in Washington before 1989 were reported to be affected with IMF, the condition being considered fatal in two cases (Munson and Montali 1990). Since then, many reports described cases of myocardial fibrosis in great apes, especially in gorillas and chimpanzees. A retrospective study on fibrosing cardiomyopathy in captive western lowland gorillas in the United States, published in 1995, devised the modern definition of fibrosing cardiomyopathy, highlighting its idiopathic aetiology. Out of 19 identified gorillas that died with cardiac disease, they found that 11 gorillas were affected with fibrosing cardiomyopathy, of which 8 died from the disease. Interestingly, 7 out of these 8 animals experienced sudden death, and the other animals that were diagnosed with cardiac conditions other than IMF presented symptoms before their death, thus establishing a clear link between IMF and sudden cardiac death in gorillas (Schulman et al. 1995).

Most reports on IMF concern chimpanzees, as it is the species with the largest number of animals kept in captivity (both in zoos and in research centres) and because IMF has a high prevalence in the captive population (Hansen et al. 1984; Munson and Montali 1990; Hubbard et al. 1991; Varki et al. 2009). A review of the clinical and necropsy records of a captive chimpanzee population that died over a 6-year period found that 81% of the chimpanzees had IMF and that all animals that suffered sudden death (36%) were affected by various degrees of IMF, thus again linking sudden cardiac death to IMF (Lammey et al. 2008a). Another analysis of sudden cardiac death cases in the chimpanzee population of the Alamogordo Primate Facility between 2001 and 2006 revealed that 12 out of 13 animals that presented with sudden death had IMF, that all had cardiac arrhythmias on clinical examination before death and most had cardiomegaly (Lammey et al. 2008b). In 2009, a review of medical records of 87 deceased chimpanzees housed at a North-American primate research centre found that 52% of the animals had idiopathic cardiomyopathy and that the disease was the primary cause of death for more than half of them (Seiler et al. 2009). This paper has been criticised by Sleeper as they state that congestive heart failure (CHF) was the most common presentation in chimpanzees with heart disease without describing which symptoms these animals suffered; furthermore, Sleeper points that the term “sudden cardiac death” should have been used rather than “acute heart failure” which is a rare cause of death in apes (Sleeper 2009). The 2017 paper from Kumar et al.

reviewing 245 chimpanzee pathological records is very vague in this aspect as it lists morphological diagnoses with cardiomyopathy being present in 67 animals and fibrosis in 21 but does not define the exact nature of the lesion nor in how many cases they occurred concurrently (Kumar et al. 2017). The possible aetiology, pathogenesis and diagnostic of IMF will be discussed further in this chapter (section 1.3).

1.2.2. Aortic dissection

Aortic dissection was first reported in 1970 in a gorilla (Morgan 1970) and later in 1994 its relatively high prevalence in this species was emphasised by Kenny et al. who surveyed 142 institutions that held gorillas and found 8 confirmed cases. Six of these cases were males, and ages ranged from 16 to 43 years old (Kenny et al. 1994). The same year, a survey of the lowland gorilla population from the Species Survival Plan (SSP) programme found aortic dissection to be the cause of 5 adult deaths out of 39, the gross lesion being diagnosed mostly in animals older than 30 years old and being more prevalent than IMF in this age category (Meehan and Lowenstine 1994). The most recent review of gorilla mortality in European zoos found 3 cases of aortic aneurism or rupture in 151 records analysed (Strong et al. 2017). Four cases have been reported in bonobos and one in a chimpanzee (Gamble 2004), interestingly no cases have been described in orang-utans (Lowenstine et al. 2016). In all cases, the dissection affected the proximal ascending aorta and was not associated with atherosclerosis. Lesions were commonly chronic, and death was ultimately due to failure of the vessel wall and haemorrhage. Hypertension had been implicated based on the fact that it is the trigger in most human cases and that left ventricular hypertrophy is observed in affected apes; however, the latter could also be a consequence of the chronicity of the dissection (McManamon and Lowenstine 2012). Other risk factors such as atherosclerosis, elevated cholesterol and pregnancy have been identified in the pathogenesis of aortic dissection in gorillas (Natterson-Horowitz and Wynne 2009).

1.2.3. Atherosclerosis

Arteriosclerosis is an age-related disease characterised by the hardening, thickening and loss of elasticity of arterial walls due to intimal fibrosis. Atherosclerosis is caused by the build-up of atheromatous plaque (lipids, fibrous tissue, and calcium), with

cellular debris being ingested by macrophages and smooth muscle cells (“foam cells”) (Miller and Gal 2017). Although the terms arteriosclerosis and atherosclerosis describe different lesions, these terms are often used interchangeably, creating confusion. Atherosclerosis, especially of the coronary arteries, is the most common cause of CVD in humans, and leads to ischemic heart disease, stroke, and peripheral arterial disease (Herrington et al. 2016). However, coronary disease is considered rare in apes (Varki et al. 2009) and atherosclerosis is often mild and in most cases found incidentally on post-mortem (McManamon and Lowenstine 2012).

Chimpanzees were used as a model for human atherosclerosis in the past partly because the composition of their plasma lipoprotein are similar to humans and respond to dietary changes in a similar way (Blaton and Peeters 1976). However, atherosclerosis is a multifactorial and complex syndrome associated with a myriad of risk factors including inflammatory disease, nutrition, genetic predisposition, toxins, stress, etc.(Thomas et al. 2014). Spontaneous atherosclerosis was recorded regularly in the seventies in apes used in research, probably due to a poor nutritional status (Schmidt 1975). However, a review of 94 chimpanzee records that died between 1990 and 2003 in zoos only found two cases of atherosclerosis (Gamble 2004). Similarly, out of 87 chimpanzee records analysed by Seiler et al. in 2009, only eight described vascular lesions, unfortunately, the animals with spontaneous arteriosclerosis or atherosclerosis were grouped in the data presented (n=8) (Seiler et al. 2009). The latest mortality review of laboratory-housed chimpanzees found that one animal with acute myocardial necrosis also presented with a thrombus in the coronary artery, however, the composition of the thrombus was not reported. They also attribute the death of 3 females to a stroke secondary to atherosclerosis (Hannah et al. 2017). The Great Ape Heart Project (GAHP) veterinary pathologist, Dr Lowenstein, reports that she has only diagnosed the condition in two zoo-housed chimpanzees and that both cases affected the aorta (McManamon and Lowenstine 2012). These findings confirm that cardiac disease is generally not associated with atherosclerosis in this species.

Interestingly, despite their “healthy” diet compared to humans, chimpanzees’ blood lipid profile could be classified as pro-atherogenic with mean cholesterol levels higher than in humans, a low-density lipoprotein (LDL) / high-density lipoprotein (HDL) ratio similar to humans and an increase in LDL levels by atherogenic diets. They also have high levels of lipoprotein-associated phospholipase A2 (LPa) and homozygous for the

APOE4 allele, both being risk factors for the development of atherosclerosis in humans (Varki et al. 2009). The 35-year review on chimpanzee pathology published in 2017 observed that 28 animals out of 245 suffered arteriosclerosis or atherosclerosis, all animals except one were middle-aged or elderly, but no mention of the exact nature, location or severity of the lesions was made. Curiously, the lesion was observed in twice as many females as males (Kumar et al. 2017).

Two deaths associated with coronary atherosclerosis have been published in gorillas (Gray et al. 1981; Schulman et al. 1995), but the condition is described as rare in these animals (McManamon and Lowenstine 2012). A study evaluating fifteen western lowland gorillas with blood lipid profile and transoesophageal echocardiography found atheroma plaques in five of them. Plaques generally affected the descending aorta with severity increasing with age and were correlated with elevated ratios of apolipoprotein B/apolipoprotein A1 and cholesterol/HDL (Baitchman et al. 2006). However, as both the presence of plaques and the lipid profiles were age-dependent, no clear relationship between the risk of coronary disease and the lipid ratios can be determined.

In orangutans, the prevalence of the condition seems to be similar to other species. One case of fatal coronary atherosclerosis in a captive orang-utan with high cholesterol levels was published in 1987 (Scott 1987). The SSP pathology advisors found atherosclerosis in nine orang-utans examined, with lesions affecting the aorta and being more severe in the caudal abdominal aorta and internal iliac vessels (McManamon and Lowenstine 2012).

The low prevalence of atherosclerosis and coronary disease in great apes is still poorly understood and its pathophysiology needs further investigation.

1.2.4. Valvular disease

Valvular heart disease is common in animals and humans, the two most common types in the latter being mitral regurgitation due to myxomatous degeneration and aortic stenosis. The prevalence of valvulopathies in humans is around 2.5% and increases sharply with age, being considered as degenerative diseases, except for infectious endocarditis (Iung and Vahanian 2014).

Valvular disease occurs infrequently in apes. Endocardiosis has been diagnosed in six adult chimpanzees from the SSP population (Gamble 2004) but no details were given about the localisation of the lesions. Valvular anomalies were found to be extremely rare in gorillas undergoing echocardiographic evaluation by the GAHP, although mitral regurgitation was observed in some animals with end-stage cardiomyopathy (Murphy et al. 2011). Lowenstine observed mitral valve myxomatous degeneration in three female mountain gorillas over thirty years old, one 42-year male orang-utan, and a 48-year old female chimpanzee, as well as a case of aortic valve mineralisation and fibrosis in a 47-year-old gorilla (Lowenstine et al. 2016). Endocardiosis was observed in 1.4% of the chimpanzees in Kumar's review, and endocarditis in 0.2% of them, but again, no mention was made of localisation, severity or clinical significance (Kumar et al. 2017). Endocarditis is known to be more common than degenerative valve disease in apes (Lowenstine et al. 2016). In 1975, Schmidt described a case of vegetative endocarditis in a 12-year-old female chimpanzee that had suffered from necrotising gingivitis. Interestingly, it affected the tricuspid valve and consisted of multiple nodular vegetations made of fibrous tissue with lymphocytes and macrophage infiltration (Schmidt 1975). Since then, infectious endocarditis has been diagnosed in a few gorillas (Lowenstine et al. 2016) and other apes (McManamon and Lowenstine 2012), although case reports are difficult to find in the literature. Endocarditis is not mentioned in the 2004 SSP chimpanzee pathologic review (Gamble 2004). It is possible that as endocarditis is generally one of several lesions of infectious processes, it is not as frequently reported as it actually occurs.

1.2.5. Infective myocarditis

Myocardial inflammation, mostly due to viral infections, is thought to be a major cause of sudden cardiac death and dilated cardiomyopathy (DCM) in young humans (Fung et al. 2016). In apes, it has been described in three young bonobos due to encephalomyocarditis virus infection. For one of the animals, the diagnosis was made presumptively based on gross and histopathological findings and clinical signs (heart and renal failure, CNS signs) (Jones et al. 2005). For the other two, who died acutely after the onset of respiratory illness, diagnosis was confirmed by immunohistochemistry and PCR (Jones et al. 2011). In chimpanzees, early reports

describe focal myocarditis characterised by necrosis with pleocellular infiltrate, diagnosed incidentally and of unknown aetiology, and a case of severe acute myocarditis in a chimpanzee with *Enterobacter cloacae* infection (Schmidt 1975). Fatal myocarditis caused by *Trypanosoma cruzi* has been reported in a 23-year old chimpanzee (Bommineni et al. 2009). Cases of viral myocarditis have also been reported in the AZA chimpanzee population (Gamble 2004). One adult zoo orang-utan died from Coxsackievirus B4 myocarditis confirmed by immunohistochemistry (Miyagi et al. 1999). An extremely high concentration of Coxsackievirus B3 was detected by real-time PCR in a chimpanzee that died during a respiratory outbreak in a Danish zoo (Abel Nielsen et al. 2012). In all these cases of viral myocarditis, the myocardium showed focal or interstitial mononuclear infiltrate. Myocarditis has been diagnosed in 21 chimpanzees out of 245 in the study by Kumar et al., however, the clinical significance and agent implicated were not detailed. One recent paper describes the successful treatment of a myocarditis in a chimpanzee, however, the diagnosis was only presumptive and based on increased white blood cell count, serum inflammatory biomarkers and reduced left ventricular function on echocardiography (van Zijll Langhout et al. 2017). This highlights the difficulty of reaching a definitive diagnosis in zoological medicine, particularly when investigating CVD in great apes. In many case reports and retrospective studies, the real significance of the pathological lesions described, and the origin of clinical signs observed remain unclear.

1.2.6. Congenital heart defects

Congenital heart defects reported in apes include mainly septal defects (McManamon and Lowenstine 2012), but their prevalence seems to be low (Kumar et al. 2017). Schmidt cites a case of patent foramen ovale in an infant chimpanzee with no related clinical signs (Schmidt 1975). A ventricular septal defect was diagnosed using *in vivo* oximetry in a 3-year-old female gorilla with a heart murmur and a history of congestive heart failure (Machado et al. 1989). One case of coarctation of the aorta in a gorilla with cerebral infarction has been described (Trupkiewicz et al. 1995).

1.3. Possible aetiologies and pathogenesis of CVD, and particularly IMF, in great apes

1.3.1. Epidemiological considerations

It is well known that in all species, including apes, CVD prevalence increases with age (Lowenstine et al. 2016). In a study on echocardiographic parameters in western lowland gorillas left ventricular wall thickness increases and left ventricular cavity decreased with age in males. Progressive left ventricular hypertrophy and cardiomyopathy was found to be predominantly a male-associated disease, with all males older than 31 years old considered affected. Interestingly, females showed few changes in cardiac parameters with age. In a similar study on chimpanzees, no differences in echocardiographic findings were noted between age groups in females nor males, however, adult males were more susceptible to cardiac arrhythmias as they aged (Sleeper et al. 2014). This is consistent with a report on sudden cardiac death in chimpanzees that concluded that males appeared to be more at risk for fatal arrhythmias than females (Lammey et al. 2008b). This report, however, found that male chimpanzees with IMF had heart enlargement, while females did not. Another study observed IMF in 14 males and 4 females presented at necropsy, of which 8 males and 1 female died of sudden death (Varki et al. 2009). No mention of the age of the affected animals was made. In a study that found IMF in 89% of a captive chimpanzee population, the younger animals were mostly not affected with IMF, although two 13-year-old chimpanzees presented with mild fibrosis. Males and females were similarly affected (Lammey et al. 2008a). Seiler et al. reported that the youngest chimpanzee that died from IMF was 13 years old (Seiler et al. 2009). In orang-utans, cardiac fibrosis has been reported in animals over 17 years-old (Munson and Montali 1990). Although these findings point toward a higher prevalence of cardiac disease in males than in females with risk increasing with age, some contradictions highlight the need for more detailed and large-scale epidemiological studies.

1.3.2. Mechanisms of myocardial fibrosis

The myocardium is composed of cardiomyocytes, fibroblasts, vascular cells and an extracellular matrix (ECM) composed of fibrillar collagen (mainly collagen I and III) that gives the tissue its structure and elasticity. While cardiomyocytes represent more than

two-thirds of the myocardial tissue volume, cardiac fibroblasts (CFBs) are very abundant in number. CFBs are responsible for ECM production, homeostasis and remodelling, and are involved in electrical activity, intercellular communication and angiogenesis, cell proliferation and apoptosis (Fan et al. 2012; Istrătoaie et al. 2015). They produce cytokines, peptides and growth factors (tumour necrosis factors TNFα, transforming growth factor TGF-β, interleukins, angiotensin II, etc.); and ECM-regulatory proteins such as matrix-metalloproteinases (MMPs) which can degrade ECM proteins and tissue inhibitors of metalloproteinases (TIMPs) (Fan et al. 2012).

In response to some stimuli, most commonly myocardial injury, CFBs proliferate and can differentiate into their activated form, myofibroblasts, which produce more ECM proteins than normal CFBs. In advanced stage of fibrosis, a subpopulation of myofibroblasts becomes able to express the α-smooth muscle actin protein (α-SMA) that enhance their contractile activity. These processes are initially adaptive to allow the maintenance of structural integrity and mechanical strength of the ventricle, however, an excess of fibroblasts and ECM leads to impaired cardiac function by increasing ventricular stiffness and impairing mechano-electric coupling of cardiomyocytes, thus leading to contractile dysfunction and risk of arrhythmogenesis and mortality (Travers et al. 2016). Both the source of myofibroblasts in the fibrotic hearts and the pathways involved in the conversion of CFBs to myofibroblasts are still under investigation in humans, but it is thought that these cells derive from the proliferation and activation of resident fibroblasts as well as from other precursors including endothelial cells, haematopoietic bone-marrow-derived cells, perivascular cells, and fibrocytes. Known mediators of fibroblast activation include TGF-β (which is likely to play the greatest role), angiotensin II, endothelin-1, serum response factor, platelet-derived growth factor and cytokines (Leask 2015).

In humans, two forms of myocardial fibrosis are defined. Replacement or reparative fibrosis is where collagen accumulation is seen focally to replace dead cardiomyocytes, forming scars. Reactive fibrosis occurs diffusely throughout the interstitial and perivascular myocardium in the absence of significant cardiomyocytes loss. Both types of fibrosis are seen after acute myocardial infarctions. Replacement fibrosis develops in the infarct areas and helps preserve heart integrity, while reactive fibrosis is seen in the non-injured myocardium, causing pathological remodelling (Talman and Ruskoaho 2016). Reactive interstitial fibrosis is also the form that

develops in the elderly population and as a consequence of either pressure or volume overload due to chronic hypertension, metabolic disorders, valvular diseases or cardiomyopathies (Gyongyosi et al. 2017).

The aetiopathogenesis of IMF in great apes is still poorly understood. Although numerous reports are describing IMF in great apes, its cause remains unknown and only one paper attempted to study the mechanism of IMF in chimpanzees (Varki et al. 2009).

1.3.3. Possible aetiopathogenesis of idiopathic myocardial fibrosis.

An age-related change?

Although fibrosis is generally related to repair following acute or chronic ischemic insults in humans, it is thought that in the normal ageing heart, an increase of haemodynamic load caused by peripheral vascular stiffening contributes to the development of cardiomyocyte hypertrophy and interstitial and perivascular fibrosis (Biernacka and Frangogiannis 2011). In humans, the ageing heart has a decreased number of myocytes, and increased myocyte size, and an increased extracellular matrix compared with younger hearts (Kwak 2013). The development of fibrosis as an age-related change could be considered in the case of IMF in apes, as in these species the prevalence of ischemic events is rare, and IMF is more prevalent in aged individuals. Both replacement and interstitial fibrosis can be observed in ape myocardium affected by IMF. Patches of replacement fibrosis are seen more frequently around small-calibre coronary arterioles which often develop arteriosclerosis, and areas of fibrosis can extend throughout the walls of all chambers (McManamon and Lowenstine 2012). Associated left ventricular hypertrophy (LVH) can be seen, particularly in aged male gorillas. When LVH is present, it is hard to determine if the fibrosis is the consequence of the hypertrophy, in response to an increased haemodynamic load as occurs in humans, or the fibrosis occurs first and leads to LVH as a compensatory mechanism. In cases of left ventricular pressure overload in other species, perivascular and interstitial fibrosis develop first together with cardiomyocyte hypertrophy, then as cardiac cells undergo necrosis, reparative fibrosis is noted (Biernacka and Frangogiannis 2011). It is unclear if the fibrosing cardiomyopathy observed in apes follows a similar mechanism.

An idiopathic process?

One may also wonder what mechanisms are involved when myocardial fibrosis is observed in young apes or in apes where the heart appears normal and no other lesions or co-existing conditions are identified, which is what occurs most frequently in chimpanzees. This phenomenon resembles idiopathic myocardial fibrosis in humans, a process that is identified in 1% to 3% of the cases of sudden cardiac deaths in young adults, and whose aetiology is still unexplained (John et al. 2004). In humans, IMF is described as myocardial fibrosis without evidence of any additional cardiac abnormalities including LVH, prior myocardial infarction, coronary luminal narrowing greater than 50%, valvular or congenital heart disease. In a paper that characterised six cases of IMF in humans, the pattern was exclusively interstitial in four cases and mostly interstitial with some areas of replacement fibrosis in the other two, with a predilection to the left ventricular wall. Although myocardial fibrosis has been linked to residual effects of myocarditis and age-related changes, in this study there was no evidence of myocardial inflammatory response nor apoptosis, and there was no correlation of lesion extend with age. However, an increased expression of tumour growth factor beta-1 (TGF-β1) was observed across all myocardial sections and particularly within myocytes, suggesting an association of this growth factor with IMF. TGF-β1 is a known mediator implicated in cardiac fibrosis, however, its production is generally sustained enough to lead to fibrosis only in cases of repeated injury, as in myocardial infarction, cardiac hypertrophy or congestive heart failure. The authors speculated that occult hypertension, novel gene defects or novel circulatory mediators could be implicated in the pathogenesis of IMF mediated by TGF- β1 in young adults (John et al. 2004).

A result of hidden hypertension?

It is well known that pressure overload exerts biomechanical stress in the myocardium that can lead to adverse remodelling and eventually to cardiac hypertrophy, cell death and further fibrosis formation (Fan et al. 2012). In humans, hypertension is the primary cause of non-ischemic cardiac fibrosis. In gorillas, the common presence of left ventricular hypertrophy together with varying degrees of median hypertrophy and hyalinisation of endomyocardial arteries and arterioles suggest the possibility of hypertension playing a role in the pathogenesis of fibrosing cardiomyopathy

(Schulman et al. 1995; Lowenstine et al. 2016). In chimpanzees, however, vascular changes and ventricular hypertrophy are only occasionally observed, which makes hypertension a less plausible cause of IMF in this species. In a captive population of chimpanzees, 29 deceased animals presented with IMF on histopathology but only 3 of them were diagnosed with systemic hypertension during their annual health examinations (Lammey et al. 2008a). Ely et al. demonstrated that in chimpanzees, hypertension increases with age in both sexes and with obesity in females (Ely et al. 2013). However, it is important to consider that blood pressure (BP) is generally measured in great apes during anaesthesia, and with oscillometric devices not validated for use in these species, it makes the significance of the results uncertain. Changes in BP throughout the day, with various levels of activities or with ageing in the different species of great apes have not been studied.

A change related to inflammation?

It is well known that cardiac injury initiates an inflammatory reaction that is the starting point for repair mechanisms. After an infarct, for example, necrotic cells release signals that activate the innate immune pathways, triggering an intense inflammatory and immune cell infiltration that clear necrotic cells. A reparative phase follows, with resolution of the inflammation, (myo)fibroblast proliferation and fibrosis (Prabhu and Frangogiannis 2016). It is thought that a disproportionately prolonged or intense inflammatory phase can lead to adverse remodelling. Similarly, in other CVD in humans, such as hypertension, myocarditis, DCM and heart failure, fibrosis is considered to be the natural consequence of inflammation (Kania et al. 2009).

In the case of myocarditis, studies in humans and animal models demonstrate that the initial beneficial role of the immune response can become detrimental if not properly regulated. Both the host immune response and viral factors can induce fibrosis, which is a feature of chronic active myocarditis (Fung et al. 2016). Viral myocarditis is a major cause of sudden cardiac deaths in young humans as it leads to myocardial inflammation, ion channel dysfunction, electrophysiological and structural remodelling that can generate life-threatening arrhythmias. Moreover, it has been shown that increased oxidative stress and inflammation can increase the release of inflammatory cytokines in the heart and that inflammation during acute myocarditis activates MMPs, contributing to fibrosis (Tse et al. 2016). Myocarditis in humans is defined as

"inflammatory infiltrate of the myocardium associated with myocyte degeneration and necrosis of non-ischaemic origin" and the criteria to reach a definitive diagnostic is a value more than 14 leukocytes/mm^2 and more than 7 T-lymphocytes/mm^2 (Caforio et al. 2013). In apes, although some case reports describe confirmed cases of viral myocarditis with, in some of them, the presence of associated myocardial fibrosis (Jones et al. 2005; Bommineni et al. 2009), most of the cases of IMF only present a minimal inflammatory infiltrate. In the retrospective study on fibrosing cardiomyopathy in captive western lowland gorillas in the US, six out of eleven fibrotic hearts had mild inflammation associated with myocyte necrosis (multifocal mild myocarditis) and three others had multifocal mild interstitial inflammation. In the former cases, it is unclear if the inflammation is the cause or result of myocyte necrosis. The authors also stated that recurrent infections such as influenza infections in gorillas could lead to cumulative myocardial damage by virus-induced autolysis, induced auto-immunity, and/or ischemia caused by thrombosed capillaries (Schulman et al. 1995).

Inflammation pathways (unrelated to myocarditis) causing cardiac fibrosis are currently extensively studied in humans and animal models (Levick et al. 2007; Dick and Epelman 2016). It is thought that many conditions associated with advanced age such as type-2 diabetes, metabolic syndrome, osteoporosis, dementia, etc. are associated with increased levels of circulating inflammatory cytokines and acute-phase proteins (Trial et al. 2016). In the mouse, it has been demonstrated that age-related interstitial fibrosis is a consequence of immune-inflammatory dysregulation (Cieslik et al. 2011).

A consequence of captive lifestyle?

Nutrition and husbandry are very different in apes maintained in captivity compared to the ones in the wild, and it is natural to think that nutritional deficiencies or environmental factors may play a role in the aetiopathogenesis of IMF. Vitamin E deficiencies have been associated with cardiomyopathy with fibrosis in gorillas (McNamara et al. 1986), and other nutritional factors such as iron overload, high salt content or unavailability of cardio-protective plants eaten by wild apes have been cited (McManamon and Lowenstine 2012).

Of interest is the possible role of vitamin-D deficiency in ape CVD and particularly IMF. In humans, the vitamin D receptor (VDR) is present in numerous organs including the

heart and blood vessels, and although solid data from randomised controlled trial is sparse, clinical and epidemiological investigations are suggesting an association between vitamin D deficiency and CVD (Wang et al. 2012c; Al Mheid and Quyyumi 2017; Wimalawansa 2018; Zittermann 2018). Inverse associations between serum 25-OHD and CDV risk at serum 25-OHD concentrations below 60 nmol/L have been reported, and some studies show an increase in mortality with levels above 125 nmol/L (Wang et al. 2012b; Zittermann and Prokop 2014). Low vitamin D values have been associated with hypertension, atherosclerosis, myocardial infarction and stroke (Public Health England 2016; Caccamo et al. 2018; Kim et al. 2020). In mice, deletion of the VDR gene in the cardiac myocyte of mice resulted in cardiac hypertrophy (Chen et al. 2011) while VDR activation reduced fibrosis (Caccamo et al. 2018). It has been demonstrated that vitamin D may act as an inhibitor of fibrosis in numerous organs and that it reduces alpha-smooth muscle actin expression and prevents TGFβ1-mediated cardiac pro-fibrotic changes in-vitro (Meredith et al. 2015a). Vitamin D deficiency in humans is highly prevalent, and it is believed that a large part of the UK population does not synthesise enough vitamin D in summer to ensure a winter serum 25-OHD concentration above 25 nmol/L (Public Health England 2016). Similarly, in captive great apes, a few studies suggest that low vitamin D levels may be widespread. Low serum 25-OHD have been found in captive chimpanzees and linked to insufficient sunlight exposure in one study (Crissey et al. 1999; Junge et al. 2000; Videan et al. 2007). A recent study assessing serum 25-OHD concentrations in two collections of captive gorillas in the US found that many individuals had values below the recommended concentrations for humans despite daily outdoor access (Bartlett et al. 2017). However, as none of these studies relates health status to vitamin D levels, the significance of the findings is unclear. No studies exist on vitamin D levels in European captive apes, and vitamin D reference ranges have not been published for captive apes or apes living in their natural environment. The correlation between vitamin-D status and CVD in captive great apes should therefore be investigated.

Metabolic abnormalities should be considered as contributing factors in great ape CVD. Murphy et al. found a positive correlation between body-weight and the development of cardiomyopathy in male gorillas between 11 and 20 years of age (Murphy et al. 2011). Diabetes or chronic hyperglycaemia could also be a plausible aetiology in some cases of myocardial fibrosis in apes. In humans, diabetes mellitus

is an important cause of non-ischemic cardiac fibrosis, and interstitial and perivascular fibrosis is a histological hallmark of diabetic cardiomyopathy, which is defined as structural and functional abnormalities of the myocardium in diabetic patients without coronary artery disease of hypertension (Miki et al. 2013). It has been shown that in patients with diabetes, cardiac fibrosis results mainly from an increase of collagen type III synthesis (Shimizu et al. 1993). Diabetes has been diagnosed in captive apes, however, no association has been made yet with this syndrome and CVD (Chilton et al. 2016). In a paper calculating references ranges for fasting blood glucose and haemoglobin A1c for chimpanzees, the overall incidence of type 2 diabetes in the population was 0.8% but increased to 3.7% in geriatric animals. These numbers are much lower than the prevalence for IMF in this species, however, insulin resistance and hyperglycaemia linked to obesity, inflammation or stress are more difficult to diagnose and could play a role in the development of IMF in captive apes (Andrade et al. 2011).

The lesions of IMF, together with the common presence of cardiomyocyte karyomegaly in ape hearts, bears a clear resemblance to human catecholamine cardiotoxicity. Early retrospective studies in humans indicate that environmental stress, via catecholamines can lead to irreversible myocardial necrosis and sudden cardiac death. The mechanisms of catecholamine cardiotoxicity and CVD due to stress are not yet fully understood but appear to be multifactorial (Golbidi et al. 2015). The severity and high prevalence of IMF in captive apes and the higher prevalence of CVD in males, that have to fight to maintain their rank within the social hierarchy, suggest a possible association between CVD and stress in apes (Lowenstine 2003; Terio et al. 2011).

The lack of exercise that great apes suffer in captive settings could also be suspected as a possible factor for the development of CVD in these species. Moderate exercise training has been shown to attenuate ageing-induced cardiac inflammation, hypertrophy and fibrosis in rats (Kwak 2013; Liao et al. 2015), and to decrease CVD risk in humans (Lavie et al. 2015). However, excessive exercise has also been correlated to myocardial damage and fibrosis (Patil et al. 2012). The link between CVD and exercise in apes has not been yet investigated.

Other proposed aetiologies

Various other factors have been shown to be associated with cardiac fibrosis in other species, and as IMF can be considered as an end-stage lesion, its aetiology may well be a combination of several aetiologies.

It is well known that the cardiovascular and renal systems are interdependent, and not only via changes in systemic blood pressure. In human medicine, cardiorenal syndrome type 2 is defined as when chronic heart disease leads to chronic kidney disease (CKD), while type 4 occurs when CKD promotes myocardial disease. Both organs are prone to developing tissue fibrosis in cardio-renal syndromes, with TGF-β playing a central role (Hundae and McCullough 2014). The renin-aldosterone system is also critical in the regulation of cardiac fibrosis (Lammey et al. 2008a). In orang-utans, a statistically significant association between renal disease and fibrosing cardiomyopathy has been found (McManamon and Lowenstine 2012), and cases of concurrent renal and cardiac disease have been reported in other ape species (Ely et al. 2010). In a laboratory-housed chimpanzee population, cardiac fibrosis with attendant glomerulosclerosis and tubulointerstitial fibrosis were observed in 69% of the animals, and a statistically significant association was observed between the two conditions. As the severity of glomerulosclerosis increased so did the severity of cardiac fibrosis (Chilton et al. 2016). Many pathways are known to play a role in concurrent renal and cardiac disease in humans and animals, but in apes, it is hard to be sure which pathways are implicated, as in most cases it is not known which condition developed first.

Varki et al. suggest that a factor involved in the difference between apes and human CVD may be explained by the change in terminal glycosylation of sialic acids and other glycans in the myocardium. Humans are the only mammal species that do not synthesise the N-glycolylneuraminic acid (Neu5Gc) and instead express the precursor Neu5Ac on cell surfaces. However, Neu5Gc from the diet can become incorporated into human endothelial and epithelial cells and generate chronic inflammation due to the presence of anti-Neu5Gc antibodies, and the authors suggested that this together with the fact that human lymphocytes are more reactive than those of chimpanzees, could accelerate the development of atherosclerotic lesions in humans (Varki et al. 2011). This does not explain however why apes are more prone to IMF than humans. The authors found evidence that the chimpanzee myocardium had a lower density of

capillary blood vessels compared to humans, implying a lower myocardial blood supply in chimpanzee and an increased risk of developing myocardial fibrosis. They also proposed that as terminal sialic acids are denser in the great ape heart and are often the target for viral pathogens, IMF could be linked to precedent viral myocarditis (Varki et al. 2009). This assumption seems to be quite conjectural considering that, as stated previously, viral myocarditis has been diagnosed concurrently with IMF in only a few great apes. The difference in sialic acid biology and its correlation with CVD and cardiac fibrosis in different species merits further investigation.

1.4. Clinical presentation and diagnostic

1.4.1. Sudden death and arrhythmic events monitoring

Ante-mortem diagnosis of CVD and especially IMF in great apes is challenging not only because of the lack of CVD diagnostic protocols and reference ranges for these species, but also because of the lack of clinical signs in diseased animals.

Sudden death without any previous symptoms is a common occurrence in apes affected with IMF (Schulman et al. 1995; Lammey et al. 2008b). In the absence of other relevant pathological findings that could lead to instantaneous death such as massive pulmonary embolism, aortic aneurysm or stroke, these deaths are considered “sudden cardiac death” (SCD) and are believed to be due to fatal arrhythmias (Lammey et al. 2008b; Sleeper 2009). In humans, SCD can occur secondary to structural heart disease (including ischemic and non-ischemic heart disease) or primary electrical abnormalities of the heart (Kuriachan et al. 2015), and cardiac arrest is commonly caused by ventricular tachycardia degenerating to ventricular fibrillation (VF) and subsequent asystole (Rubart and Zipes 2005). An increased number of premature ventricular complexes, altered QT interval and reduced heart rate variability have been associated with fatal cardiac arrhythmias in humans (Artigos 2014). In human idiopathic myocardial fibrosis, it is postulated that the diffuse increase in myocardial collagen could promote the genesis of re-entrant ventricular arrhythmias (John et al. 2004).

In a study on electrocardiogram (ECG) abnormalities in chimpanzees, ventricular premature complexes (VPCs) have been reported to be the most common arrhythmia,

and the mortality was significantly higher in animals with multiform VPCs than in those without. Other abnormalities detected were partial right bundle branch block, second-degree AV-block, bradycardias, and mixed arrhythmias. The risk of arrhythmias in this species appeared to increase in the third and fourth decades of life and in males. Interestingly, the incidence of cardiac arrhythmias was not significantly higher in animals with hypertension, hyperlipidaemia, or chronic viral infections. Unfortunately, no comparison was made between the detection of arrhythmias and the presence and severity of IMF on post-mortem (Doane et al. 2006). In one retrospective study on SCD in 13 captive chimpanzees, all the animals that died suddenly had ventricular ectopy on ECG antemortem, and twelve of them presented IMF (Lammey et al. 2008b).

ECG is an affordable and accessible diagnostic tool that is used routinely during cardiac screening in great apes. On the basis of apes' anatomic similarity with humans, a 12-lead ECG is preferably performed, and electrodes are placed in accordance with human standard locations. ECG reference intervals have been published for clinically normal chimpanzees from an African sanctuary. It is worth noticing that the number of arrhythmias detected in this population was much lower than in previous studies on zoo-housed animals. This may be due to the lower age of the studied wild-born animals but could also be related to a lower prevalence of IMF. Interestingly, 47% of young chimpanzees and 61% of adult chimpanzees would have been classified as having LVH if the human criteria was applied, however, these findings were not compared with cardiac imaging which made it not possible to define ECG criteria for LVH for this species (Atencia et al. 2015). A later study found a relationship between results of electrocardiography and cardiac morphology via echocardiography in 341 sanctuary chimpanzees, but ECG-generated predictive models to predict cardiac structure had low accuracy (Drane et al. 2020).

One of the limitations of ECG measurements in apes is that there are generally performed on animals under general anaesthesia. This means that the electrical activity of the heart is recorded for a few minutes only, and the physiological effects of different anaesthetic protocols need to be considered, making the clinical significance of arrhythmias detected on ECG unclear. Implantable loop recorders (ILR) have been used in chimpanzees to monitor cardiac arrhythmias and to investigate an animal with a history of collapse. The device, which is the size of a small USB stick, is implanted

subcutaneously in the back or the chest of anaesthetised animals. The device stores ECG data when it is manually activated or when a rhythm alteration (corresponding to programmed thresholds) is detected. Data need to be downloaded periodically before the memory space is filled, and this can be easily achieved in a trained conscious animal. ILRs are very promising devices for the long-term investigation of arrhythmias in great apes without the confounding factor of the anaesthesia, however, more studies are needed to link the ILRs observations with clinical signs, behaviour, and pathological findings (Lammey et al. 2011; Magden et al. 2016).

1.4.2. Imaging techniques

Cardiac ultrasound

Together with electrocardiography, echocardiography is the most frequently used diagnostic tool for cardiac health assessment in both humans and animals. It is particularly useful to detect cardiomyopathies, valvular diseases, cardiac tissue alterations and to assess the cardiac blood-flow. Reference ranges have been published for gorillas and chimpanzees (Murphy et al. 2011; Sleeper et al. 2014), and cardiac ultrasound parameters have been described for 6 healthy non-anaesthetised bonobos (Clyde et al. 2002). Guides on echocardiographic assessment of cardiac structure and function in great apes are available (Shave et al. 2014; Boyd et al. 2020). However, species-, age- and gender-specific reference ranges are not available for most species, making the interpretation of echocardiographic findings complicated. The GAHP, based at Zoo Atlanta, centralises and analyses great ape (especially gorilla) echocardiographic exams in a purpose-designed database, and has published the most comprehensive dataset for captive western lowland gorillas. They classified adult male gorillas as affected or unaffected based on different cardiac parameters, however, as stated previously, the presence or absence of cardiac disease was not confirmed by other diagnostic technique, which makes this categorisation questionable, especially considering the fact that all males gorillas older than 31 years of age fell into the affected category (Murphy et al. 2011). As for ECG and ILR, there is a need for longitudinal studies in great ape echocardiography, comparing cardiac ultrasound findings with other clinical parameters and post-mortem findings, especially for the detection of IMF when no other cardiac structural or functional disease is present.

Tissue Doppler is used in humans to assess myocardial function, and it has been proven that myocardial velocities measured via tissue Doppler reflect the degree of myocardial fibrosis (Nikitin and Cleland 2002). The practical guide for echocardiographic assessment in great apes discusses the tissue Doppler methodology but states that this technique has not been evaluated in great apes (Shave et al. 2014).

It is also worth mentioning that in humans, regional ultrasonic reflectivity, evaluated by a real-time integrated backscatter analysis, has been shown to correlate with myocardial fibrosis in patients with dilated or hypertrophic cardiomyopathy and extensive fibrosis (Picano et al. 1990; Prior et al. 2015). There are no reports on the utilisation of ultrasonic backscatter for the detection of myocardial fibrosis in apes.

Other imaging techniques

Late gadolinium enhancement (LGE) cardiac magnetic resonance imaging (MRI) has been frequently used in humans to assess myocardial scarring, as the contrast agent remains longer in fibrotic than in healthy tissue. With this method, however, only focal areas of replacement fibrosis can be detected. The novel T1 mapping technique can be used to detect diffuse interstitial myocardial fibrosis by measuring the native T1 value of the tissue and providing a direct measurement of the extracellular volume fraction (ECV) of the myocardium. Both measurements correlate well with histological fibrosis in humans (Everett et al. 2016). Another technique, ultrashort echo time (UTE), has been shown to be able to detect myocardial fibrosis without the use of any contrast agent (De Jong et al. 2011). However, there are obvious limitations to the use of MRI in great apes. Techniques are expensive, generally not available on-site and require prolonged anaesthesia that is considered risky in animals with suspected CVD.

Computed tomography (CT) and CT-angiography are used in human medicine to detect a variety of cardiac diseases such as coronary artery disease or congenital diseases and to assess left and right ventricular function as well as myocardial perfusion and viability (Thilo et al. 2010). CT is however not currently used for the detection of diffuse myocardial fibrosis in humans.

Except for an anatomical study comparing the cardiac position and innervation in orang-utans, chimpanzees, and gorillas (Kawashima and Sato 2012), no reports exist of the use of CT or MRI to assess cardiac function or structure in great apes.

1.4.3. Cardiac biomarkers

Numerous blood-based biomarkers have been proposed as diagnostic tools to evaluate cardiac health in humans and animals. In veterinary medicine, N-terminal pro-B type natriuretic peptide (NT-proBNP) and cardiac troponin I (CTnI) are widely available and commonly used for the diagnostic and clinical assessment of heart disease (Oyama 2015).

Cardiac troponins

Cardiac troponin I and T (CTnI and CTnT) are highly specific and sensitive markers of myocardial cell injury or necrosis (Oyama 2015). They have become an important asset for the diagnosis of myocardial infarction and heart failure in humans (Gaggin and Januzzi Jr 2013). Ranges for CTnI in normal dogs and cats have been published defining an upper tolerance limit of 0.07 ng/ml for dogs and 0.16 ng/ml for cats (Sleeper et al. 2001). One of the limitations of the available veterinary tests is that the limit of detection is quite high (approximately 0.2 mg/ml) and higher sensitivity assays are needed to detected mild chronic heart disease such as mitral valve disease. Another problem is that CTn can be falsely elevated in the presence of renal disease and after strenuous exercise (Shave et al. 2010), furthermore, levels differ with age (Oyama 2015). It is thought that CTnI is highly conserved across species, and assays have been used and/or validated in a few non-domestic species (Feltrer et al. 2016). In a study on cardiac biomarkers in chimpanzees, mean CTnI levels were slightly more elevated in CVD cases than in healthy controls (0.18 ng/ml versus 0.14 ng/ml), and a significant difference was found with sex; males having higher levels than females. Moreover, cardiomyopathy and valve disease, but not hypertension, were associated with elevated levels of CTnI (Ely et al. 2011b). Although the authors conclude that level of CTnI above 0.20 ng/ml appeared to be clinically relevant, the study included only a small number (28) of animals with CVD and cardiac lesions were not confirmed with post-mortem histopathology. In one case of suspected fatal arrhythmogenic right ventricular cardiomyopathy in a chimpanzee, the animal presented levels of CTnI of 0.48 ng/ml the year before his death and marked replacement myocardial fibrosis with areas of marked myocyte hypertrophy with degenerate myocytes were observed on cardiac histopathology (Tong et al. 2014).

Natriuretic peptides

Natriuretic peptides are considered the gold standard biomarkers in heart failure in humans, and they are believed to be structurally conserved across multiple species. The atrial natriuretic peptide (ANP) and the B-type natriuretic peptide (BNP) are primarily produced in the myocytes of the atria and ventricles respectively, in response to myocardial stretch due to pressure or volume overload. The induction of the BNP genes in the myocardium results in the secretion of the pro-hormone pro-BNP which is cleaved into two fragments: the biologically active and short-lived BNP (also called C-BNP) and the inert but more stable NT-proBNP. The two fragments, as well as the pro-hormone, can be detected in the circulation. In humans, a BNP cut-off value of 100 pg/ml has good sensitivity and specificity for the detection of heart failure, whereas the cut-off values for NT-proBNP are published by age group (450 pg/ml for age <50 years, 900 pg/ml for age 50-75 years, and 1800 pg/ml for age >75 years) (Gaggin and Januzzi Jr 2013). In dogs and cats, natriuretic peptide levels appear to be elevated in mitral valve diseases, dilated and hypertrophic cardiomyopathies, but also in hyperthyroidism and systemic and pulmonary hypertension (Oyama 2015). As with CTnI, renal disease can also lead to an increase in NT-proBNP levels. Serum NT-proBNP concentration > 445 pmol/L has been proposed to discriminate dogs with cardiac disease from healthy dogs (Oyama et al. 2008). Testing procedures and handling of the samples account for the relatively high variability in natriuretic peptide measurements (Oyama et al. 2013).

In the study on cardiac biomarkers in chimpanzees mentioned previously, BNP levels showed no significant difference by decade of life nor sex, but cases with CVD had an average level of 100 pg/ml versus 55 pg/ml for healthy controls, and BNP was found to be a significant predictor of CVD status. They suggest an upper value of 163 pg/ml as the upper limit for heart-healthy animals (Ely et al. 2011b), but as stated before, the cardiovascular status of the animals participating in the study was not confirmed by post-mortem data. In gorillas, the BNP levels measured in two cases and compared with echocardiography findings suggest that BNP may be an effective method for the diagnostic and monitoring of cardiac disease in this species (Hope et al. 2008). In the case of a chimpanzee with suspected fatal arrhythmogenic right ventricular cardiomyopathy, levels of BNP were 259 pg/ml the year before the death (Tong et al. 2014).

As Ely et al. highlighted, mortality and post-mortem histopathology data are necessary to confirm that circulating levels of BNP, CTnI, or any other biomarker are reliable surrogate endpoints for CVD-related mortality (Ely et al. 2011b).

Biomarkers of myocardial fibrosis

In humans, numerous circulating biomarkers have been proposed for the assessment of myocardial fibrosis, however, the validity of most of them is still highly controversial. The clinical validation of a molecule as a biomarker for myocardial fibrosis involves comparing its level with the myocardial collagen volume fraction (a relative quantification of the collagen content in the tissue on histopathology) measured on endomyocardial biopsy or post-mortem histopathology; or by comparing its level with the myocardial extracellular volume assessed by MRI (López et al. 2015). Two biomarkers have been proven to be associated with myocardial fibrosis in humans: the carboxy-terminal propeptide of procollagen type I (PICP) and the amino-terminal propeptide of procollagen type III (PIIINP). Both are formed during the conversion of the molecules of procollagen to collagen (type I and III) and released into the blood. PICP levels have been found to be highly correlated to the cardiac collagen volume fraction in patients with hypertensive heart disease and CVD, with levels changing in parallel to therapy. A ratio of 1:1 exist between the number of molecules of collagen I produced and the number of PICP molecules released into the blood. PIIINP levels are also reported to be highly correlated with collagen type III volume fraction in patients with heart failure due to ischemic heart disease or dilated cardiomyopathy. However, limitations need to be taken into account, for example, PICP levels correlate with growth velocity in children, whereas PIIINP levels increase with age and body mass index. Also worth mentioning is that these biomarkers are not cardiac-specific and their levels would be expected to raise in the case of fibrosis in other organs (Querejeta et al. 2000; López et al. 2015; Gyongyosi et al. 2017).

Other biomarkers currently under investigation include matrix metalloproteinase, TGF-β1, galectin-3, soluble ST2, micro-RNAs, etc. (Gyongyosi et al. 2017).

A pilot study explored the association of 5 biomarkers of collagen type I and III metabolism with CVD in chimpanzees. The biomarker MMP1 did not cross-react in chimpanzee sera, while TIMP1 and PINP (Procollagen carboxyl-terminal telopeptide) showed no association with CVD. ICTP (Initial carboxyl-terminal telopeptide) and

PIIINP were increased mostly in cases of CVD concurrent with renal disease (Ely et al. 2010). However, the determination of CVD status was made based on clinical evaluation and only one case had cardiomyopathy without renal disease. Further studies comparing serum levels of different biomarkers degree of IMF on histopathology are needed in great apes.

1.4.4. Histopathology

The gold-standard investigative procedure for diagnosis of myocardial fibrosis in all species is histopathological examination (Gyongyosi et al. 2017). In humans, endomyocardial biopsies can be performed but are mainly indicated for the surveillance of cardiac allograph detection, in young patients with suspected myocarditis, and in older patients with suspected infiltrative cardiomyopathy. The use of endomyocardial biopsy for the investigation of other cardiomyopathies or unexplained arrhythmias is considered only when the benefits of biopsy out-weigh the procedural risks (From et al. 2011). This procedure has never been described in great apes, probably due to its invasive nature and the unknown complication rate in these species.

In great apes, all the confirmed cases of IMF have been diagnosed via post-mortem (PM) histopathological examination. Lesions vary from mild to marked and can be diffuse (interstitial), focally extensive, multifocal or focal (replacement) fibrosis. In gorillas, various degrees of vascular changes (tunica media hypertrophy with lumen narrowing) are commonly observed. In chimpanzees, however, arterial changes are not so often detected. Myocyte necrosis and contraction bands may be observed in severely affected areas. The presence of a thickened ventricular wall together with myofibre disarray is suggestive of hypertrophic cardiomyopathy and is sometimes observed together with IMF. Degenerative changes such as increased left ventricular thickness, myofibre hypertrophy, polyploidy, and vascular stiffening should be interpreted with caution as they can be intrinsic ageing changes, although they often appear exaggerated in cases of sudden cardiac death (Lowenstine et al. 2016). Detailed cardiac post-mortem and histopathology protocols are available through the GAHP website, based on recommendations for human cardiac autopsy (GAHP Recommended Cardiac Trimming Protocol for Pathologists n.d.; Sheppard 2012). However, a need for consistency in cardiac post-mortem and histopathological

trimming is still needed in zoos across the globe. The use of different protocols together with the inter-observer variability inherent to the subjectivity of the observation makes the comparison of different cases difficult. Quantitative methods for the assessment of fibrosis are available, for example, collagen volume fraction (CVF), a computer-assisted method to determine collagen content from histologic sections stained with picrosirius red of Masson's trichrome have been developed. Immunohistochemistry with antibodies specific to different types of collagen fibres can also be performed. Although Masson's trichrome stain is commonly used to better evaluate the areas of fibrosis in great apes (Lammey et al. 2008a; Varki et al. 2009; Tong et al. 2014; Chilton et al. 2016), no cases with quantitative evaluation of myocardial fibrosis in great apes have been published.

2. Comparison of invasive and non-invasive blood pressure measurements in chimpanzees.

Obtaining accurate blood pressure readings is essential to detect hypertension that could be linked to cardiac disease in great apes, and to ensure the maintenance of physiological blood pressure during anaesthesia. At Twycross zoo, blood pressure readings are routinely recorded every five minutes during all ape anaesthetic procedures, using two different oscillometric devices (one designed for veterinary patients and one designed for humans). However, both devices were not validated for use in apes, and therefore this study was designed to compare their accuracy in anaesthetised chimpanzees during a comprehensive health-check. Although neither devices met all the requirements specified by the American College of Veterinary Internal Medicine, the small animal device demonstrated a relatively good agreement with the invasive blood pressure readings and could be used to monitor trends during anaesthesia. These results of this study have improved the accuracy of data collection for subsequent chimpanzee procedures, especially during echocardiography where estimates of heart function need to be compared with accurate blood pressure readings. The manuscript of this study, detailed below, is currently in press in Journal of Veterinary Anaesthesia and Analgesia and is titled “Evaluation of the agreement of two oscillometric blood pressure devices with invasive blood pressure in anaesthetised chimpanzees (Pan troglodytes)”.

The main co-author contributions for this manuscript were the following:

- Sophie Moittie (myself): designed the study, selected the animals, collected the data (invasive and non-invasive readings), analysed the results, wrote the manuscript and its subsequent revisions.

- Kate White: directed the study design and data collection, assisted with data analysis, reviewed the manuscript and its subsequent revisions.

- Matyas Liptovszky: participated in the study design, data collection, and manuscript revision.

2.1. Introduction

Measurement of arterial blood pressure (BP) is performed routinely in anaesthetised apes as part of anaesthetic monitoring and cardiovascular assessment. Idiopathic myocardial fibrosis is an important cause of morbidity and mortality in captive chimpanzees (*Pan troglodytes*) and it has been proposed as the major cause of sudden cardiac death commonly observed in great apes (Lammey et al. 2008b; Strong et al. 2016, 2018a, 2020). Anaesthesia related death is not rare and accurate anaesthetic monitoring is vital in these species (Strong et al. 2016). It is also paramount to relate echocardiography findings under general anaesthesia with accurate BP measurements, as the pharmacodynamic effects of anaesthetic drugs on the cardiovascular system must be considered. In chimpanzees, BP increases with age in both sexes and with obesity in females (Ely et al. 2013). Invasive blood pressure measurement (IBP) is the gold standard technique in both human and veterinary medicine; however, it is not always achievable in zoo and field settings therefore non-invasive techniques (NIBP) are more often used. BP reference intervals have been published for healthy adult chimpanzees under anaesthesia using NIBP readings (Eichberg and Shade 1987; Ely et al. 2011a). However, no studies have validated the use of NIBP equipment in great apes. In humans and animals, agreement between NIBP and IBP techniques can be poor, and accuracy depends on a variety of factors such as equipment type, calibration, animal or patient positioning, cuff size and location, and presence of hypo- or hypertension (Marks and Groch 2000; Bosiack et al. 2010; Meng et al. 2013; Yamaoka et al. 2017; Kaur et al. 2019). In human medicine, it is accepted that all devices must be validated independently, and several guidelines have been published (Prisant et al. 1995; O'Brien et al. 2010; Sharman et al. 2017). The development of a universal standard for device validation was recently announced (Stergiou et al. 2018). In veterinary medicine, a consensus statement for the identification, evaluation, and management of systemic hypertension in dogs and cats has been published by the American College of Veterinary Internal Medicine (ACVIM) and includes recommendations for validation of devices based on the Association for the Advancement of Medical Instrumentation (AAMI) guidelines (Brown et al. 2007). Agreement between different oscillometric equipment and IBP have been published in several animal species such as camelids, sheep, cheetahs, dogs, giraffes, pigs,

horses, rhesus macaques and cats (Aarnes et al. 2012; Trim et al. 2013; Sant Cassia et al. 2015; da Cunha et al. 2016; Bertelsen et al. 2017; Tuohy et al. 2017; Yamaoka et al. 2017; France et al. 2018; Kang et al. 2019; Cremer et al. 2020).

The objective of this study was to determine the agreement of two oscillometric BP devices with IBP measurements in anaesthetised healthy adult chimpanzees.

2.2. Material and methods

This study was approved by the ethics committee of The University of Nottingham (1843 160905).

2.2.1. Animals

A total of 11 adult chimpanzees, three males and eight females aged 14 to 52-year-old [mean ± standard deviation (SD) 33.4 ± 11.2 years] with body weight ranging from 52 to 69.5 kg (mean 58.8 ± 5.7 kg) were included in the study. Animals were part of a group of 13 zoo chimpanzees that were relocated to a new enclosure and required anaesthesia for transport and full health assessment. Owing to difficulties with intra-arterial catheter placement, two animals were excluded from the study. Food, but not water, was withheld for 16 to 24 hours prior to anaesthesia.

2.2.2. Induction and maintenance of anaesthesia

All chimpanzees were offered 0.49 ± 0.04 mg kg^{-1} midazolam (Hypnovel Roche, UK) orally. Anaesthesia was induced 30 minutes later with intramuscular (IM) medetomidine 0.02 ± 0.002 mg kg^{-1} (Kyron Prescriptions, RSA) and tiletamine-zolazepam 2.2 ± 0.5 mg kg^{-1} (Zoletil 100, Virbac, UK) via hand-injection, except one elderly animal that was administered tiletamine-zolazepam (3.5 mg kg^{-1}) only.

Animals were transported to the new enclosure 10 minutes after induction of anaesthesia and were weighed and positioned in dorsal recumbency on arrival. The trachea was intubated with a cuffed silicone endotracheal tube (7 to 9.5 mm internal diameter, Smith Medical, UK) and anaesthesia was maintained with isoflurane (Isoflo, Abbott Laboratories, UK) in oxygen via a circle breathing system (Cyclo-Flo, Burtons Medical Equipment Ltd, UK). A 20-gauge cannula (Jelco, Smiths Medical, UK) was placed in the right or left cephalic vein and lactated Ringer's solution (Vetivex 11,

Dechra, UK) administered (2-15 mL kg^{-1} $hour^{-1}$). The chimpanzee administered tiletamine-zolazepam was also given two intravascular (IV) ketamine (Ketamidor 100 mg/mL solution for injection, Chanelle Pharma, UK) boli (2.63 and 1.75 mg kg^{-1} 15 and 50 minutes after induction respectively).

A multiparameter veterinary monitor (Surgivet Advisor Vital Signs monitor V9203, Smiths Medical, UK) continuously monitored heart rate (HR) and rhythm, respiratory rate (f_R), haemoglobin oxygen saturation using pulse oximetry, end-tidal carbon dioxide partial pressure, and oesophageal temperature. End tidal isoflurane was also measured (Datex Ohmeda S/5, Finland). Palpebral reflex, muscular tone, HR and rhythm, f_R and pulse rate were also manually monitored. All anaesthetic variables were recorded at 5-minute intervals. Each chimpanzee underwent a comprehensive health assessment and some animals also underwent minor surgical procedures such as contraceptive implant placement or dental extractions (n = 10).

At the end of the procedure, the animals were positioned in lateral recumbency and flumazenil 0.2 mg kg^{-1} was given IV and atipamezole 0.1 ± 0.01 mg kg^{-1} IM. Oxygen was delivered (3 L $minute^{-1}$) until a swallowing reflex returned, at which point the tracheal tube was then removed. Recovery was monitored until the animals were able to walk.

2.2.3. Non-invasive blood pressure measurements

Mid upper brachium circumference was measured and a 14 cm wide two-tube cuff with 360° bladder (Technicuff, FL, USA) was placed on the right arm, with the bottom edge of the cuff positioned approximately 2 cm above the antecubital fossa. That cuff was chosen as its width was the closest to 40% of the arm circumference in all chimpanzees (Pickering et al. 2005). The cuff was connected to the veterinary multiparameter monitor (Surgivet Advisor Vital Signs monitor V9203, Smiths Medical, UK) and systolic (SAP) and diastolic (DAP) arterial pressures were recorded at 5-minute intervals.

Wrist circumference was measured and a 7.5cm wide cuff was placed immediately proximal to the left carpus (on the opposite arm to the Surgivet cuff), with the upper brachium resting on the bed and the antebrachium slightly elevated in order for the carpus to be levelled with the heart. The cuff was integrated to a battery powered

portable oscillometric BP monitor designed for use on the human wrist (Omron R1 HEM-601, OMRON Healthcare UK Ltd, UK). SAP and DAP readings were obtained and recorded at 5-minute intervals.

The HR displayed by both NIBP devices were compared to the monitored ECG and auscultation at the time of the BP readings.

2.2.4. Invasive blood pressure measurements

In 11 animals, after hair clipping and sterile skin preparation, a 20-gauge 33mm cannula (Jelco, Smiths Medical, UK) was inserted percutaneously into the right femoral artery for monitoring IBP via a saline-filled noncompliant tubing connected to a pressure transducer (BD DTX Plus; Becton Dickinson, UT, USA) and monitor (Datex Ohmeda S/5, Finland). Once the cannula was *in situ*, a square wave test at 300 mmHg flushing pressure was performed by pulling and quickly releasing the built-in fast flush tab of the transducer to generate a square wave (Kleinman et al. 1992). Dynamic response was judged adequate when observing less than two post fast flush oscillations of an amplitude less than a third of the previous waveform, presence of one distinct dicrotic notch and absence of artefacts within the waveform. Corrections to the system were made when the system appeared over or under damped (Saugel et al. 2020). The arterial cannula was flushed continuously with heparinized 0.9% saline (Heparin Sodium Flushing Solution 100 IU mL^{-1}, Wockhardt, UK) at 3 mL $hour^{-1}$ and flushed manually every 10-15 minutes (2 mL in 1 second). The pressure transducers were calibrated against a mercury manometer using a three-point calibration technique (50, 100 and 150 mmHg) and zeroed to atmospheric pressure at the level of the phlebostatic axis (corresponding to the anatomic projection of the right atrium) before the beginning of data collection (Saugel et al. 2020). Systolic and diastolic IBP readings were recorded every 5 minutes, simultaneously with the NIBP measurements, ensuring that the transducer was levelled to the phlebostatic axis at all time. A small number of cannulas were replaced during the procedure due to their displacement during repositioning of the animal.

2.2.5. Statistical analysis

Statistical analysis was performed using GraphPad Prism Version 8.1.2. (GraphPad Software Inc., CA USA) and MedCalc version 19.5.1 (MedCalc Software Ltd,

Belgium). Normality was assessed using Shapiro-Wilk test. Mean biases and limits of agreement [LOA = mean bias ± 1.96 times the standard deviation (SD)] between IBP and NIBP were calculated by the modified Bland-Altman method (bias = IBP - NIBP $_{SURGIVET}$ or NIBP $_{OMRON}$), where positive or negative biases respectively correspond to underestimation or overestimation of the BP by the oscillometric device (Bland and Altman 2007). The 95% confidence intervals (CI) of the mean bias and limits of agreements were calculated to assess the significance of the bias and to estimate the size of possible sampling error (Giavarina 2015). Linear regression of the differences was plotted on the Bland-Altman graph to detect proportional bias. Outliers were not removed. Spearman's correlations and corresponding 95% CI were calculated between NIBP and IBP measurements, and between the differences in measurements and the ratios cuff width/wrist circumferences and cuff width/arm circumferences. Percentages of oscillometric readings within 10 and 20 mmHg of the reference method were calculated.

2.2.6. Validation criteria

The recommendations for validation of BP measurement devices published by the ACVIM (Brown et al. 2007) were used to assess the two NIBP devices for SAP and DAP measurements in chimpanzees. Devices can be validated if the mean difference of paired measurements for SAP and DAP treated separately is ≤ 10 mm Hg with a standard deviation of ≤ 15 mm Hg; the correlation between paired measures for SAP and DAP treated separately is > 0.9 across the range of measured values of BP; 50% of all measurements for SAP and DAP treated separately lie within 10 mmHg of the reference method; 80% of all measurements for SAP and DAP treated separately lie within 20 mm Hg of the reference method.

2.3. Results

A total of 87 paired measurements were obtained for the $NIBP_{SURGIVET}$ and IBP and 84 paired measurements for $NIBP_{OMRON}$ and IBP, in a total of eleven chimpanzees. Between 3 and 16 paired measurements were obtained for each chimpanzee. The SAP_{IBP} values ranged from 61 mmHg to 202 mmHg and from 30 mmHg to 162 mmHg

for DAP_{IBP}. BP variations occurred naturally during the anaesthetic although fluid therapy rate was increased in animals showing a mean IBP lower than 60 mmHg.

Mid upper arm circumference was measured in 10 chimpanzees and ranged from 30.5 to 36 cm (32.85 ± 1.67 cm) (mean ± SD), which resulted in a cuff width-to-arm circumference ratio between 38.9 and 45.9 %. Wrist circumference was measured in 7 chimpanzees and ranged from 18 to 20.5cm (19.43 ± 0.79 cm), (mean ± SD), which represented a cuff-to wrist ratio between 36.6 and 41.7 %.

The differences between the NIBP readings and the corresponding IBP readings were normally distributed for $DAP_{SURGIVET}$ and SAP_{OMRON}, but not for $SAP_{SURGIVET}$ and DAP_{OMRON}. The ratios cuff width/arm circumferences and cuff width/wrist circumferences were not normally distributed.

Table 2.1. Bias, standard deviation (SD), limits of agreements (LOA), and correlation coefficient with respective 95% confidence intervals (CI) for systolic (SAP) and diastolic (DAP) blood pressures (mmHg) measured by two oscillometric devices (the Surgivet Advisor and the Omron R1) compared with invasive blood pressure in anaesthetised chimpanzees.

Variable	Bias (mmHg)	95% CI	SD (mmHg)	Lower LOA (mmHg)	95% CI	Higher LOA (mmHg)	95% CI	Spearman's r correlation	95% CI
$SAP_{SURGIVET}$	8.55	4.72 to 12.38	18.19	-27.11	-33.68 to -20.53	44.21	37.63 to 50.78	0.86	0.79 to 0.91
$DAP_{SURGIVET}$	8.4	6.32 to 10.49	9.91	-11.02	-14.59 to -7.44	27.82	24.24 to 31.41	0.85	0.78 to 0.90
SAP_{OMRON}	-21.12	-26.53 to -15.71	24.93	-69.99	-79.27 to -60.71	27.75	18.47 to 37.04	0.64	0.49 to 0.75
DAP_{OMRON}	-17.81	-21.05 to -14.57	14.95	-47.11	-52.68 to -41.55	11.49	5.93 to 17.06	0.72	0.59 to 0.81

Bland-Altman and correlation results for the Surgivet are shown in table 2.1. Results showed significant positive bias: the Surgivet tended to underestimated SAP and DAP. On the Bland-Altman plot, linear regression line slope was significantly different from zero for SAP (slope = 0.33, X-intercept = 82.26, $p < 0.0001$) indicating a significant proportional bias: SAP tended to be overestimated at low BP values (when SAP < 82.26 mmHg as represented by the X-intercept of the regression line) and underestimated above this value, with the underestimation increasing as BP increased. No proportional bias was detected for DAP (slope = 0.08, X-intercept = -47.82, $p = 0.11$). Figure 2.1. Correlations between Surgivet and IBP values were significant for both SAP and DAP, with both $p < 0.000\ 1$.

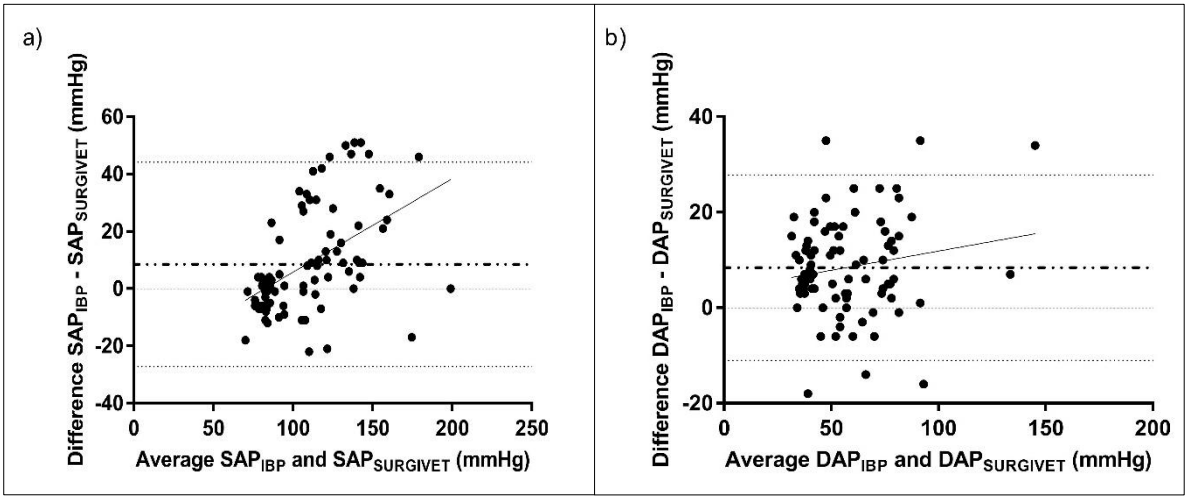

Figure 2.1. Bland-Altman plots with multiple measurements per subject for assessment of the agreement between systolic (a) and diastolic (b) blood pressure recorded by the Surgivet Advisor ($SAP_{SURGIVET}$ and $DAP_{SURGIVET}$) and invasive blood pressure (SAP_{IBP} and DAP_{IBP}) in 11 isoflurane anaesthetised chimpanzees. Dot-dash line: mean bias. Dotted lines: limit of agreements. Solid line: regression line. Horizontal dashed line: zero line.

The percentages of the Surgivet measurements that lay within 10 mmHg of the IBP values were 62.07% for SAP and 59.77% for DAP. Percentages of the Surgivet measurements that laid within 20 mmHg of the IBP values were 74.71% for SAP and 93.10% for DAP.

The correlation between the cuff width/arm circumference ratio and the differences between SAP_{IBP} and $SAP_{SURGIVET}$ was significant (r_S=0.42; $p < 0.0001$), with SAP tending to be overestimated when the ratio was lower than 41.20% (larger arms) and underestimated when the ratio was higher than 41.20% (smaller arms); 41.20 representing the X-intercept of the regression line. The correlation between the cuff to

arm circumference ratio and the differences between DAP_{IBP} and $DAP_{SURGIVET}$ was not significant (r_s=-0.21; p=0.06). Figure 2.2.

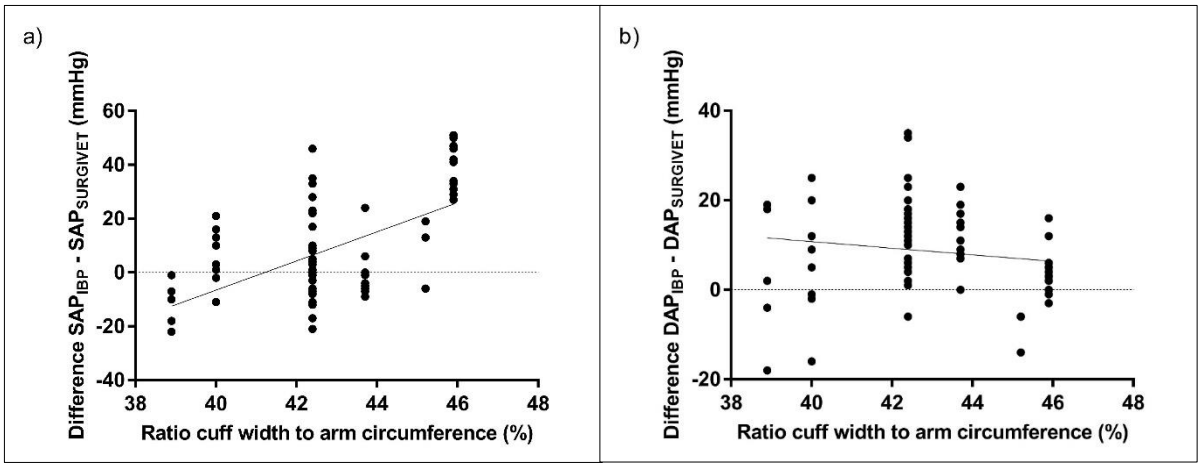

Figure 2.2. Correlation between the cuff width to brachium circumference ratio and the differences between the invasive (IBP) and non-invasive (NIBP) measurements for systolic (a) and diastolic (b) blood pressure by the Surgivet Advisor in 11 isoflurane anaesthetised chimpanzees. Solid line: regression line. Horizontal dashed line: zero line.

Bland-Altman and correlation results for the Omron are shown in Table 2.1. Results showed significant negative bias: the Omron tended to overestimate SAP and DAP. On the Bland-Altman plot (Fig 3), linear regression line slope was not significantly different from zero for SAP (*p*=-0.02) but was significantly different from zero for DAP (slope=-0.26, X-intercept=-2.1, *p*=0.003), indicating a proportional bias for DAP only: the magnitude of the DAP overestimation by the Omron increased at higher diastolic BP. Figure 2.3. Correlations between the Omron and IBP values were significant for both SAP and DAP, with both $p < 0.0001$.

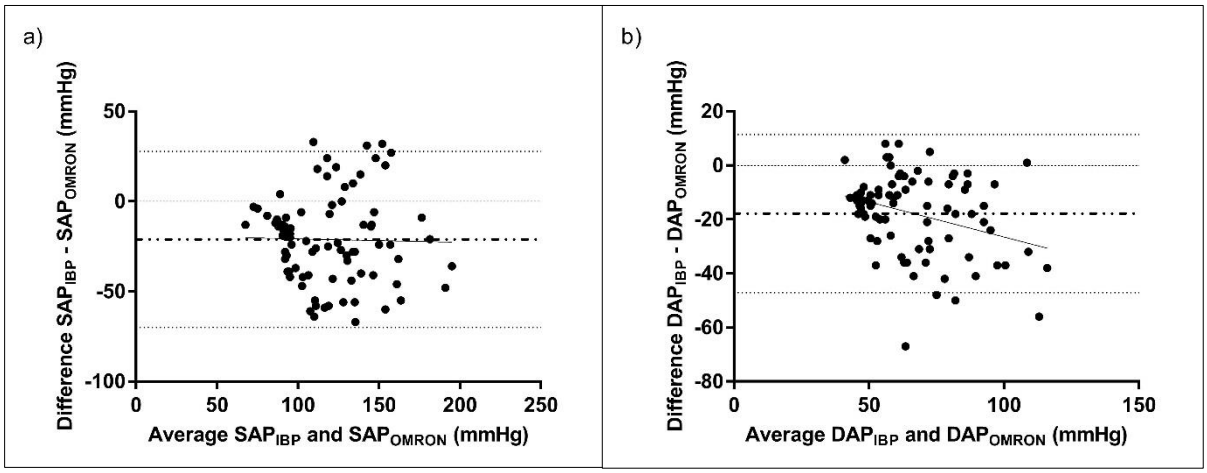

Figure 2.3. Bland-Altman plots with multiple measurements per subject for assessment of the agreement between systolic (a) and diastolic (b) blood pressure recorded by the Omron R1 (SAP_{OMRON} and DAP_{OMRON}) and invasive blood pressure (SAP_{IBP} and DAP_{IBP}) in 11 isoflurane anaesthetised chimpanzees. Dot-dash line: mean bias. Dotted lines: limit of agreements. Solid line: regression line. Horizontal dashed line: zero line.

The percentage of the Omron measurements that were within 10 mmHg of the IBP values were: 16.67% for SAP and 30.95% for DAP. The percentages of the Omron measurements that were within 20 mmHg of the IBP values were: 40.48% for SAP and 64.29% for DAP.

The correlation between the cuff width/wrist circumference ratio and the differences between SAP_{IBP} and SAP_{OMRON} was significant (r_s=0.63; $p < 0.0001$), with SAP tending to be overestimated when the ratio was lower than 40.51% (larger carpi) and underestimated when the ratio was higher than 40.51% (smaller carpi); 40.51 representing the X-intercept of the regression line. Correlation between the cuff width/wrist circumference ratio and the differences between DAP_{IBP} and Omron DAP_{OMRON} was also significant (r_s=0.28; p = 0.035), with DAP tending to be overestimated in all chimps (regression line slope not significantly different from 0). Fig 2.4.

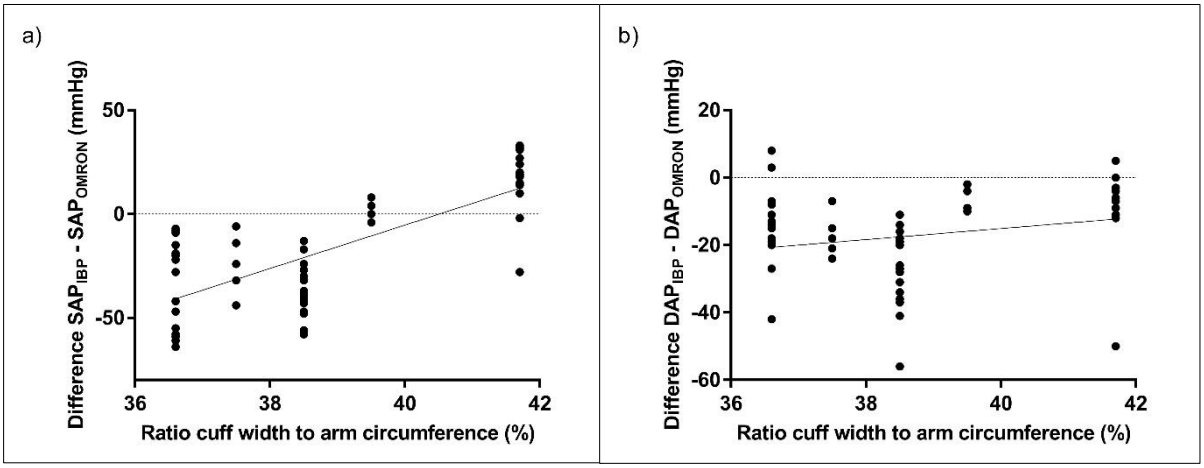

Figure 2.4. Correlation between the cuff width to carpus circumference ratio and the differences between the invasive (IBP) and non-invasive (NIBP) measurements for systolic (a) and diastolic (b) blood pressure by the Omron R1 in 11 isoflurane anaesthetised chimpanzees. Solid line: regression line. Horizontal dashed line: zero line.

2.4. Discussion

In this study, the Surgivet instrument displayed a better agreement with the IBP than the Omron device. However, neither of them fulfilled all the criteria recommended by the ACVIM. For the Surgivet, the mean difference of paired measurements for SAP and DAP treated separately were 10 mm Hg or less, standard deviation was 15 mm Hg or less for DAP but not for SAP; the correlation between paired measures for systolic and diastolic pressures were not superior to 0.9; and finally, although more

than 50% of all measurements for SAP and DAP were within 10 mm Hg of the reference method, only for the DAP did more than 80% of measurements lie within 20 mm Hg of the reference method. The Omron device did not meet any of the criteria except that more than 50% of the measurements for DAP_{OMRON} were within 20 mmHg of the DAP_{IBP} measurements.

Direct intra-arterial BP measurement is considered the most accurate technique especially during haemodynamic instability and allows continuous beat-to-beat monitoring and the calculation of other parameters such as cardiac output and vascular resistance via arterial waveform analysis (Esper and Pinsky 2014). However, IBP measurements can also present inaccuracies due to mispositioning of the transducer, over or underdamping (resonance artifact), calibration errors, or movement artifacts (Romagnoli et al. 2014). The use of the femoral artery to measure IBP in these chimpanzees was chosen rather than more peripheral sites to reduce IBP inaccuracy and variability, as distal sites result in arterial tree pressure amplification and an increase in SAP and decrease in DAP compared to central measurements (Esper and Pinsky 2014). Heart rate auscultation and digital palpation of pulse were performed concomitantly to IBP measurements to ensure that device was measuring oscillations correctly (Grosenbaugh and Muir 1998). Although the damping coefficient and system frequency were not measured, the fast-flush tests were performed to assess the dynamic response of the equipment and detect artefacts such as excessive resonance, summation of reflected waves or occlusion (Kleinman et al. 1992). An overdamped system would have resulted in a systematic overestimation of DAP and underestimation of SAP, and conversely an under damped system would have underestimated DAP and overestimated SAP. Although neither scenarios explain the differences seen between the IBP and the Omron or Surgivet, it is possible albeit unlikely that inadequate damping contributed to the observed differences. Future studies could incorporate the calculation of the damping coefficient and the natural frequency of the BP waveform.

The Surgivet Advisor (V9200 series) is a multiparameter monitor commonly used in veterinary practices. It was judged clinically acceptable in anaesthetised horses for SAP, MAP and DAP although correlation results did not fit the recommendations; in hypotensive greyhounds it showed good agreement for DAP and MAP but not for SAP; in sheep it was acceptable by ACVIM standards for MAP measurements only, and in

pigs it showed consistent underestimation of DAP, SAP and MAP (but especially for SAP) thus was judged of limited clinical usefulness (Drynan and Raisis 2013; Trim et al. 2013; Drynan et al. 2016; Tuohy et al. 2017). In our study, the Surgivet showed acceptable bias for all measurements and relatively good correlation but SD and LOA were wide, especially for SAP. The bias, 95% CI and LOA values showed that the Surgivet tends to underestimate both parameters and especially SAP. Interestingly, the magnitude of the underestimation of SAP by the Surgivet increases at higher BP but an overestimation of SAP tends to happen at very low BP (when SAP is less than 82 mmHg as under this value the predicted differences IBP-NIBP are negative) (Ho 2018). This happening has also been observed in oscillometric BP measurements in humans and may be due to several factors such as oscillometric device algorithm-related error in calculating SAP at high and low pressures and with varying pulse pressures, or to the abolishment of peripheral BP amplification due to hyperaemia in the arm (Gourdeau et al. 1986; Pannarale et al. 1993; Wax et al. 2011; Babbs 2012; Liu et al. 2013; Kuck and Baker 2017). It may also reflect an attenuation of the IBP signal due to disturbance to laminar flow at low BP, a phenomenon that is exaggerated in response to vasodilation due to anaesthetic agents (Ercole 2006).

Automatic wrist BP devices are practical and inexpensive, they are however known to have limited accuracy compared to other BP devices and are generally not recommended for NIBP monitoring in humans, except for obese patients (Parati et al. 2013; Mostafa et al. 2020; Picone et al. 2020). The lack of accuracy is believed to be caused by the distal site of the cuff, the impact of the body and wrist position (level, flexion and orientation), and the fact that two arteries contribute to the signal (Kikuya et al. 2002; Mourad et al. 2005; Parati et al. 2013; Kuwabara et al. 2019). In one study, although the Omron R1 bias was small compared with auscultation, the SD was large, thus the device failed to reach the AAMI standards and was deemed inadequate for clinical or practical use (Kikuya et al. 2002). In another study, the Omron R1 was found to underestimate both SAP and DAP in children and adolescents, especially in those with a wrist smaller than 13.5cm (Bald et al. 1996). We elected to assess the Omron R1 accuracy here as a small, easy to use and battery powered device present clear benefits for field clinical work. However, it presented poor agreement with the IBP, with large SD and LOA for both SAP and DAP, and a significant overestimation of SAP and DAP. The magnitude of the differences seemed to increase for DAP at higher

blood pressures, but not for SAP. This observed proportional bias, similarly to the proportional bias found for $SAP_{SURGIVET}$, may be due to a combination of factors affecting the accuracy of the oscillometric algorithm when changes in arterial compliance or arterial pulse occur in chimpanzees (Kuck and Baker 2017). Although the correlation between the Omron and the IBP measurements was significant, the correlation coefficients were relatively low.

A well-known factor in the accuracy of NIBP measurements is the size of the cuff related to the size of the limb where it is placed, with too small cuff resulting in over-estimation and too large cuff resulting in underestimation (Marks and Groch 2000; Parati et al. 2013). In this study, the magnitude of the error for NIBP measurements were significantly correlated with the ratio cuff size/limb circumference except for the $DAP_{SURGIVET}$, but correlation coefficients were low. The calculated optimal ratio for the arm cuff was 41.20% which represent a 33.9 cm arm circumference, meaning that for arms smaller than that, the magnitude of the underestimation was greater. Conversely, the magnitude of the Omron SAP overestimation decreased with smaller wrist, and the calculated optimal ratio was 40.51% (18.5 cm wrist circumference), meaning that for wrists larger than that (which was the case for most of our chimpanzees), the magnitude of the overestimation was greater. Although the Omron R1 is designed for human wrists of between 13.5 cm and 19.5 cm, results of our study indicate that the Omron cuff was likely too small for most of our chimpanzees.

Limitations of our study include the relatively small numbers of animal used, although more than eight animals were used in accordance with the ACVIM guidelines. Chimpanzees are routinely anaesthetised in zoo settings only for regular health-checks (generally every two to three years) or for enclosure moves, and due to health and safety concerns for both chimpanzees and staff, procedures are kept as short as possible. In our study, the length of the anaesthesia varied for each animal, and some chimpanzees had significantly higher numbers of readings than others. The BP range, however, was wide with recorded SAP and DAP values from well under to well above the median normotension values reported for adult healthy chimpanzees (Ely et al. 2011a). It is important to stress that our results evaluate the accuracy of two specific NIBP monitors, and that the accuracy of these monitors could vary with changes of algorithm by the manufacturer. Moreover, it has been shown that different monitors respond differently to artefacts and that successive determinations by the same

monitor varied when presented with the same oscillometric waveform (Amoore et al. 1997). These intra-monitor variations have not been evaluated in our study. Another limitation of our study is that the recordings of MAP were not included in our research design, partly because the ACVIM recommendations for device validation do not include the assessment of MAP, and because the Omron does not show the MAP. Nevertheless, the study of the agreement between $MAP_{SURGIVET}$ and MAP_{IBP} could have been a useful addition to assess the clinical usefulness of the Surgivet, as MAP is often used to diagnose hypotension and guide its treatment during anaesthesia.

Finally, it is worth pointing out the relative uniform body size of the chimpanzees studied, as all were adults with no juvenile represented. This may be of importance as the ratio cuff width/limb size seemed to have a significant impact on the accuracy of some of the measurements; future studies may be warranted to assess if the Omron presents better accuracy in smaller apes, and if the use of a smaller cuff may reduce the underestimation of the Surgivet in small chimpanzees.

The ACVIM recommendations are derived from the AAMI standards and designed to validate devices for the detection and monitoring of hypertension in conscious dogs and cats (Brown et al. 2007). Although these guidelines may be applicable to other species, it is advisable to recognise the limitations of such standards (for example, devices with wide LOA may still conform to the ACVIM standards) and use other evidence together with clinical judgement when planning and managing interventions (Yamaoka et al. 2017).

Conclusions

Although the Surgivet device did not meet all the criteria recommended by the ACVIM for validation, it presented a better agreement with invasive blood pressure values that the Omron. The Omron human wrist portable device presented poor accuracy and its use in adult chimpanzees should be avoided.

3. Implantable loop recorders as a diagnostic tool to detect arrhythmias in chimpanzees.

3.1. Introduction

Antemortem diagnostic of heart disease is challenging, and sudden death, without prior clinical signs, is a common occurrence in apes. Sudden death is believed to be due to fatal arrhythmias (Lammey et al. 2008b), often secondary to idiopathic myocardial fibrosis (IMF) found at post mortem. The assessment of cardiovascular health in zoo-housed great apes commonly include clinical examination, blood-pressure measurement, cardiac ultrasonography, cardiac biomarkers determination in serum and 12-lead electrocardiography (Shave et al. 2014; Boyd et al. 2020). However, the sensitivity and specificity of these tests to detect cardiac disease and especially IMF in chimpanzee is as yet unclear (Ely et al. 2011b), partly due to the lack of longitudinal studies including ante-mortem clinical data and cardiac histology. Moreover, due to the size and strength of chimpanzees, cardiac assessments are usually performed under general anaesthesia, complicating clinical interpretation as the effects of the anaesthetic drugs on the cardiovascular system need to be taken into account when interpreting results from echocardiography, electrocardiography or blood pressure measurements (Napier et al. 2013; Strong et al. 2018b). Although echocardiography is a crucial tool to assess cardiac function and structure in chimpanzees (Drane et al. 2019), IMF often occur without any significant echocardiographic changes, and in humans more advanced imaging methods such as cardiac-MRI and integrated ultrasonic backscatter are needed to detect myocardial fibrosis (Picano et al. 1990; Maceira et al. 2002; Kosmala et al. 2012). Electrocardiography allows for the detection of cardiac arrhythmias in chimpanzees and reference ranges have been published (Doane et al. 2006; Atencia et al. 2015). Ventricular premature complexes have been reported to be the most common arrhythmia and may be linked to IMF and sudden death in this species (Doane et al. 2006; Lammey et al. 2008b). In humans, cardiac fibrosis is known to cause altered cardiac conduction such as blocks, atrial and ventricular fibrillation, and ventricular tachycardia (Karagueuzian et al. 2013; Morita et al. 2014).

Implantable loop recorders (ILR) can be used in chimpanzees to monitor cardiac arrhythmias detected on short-term electrocardiograms (ECG), and to investigate animals with clinical signs compatible with cardiac disease (Lammey et al. 2011), while fully conscious and thus without the confounding influence of anaesthetics. The device stores single-lead ECG data when a rate-triggered limit is reached such as with an arrhythmia. It is implanted subcutaneously in anaesthetised animals, and data needs to be downloaded periodically. Although two reports on the use of ILRs to detect and monitor arrhythmias in chimpanzees have been published, a limited amount of ILR data were retrieved for each animal and no histological diagnostics were available (Lammey et al. 2011; Magden et al. 2016).

The objective of this study was to assess the value of ILRs as a screening and diagnostic tool in chimpanzees considered at risk of developing cardiac disease, by comparing the ILR data obtained with available clinical and post-mortem data.

3.2. Animals, Material and Methods

3.2.1. Animals

Three chimpanzees, named here C1, C2 and C3 were recruited to the study. Chimpanzees that were considered at risk for heart disease were chosen for ILR implantation considering available clinical, demographic, and/or behavioural data. Chimpanzees' attitude towards training was also taken into consideration, ensuring that the selected animals would readily present their chest to the keepers for ILR data downloads. Details on each individual and reasons for selection are summarised in table 3.1.

Table 3.1. Rationale for chimpanzee selection

Individual	Sex	Age (at implantation)	Previous cardiac findings	Behavioural data	Reasons for selection	Date of ILR implantation
C1	Female	39	Reduced systolic cardiac function with low ejection fraction & reduced systolic tissue velocities, LV dilated. ECG abnormal	Calm individual	Previous cardiac findings, easy to train	January 2015 April 2018
C2	Male	20	Not assessed previously	Agitated individual with abrupt changes of mood, socially inept (hand-raised)	Gender, behaviour, easy to train	September 2016
C3	Male	32	No abnormalities detected in 2012	Anxious individual, difficult social position within group	Age, gender, social status, easy to train	April 2018

3.2.2. Anaesthetic protocol

Animals were anaesthetised in order to perform vasectomy (C2) or to move to a new enclosure (C1 and C3). Food, but not water was withheld 15 to 24 hours before the procedure. Animals were premedicated with 0.5mg kg^{-1} midazolam (Hypnovel Roche, UK) orally and aesthesia was induced with 2 mg kg^{-1} tiletamine-zolazepam (Zoletil 100, Virbac, UK) and 0.02mg kg^{-1} medetomidine (Kyron Prescriptions, RSA) intramuscularly. Once the animals had achieved a light plane of anaesthesia, the trachea was intubated with a cuffed silicone endotracheal tube (7 to 9.5 mm internal diameter, Smith Medical, UK) and anaesthesia was maintained with isoflurane (Isoflo, Abbott Laboratories, UK) in oxygen (3 litre min^{-1}) via a circle breathing system (Cyclo-Flo, Burtons Medical Equipment Ltd, UK). A cannula was placed in the left or right cephalic vein and Hartmann's solution (Vetivex 11, Dechra, UK) was administered during the procedure, at a standard rate of 10ml/kg/h and increased in case of low blood pressure readings. Heart rate, respiratory rate, end-tidal carbon dioxide, oxygen saturation, rectal temperature and oscillometric blood pressure were measured throughout via a multiparameter monitor (Surgivet Advisor Vital Signs monitor V9203, Smiths Medical, UK), and recorded at five-minute intervals.

At the end of the procedure, atipamezole (Atipam 5.0 mg/ml, Dechra, UK) was administered intramuscularly at five time the medetomidine dose. C3 also received 0.2mg of flumazenil IV before removal of the intravenous cannula. The animals were placed in lateral recumbency with 3 litre min^{-1} oxygen until extubation.

3.2.3. Cardiac biomarkers

Up to 50 ml of blood was taken from each animal's femoral vein for routine health-checks, following standard operating procedures in great ape. Whole blood samples were allowed to clot at room temperature for 2 hours and centrifuged for serum separation. Serum aliquots were sent to an external laboratory for cardiac biomarkers measurements. Troponin I and NT-ProBNP concentrations were measured using chemiluminescent microparticle immunoassays: the Architect High-Sensitivity Troponin I assay and the Alere Abbott NT ProBNP assay, both on the Architect iSR2000-system (Abott, Maidenhead, UK).

3.2.4. Echocardiographic examination

A complete cardiac ultrasound (GE Vivid i) was performed following guidelines developed by the European Ape Heart project (Strong et al. 2015), which were based upon the British Society of Echocardiography Minimum Dataset for humans (Wharton et al. 2015). See appendix 1 for details on ecochardiographic examination.

3.2.5. 12-lead ECGs

A 12-lead ECG was performed in each animal during anaesthesia, with limb and chest electrodes placed according to described human and chimpanzee protocols (Kligfield et al. 2007; Atencia et al. 2015), using a MAC 1200 ECG machine (Marquette Hellige GmbH, Freiburg, Germany). C1 underwent four ECGs (in January 2015, January 2017, April 2018 and July 2019). C2 underwent on ECG in September 2016, and C3 underwent one ECG in April 2018.

3.2.6. ILR implantation and downloads

The ILR system used in this study consisted of the programmer (CareLink programmer with FullView software Model SW026, Medtronic, UK), the ILR itself (Reveal LINQ Model LNQ11 Insertable Cardiac Monitor, Medtronic, UK), and the Patient Monitor (MyCareLink Patient Monitor Model 24950, Medtronic, UK). The three ILRs used in this study were second-hand devices donated to the Ape Heart Project by human hospitals and re-sterilised using ethylene oxide before implantation in the chimpanzees. The specific model used (Reveal Linq LNQ11) is among the smallest

insertable cardiac monitors available, with dimensions of 44.8 x 7.2 x 4 mm and 2.5g of weight. Their projected longevity is up to 3 years, although this was reduced in these cases due prior usage before implantation.

Shortly before implantation (while ILR still in its sterile package) the patient details and arrhythmia detection parameters were programmed into the specific ILR with the Carelink Programmer. The devices were programmed to detect episodes of bradycardia, tachycardia and pauses, but not atrial fibrillation. Specific parameters set up for each device are detailed in table 3.2. The first device used for C1 was reprogrammed 21 months after implantation because of frequent false bradycardia detection: the automatic detection of bradycardic events was turned off and tachycardia detection was reduced from 170 to 158 beats/min (380ms) for a minimum of 12 beats. These parameters were later used for C2. The C3 device was reprogrammed in September 2018 to increase the number of tachycardic events detected.

Table 3.2. Parameters of arrhythmia detection set up for each ILR device.

Individual	Arrhytmia detection	Duration	Rate (Interval)	Sensitivity	Blanking	Comments
C1	Tachycardia	16 beats	171 bpm (350ms)	35 µV	150 ms	Until Sept 2016
	Tachycardia	12 beats	158 bpm (380ms)	35 µV	150 ms	From Sept 2016
	Bradycardia	4 beats	30 bpm (2000ms)	35 µV	150 ms	Turned off in Sept 2016
	Pause	4,5 seconds		35 µV	150 ms	
C2	Tachycardia	12 beats	158 bpm (380ms)	35 µV	150 ms	
	Pause	3 seconds		35 µV	150 ms	
C3	Tachycardia	16 beats	167 bpm (360ms)	35 µV	150 ms	Until Sept 2018
	Tachycardia	12 beats	154 bpm (390ms)	35 µV	150 ms	From Sept 2018
	Pause	3 seconds		35 µV	150 ms	
	Bradycardia	4 beats	30 bpm (2000ms)	35 µV	150 ms	

Surface mapping was carried out with the anaesthetised chimpanzee in both dorsal recumbency and sitting position to identify the location of the chest with the highest and most stable R-wave, using the CareLink programmer. For all 3 animals, the optimal insertion location was immediately to the left of the sternum near the fourth intercostal space. This area was surgically prepared with diluted chlorhexidine gluconate (Hibiscrub, Molnlycke Health Care Ltd, Dunstable, UK) and 3 ml of lidocaine (Lignol 2.0% w/v Solution for Injection, Dechra Veterinary Products, UK) was infiltrated intradermally and subcutaneously. A 1cm long incision was made through the skin and a 4 cm-long subcutaneous tunnel was created (figure 3.1). The ILR device was then inserted under the skin in the deeper part of the tunnel using artery forceps, with the electrodes facing towards the heart. A single suture was placed to close the subcutaneous pocket and the skin was closed with 3 simple intradermal sutures (Vycril 4/0, Ethicon Inc, Livingston, UK). Figure 3.2. An initial device interrogation was performed to ensure that the device was fully functioning.

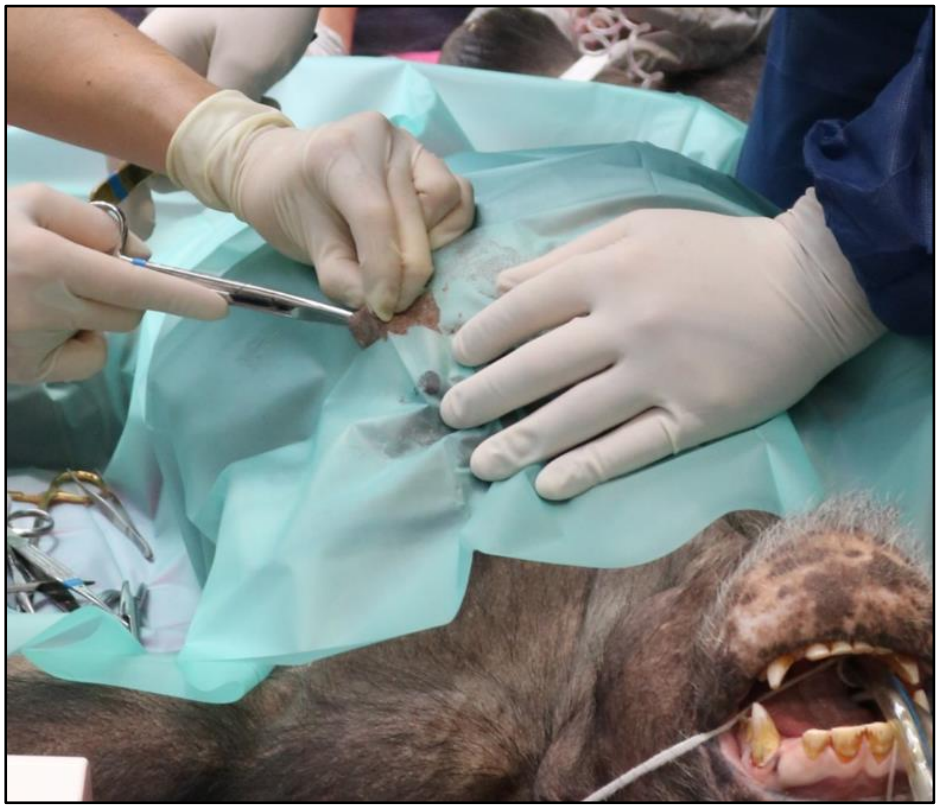

Figure 3.1. Subcutaneous tunnelling for ILR implantation.

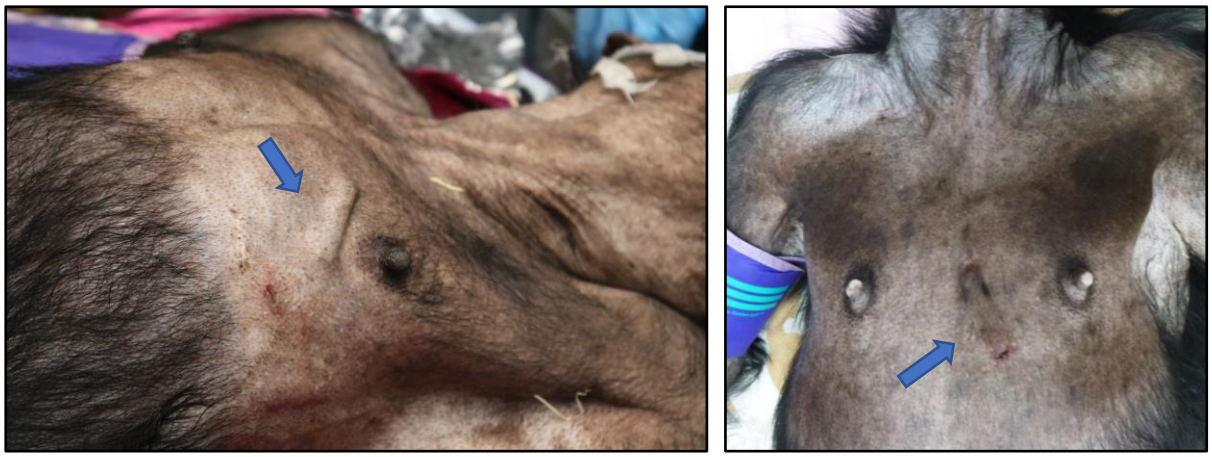

Figure 3.2. Positioning of the ILR (arrows) in C1 and C2.

In one animal (C1) that was implanted with an ILR device twice, the second ILR device was implanted after extracting the old device, in the same location.

All animals were administered meloxicam (Metacam 20 mg/ml solution for injection for cattle, pigs and horses, Boehringer Ingelheim, UK) at a dose of 0.2mg/kg orally until the surgical site had healed completely.

3.2.7. ILR interrogation

All three animals were trained using positive reinforcement techniques for chest presentation through the enclosure mesh in order to interrogate the ILR device when needed. Interrogations were performed by zookeepers with a variable frequency depending on keeper availability and number of episodes recorded in previous interrogations, with an aim of one interrogation weekly. See figure 3.3.

Figure 3.3. Left: C3 performing chest presentation via operant conditioning for device interrogation. Right: patient monitor used for ILR interrogations

3.2.8. ILR data analysis

After each device interrogation, ILR recordings were accessed via the Medtronic website. Full reports with details of all episodes recorded by the ILR device between two interrogations could be accessed for all devices implanted. Each report starts with a summary of recorded episodes, current ECG during download, and a "cardiac compass" showing average ventricular rate, patient activity and heart rate variability during the last 90 days (see Figure 3.4). Consequently, the ECG trace of each recorded episode (tachycardia, bradycardia or pause) together with time of detection and details on parameters settings are shown (Figure 5). Each recorded episode was examined and abnormalities such as ventricular premature complexes (VPCs) were circled; episodes were then reviewed by a veterinary cardiologist.

3.2.9. Heart histopathology

Two of the three studied chimpanzees (C1 and C2) died respectively 29 and 13 months after their ILR had ceased functioning and underwent complete post-mortem examination, including detailed cardiac histopathological examination following the Ape Heart Project exhaustive protocol detailed elsewhere (Strong et al. 2018c, 2020).

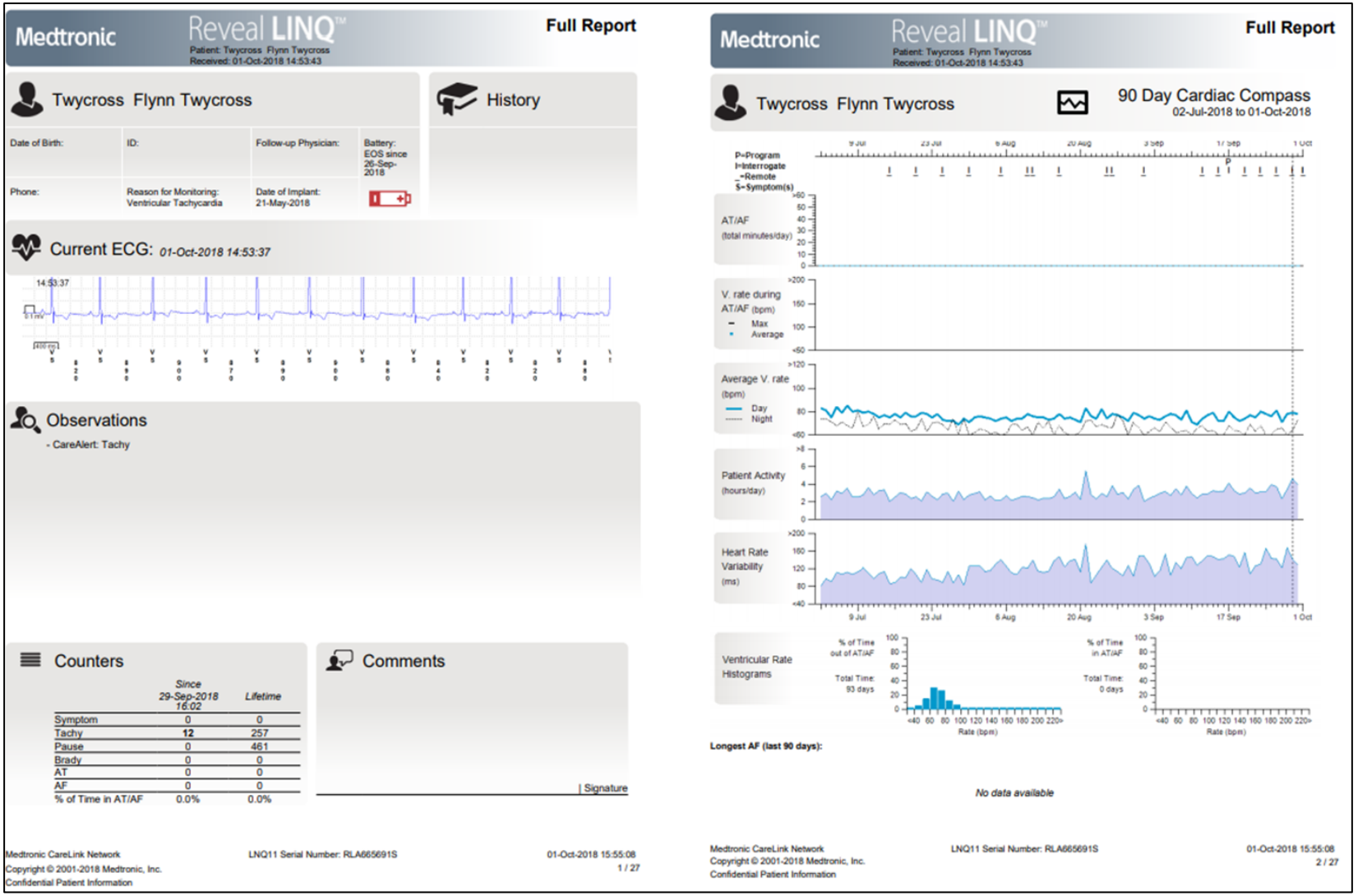

Figure 3.4. First page of ILR interrogation report with current ECG during interrogation, episode summary and 90-day compass.

3.3. Results

3.3.1. ILR findings

Two implants (C1 first implant and C3 implant) were very well accepted and were functional for 34 months for C1 and for 10 months for C3 (until the battery expired). C1's second implant and the C2 implant were removed by the chimpanzees 25 and 18 days after implantation, respectively. In both cases, surgical wounds appeared totally healed and the non-steroidal anti-inflammatory had been discontinued 11 days (C1) and 14 days before (C2).

The total number of usable interrogations were 86 for C1, 4 for C2 and 61 for C3. Although C1 was implanted in January 2015, most interrogations were performed from September 2015 until end of October 2017 when the first device ran out of battery. The number of detected tachycardic or bradycardic events with recorded ECG traces are represented in table 3.3. Although most of the detected episodes had a corresponding ECG trace, in some cases when the maximum of episodes that could be stored on the device was reached, detected episodes lacked an ECG trace. Some episodes for C2 and for C1 before reprogramming of the ILR were also falsely detected as bradycardia or pause due to small QRS complexes.

Table 3.3. Details on active ILR device period and numbers of interrogations and episodes for each chimpanzee.

Individual	Period of active ILR device	Number of ILR interrogations	Number of recorded episodes with ECG trace	Reason for end of active ILR
C1	08 January 2015- 29 October 2017	86	1797	End of battery life
	12 April 2018- 07 May 2018	0	0	Removed by chimp
C2	20 September 2016- 08 October 2016	4	49	Removed by chimp
C3	9 May 2018- 17 February 2019	61	501	End of battery life

For both C1 and C3 a fourteen-month cardiac compass representing trends in the frequency of arrythmias, physical activity and heart rates were available (see figure 3.5 and 3.6).

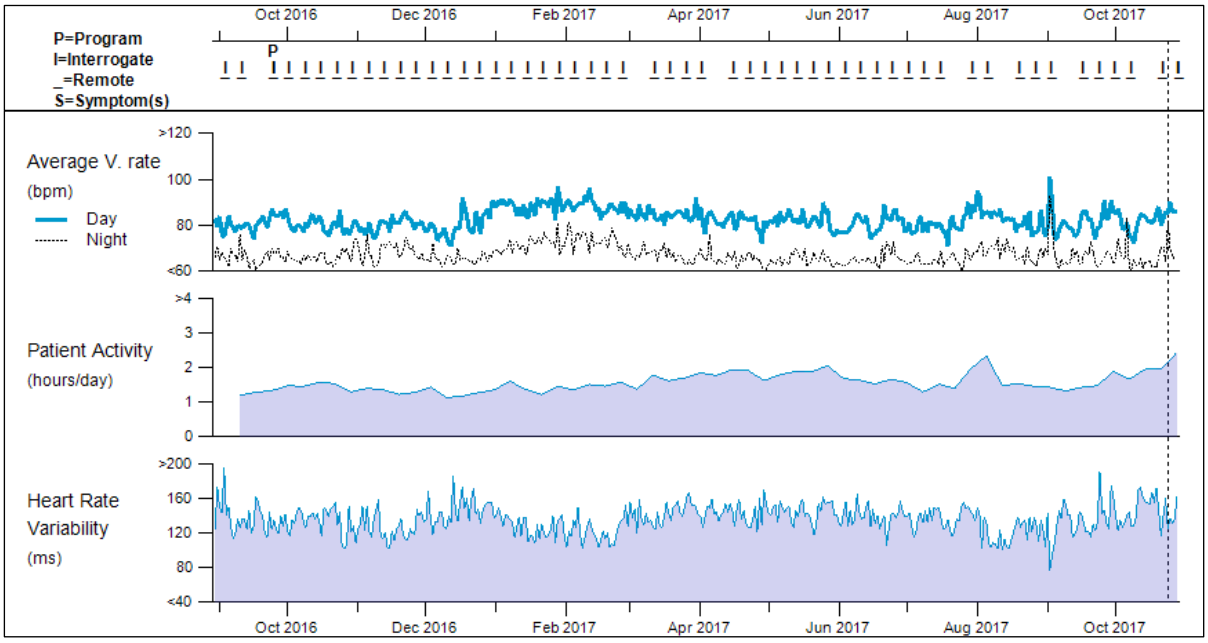

Figure 3.5. 14-month cardiac compass for C1 (from 30 August 2016 to 29 October 2017).

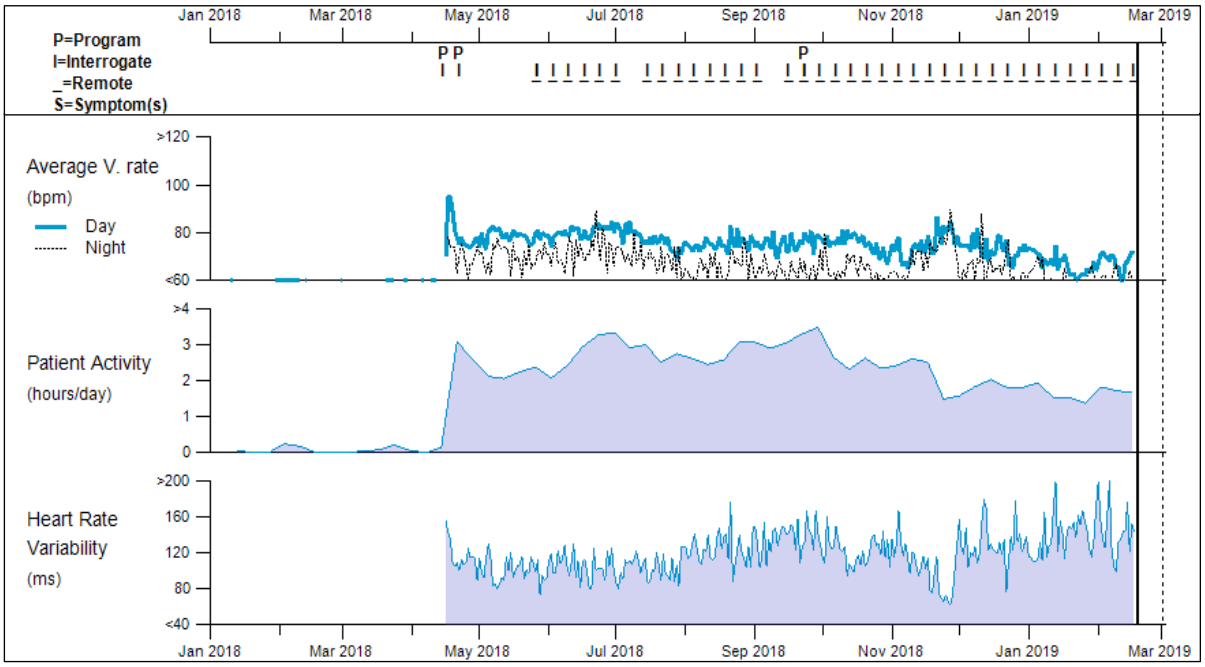

Figure 3.6. 14-month cardiac compass for C3 (from 02 January 2018 to 03 March 2019).

The median ventricular rate for C1 during tachycardic events recorded in 2016 averaged 174 bpm (tachycardia trigger was set at 171 bpm) and averaged 175 bpm for C2 for all recorded tachycardic events (tachycardia trigger was set at 158 bpm). Mean heart rate during interrogations (resting ECG) was 100 bpm for C1 (SD=12), and 82 bpm (SD=10) for C3. The resting heart rates were not normally distributed for C2 due to low number of interrogations (median 66 bpm, ranging from 60 to 108 bpm).

Sinus bradycardia and pauses were detected mostly at nights, presumably while sleeping (see figure 3.7) and tachycardic events were detected mostly during the day (see figure 3.8).

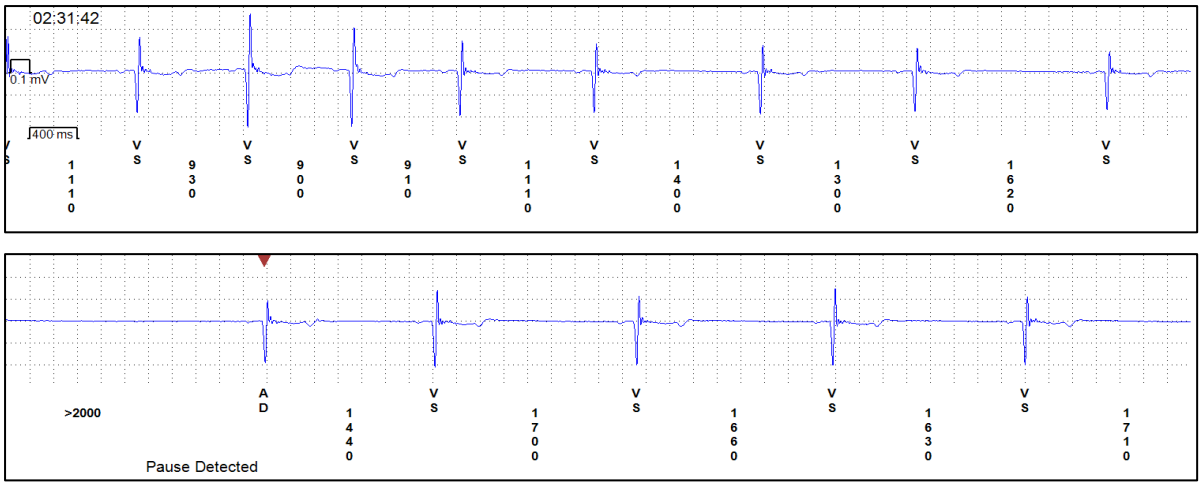

Figure 3.7. Nocturnal pause greater than 2000ms detected on C3 ILR. VS: ventricular sense. AD: asystole detected.

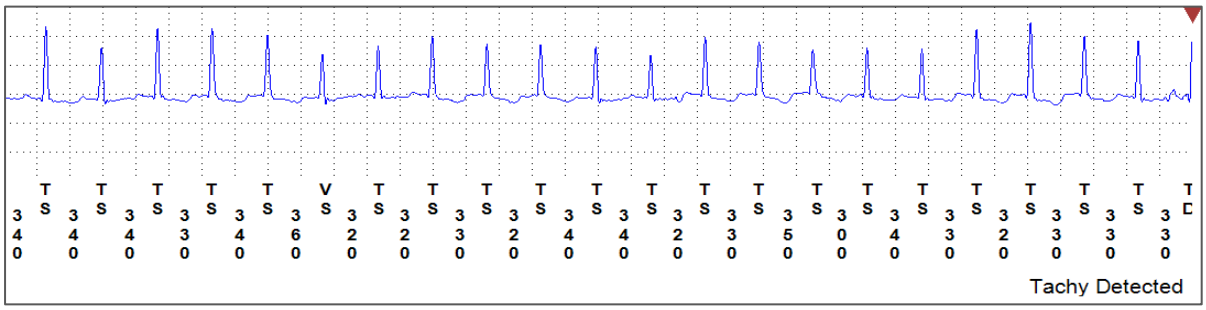

Figure 3.8. Sinus tachycardia detected on C3 ILR. TS: tachycardia sense, red arrowhead indicates trigger time point.

Ventricular premature complexes (VPCs) were the most common arrhythmia detected during tachycardic events, with both C1 and C3 presenting moderate numbers of unimorphic and multimorphic VPCs, couplets, triplets, as well as ventricular bigeminy and trigeminy (see figures 3.9 and 3.10). On eight occasions for C1 and four occasions

for C3, single VPCs were detected on the resting ECG taken during the device interrogation (thus outside of tachycardic events).

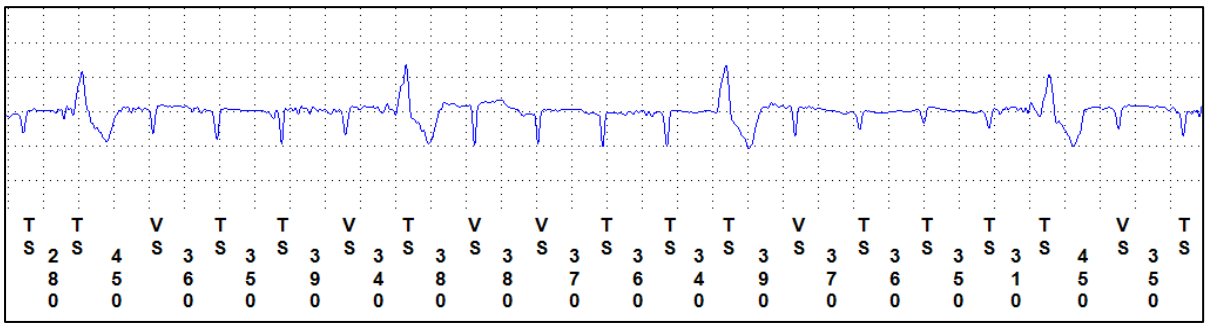

Figure 3.9. Unimorphic VPCs in C1. Note the downward QRS complex due to mispositioning of the ILR device.

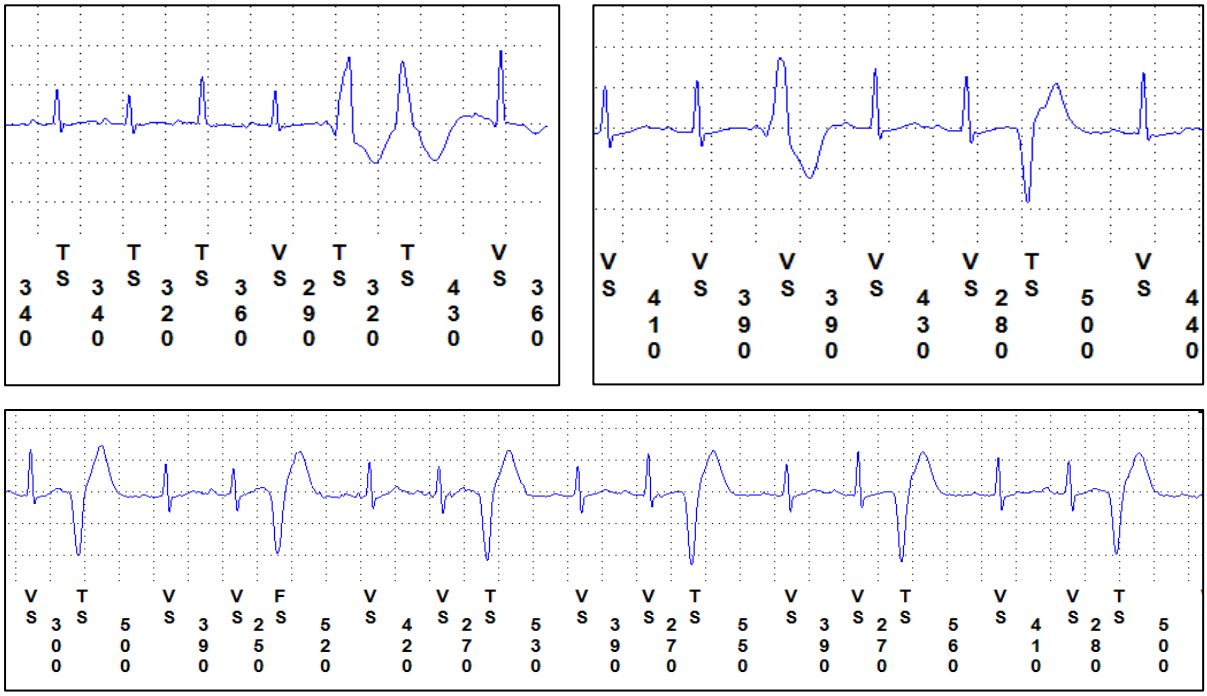

Figure 3.10. Ventricular premature complexes detected on C3 ILR. VS: ventricular sense. TS: tachycardia sense. Note the couplet in upper left trace, multifocal VPCs in upper right trace, and trigeminy in bottom trace.

The number of VPCs per recorded tachycardic event varied greatly. Although many tachycardic events for C1 and C3 had none to less than five VPCs recorded, some tachycardic episodes had up to 23 VPC for C1 (in February 2016) and up to 40 VPCs for C3 (August 2018). For C1, longer periods of tachycardia seemed to have more numerous VPCs than shorter tachycardic events.

There was no increase in frequency and numbers of VPCs with time for C1 or C3. For C2, recorded episodes did not show any VPCs except for three tachycardic episodes that presented one clear VPC each. C3 presented 5 episodes of short run of ventricular

tachycardia (see figure 3.11). C1 showed one episode of suspected ventricular tachycardia in October 2017.

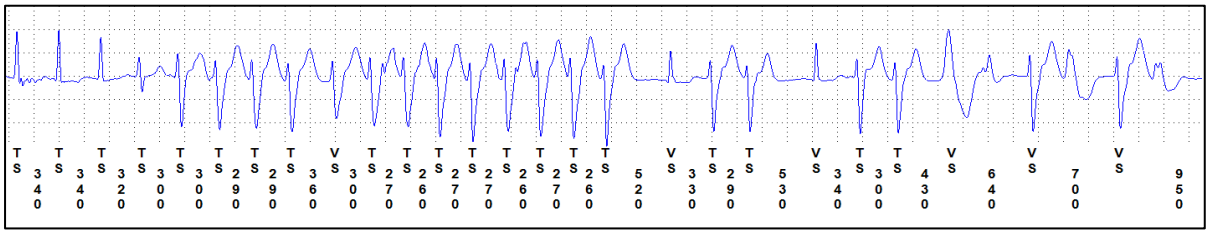

Figure 3.11. Run of ventricular tachycardia of approximately 200 bmp followed by ventricular premature complexes in C3.

3.3.2. Cardiac biomarkers

Results of biomarker concentrations are represented in figure 3.12. Treatment with spironolactone and enalapril orally was initiated in August 2019 for C1 due to increasing concentrations of cardiac biomarkers and changes on echocardiography.

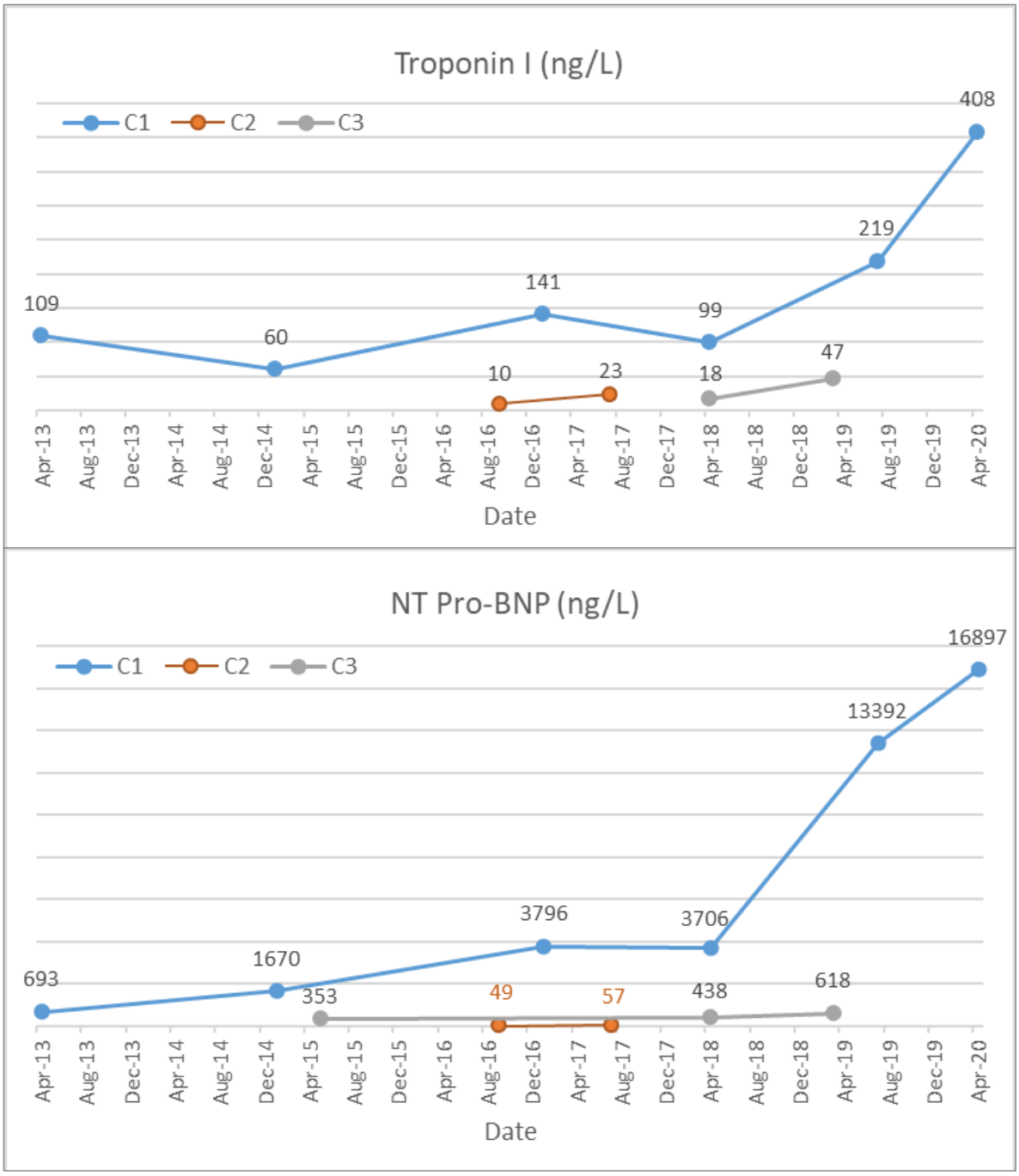

Figure 3.12. Serum concentrations of cardiac biomarkers in C1, C2 and C3.

3.3.3. Cardiac ultrasound findings

C1 underwent three cardiac ultrasounds during the period of study. The first cardiac ultrasound, on the day when the first ILR was implanted in January 2015, showed reduced systolic function and mild mitral regurgitation. Two years later echocardiography showed mild dilation of left ventricle, raised myocardial echogenicity and reduced systolic and diastolic functions. In April 2018, when the ILR device was replaced, echocardiography showed a dilated left ventricle with very poor systolic function and contractility.

C2 underwent one cardiac ultrasound on the day of the ILR implantation, which showed trivial mitral regurgitation. Mild reduction in left ventricular contractibility was also noted but difficult to differentiate from the effects of anaesthesia.

C3 also underwent a cardiac ultrasound on the day of implantation in April 2018, which showed trivial tricuspid regurgitation and a mild reduction in left ventricular function potentially linked to the effect of the anaesthetic drugs. See appendix 1.

3.3.4. 12-lead ECG findings

The four 12-lead ECGs performed on C1 showed normal sinus rhythm. Although a minor ST elevation was detected in the anterior chest leads in 2015, ST segments were normal in the subsequent ECGs. In the 2017 ECG, leads 2 and 3 showed a slight notch in upstroke of the QRS complex, but this was not visible in the subsequent ECGs. Although R wave amplitude on chest leads in 2017 and 2018 could have indicated an axis shift, this was not visible on the 2019 ECG.

C2's 12-lead ECG showed a normal sinus rhythm and some movement artefacts, no abnormalities were detected.

The 12-lead ECG for C3 showed normal sinus rhythm and mild elevation of the ST segment in chest anterior leads V2, V3 and V4. QRS was greater in V3 and V4 than V5 and V6.

3.3.5. Cardiac post-mortem findings for C1 and C2

C1 was euthanised in April 2020 (29 months after the last ILR download) due to acute lethargy and suspected thrombosis in the left arm. Histopathology performed at an

external laboratory (on all organs except the heart) revealed subacute to chronic occlusive vascular thrombosis with segmented chronic lymphoplasmacytic fibrosing arteritis with vascularisation of the arterial wall affecting the left axillary artery. There was no evidence of systemic underlying vascular pathology or systemic inflammatory process. The heart was examined and trimmed following the comprehensive Ape Heart Project protocol (Strong et al. 2018c, 2020), and showed chronic, multifocal, marked replacement fibrosis with interstitial and perivascular fibrosis; acute, multifocal contraction band necrosis, oedema, and multifocal acute myocytolysis; and chronic, mild to focally moderate lymphocytic pericarditis and aortic perivasculitis and focal, acute adventitial haemorrhage. There were also marked signs of acute myocardial damage with intraluminal thrombus formation.

C2 died in November 2017 (13 months after the last ILR download) during the recovery from an anaesthetic procedure to treat numerous severe bite wounds. Histopathology performed at an external laboratory was mostly unremarkable, however the heart examination following the Ape Heart Project protocol revealed diffuse, mild to moderate, chronic interstitial fibrosis and perivascular fibrosis; multifocal, mild, acute myocardial and epicardial haemorrhages as well as multifocal, acute to subacute areas of rhabdomyolysis with contraction bands and mineralisation.

3.4. Discussion

This study confirms that ILRs implantations and interrogations are achievable in chimpanzees, with a surgical procedure that is minimally invasive and with no identified side effects in the selected animals. Although no animal showed any discomfort after device implantation, unfortunately two devices out of four were removed by the chimpanzee 18 and 25 days after implantation, when the surgical wounds appeared externally healed and the non-steroidal anti-inflammatory medication had been discontinued. Longer periods of analgesic medication may be required in chimpanzees after ILR implantation, because foreign body granulation tissue reaction within the subcutaneous tissue may cause discomfort weeks after implantation. The dislodgment of the devices may also have been avoided if the ILR had been placed under the skin of the back instead of the chest, as suggested in other studies (MacKie et al. 2010; Furukawa et al. 2011). We chose chest placement in

these animals to avoid interference due to muscle movement on the ECG trace when the device is place on the back, and because training chimpanzees for chest presentation is easier than for back presentation, but this may need to be reconsidered in the future to minimise the risk of removal.

Training for chest presentation was well accepted and most ILR interrogations were readily achieved by the keepers, however during some periods the social grouping of chimpanzees and tension within the group hindered ILR interrogations. Data analysis of C1's ILR revealed frequent under sensing of QRS complexes thus re-programming was necessary. In humans, R-wave under sensing and false detection of bradyarrhythmia is also a common occurrence in patients implanted with ILRs (Maines et al. 2018).

ILR data analysis showed that VPCs were the most common arrhythmias detected in the study animals, but it is not possible to clearly associate the number or nature of the VPCs with other clinical or pathological findings, mainly due to the low number of animals studied. Both C1 and C3 presented numerous VPCs, and although C1 had cardiac disease diagnosed via echocardiography, biomarkers values and marked IMF confirmed on histopathology; C3 showed relatively normal echocardiography and cardiac biomarkers values. C2 had mild to moderate IMF on histopathology, and unfortunately only had a few ILR interrogations, little VPC occurrence, and presented the lowest cardiac biomarkers of the three animals. Its death may have been related to the observed prominent areas of acute to focally subacute myocardial infarction that are often associated with terminal dysrhythmic events, thus related to more acute cardiac changes compared to C1. Unfortunately, neither C1 nor C2 had an active ILR device at the time of their death.

In humans, a VPC burden >10% is considered significant and requires monitoring and sometimes treatment (Lee et al. 2019), as repetitive VPCs may trigger ventricular fibrillation and sudden cardiac death (Ip and Lerman 2018) even in structurally normal hearts. In young humans showing VPCs without evidence of cardiac disease; right ventricular biopsy revealed cellular hypertrophy, fibrosis and degenerative changes in 42% of the studied individuals, but the results of Holter monitoring did not correlate with the severity of histopathological findings (Biase et al. 1992). Although determining the origin of the VPC via the 12-lead ECG is advisable, in our cases the single lead ECG captured by the ILR did not allow localisation. Treatment for cardiac disease was

initiated for C1 months after her second device had been removed, thus it was not possible to assess the effect of treatment on the frequency of arrhythmias.

Interestingly, 12-lead ECGs performed in the study animals under anaesthesia revealed little abnormalities. The four 12-lead ECGs performed on C1 showed normal sinus rhythm and normal ST segments except for the first ECG performed in 2015 that showed slight elevation of the ST segment. The slight notch in upstroke of the QRS complex seen in C1's ECG in 2017 might indicate fibrosis or ischaemia, but it is unclear why this was not visible in the subsequent ECGs. Although R wave amplitude on C1's chest leads in 2017 and 2018 could have indicated an axis shift, the fact that this was not visible on the 2019 ECG probably indicates a slightly inaccurate chest lead placement in the two previous ECGs. In C3's ECG, a QRS greater in V3 and V4 than V5 and V6 might suggest a change in vector direction, or a slightly inaccurate lead placement. C3 also presented ST segment elevation in the anterior chest lead, in humans this is indicative of anterior infarct, but it also may occur in athletic hearts; in C3 this finding could indicate the presence of myocardial fibrosis in the anterior myocardium or a slightly hypertrophied heart muscle.

Of interest are the raising values of biomarkers presented by C1 since 2013. Although no reference ranges for troponin I nor NT-proBNP have been published in chimpanzees, by 2020 C1 presented troponin I concentrations well above the suggested clinically relevant value of 200 ng/L for chimpanzees (Ely et al. 2011b), and her NT-proBNP values were also above the cut-off of 7611 ng/L suggested for humans between 50 and 75 years of age (Gaggin and Januzzi Jr 2013). C2's biomarkers concentrations were low four months before his death, supporting the theory of a death due to acute rather than chronic cardiac changes. Although C3´s cardiac biomarkers concentrations can be considered low, they seem to be slowly rising with time and will continued to be monitored.

The ILR devices used in this study were offered free of charge to the Ape Heart Project by human hospitals. Unfortunately, several attempts made to source additional ILR devices for our three study animals were unsuccessful. Nonetheless, the number of ILR interrogations achieved in this study is unmatched and offer a unique insight into the electrical activity of the chimpanzee heart. This study is also exceptional due to its longitudinal nature and the availability of other clinical and post-mortem data. We hope

that more ILR devices will be available to the Ape Heart Project in the future to continue investigating chimpanzee cardiac rhythm.

4. Assessment of the dried blood spot method to assess vitamin D status in chimpanzees.

This chapter has been published as “Comparison of 25-hydroxyvitamin D concentration in chimpanzee dried blood spots and serum” in Journal of Veterinary Clinical Pathology, **https://doi.org/10.1111/vcp.12863**

4.1. Introduction

Vitamin D is a fat-soluble vitamin that includes vitamin D_3, produced in the skin from sun exposure, and vitamin D_2, which is obtained from food. In humans and other primates, the predominant circulating form of vitamin D is 25-hydroxyvitamin D (25-OHD) comprising 25-hydroxyvitamin D_2 and 25-hydroxyvitamin D_3. Although Vitamin D’s major function is to maintain adequate serum calcium and phosphorus concentrations in the blood, it has a wide range of other biological actions(Hossein-Nezhad and Holick 2013). Low concentrations of vitamin D in humans have been associated with both an increased risk of mortality and with a variety of disorders including musculoskeletal diseases, diabetes mellitus, cardiovascular diseases, autoimmune diseases, and cancer (Pilz et al. 2011; Christakos et al. 2013).

Few studies have assessed the concentrations of vitamin D in non-human primates (Crissey et al. 1999; Videan et al. 2007), but vitamin D deficiency has been diagnosed in juvenile chimpanzees with rickets (Junge et al. 2000) and one study suggested that adult captive chimpanzees experienced vitamin D deficiency when housed without regular access to unfiltered sunlight (Videan et al. 2007). Another study measuring nutritional parameters in nine species of captive primates found that most of them had serum 25-OHD levels below published levels for humans and other primates, and that chimpanzees had the lowest serum levels (Crissey et al. 1999). However, as none of these animals showed clinical signs of vitamin D deficiency, the significance of the findings is uncertain and the question of normal serum vitamin D values in chimpanzees is unanswered. To establish reference ranges for this taxon, ideally concentrations should be measured in healthy individuals living in their natural geographical range with unlimited sun exposure. This represents a challenge because

of limited access to samples from these populations and little availability of micronutrient analysis *in-situ*.

Precision and reliability of 25-OHD measurements in serum vary depending on the laboratory, analytical technique and other factors such as equipment calibration and maintenance (Black et al. 2015). The Vitamin D External Quality Assessment Scheme (DEQAS) is the largest specialist external quality assessment scheme for the vitamin D metabolites that assess and monitor the accuracy of results produced by its certified laboratories, that must produce 75% of results within +/-25% of the target value (Carter et al. 2017). At present, it is accepted that liquid chromatography-tandem mass spectrometry (LC-MS/MS) offers the best accuracy for vitamin D metabolite measurements and is considered as the gold-standard technique (Galior et al. 2018). However DEQAS 2016/2017 review reports that in April 2017, the mean bias of LC-MS/MS assays (against target values assigned by the US National Institute of Standards and Technology) among DEQAS accredited laboratories was 9.3%, over the Vitamin D Standardisation Program (VDSP) acceptable bias of 5%, and the mean coefficient of variation (CV) was 9.4% (just below the VDSP threshold of 10%) (Binkley and Sempos 2014; Vesper and Cook Botelho 2014; DEQAS review 2016/2017 2016).

Although serum or plasma are the standard biological specimens used for measuring 25-OHD concentrations in human medicine, it has been shown that measurements of 25-OHD concentration in dried blood spots (DBS) are accurate and precise (Heath et al. 2014). DBS-drops of capillary blood collected on filter paper represents a minimally invasive and low-cost technique that requires limited sample processing and can be applied easily in field-based research settings. One of the big advantages of DBS samples is that they do not need to be centrifuged, separated or frozen following collection. In veterinary medicine, the DBS method has been used for detection of toxins in mammals and birds (Fairey et al. 2001; Lehner et al. 2017), pharmacokinetic studies in rats and mice (Cvan Trobec et al. 2014) and avian sexing with PCR (Suriyaphol et al. 2014). However, this technique has not been validated for any testing in primates.

The objective of this study was to measure 25-OHD ($25\text{-}OHD_3$+$25\text{-}OHD_2$) in captive chimpanzee dried blood spots and calculate the intra- and inter-assay imprecision and the inaccuracy compared to the measurements in serum. Measurements in serum at two different laboratories were also compared. This project aims to contribute to the

field of zoological medicine by evaluating an easy and affordable sampling technique to measure an important metabolic variable in great apes.

4.2. Material and Methods.

4.2.1. Sample collection

Routine health-checks were carried out between April and September 2018 on 7 male and 10 female chimpanzees (*Pan troglodytes*) held at Twycross Zoo, UK, that needed to be transferred into a new enclosure. Ages ranged from 11 to 54 years. Premedication consisted of 0.5mg/kg midazolam orally 30 minutes before anaesthesia was induced with medetomidine (0.02mg/kg) and tiletamine-zolazepam (2 mg/kg) administered via hand injection intramuscularly. Anaesthesia was maintained with isoflurane in oxygen. Respiratory rate, heart rate, body temperature, invasive and non-invasive blood pressure, end-tidal CO_2, oxygen saturation, and end-tidal isoflurane were monitored continuously. A complete health-check was performed on each animal including a full physical examination, haematology and biochemistry, abdominal and cardiac ultrasound, dental examination, urine analysis, and tuberculosis skin testing. Following standard operating procedures for great ape routine health-check, 60 ml venous blood was collected from the femoral vein of all animals for analysis and storage. Three individual DBS cards were prepared for each animal by applying 4 drops of whole blood directly from the syringe (after removing the needle) on each card. The cards were provided by the Sandwell and West Birmingham NHS Hospital clinical biochemistry department (Whatman 903, GE Healthcare). Considering that each drop of blood collected on the paper card had an estimated volume of 50 µL, it was calculated that approximately 200 µL of whole blood was needed for each DBS card.

4.2.2. Sample processing

For serum preparation, whole blood samples were allowed to clot at room temperature for one to three hours, they were then centrifuged (1000G for 10 minutes) and serum was separated using a Pasteur pipette and apportioned into 0.5 to 1.5 ml aliquots. Two 0.5 ml serum aliquots were stored at 7°C overnight and sent to different external laboratories the following day: Sandwell and West Birmingham NHS Hospital Clinical

Biochemistry department (“Laboratory A”) and Laboratory Medicine-Central Manchester University Hospitals (“Laboratory B”).

At laboratory B, samples were prepared for analysis by adding 150 µL of Internal Standard (IS) solution (25-OHD_2-d3 and 25-OHD_3-d6) in acetonitrile to 75 µL of serum sample, vortex mixed for 5 minutes and centrifuged for 4 minutes. 30 µL of the resultant supernatant was injected into a Transcend™ II liquid chromatography sample preparation system, utilising TurboFlow™ online sample preparation technology. After automated online sample preparation (TurboFlow™ C8 XL column [0.5 x 50 mm]) the analytes were separated by the analytical column (Accucore C8, [2.6 µm, 2.1 x 50 mm]) maintained at 60°C. The aqueous mobile phase (AMP) was 10mM ammonium acetate with 0.1% formic acid in water and the organic mobile phase (OMP) was 10mM ammonium acetate with 0.1% formic acid in methanol. Chromatographic separation was achieved with a gradient program of: 0-2.33 min at 15% OMP; 2.33-3.08 min at 80% OMP; 3.08-3.83 min with a linear gradient of OMP from 80 to 90%; 3.83-4.83 min at 100% OMP; returning to 15% OMP for 4.83-5.83 min to re-equilibrate the column. The flow rate was 0.6 mL/min. Mass spectrometric detection was performed using a TSQ Endura tandem quadrupole mass spectrometer (Thermo Scientific) with atmospheric pressure chemical ionisation in positive mode at 400°C. Analyte quantification was determined against Chromsystem Multi-Level Serum 25-OH-Vitamin D3/D2 calibrators, using TraceFinder™ (version 3.2) system control and data acquisition software. Reported coefficients of repeatability for 25-OHD_3 measurements in human sera were 4.6% at 29.3 nmol/L and 3.7% at 85.8 nmol/L. Dynamic ranges (quantitative reporting ranges) for the assay are 5 - 128 nmol/l for 25-OHD_2 and 5 - 173 nmol/L for 25-OHD_3.

At laboratory A, liquid-liquid extraction was performed adding 150µl sample, calibrator or control to 25µl of IS solution to 150µl 0.2M zinc sulphate solution, 300µl methanol and 700µl hexane, then vortexed and centrifuged. The hexane layer was transferred to a 96-well plate and left to evaporate to dryness, then each well was re-constituted with 80µl of 70% methanol:water loading solvent and 20µl of sample injected onto the column: Waters Acquity UPLC BEH Phenyl 1.7µm, 2.1x50mm, temperature 35^{o}C. Chromatographic separation was performed with a similar gradient than at laboratory B and with a run time of 4.5mins at 0.45ml/min, using an electrospray ionisation source in positive ion mode. Mass spectrometric detection was performed using a Waters

Xevo TQD mass spectrometer with a qualifier transition as an added assurance. Chromsystem Multi-Level Serum 25-OH-Vitamin D3/D2 calibrators and Targetlynx data processing software were used for quantification. Reported intermediate precisions for 25-OHD_3 measurements in human sera were 7.1% at 27.9 nmol/L and 4.8% at 97.8 nmol/L. Dynamic ranges for this assay are 2.8 – 450 nmol/L for 25-OHD_2 and 7.5 – 450 nmol/l for 25-OHD_3.

Both laboratories are accredited by the United Kingdom Accreditation Service (UKAS), hold an ISO-15189:2012 certification and participate in DEQAS external quality assurance (Carter et al. 2017).

The DBS cards were allowed to dry for two hours at room temperature and then placed into hermetically sealed plastic bags containing silica gel and stored at room temperature. Two of the cards for each animal (DBS1 and DBS2) were sent to laboratory A the day after collection and analysed within the same batch, and the third card (DBS3) was sent to the same laboratory one to two weeks after collection in order to be analysed in different batches. Samples were analysed using LC-MS/MS on a Waters Acquity UPLC Waters TQS Mass Spectrometer, following a liquid-liquid extraction, as previously described in the literature (Eyles et al. 2009). This assay has been standardized for humans against their conventional serum and plasma 25-hydroxyvitamin D_3 and D_2 LC-MS/MS (Waters TQD and Acquity UPLC) using specific blood calibrators (with a standard haematocrit of 45%); hence, blood spot results in humans are equivalent to the serum/plasma concentrations if a venous sample has been collected; without requiring any conversion factor. For the preparation of calibration and quality control samples, raw 25-OHD concentrations in DBS are corrected for haematocrit fractions using the following formula (values in nmol/L) (Eyles et al. 2009): Plasma $_{25OHD}$ = DBS $_{25OHD}$ / (1- haematocrit fraction). The laboratory-derived intra-assay variation for 25-OHD in human DBS is < 10% and the inter-assay variation was <15%. All DBS samples were analysed in duplicate by the laboratory, taking a central 3mm punch each from two best blood spots and reporting the results as the average of the two. Dynamic ranges of the DBS assay are 2.8 – 450 nmol/L for 25-OHD_2 and 7.5 – 450 nmol/l for 25-OHD_3.

4.2.3. Data analysis

As the concentrations of 25-OHD_2 were reported to be less than 5 nmol/L in all samples analysed at laboratory B and equal to 2.8 nmol/L in all samples analysed at laboratory A, only 25-OHD (vitamin D total) results were included. Mean results for DBS1 and DBS2 pairs were calculated and thereafter called DBS12.

Results were analysed using GraphPad Prism 8.0.2. Shapiro-Wilk test was used to test 25-OHD concentrations and calculated differences (serum lab B-serum lab A, DBS12-serum lab A, DBS3-DBS12) for normality (alpha=0.05).

Results from serum at laboratory A and laboratory B were analysed using non-parametric Spearman correlation and Deming regression, and agreement was evaluated with Bland-Altman analysis of the differences (Giavarina 2015). Standard deviations (SD) used for Deming regression were estimated from the reported intra-assay variations using the formula SD = CV/100 x Mean. One-sample t-tests were performed on calculated differences (Lab A – Lab B) and linear regression of the differences was plotted on the Bland-Altman graph to detect proportional bias. Outliers were not removed.

The coefficients of variation and SD for the DBS were calculated using the formulas for the CV and SD based on duplicate samples (Synek 2008; Hyslop and White 2009).

Laboratory A (serum lab A) was considered the reference method as their DBS technique has been calibrated against their conventional LC-MS/MS on serum. Results from DBS12 and serum laboratory A were compared and analysed with the same statistical methods used for the comparison between laboratory A and B. and acceptability of the DBS method was judged by calculating the percentage of DBS12 results that lies within +/- 25% of serum laboratory A results, as this corresponds to DEQAS performance target and has been suggested as the acceptable performance for 25-OHD measurements (NOTES ON INTERPRETING DEQAS REPORTS (25-OHD) Definitions Target Value n.d.; Holmes et al. 2013; New York State Department of Health 2015).

Differences between DBS12 and DBS3 results were calculated and analysed with a one-sample t-test. Differences expressed in percentage of DBS12 were calculated and plotted against DBS12.

Finally, the absolute differences between the haematocrit results and a standard haematocrit of 45% were calculated, tested for normality with Shapiro-Wilk test and compared with the absolute differences between DBS12 and lab A with a Pearson correlation.

This project has received the approval of the ethical review committee of the University of Nottingham's School of Veterinary Medicine and Science.

4.3. Results

Total 25-OHD concentrations measured in serum and dried blood spot cards, calculated differences, and haematocrit results, are shown in Table 4.1.

25-OHD concentrations in serum at laboratory A and B were not normally distributed, and Spearman correlation coefficient r_s was 0.5 (95% CI=0.02 to 0.8; p=0.04). Estimated SD at a mean 25-OHD concentration of 82 nmol/L were 3.93 for laboratory A and 3.00 for laboratory B. These SD were used to compute Deming regression, which values were: slope 1.46 (95% CI=0.66 to 2.25); Y-intercept -35.82 (95% CI=-98.03 to 26.40). Differences between results at the two laboratories were normally distributed. Bland-Altman analysis revealed a mean bias of -1.25 (SD=14.83) that did not differ significantly from 0 on a one-sample t-test (t=0.347, d.f=16, p=0.733). On the Bland-Altman plot, magnitudes of the differences did not seem to increase at lower or higher concentrations of 25-OHD: linear regression line slope was -0.28 (95% CI= -0.65 to 0.1), not significantly different from 0 (p=0.14). 95% limits of agreements were -30.31 to 27.61. Chimp 15 was identified as an outlier on the Bland-Altman plot with a bias of 36.60 (Figure 4.1).

Table 4.1. Total 25-OHD concentrations measured in serum and dried blood spot cards, calculated differences, and haematocrit results. DBS12 refers to the mean between DBS1 and DBS2.

	Serum lab A	**Serum lab B**	**DBS1**	**DBS2**	**DBS3**	**PCV** *(%)*	**DBS12**	**Serum lab A - serum lab B**	**DBS12 - serum lab A**	**DBS3-DBS12**	**DBS3-DBS12** (*% of DBS12)*
	Total 25-OH vitamin D concentrations, in nmol/L										
Chimp 1	81.3	54	76.3	80.6	81.3	41.6	78.45	27.3	-2.85	2.85	3.63
Chimp 2	89.1	70.3	115.7	107.1	81.1	36.2	111.4	18.8	22.3	-30.3	-27.20
Chimp 3	76.3	64	46.4	48.4	51.1	45.8	47.4	12.3	-28.9	3.7	7.81
Chimp 4	81.0	82.8	59.8	55.2	62.9	38.1	57.5	-1.8	-23.5	5.4	9.39
Chimp 5	59.1	59.9	62.5	63.5	52.1	39.9	63	-0.8	3.9	-10.9	-17.30
Chimp 6	69.1	72.8	45.9	49.9	46.1	55	47.9	-3.7	-21.2	-1.8	-3.76
Chimp 7	64.2	72	83.6	75.9	71.2	51	79.75	-7.8	15.55	-8.55	-10.72
Chimp 8	70.2	83.1	51.7	52.2	59.7	42.9	51.95	-12.9	-18.25	7.75	14.92
Chimp 9	72.9	74.8	57.4	63.8	57.5	37.8	60.6	-1.9	-12.3	-3.1	-5.12
Chimp 10	78.7	60.5	71.8	66.5	59.1	32.4	69.15	18.2	-9.55	-10.05	-14.53
Chimp 11	69.7	74.1	60.1	52.6	45.6	60	56.35	-4.4	-13.35	-10.75	-19.08
Chimp 12	66.1	65	46	44.9	52.2	48.3	45.45	1.1	-20.65	6.75	14.85
Chimp 13	124.7	123.7	175.4	157.5	135.3	24.1	166.45	1	41.75	-31.15	-18.71
Chimp 14	122.8	135.1	132.8	125.6	105.2	42.9	129.2	-12.3	6.4	-24	-18.58
Chimp 15	74.3	110.9	100.9	92.6	66.3	28.2	96.75	-36.6	22.45	-30.45	-31.47
Chimp 16	98.9	112.5	106.5	107.7	95	38.3	107.1	-13.6	8.2	-12.1	-11.30
Chimp 17	87.3	91.4	84.7	101.6	78.8	41.2	93.15	-4.1	5.85	-14.35	-15.41

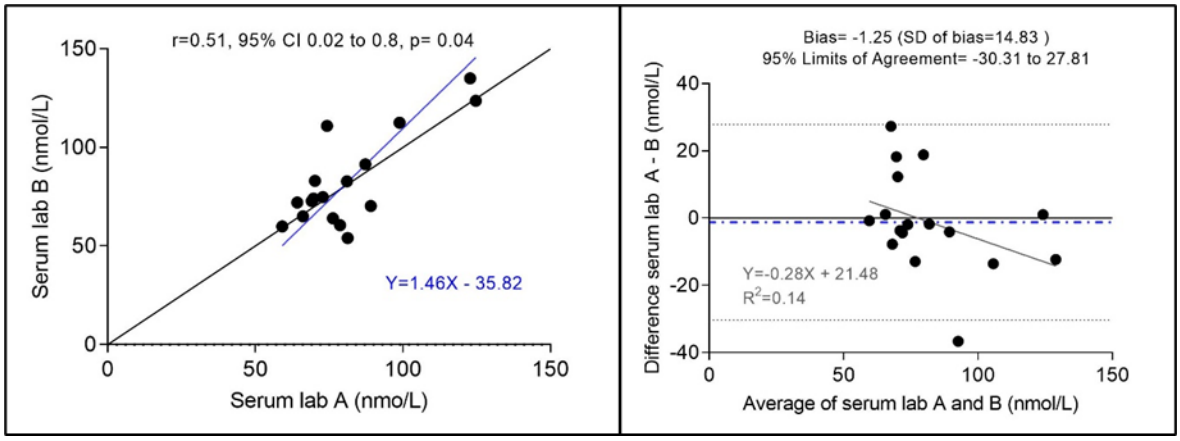

Figure 4.1. Spearman correlation and Bland-Altman analysis assessing agreement between total 25-OHD measurements in serum at Laboratory A and Laboratory B. Blue continuous line: Deming regression line. Blue dashed line: mean bias. Gray continuous line: linear regression line. Black dotted lines: 95% limits of agreement (+/- 1.96 SD). The identify line (Y=X) is also provided on the correlation graph.

The coefficient of variation for the DBS1 and DBS2 pairs was 6% and the CV computed between the mean of DBS1 and DBS2 with DBS3 was 12.6%. Calculated SD for the DBS12 pairs was 5.55.

Mean results of the pairs DBS1 and DBS2 (thereafter called DBS12) were not normally distributed. The Spearman correlation computed between DBS12 and laboratory A results yield a correlation coefficient of 0.7 (95% CI= 0.31 to 0.89; p=0.024). Values for Deming regression (using SD=3.93 for lab A and SD=5.55 for DBS12) were: slope 1.86 (95% CI= 1.17 to 2.55); Y-intercept -71.41 (95% CI= -125.8 to -17.05). Differences in 25-OHD concentrations between DBS12 and laboratory A were normally distributed. Bland-Altman analysis revealed a mean bias of -1.42 (SD=19.58), that was not significantly different from 0 on one-sample t-test (t=0.299, df=16, p=0.769). 95% limits of agreements were -39.80 to 36.96, with chimpanzee 13 identified as an outlier with a bias of -41.75 (Figure 4.2). Linear regression analysis of the differences identified a significant positive proportional bias (slope=0.6; 95% CI= 0.34 to 0.87; p=0.0002) and a negative constant bias (Y-intercept=-50.30; 95% CI= -72.70 to -27.89) which resulted in average negative bias at results less than 83.15 nmol/L (X-intercept) but positive bias above this concentration (Figure 4.2). Only 9/17 (53%) of the DBS12 results were within +/-25% of laboratory A results (Figure 4.3).

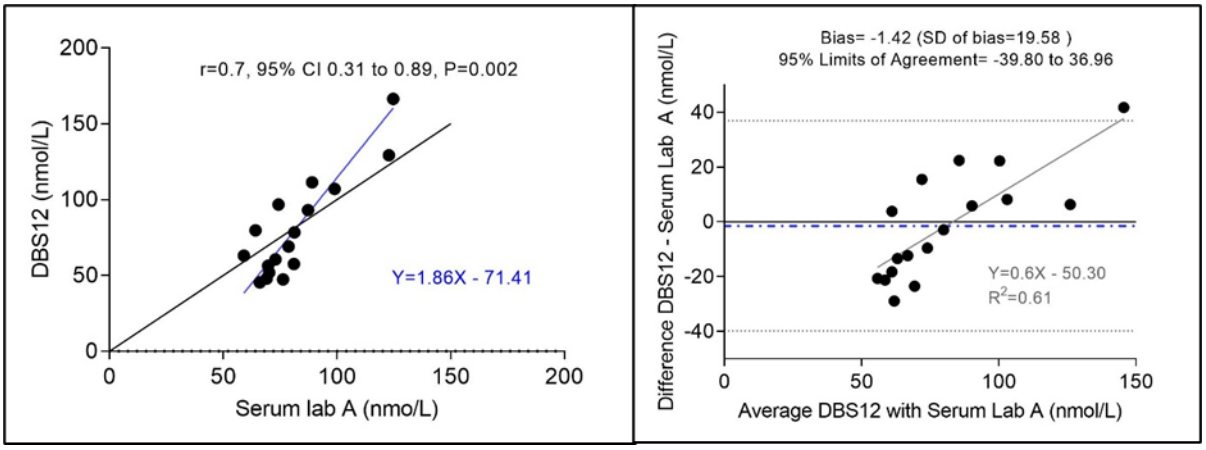

Figure 4.2. Spearman correlation and Bland-Altman analysis assessing agreement between total 25-OHD measurements in serum at Laboratory A and dried blood spots of the DBS1 and DBS2 pairs (DBS12). Blue continuous line: Deming regression line. Blue dashed line: mean bias. Gray continuous line: linear regression line. Black dotted lines: 95% limits of agreement (+/- 1.96 SD). The identify line (Y=X) is also provided on the correlation graph.

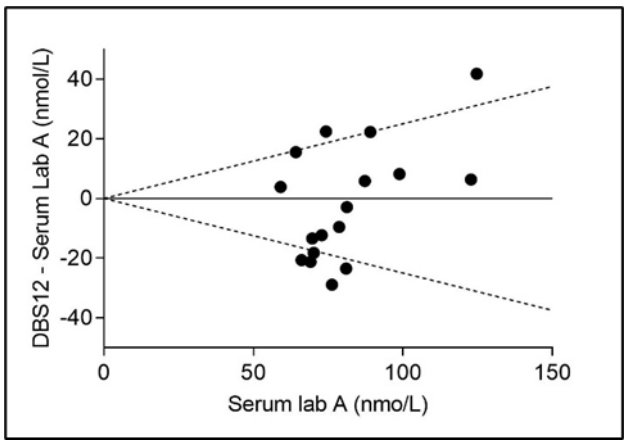

Figure 4.3. Differences between total 25-hydroxyvitamin D (25-OHD) measurements in dried blood spots of the DBS1 and DBS2 pairs (DBS12) and serum at Laboratory A showing the +/-25% acceptability lines (black dashed lines)

When comparing results from DBS3 with DBS12, differences were normally distributed and the mean difference was -9.47 (SD=13.22, 95% CI= -16.27 to -2.68) which differed significantly from 0 on a one-sample t-test (t=2.96, df=16, p=0.009), showing that 25-OHD concentration in DBS3 card was generally lower than in DBS1 and DBS2. When expressed in percentage of DBS12, the differences were between -31.47% and 14.92% (mean difference -8.39% +/-14.21) (Figure 4.4).

The calculated absolute differences between the haematocrit results and a standard haematocrit of 45% were normally distributed. Spearman correlation between these differences and the absolute differences between DBS12 and lab A was not significant (α=0.05) with r=0.11 (95% CI= -0.40 to 0.57, p=0.67).

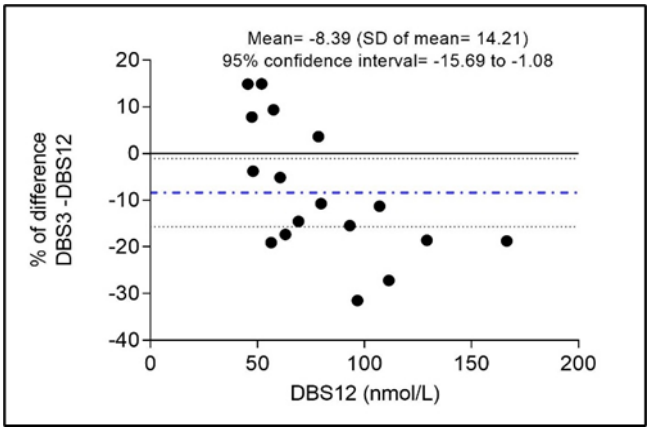

Figure 4.4. Percentage of difference between DBS3 and the DBS1 and DBS2 pairs (DBS12), plotted against DBS12. Blue dashed line: mean % difference. Black dotted lines: 95% confidence interval.

4.4. Discussion

Correlation between 25-hydroxyvitamin D measurements in chimpanzee dried blood spots and serum may be considered as strong using traditional approaches to interpreting correlation coefficient (Schober and Schwarte 2018). However, limits of agreements were wide, and both constant and proportional error was identified in the DBS method when compared to measurements in serum at the reference laboratory. Only 53% of DBS results showed an error within acceptance limits used in humans. Correlation was moderate between the measurements in serum at the two different laboratories; however, no significant constant nor proportional error was identified.

Liquid chromatography-tandem mass spectrometry (LC-MS/MS) is currently established as the gold standard for measurement of vitamin-D compounds due to improved analytical specificity and sensitivity and wider dynamic range compared to immunoassay methods (Galior et al. 2018). It is widely recognised that there are substantial differences in human serum 25-hydroxyvitamin D measurements not only between assays but also between laboratories using LC-MS/MS (Black et al. 2015). Due to this analytical variability and pre-analytical factors for serum 25-OHD variation (season, sun exposure, skin type, etc.), no evidence-based international consensus on human vitamin D reference range exist (Ferrari et al. 2017). It is however recognised that 25-OHD concentrations below 30 nmol/L increase the risk of poor musculoskeletal health, while concentrations between 50-125nmol/L appear to be safe and sufficient (Public Health England 2016; Sempos et al. 2018; Bjerg et al.

2019). Cases of vitamin D toxicity are rare and associated with serum 25-OHD concentrations above 300 nmol/L (Public Health England 2016).

The presented comparison between 25-OHD measurements in chimpanzee serum at two accredited laboratories allows contextualising the variation found between serum and DBS technique. A maximum bias of 36.60 nmol/L and limits of agreements as wide as -30.31 to 27.81 between chimpanzee serum samples stresses the fact that results of vitamin D levels in chimpanzees must be interpreted with care regardless of the sample type, especially for values close to human published cut-off points. For this study, serum samples were sent at ambient temperature as it has been shown that 25(OH)-vitamin D3 in its natural state bound to vitamin D-binding protein is very stable at room temperature, and decreases noted after three days at around 20ºC under common pre-analytical conditions are less than analytical inter-assay precision (Wielders and Wijnberg 2009).

DBS matrix-matched calibrators used by laboratory A are produced with a human haematocrit of 45%. As most of 25-OHD is present in serum and not in red blood cells, extreme values of haematocrit in the analysed samples could lower the accuracy of the 25OHD results in DBS compared to serum. The chimpanzees in this study had a wide range of haematocrit levels, ranging from 24.1% to 60%. Interestingly, chimpanzee 13, who had the lowest value of haematocrit, was an outlier in the Bland-Altman analysis comparing serum and DBS results. Although statistical analysis failed to reveal a correlation between the differences in haematocrit (compared with standard 45%) and differences in vitamin D levels between assays, veterinarians should be aware that vitamin D concentration measured in DBS may be falsely increased in animals with very low haematocrit and falsely decreased in animals with very high haematocrit.

The coefficient of variation of 6% calculated between the DBS1 and DBS2 pairs encompass both the within-batch analytical CV of the assay for chimpanzees (intra-assay variation) and the variations due to DBS quality (spot size, diffusion of blood, etc). The result is comparable to the quoted intra-assay CV for the human DBS assay of <10%, thus suggesting little variation due to DBS quality in this study. The CV of 12.6% calculated between mean DBS12 and DBS3 additionally incorporates the batch assay variation but also the stability of vitamin 25-OHD in dried blood spots. This result is also comparable to the inter-assay CV of <15% quoted by laboratory A for human

DBS. The fact that the third blood spot card, analysed at a later time point showed generally lower values than the first two DBS may put into question the stability of vitamin 25-OHD in chimpanzee's dried blood spot. However, in unprocessed whole blood, vitamin D metabolites are considered very stable (Wielders and Wijnberg 2009) and a study found no significant effect of different storage condition (-20ºC, 2 weeks in dark at room temperature and 2 weeks in full light and open box at room temperature) on vitamin D levels in DBS (Eyles et al. 2009). All the DBS cards in this current study were stored in sealed plastic bags with desiccant gel in the dark, to minimise analyte degradation. The difference between the third DBS and the other DBS could thus be attributable to inter-assay variation only, or to the limited number of samples.

The blood sample used to prepare the DBS in this study was from one single venous blood sample in order to avoid multiple sampling. DBS cards are designed and calibrated for the use of capillary blood, however, excellent agreement was found between venous and capillary serum 25-OHD concentrations measured by LC/MS-MS in humans(Jensen et al. 2016). A known source of inaccuracy and variation in DBS results come from the quality of the blood spots on the Whitman paper. In a field setting, creating well-sized and homogeneous blood spots is challenging. The laboratory used in this study tries to overcome this problem by performing duplicate measurements using a central 3mm punch from two of the best spots on the card and providing the mean concentration.

Important study limitations were the relatively low number of samples included and the fact that most of the measured 25-OHD concentrations were in the middle to high part of the analytical range and did not cover the whole working range of the method. This does not adhere with recommendations for method comparison experiments (Jensen and Kjelgaard-Hansen 2006); however, adequate sample number and range is difficult to achieve when working with zoo species that can only be sampled opportunistically during health-checks or translocations.

Recommendations to calculate the total allowable analytical error for new laboratory methods (Jensen and Kjelgaard-Hansen 2006) are difficult to apply in this current study because the inherent imprecisions of the methods used are unknown for chimpanzees, and acceptance limits based on analytical quality specifications can only be estimated following recommendations from humans. However, as the

imprecision estimated for the DBS technique in chimpanzees was similar to the reported imprecisions for human serum and DBS, the use of acceptance limits based on External Quality Assessment scheme for human 25-OHD seems reasonable. 25-OHD concentrations in serum at laboratory A were considered as references when estimating the DBS technique acceptability. The fact that only 9/17 of the DBS12 results were within +/-25% of laboratory A serum results categorises the DBS technique in chimpanzees as unacceptable according to human quality schemes. However, an important limitation of our study is that the true total-25OHD concentration is unknown; thus, the accuracy of the dry blood spot method in chimpanzees can only be estimated. To validate the DBS method for vitamin D measurement in chimpanzees, further within-laboratory experiments for this sample type are needed, including accuracy measurement against a “true” value, recovery and interference studies, additional tests on imprecision, and the creation of specific reference intervals (Lumsden 2000).

Until further validation studies are carried out, zoo and wildlife veterinarians should only use DBS samples to estimate vitamin D status in chimpanzees when serum collection and/or storage is not possible, and avoid making clinical diagnostics based on 25-OHD results from DBS, as the analytical error of this method may not allow discriminating between normal and abnormal values.

5. Assessment of the vitamin D status of the British and European chimpanzee population.

5.1. Introduction

Vitamin D deficiency in humans is being described as a pandemic, and is associated with costs of hundreds of billions of Euros in Europe (Cashman et al. 2016). Studies on vitamin D status in the European population show very different estimates of prevalence of vitamin D deficiency, partly due to differences in analytical methods, and although it has been suggested to use centralised laboratories to make these studies more reliable, this has not yet been achieved (Spiro and Buttriss 2014; Cashman et al. 2016).

Vitamin D_3 (cholecalciferol) synthesised in the skin from exposure to UVB radiation is the main source of vitamin D for most people, but vitamin D_3 and D_2 (ergocalciferol) obtained from the diet become important sources when exposure to UVB is restricted (O'Neill et al. 2016; Public Health England 2016). As UV transmission is hindered by melanin, dark skin is a well-known risk factor for insufficient cutaneous vitamin D synthesis, especially at northern latitudes (Libon et al. 2013; Åkeson et al. 2016). Other factors include little skin exposure to the sun, sunscreen usage, and environmental factors such as weather or pollution(O'Neill et al. 2016). The prevalence of vitamin D deficiency is widespread even in Southern Europe (González-Molero et al. 2011; Cardoso et al. 2017; Rodríguez et al. 2019). Interestingly, some Scandinavian populations show higher values of serum 25-OHD than in Southern Europe due to the consumption of oil-rich fish, dairy products and vitamin D supplements (Bouillon 2017). The definition of vitamin D deficiency is still under debate, and recommendations for nutritional supplementation vary depending on countries (Bouillon 2017; Sempos et al. 2018). Public Health England recommends a daily intake of 400 IU of vitamin D in the UK population over 4 years of age (Public Health England 2016).

Vitamin D_2 and D_3 are converted in the liver to 25-hydroxyvitamin D (25-OHD) which is widely used as a biomarker of vitamin D status due to its long half-life in the blood (10 to 89 days depending on studies) (Public Health England 2016; Datta et al. 2017). Although the main limitation to the use of 25-OHD as a biomarker of vitamin D status

is its analytical variability, other factors such as body mass index, genetic variation and the presence of an underlying inflammatory state can impact concentrations of circulating 25-OHD independently of vitamin D supply. The active metabolite $1,25(OH)_2D$ (calcitriol) formed by further hydroxylation of 25-OHD in the kidneys, is under tight homeostatic control and its measurement is only relevant to diagnose specific conditions leading to altered vitamin D metabolism (Dirks et al. 2018). The high-affinity receptor (VDR) for calcitriol is present in most tissues and cells in the body and it has been shown that in humans there are up to 2000 genes directly or indirectly regulated by calcitriol (Hossein-Nezhad and Holick 2013; Kim et al. 2020). Clinical investigations in humans suggest an association between vitamin D deficiency and cardiovascular disease such as cardiomyopathy and heart failure and respiratory infections such as influenza and SARS-CoV-2, although further research is needed to assess the observed association (Gardner et al. 2011; Wang et al. 2012b; D'avolio et al. 2020; Grant et al. 2020).

The effects of vitamin D status are likely to be similar in great apes and people, thus vitamin D deficiency in great apes has a potential dramatic negative impact on their health, welfare and breeding success and ultimately might compromise the sustainability of the zoo population. Although reference intervals for serum 25-OHD have not yet been established in chimpanzees, several studies suggest that both juvenile and adult captive chimpanzees may suffer from vitamin D deficiencies despite vitamin D supplementation (Crissey et al. 1999; Junge et al. 2000; Videan et al. 2007). However, clinical relevance of these results is unclear as no data exist on vitamin D values in healthy apes living in their natural geographical and ecological environment.

According to Species360 Zoological Information Management System, there are more than 700 chimpanzees in zoos in Europe and 79% of this population live at latitudes over 46°North (ZIMS data, March 2021), potentially being affected by a low amount of direct sunlight most of the year. Despite this, no recommendations for minimal UVB exposure nor vitamin D supplementation in great apes exist currently.

As described previously, one of the main limitation when assessing vitamin D concentrations in serum is the high analytical variability, which makes it unadvisable to compare concentrations measured at different laboratories (Holmes et al. 2013; Ferrari et al. 2017). The objective of this study was to assess the concentrations of 25-OHD in serum of European zoo-housed chimpanzees using the same laboratory and

liquid chromatography–mass spectrometry gold-standard assay, and to analyse the effects of the zoo's latitude, period of the year, and husbandry practices on vitamin D status.

5.2. Material and Methods

Serum samples from chimpanzees kept in European zoos were used for this study. Samples were sent directly from European zoological institutions or from the European Association of Zoo and Aquaria (EAZA) Biobank across Europe at ambient temperature or refrigerated and immediately stored at -80°C upon arrival. Samples were subsequently sent to a UKAS accredited laboratory (Laboratory Medicine - Central Manchester University Hospitals) and analysed for 25-OHD_2, 25-OHD_3 and total 25-OHD using liquid-liquid extraction method and tandem mass spectrometry (LC-MS/MS), as detailed in chapter 3 (Moittié et al. 2020b).

The following information for each animal at the time of sampling was obtained from participating zoos: age, sex, health and pregnancy status, body condition score (1-emaciated to 9-markedly overweight), skin tone (dark or light), presence of alopecia (0-normal coat to 3-total lack of hair), diet sheet including any vitamin D supplementation given at time of sampling; and details about outdoor access in the two months before sampling (limited/unlimited).

The geodetic latitude for each zoo was determined using Google Maps.

Statistical analysis was carried out using Graph Prism version 9.0.2. For each analysis, normality of the data was assessed with Shapiro-Wilk test and parametric or non-parametric tests were subsequently used. Parametric tests were chosen over non-parametric tests when at least one of the two group had a normal distribution, provided that each group had a sample size greater than 15 (de Winter and Dodou 2010). A Mann-Whitney test was chosen as the non-parametric alternative of the Student's t-test. Significance was set at $p<0.05$.

Animals were classified as healthy when reported as such or when reported to suffer from acute traumatic injuries only.

Daily and unlimited outdoor access was considered equivalent for statistical analysis.

Sampling season was categorised as winter from 21st of December to 20th of March, Spring from 21st of March to 20th of June, Summer from 21st of June to 21st of September and fall from 22nd of September to 20th of December. The year was also divided in two UV index periods: samples taken from beginning of October to end of March were classified into the low UV index period, and samples taken from beginning of April to end of September were classified into the high UV index period (O'Neill et al. 2016; Vitt et al. 2020).

The time of sample storage before analysis was calculated in months.

Northern Europe was defined for latitudes above 46 degrees North, where levels of UVB are too low to allow cutaneous vitamin D_3 synthesis for most of the year (Jablonski and Chaplin 2010).

5.3. Results

A total of 213 serum samples were analysed, from 127 individuals from 27 zoos.

One sample that had a total 25-OHD concentration below the detection limit of 5 nmol/L was not included in the statistical analysis as its true value was unknown.

The numbers of samples sent per zoo ranged from 1 to 105. The largest number of samples were obtained from Twycross Zoo (n=105, latitude 52.65°) followed by Copenhagen Zoo (n=16, latitude 55.67°), Zoological Society of London (n=13, latitude 51.53°) and Burgers Zoo (n=12, latitude 52.01°)). Only 24 samples were obtained from Southern Europe, with 10 samples obtained from Madrid Zoo (latitude 40.41°). The histogram of latitude, represented in figure 5.1, shows a clear overrepresentation of Northern European chimpanzee samples and especially of Twycross Zoo chimpanzees.

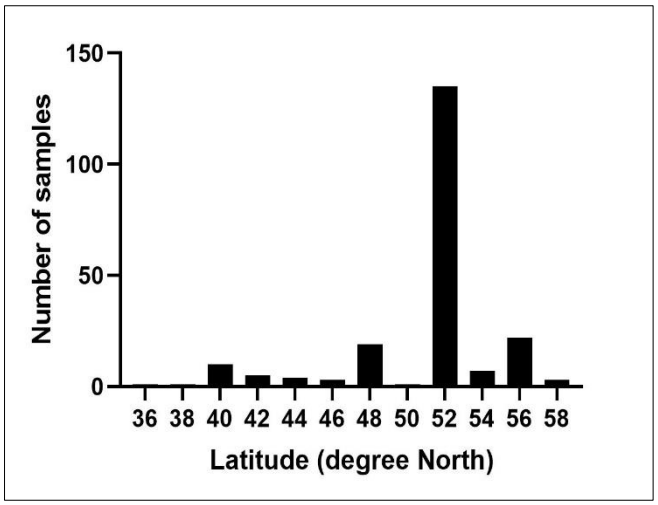

Figure 5.1. Distribution of sample number per latitude (n=211).

Chimpanzees' median age at the time of sampling was 28 years (range 2 to 53 years), with 36 samples corresponding to juvenile individuals (2-14 years), 114 to adults (15-34 years) and 50 to elderly (over 35 years).

Samples were stored for up to 166 months before analysis, with a median of 77 months of storage.

A total of 17 zoos (63%) filled out the questionnaire about the animals and their husbandry at the time of sampling. Some zoos were not able to provide all the information required on the questionnaire, especially in the case of samples taken more than five years ago.

Information on the chimpanzee diet at the time of sampling was available for 174 samples. For 98.3% of these samples, the animals were reported to eat primate pellets as part of their diet at the time of sampling. Diets were largely based on green and root vegetable, pellets, fruits, nuts and occasional extras such as eggs, vegetable oil, and meat. The total and relative amount eaten by each animal was not possible to ascertain, as diets were reported for whole chimpanzee group.

A total of 23 animals (from 7 different zoos) were known to receive extra vitamin D supplementation (on top of the vitamin D present in the pellets) at the time of sampling, one sample was discarded for statistical analysis as 25-OHD concentration was below the level of detection.

The concentration of 25-OHD_2 (ergocalciferol) was less than 5 nmol/L thus negligible for all samples except for three samples: one chimpanzee from Twycross zoo with 25-

OHD_3=26.2 nmol/L and 25-OHD_2=14.8 nmol/L, one chimpanzee from Copenhagen zoo with 25-OHD_3=23 nmol/L and 25-OHD_2=15.7 nmol/L, and another chimpanzee from Copenhagen zoo with 25-OHD_3=25.9 nmol/L and 25-OHD_2=27.7 nmol/L. Thus, apart for these 3 chimpanzees, the total 25-OHD results in this study were equivalent to the concentrations of 25-OHD_3.

The analysis of vitamin D concentrations independently of latitudes or seasons showed that 25-OHD concentrations were not normally distributed and ranged from 12.60 nmol/L to 151 nmol/L with a median of 62 nmol/L (see figure 5.2). A total of 64 samples (30.2%) had concentrations of 25-OHD below 50 nmol/L. Interestingly, 10 of these samples were from chimpanzees living in Southern European zoos.

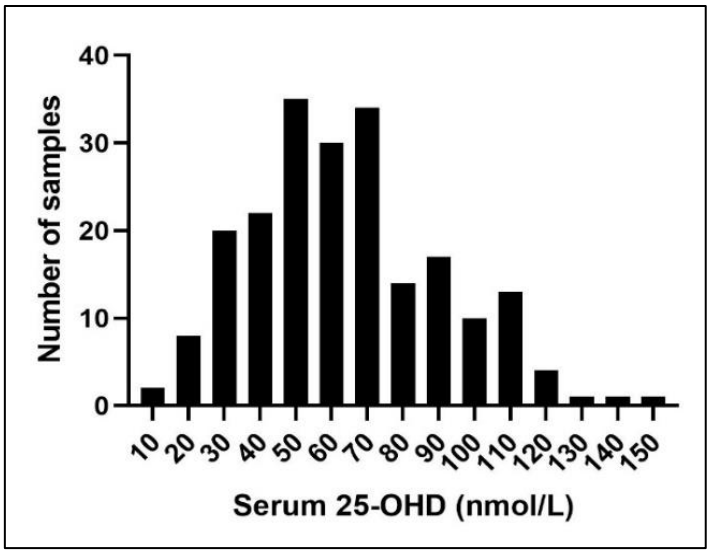

Figure 5.2. Distribution of 25-OHD concentration for all samples.

Mean 25-OHD concentrations per sampling month are represented in figure 5.3. When dividing samples into four sampling seasons, 25-OHD concentrations were normally distributed and there was a significant difference in 25-OHD concentrations between seasons (Anova $F(3,207)=11.14$, $p<0.0001$), with mean 25-OHD concentration of 49.5 nmol/L (SD 20.4) in winter, 65.96 nmol/L (SD 24.34) in spring, 80.83 nmol/L (SD 30.86) in summer, and 60.72 nmol/L (SD 24.92) in fall. Results are represented in figure 5.4.

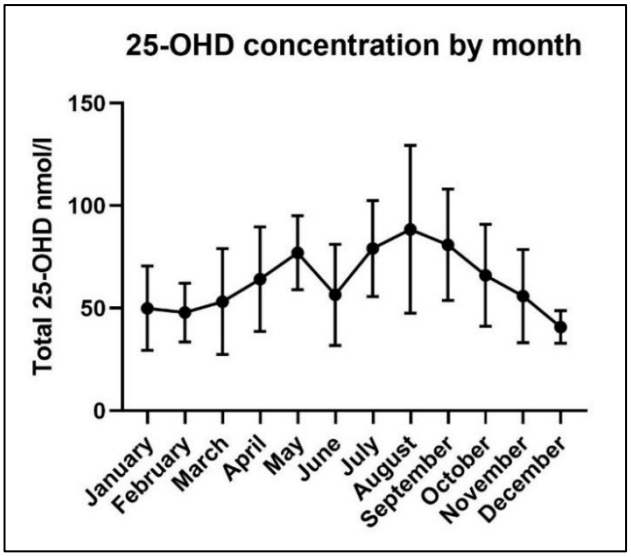

Figure 5.4. Mean 25-OHD concentration (and SD) for all samples (n=212) by sampling month.

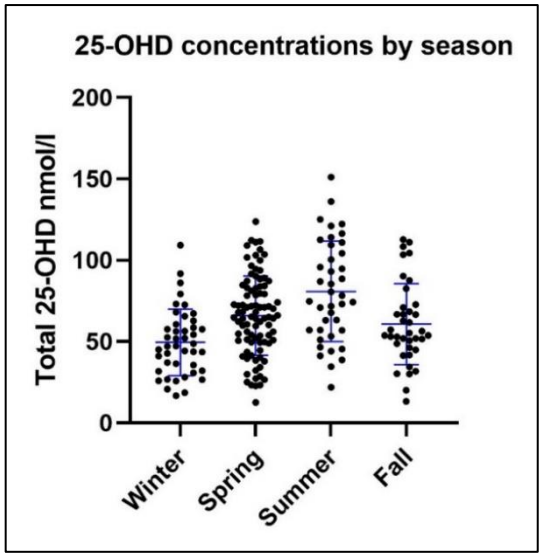

Figure 5.4. 25-OHD concentrations for all samples (n=212) by sampling season. Blue bars represent means and SD.

A total of 79 samples were taken during low UV index season (October-March), and 132 were taken during high UV index season (April-September). The concentration of 25-OHD was significantly different between these two UV index periods (t-test t (209)=4.32, p>0.0001) with a mean 25-OHD in the low season of 54.56 nmol/L (SD=22.89 nmol/L) and a mean 25-OHD of 70.42 nmol/L (SD=27.38 nmol/L) in the high UV index season. During low UV season, mean 25-OHD was 57.17 nmol/L (SD=22.67) for chimpanzees in Northern Europe (n=67), and 40 nmol/L (SD=18.94 nmol/L) for chimpanzees in Southern Europe (n=12). During high UV season, mean 25-OHD was 69.62 nmol/L (SD=26.50 nmol/L) in Northern Europe (n=121) and 79.25 nmol/L (SD=36.10 nmol/L) in Southern Europe (n=11). Percentages of samples with 25-OHD concentrations below 50 nmol/L during high UV season was 23.5% (31/132) and 41.8% (33/79) during low UV season. Two chimpanzees from Southern Europe presented 25-OHD levels below 50 nmol/L during the high UV season.

When considering the impact of skin tone on vitamin D concentration (for all seasons/latitudes) there was a significant difference in 25-OHD concentration depending on the skin tone (t-test t (158)=2.65, p=0.0045) with mean 25-OHD concentrations of 62.60 nmol/L (SD=23.43 nmol/L) in chimpanzees with dark skin (n=108) and 25-OHD concentrations of 74.54 nmol/L (SD=32.55 nmol/L) in chimpanzees with light skin (n=52). When considering Twycross zoo samples taken in high UV season only to minimize confounding factors, mean 25-OHD concentration

was 75.32 nmol/L (SD=19.59 nmol/L) in chimpanzees with dark skin (n=47) and 91.68 nmol/L (SD=29.53) in chimpanzees with light skin (n=21) (t-test t (66)=2.7, p=0.009).

There was no significant difference in 25-OHD levels between males and females across all samples (t(209)=0.17, p=0.86) nor when considering samples collected during high UVB season only (t(130)=0.68, p=0.49).

There was no significant difference in mean 25-OHD concentration between age groups when considering all samples (Anova F (2, 197)=1.92, p=0.15), nor when considering samples taken during high UV season only (Anova F (2, 128)=2.25, p=0.11).

For statistical analysis, levels of alopecia 1 and 2 were grouped due to a low number of chimpanzees categorised as level 2. Across all samples, there was no significant statistical difference in concentrations of 25-OHD depending on grades of alopecia (Anova F (2, 141)=1.76, p=0,18). Additionally 25-OHD mean concentrations did not differ significantly between alopecic levels (Anova F (2, 93)=0.82, p=0.44) in samples taken only in the high UV season.

The amount of vitamin D present in commercial pellet food varied greatly depending on the brand of pellet used. Moreover, several zoos were unable to ascertain exactly which type of pellets the animals were eating at the time of sampling. At least 7 different types of primate pellets were identified as offered to zoo chimpanzees in Europe. One food distributor reported to have changed markedly the vitamin D amount in their leafeater pellets in 2018 (raising the vitamin D_3 amount from 3500 to 8500 IU/kg). The amount of vitamin D_3 in pellets ranged from 1600 to 10170 IU/kg. It was not possible to statistically assess the effect of pellet type on serum 25-OHD concentrations, due to the limited sample number for each type of pellet and the presence of numerous confounding factors.

To assess the effect of storage time on 25-OHD concentration, correlation between the 25-OHD concentration and number of months of storage were calculated for Twycross zoo samples only, for both low UV season and high UV season. Correlation was not significant for samples taken during low UVB season (Pearson r=0.015, p=0.94) nor for samples taken during high UVB season (Pearson r= 0.11, p=0.67).

Information on vitamin D supplementation (on top of the vitamin D present in vegetables and pellets) was available for 130 animals. For the 23 animals reported to

receive extra vitamin D supplementation, it was difficult to know the exact amount of vitamin D received by each animal, due to the zoo mixing the supplementation to the diet, or lack of details on exact cholecalciferol amount present in the supplementation. Madrid zoo reported a dose of one teaspoon of supplement containing 0.00013% cholecalciferol (52 IU per gram) and 60g of another diet supplement containing a total of 800 IU of vitamin D given to the chimpanzee group (n=4). If we suppose that a teaspoon weighs approximately 4g, we could assume that each chimpanzee could receive approximately 252 IU of vitamin D per day. Another zoo in France reported feeding their chimpanzees a supplement containing 400 IU of vitamin D_3 per litre, however the amount received by each chimpanzee was not reported. Copenhagen zoo reported that three of their chimpanzees were receiving 1200 IU of cholecalciferol supplementation daily at the time of sampling.

Median 25-OHD concentrations in animals reported to get extra vitamin D supplementation (n=22) at the time of sampling was 48.95 nmol/L (range 20.70 to 114 nmol/L), which was lower and not significantly different from the animals not receiving vitamin D supplementation (Man Whitney U=945, p=0.13), with these animals (n=108) presenting a median 25-OHD of 58.90 nmol/L (range 12.60 to 151 nmol/L). When considering samples taken during low UV season only, mean 25-OHD in animals receiving supplementation (n=10) was 40.14 nmol/L (SD=18.88 nmol/L)), which was not significantly different from animals not receiving supplementation (n=31) who had a mean 25-OHD of 47.62 nmol/L (SD=16.75) (t-test t(39)=1.19, p=0.24).

The impact of unlimited daily outside access in the two months before sampling on 25-OHD concentrations, was significant across all samples (t-test t(148)=6.18, p>0.0001). The mean 25-OHD concentration was 69.98 nmol/L (SD=27.66 nmol/L) in chimpanzees with unlimited outside access and 44.10 nmol/L (SD=17.87 nmo/L) in chimpanzee with limited outside access. For the samples taken only during the high UV index season (as some zoos have to keep their animals inside during low UV season due to very cold temperatures), the difference in 25-OHD concentration between animals with limited and unlimited outside access was significant (t-test t(94)=7.38, p<0.0001), with mean 25-OHD of 45.49 nmol/L (SD=15.58) in animals with limited outside access (n= 35) and of 80.47 nmol/L (SD=25.40) in animals with unlimited outside access (n=61).

When assessing the impact of health status on vitamin D concentrations, considering all samples chimpanzees with abnormal health status had significantly lower serum 25-OHD (median of 52.10 nmol/L, range 13.20 to 151 nmol/L) than chimpanzees with normal health status (median 64.70 nmol/L, range 18.50 to 136 nmol/L) (Mann-Whitney U= 2136, p=0.048). Differences were however not significant when considering samples taken only during high UVB season or only during low UVB season, nor when considering Twycross zoo samples only.

5.4. Discussion

This preliminary study represents the first survey on serum vitamin D concentrations in captive European chimpanzees, and its methods are unique as it ensured a reduction in analytical variability by analysing all the samples at the same laboratory with the same gold-standard assay, thus allowing a more accurate comparison between results. Although pre-analytical factors such as storage and shipment conditions were not homogeneous, the high stability of 25-OHD in serum samples, even at room temperature, justified our choice of study methods (Wielders and Wijnberg 2009; Agborsangaya et al. 2010).

In humans, the suggested definition of vitamin D deficiency vary depending on sources, but levels between 50 and 125 nmol/l are generally considered sufficient and safe, while levels below 30 nmol/L can increase the risk of developing diseases such as rickets or osteomalacia (Public Health England 2016; Sempos et al. 2018). Public Health England recommends that serum 25-OHD concentration should not fall below 25 nmol/L at any time of the year (Public Health England 2016). If we apply a 50 nmol/L cut-off for chimpanzees in our study, more than 30% of all samples could be considered deficient in vitamin D (rising to 41.8% during low UVB season) which represent a concerning finding. Interestingly, low vitamin D levels seem also relatively common in Southern Europe, especially during the low UV season.

Unsurprisingly, there was a clear difference in mean vitamin D concentration between seasons, and higher means were observed in July to September while lower means were observed in December to February. It seems, however, that for a large proportion of chimpanzees even the end of summer serum vitamin D concentrations may not be high enough to ensure that they will not become deficient by winter. In humans in the

United Kingdom it has been calculated that 25-OHD serum levels in September should be at least 80.5 nmol/L in order to exceed a concentration of 25 nmol/L in February (Webb et al. 2018).

Hypovitaminosis D is a public health concerns in humans and it has been linked to numerous chronic conditions and a higher risk of mortality (Caccamo et al. 2018). Growing evidence suggests that low vitamin D levels are associated with cardiovascular disease such as hypertension, coronary heart disease, stroke, myocardial infarction, and cardiac fibrosis (Gardner et al. 2011; Meredith et al. 2015b; Milazzo et al. 2017; Zittermann 2017). It is thus natural to think that vitamin D deficiency is also likely a risk factor for cardiac disease in the European chimpanzee population. Considering the results of this study, together with the high prevalence of cardiac disease in European zoo chimpanzees (see chapter 6), the relationship between vitamin D status and cardiovascular disease in this population should be further investigated. Beyond cardiovascular diseases, vitamin D insufficiency could result in zoo chimpanzees being more susceptible bacterial or viral upper respiratory tract infections or pneumonia which are a common cause of morbidity in this species (Unwin et al. 2013; Ianevski et al. 2019; Grant et al. 2020).

There was a clear association between vitamin D levels and skin tone, which is consistent with what is known in humans, where increased skin pigmentation hinders pre-vitamin D_3 cutaneous production (Holick et al. 2007; Martin et al. 2016). Although in chimpanzees areas of skin covered with hair are generally only lightly pigmented, areas of exposed skin such as the face vary greatly in pigmentation and becomes darker with age and sun exposure (Jablonski and Chaplin 2000). The skin of adult chimpanzees is thus likely poorly adapted to low UVB environments (Jablonski and Chaplin 2010).

The provision of unlimited daily outside access was associated with higher 25-OHD concentrations year-round. Although the provision of outside access during the majority of the year is recommended by the American Association of Zoo and Aquaria Chimpanzee Species Survival Plan (Ross et al. 2010), outside access can be restricted in some zoos due to climate or husbandry requirements. It may be necessary to raise awareness about the importance to stimulate animals to spend time outside during sunny days when the cutaneous vitamin D synthesis is possible. In Caucasian humans in the UK, only nine minutes of daily sunshine exposure during the

high UV season is necessary to maintain vitamin D levels above 25 nmol/L throughout winter (Webb et al. 2018). Moreover, it may be safer to recommend daily sun or UVB exposure for zoo chimpanzees, rather than advocate for vitamin D supplementation in the diet, as hypervitaminosis D can occur with supplementation, but not with UVB exposure (Towler 2011; Spiro and Buttriss 2014). Vitamin D toxicity could be a concern in the case of vitamin D supplements mixed in the diet offered to a chimpanzee group rather than individually, as it would be difficult to ascertain the exact amount received by each individual.

The relationship between vitamin D levels and health status was unclear in our study and needs further clarification. Chimpanzees with an abnormal health status in our study showed a significantly lower serum vitamin D level but future studies will need to investigate and prove a correlation. Moreover, in humans vitamin D deficiency can not only lead to ill-health, but the inverse relationship is also observed, as chronic and acute inflammation can lead to decrease in 25-OHD levels (Mangin et al. 2014; Public Health England 2016).

The significance of some of the observed (or not observed) associations between vitamin D serum concentrations in European zoo chimpanzees and demographical or husbandry data is yet unclear, mostly because of the presence of numerous confounding factors. The low number of samples from Southern Europe made it impossible to establish the effect of the zoo latitude on serum vitamin D concentration. The overrepresentation of Twycross Zoo samples also likely led to bias when analysing the data. In order to have a clearer picture of vitamin D status in chimpanzees in Europe, ideally a wider and more balanced representation of latitudes will be needed, with a similar number of samples from Northern and Southern European zoos. This may however be difficult to achieve, as less than a quarter of the European zoo chimpanzee population live in Southern Europe.

Another limitation of our study is the inconsistency of the information on chimpanzee husbandry at the time of sampling received by the zoos. Some institutions simply did not send back the requested questionnaire, while many others sent incomplete information, which significantly affected data analysis. Additional efforts will be made in the future to obtain more information for each sample in order to obtain better quality data. However, it is obvious that some information will still be impossible to obtain especially for old samples for which zoos have incomplete records.

This study is only a preliminary step to a PhD project that will investigate more extensively and accurately the role of vitamin D as a possible risk factor for cardiovascular disease in zoo and wild chimpanzees.

6. Post-mortem cardiac examination of European Zoo's great apes.

6.1. Introduction

Ante-mortem diagnoses of disease processes such as myocardial fibrosis or other cardiovascular changes in great apes continue to be a major challenge, thus detailed post-mortem examination remains a crucial tool for the study of cardiac diseases in these species. The detection of cardiovascular lesions requires a skilled and detailed macroscopical and histological examination performed by an experienced pathologist in order to detect structural changes that are often subtle in great apes (Cooper 2017). A retrospective review published by the Ape Heart Project (AHP) analysing cardiovascular disease epidemiology and pathology of zoo-housed great apes between 2004 and 2014 highlighted a critical need for improvement in great ape post-mortem examination and reporting of cardiovascular lesions (Strong et al. 2018a). Guidelines for consistent cardiovascular post-mortem examination and sampling in European Zoo great apes were consequently published (Strong et al. 2018c). A cardiac trimming protocol for pathologists is also available on the American Great Ape Heart Project webpage (GAHP Recommended Cardiac Trimming Protocol for Pathologists n.d.). Both protocols are based on a published analysis of the dissection of the human heart and have been developed to minimise variation and to improve consistency in post-mortem examination and sampling (Sheppard 2012).

Although some studies have been published reporting cardiac post-mortem findings in captive chimpanzees and gorillas, little information is available on orangutans and bonobos (Schulman et al. 1995; Lammey et al. 2008a; Lowenstine et al. 2008a; McManamon and Lowenstine 2012; Tong et al. 2014). Moreover, most reports describe cases from North-American zoos, and until 2020 no information on European zoo great apes pathological findings had been published apart from the cases included in the AHP retrospective study on great ape cardiovascular disease epidemiology and pathology (Strong et al. 2018a).

The aim of this study was to detect and describe the changes affecting the hearts of European zoo great apes received by the Ape Heart Project between 2017 and 2020, using the AHP comprehensive and systematic cardiac trimming and reporting guidelines.

6.2. Materials and Methods

European zoos interested in sending great ape hearts to the project could follow the guidelines available on the Twycross Zo website and/or contact the AHP via email for assistance on sample preparation and shipment. Zoos were required to provide basic information on the samples by completing a sample submission form (see Appendix 2) and providing the local post-mortem reports of the animal. The heart was ideally sampled by the zoo veterinarian or pathologist following the AHP project protocol (Strong et al. 2018c), fixed in 10% neutrally buffered formalin for a minimum of 72 hours and then wrapped in saline or formalin-soaked swabs, placed in a waterproof container and sent by normal mail or courier service. In the case of samples originating from outside of the European Union (i.e Switzerland), Cites export and import permits were included with the sample shipment.

Once the heart was received by the AHP, it was placed back immediately in 10% neutrally buffered formalin for storage. It was then examined and trimmed following the AHP guidelines (Strong et al. 2018c). Briefly, the heart was weighed, and standard measurements were taken (heart circumference and length, valve diameters, ventricular thicknesses). The quality of the sample (e.g previous sectioning, quality of preservation) was evaluated and scored from 1 (very good quality whole heart, sampled as per project protocol) to 4 (poor quality sample, with extensive sectioning or artefacts making some assessments difficult). The amount of epicardial fat was noted (from 1: less than expected to 3: more than expected for an average body condition score). The overall heart shape and the appearance of the pericardium, epicardium, myocardium, endocardium, valves, chambers, and vessels were described. Finally, a minimum of 12 standard samples were taken from predetermined and consistent locations for microscopic examination; as well as samples from any macroscopic abnormality detected. A data record sheet was filled up describing the findings of the macroscopical examination.

Samples were routinely processed for histopathology and stained with haematoxylin-eosin. If needed, special stains such as Elastic Van Gieson, Ziehl-Neelsen, Periodic Acid-Schiff, Gram, Warthin-Starry, and Masson Trichrome were used with adequate positive controls and established staining methods (Morris et al. 2018).

Microscopical examination was performed together with a board-certified pathologist member of the European College of Veterinary Pathology. Findings from each slide were noted on the data collection form and archived. Where provided by the submitting zoo, the clinical history and results from the post-mortem examination of other organs were reviewed to establish a clinical context for the identified cardiac changes. A final report describing the results of the macroscopical and microscopical cardiac examination including histological diagnoses and interpretation was generated and sent to the submitting zoo.

Data analysis was performed using GraphPad Prism 8.1.2. Shapiro-Wilk test was used to assess normality. Significance was set at 0.05. Levels of interstitial and replacement fibrosis (Hinderer and Schenke-Layland 2019) were assigned numerical ranks for statistical analysis: level 0 (no fibrosis), minimal level 1 (minimal fibrosis), level 2 (mild fibrosis), level 3 (mild to moderate fibrosis), level 4 (moderate fibrosis), level 5 (moderate to marked fibrosis), and level 6 (marked/severe fibrosis). Animals above 15-years old were considered adults (Hamada et al. 1996). The weight of the heart was included only for whole hearts with minimal sampling from the zoo of origin, and other macroscopical measurements were included only when not affected by sampling artefacts such as iatrogenic cuts or deformation.

6.3. Results

6.3.1. Chimpanzees

General macroscopical findings

This result section will expose the main findings from the hearts received by the AHP between 2017 and 2020. A total of 22 chimpanzee hearts were received and examined by the AHP (C21 to C42). Results are summarised in table 6.1. Findings related to fifteen of these hearts (from C21 to C35) together with the previous 20 hearts

examined by the project from 2014 to 2017 were published in Journal of Veterinary Pathology (Strong et al. 2020).

Fourteen of the 22 hearts were from females (63.6%), and eight from males (36.4%). Two hearts (C28 and C36) were from juveniles, the rest were from adult individuals. Ages ranged from 2 years to 58 years old (mean 34 years). Body weight ranged from 12 to 82 kg (mean 52 kg).

Sample quality was generally good, except for two hearts (C24 and C27) that had suffered extensive sectioning that made shape assessment difficult.

Mean adult fixed weight (n=16) was 380.3g (SD 113.3g) and mean fixed heart weight to body weight ratio (n=15) was 0.7% (SD 0.26%). Adult heart circumference (n=19) ranged from 21.4cm to 32.5cm (mean 27.67cm, SD 2.96) and heart length (n=18) ranged from 6.1 to 13cm (mean 9.37cm, SD 1.91). Adult fixed heart weight was not significantly different between males and females (unpaired t-test t=0.28, p=0.79), nor was the heart circumference (unpaired t-test t=0.67, p=0.51).

Adult fixed heart weight was not significantly correlated with body weight (Pearson r=0.19, p=0.53) nor with age (Pearson r=0.36, p=0.19).

Left ventricular wall thickness in adults ranged from 1 to 1.8cm (mean 1.4 cm, SD 0.24cm, n=20), interventricular wall thickness had similar range (mean 1.38cm, SD 0.22cm, n=20), and right ventricular wall ranged from 0.2 to 0.6cm (mean 0.30cm, SD 0.11, n=20).

Mean adult valve diameters were 8.72 cm for the mitral valve (SD 1.03, n=20), 10.81 cm for the tricuspid valve (SD 1.17, n=20), 5.18 cm for the aortic valve (SD 0.68, n=18), 6.1 cm for the pulmonary valve (SD 0.84, n=20).

The amount of epicardial fat was moderate (level 2) for 14/22 chimpanzees; three chimpanzees presented little fat (level 1) while four presented a moderately large amount of fat (level 3).

The shape of the heart appeared overall normal for most individuals, except for C23 which presented a visibly hypertrophied left ventricle (chronic asymmetric moderate hypertrophy), and C27 which heart appeared slightly rounded, although assessment was made difficult due to previous sectioning. C29 had subjectively mildly dilated atria

and left ventricle, as well as an increased mitral valve circumference (see case detailed below). C26's heart had a slightly rounded shape.

The presence of small, focal, white areas on the epicardium was a common finding (n=11) and was generally interpreted as so-called "soldier patches" or collagen plaques, which are a common occurrence in humans and believed to result from contact of the heart with adjacent sternum or vertebrae (Roberts 2005; Sheppard 2012). See figure 6.1.

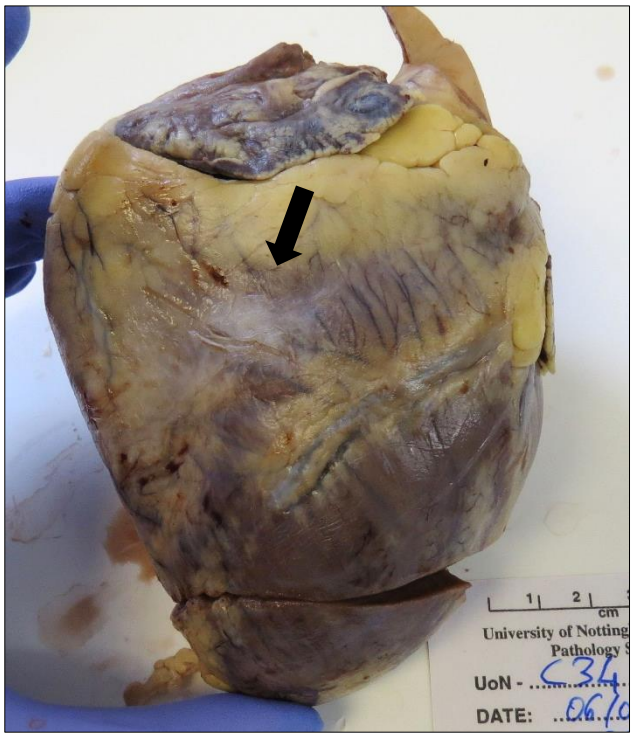

Figure 6.1. Collagen plaque (arrow) on the right ventricular epicardium of C34.

Myocardial cross sections appeared normal in 9/22 individuals, while variably sized paler areas in the heart muscle were visible in 11/22 hearts (Figure 6.2). Three hearts presented dark red mottled areas across the myocardium, interpreted as congestion. C26 presented thickened left ventricular wall and interventricular septum.

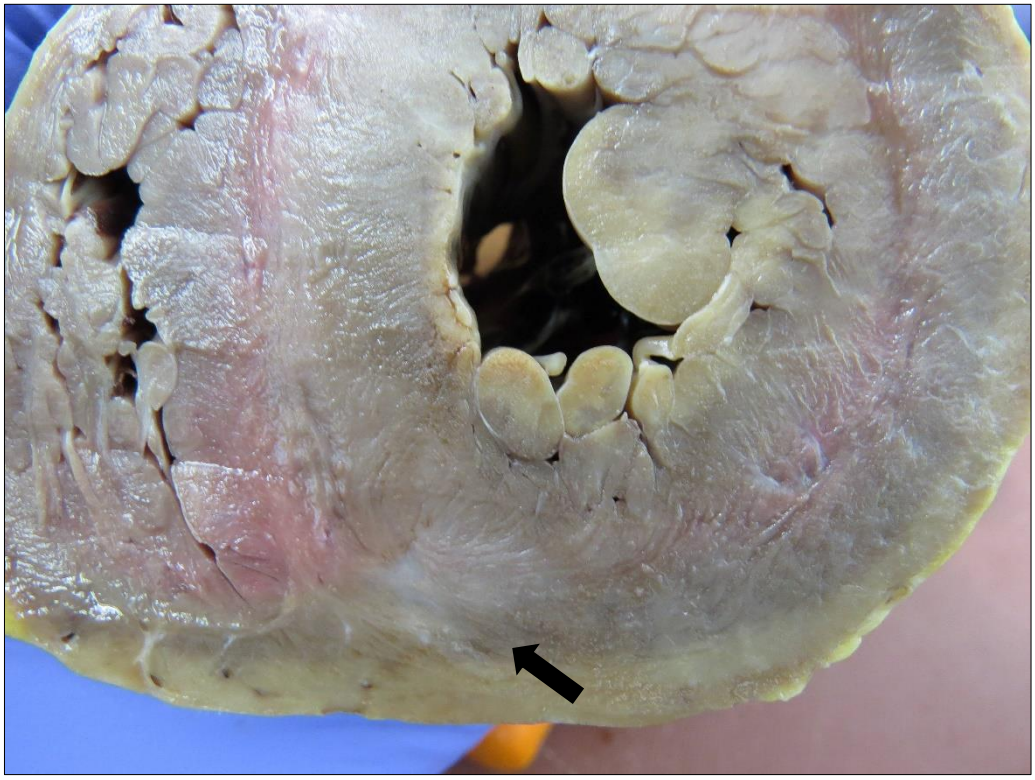

Figure 6.2. C35 myocardial cross section showing marked area of pallor, compatible with myocardial fibrosis. Note the pink areas denoting lack of formalin intake.

Eleven chimpanzees presented some macroscopical changes on the cardiac valves. These consisted of valvular thickening or small nodules on the cusps of the mitral (n=9), tricuspid (n=3) or aortic valves (n=3). Valvular changes were generally mild, except for a few animals that presented moderate mitral valve endocardiosis such as C34 (a 42-year-old female) (figure 6.3) or C31, the oldest chimpanzee of our study with an estimated age of around 60 years old, that presented mild endocardiosis of the tricuspid valve and aortic valve and moderate endocardiosis of the mitral valve. C27, a 47 years-old male, presented both mitral valve endocardiosis and aortic stenosis: the left coronary cusp of the aortic valve was diffusely thickened and stiffened by fibrous tissue (see case detailed below). C39 presented a moderately large nodule (1cm greatest diameter) on one of the leaflets of the tricuspid valve (see case detailed below).

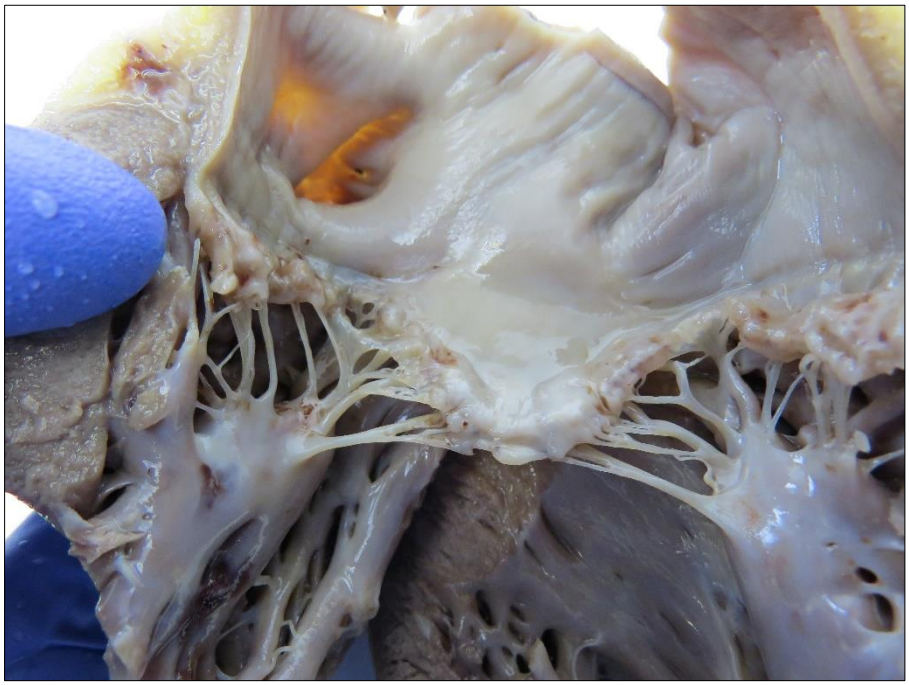

Figure 6.3. Mitral valve of C34 showing moderate chronic endocardiosis.

Macroscopical changes in great vessels were seen in 11/22 individuals and mostly consisted of gritty yellow to orange raised areas on the aortic intima. Although mostly interpreted as ‘intimal thickenings’ or “fatty streaks” and considered age related and incidental (Xu et al. 2016) (see figure 6.4), these areas were consistently sampled for histopathology to rule out atherosclerosis.

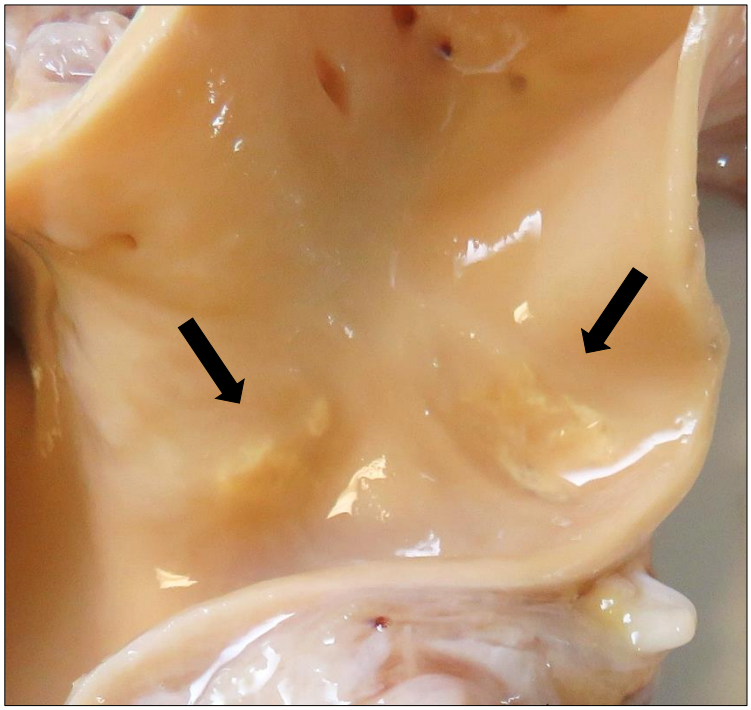

Figure 6.4. Fatty streaks on the aortic intima of C42.

General microscopical findings

Histopathological examination consistently showed a mild variation in myocardial nuclear size (anisokaryosis) that was considered a normal finding in hominids (Strong et al. 2020).

A total of 19 out of 22 hearts (86.4%) presented some degrees of interstitial fibrosis with minimal to mild levels in eight individuals, mild to moderate levels in five individuals, moderate to marked levels in four individuals, and marked levels in two individuals. The distribution of the interstitial fibrosis was generally diffuse. Mild to focally moderate perivascular fibrosis was also a common finding and often correlated with the identified degree of interstitial fibrosis. Replacement fibrosis was a feature in 18 hearts (81.8%), with four hearts presenting a minimal to mild degree, nine hearts presenting a mild to moderate degree, one heart presenting a moderate degree, two hearts presenting moderate to marked degrees, and one heart (C41) presenting a marked degree of replacement fibrosis. One heart (C35) presented mild to moderate but focally extensive replacement fibrosis (presumed old, focal infarct of unknown aetiopathogenesis). The distribution of the replacement fibrosis was random and multifocal. Occasionally, areas of replacement fibrosis also revealed a mild, scar associated fibre disarray which was interpreted as an acquired, focal and reactive change. Six hearts presented variably sized areas of granulation tissue formation indicating a more recent myocardial injury. Inflammatory cell infiltrations were seen in 18 hearts and were generally of a minimal to mild degree, composed of a mixed leukocytic population depending on the timeline of the myocardial injury and focally associated with areas of replacement fibrosis, myocytolysis or granulation tissue formation. Areas of fibrosis were mostly associated with a minimal to mild lymphohistiocytic infiltrate or mixed lymphoplasmacellular and histiocytic population. Acute myocardial damage was often accompanied by a granulocytic infiltrate like neutrophils and/or eosinophils.

Myocytolysis (acute vacuolar cell degeneration with hypereosinophilia, loss of cross striation and neutrophilic infiltrations) was seen in 10/22 hearts while contraction band necrosis (peracute area of fibre necroses with loss of nuclei, cross striation, fragmentation and irregular wavy contraction bands) was a feature in 8/22 hearts.

C23 (a 44-year-old female that died of sudden death) and C26 (a 28-year-old male that died during an anaesthetic event) presented macroscopical and microscopical evidence of left ventricular hypertrophy with mild hypertrophy of cardiomyofibres. C23 also presented diffuse, moderate interstitial fibrosis and moderate to focally marked, chronic replacement fibrosis with mild lymphohistiocytic and eosinophilic scar-related infiltrate, while C26 only presented mild interstitial and replacement fibrosis. C33, a 47 years-old female with reported kidney failure presented marked random myofibre

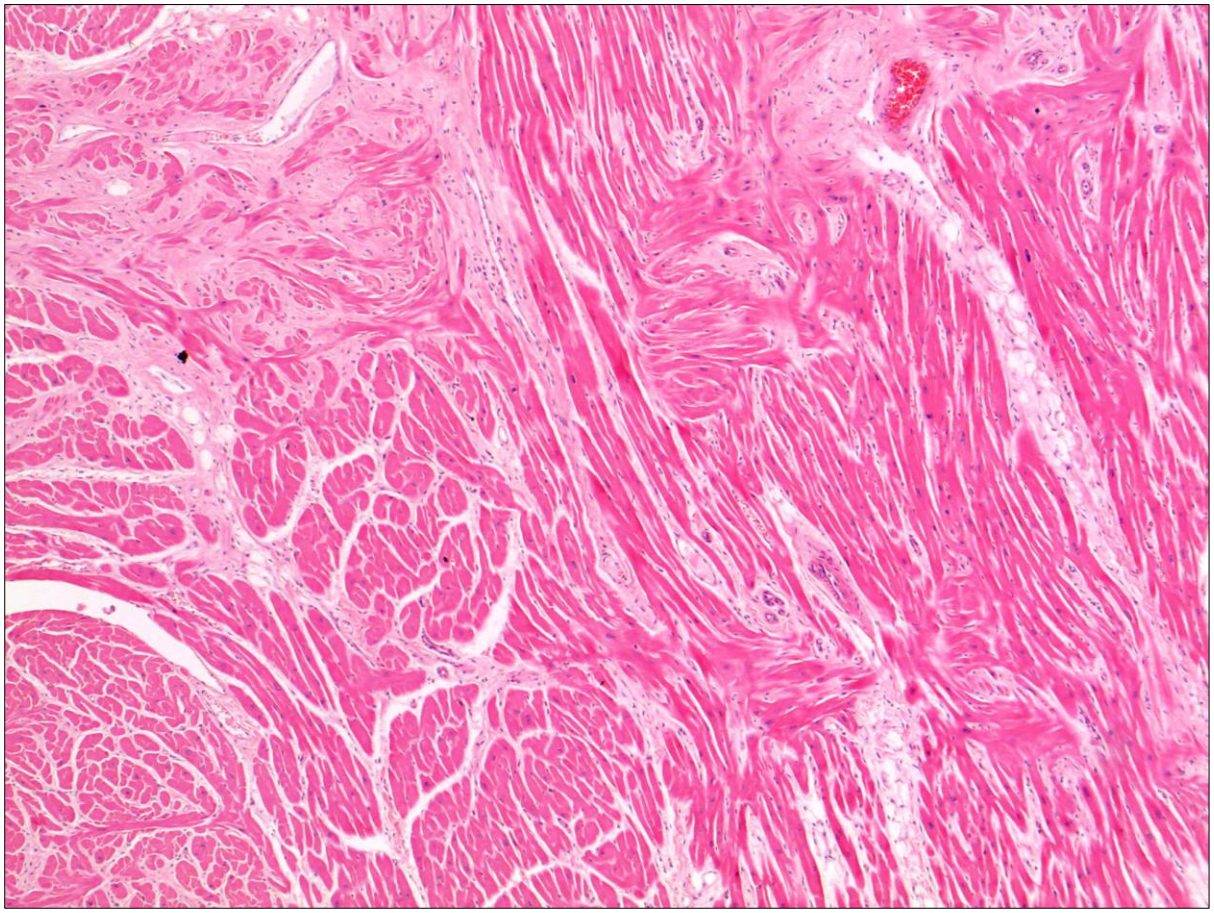

Figure 6.5. Areas of chronic replacement fibrosis and random fibre disarray in C33 (x50 total magnification).

disarray with fibre hypertrophy and was thus diagnosed with primary hypertrophic cardiomyopathy (HCM) (figure 6.5).

Assigned levels of myocardial fibrosis were significantly associated with age (Spearman r=0.61, p=0.003); however, the correlation coefficient was low when considering only adult chimpanzees (Spearman r=0.47, p=0.04). Levels of fibrosis in adult chimpanzees were not associated with heart weight, heart weight/body weight ratio, nor heart circumference. Levels of fibrosis did not appear significantly different

between chimpanzees that died of disease, accident or euthanasia and chimpanzees that died of sudden or perianaesthetic death (Mann-Whitney U=40.5, p=0.2).

Although four animals were reported to die of “sudden death” possible implying sudden cardiac death, one was C27 that presented with syncopes the previous 2 weeks and for which cardiac changes were mostly linked to aortic stenosis (see details below) thus this was ruled out as a case of sudden cardiac death. The other three animals (C23, C37 and C40) who died suddenly presented areas of acute myocytolysis (with associated eosinophil and neutrophil infiltrations), with C37 additionally presenting areas of subacute infarcts with mixed leucocytic infiltrate. C23 and C40 presented areas of contraction band necrosis denoting peracute myocardial necroses. Areas of interstitial and replacement fibrosis with associated leucocytic infiltrates were present in all three hearts.

Histological changes in cardiac vessels were observed in 12 animals. For seven of them, changes consisted in age-related, non-progressive, non-atherosclerotic, clinically silent ‘intimal thickenings’ of the coronary artery (C34, C39) or/and aorta (C25, C26, C29, C30, C42), which consisted of smooth muscle cell proliferation in the intima, and only occasionally well-demarcated subendothelial smooth muscle cell accumulation with scattered foamy macrophages (so-called ‘fatty streaks’ or ‘intimal xanthomas’). C23 presented areas of mineralisation underneath the aortic intima, likely also a reflection of the ageing process (see chapter 7).

Two animals (C33 and C34) presented changes in cardiac vessels compatible with systemic hypertension. Changes were mild in C34 and consisted of scattered intimal and hyaline media thickening of small branches of the coronary arteries. However, C33 (the 47-year-old female that reportedly died of kidney failure) showed marked intimal thickening and arteriolosclerosis in medium-sized branches of the coronary artery in the left ventricle, as well as multifocal hyaline media thickening of small to medium arteries of the interventricular septum. This female also showed evidence of mild to moderate left ventricular hypertrophy and primary HCM (see above).

C24, a 46-year-old female that was euthanised after not recovering fully from an anaesthetic event to investigate an episode of collapse, presented an idiopathic, acute and focally marked leukocytoclastic arteritis with fibrinoid wall necrosis of a major branch of a coronary artery of the right ventricular wall; this may have contributed to

the ischaemic and hypoxic changes leading to acute cardiomyocyte necrosis and observed terminal clinical signs.

Although the presence of occasional small clusters of lymphocytes in the aortic adventitia was considered normal, two animals (C27 and C41) presented mild to moderate lymphocytic perivascular infiltrates around the aortic adventitia, which may be related to a reactive response to the ongoing cardiac failure. C41 also presented multifocal fragmentation of the aortic media and focal extravasation of red blood cell in aortic the media and adventitia (see chapter 3, chimp “C1”).

Table 6.1.Available information and cardiovascular diagnoses on chimpanzee hearts received by the AHP between 2017 and 2020.

Study ID	Sex	Age at death (years)	Body weight (kg)	Recent clinical history/ circumstances of death	Manner/ cause of death	Main reported PM findings	Cardiovascular diagnoses
C21	Female	59	47	Multiple age-related pathologies	Euthanasia	Multiple degenerative changes, atherosclerotic changes in aorta, nephritis, myocarditis	Mild to moderate, diffuse, interstitial fibrosis Mild to moderate multifocal replacement fibrosis and perivascular fibrosis Multifocal, mild, lymphohistiocytic infiltrates
C22	Male	22	50	Chronic colitis	Euthanasia	Emaciation	Multifocal mild, to focally moderate interstitial and replacement fibrosis Acute, multifocal myocardial necrosis
C23	Female	41	55	Sudden death	Natural: sudden	Cerebral haemorrhage, hypertrophic left ventricle (heart), uterine leiomyoma	Chronic asymmetric moderate hypertrophy, left ventricle Diffuse moderate interstitial fibrosis Moderate to focally marked chronic replacement fibrosis with mild lympho-histiocytic and eosinophilic scar-related infiltrate. Multifocal acute cardiomyofibre lysis with neutrophil and eosinophils infiltrates and contraction bands
C24	Female	47	38	Collapse, did not recover from anaesthetic to investigate, euthanised	Euthanasia	Not disclosed	Coronary artery: acute and focally marked leukocytoclastic arteritis with fibrinoid wall necrosis Mild to moderate interstitial, perivascular and multifocal, random replacement fibrosis with minimal to mild mixed inflammatory infiltrate Multifocal acute cardiomyocytes necrosis
C25	Female	21	-	Not disclosed	Euthanasia	Not disclosed	Small focal acute haemorrhage, right ventricle Focal intimal thickening, aorta
C26	Male	28	75	Suspected tetanus	Euthanasia	Many deep wounds	Mild left ventricular hypertrophy Mild to moderate interstitial and replacement fibrosis
C27	Male	48	76	Died suddenly after presenting syncopes the previous 2 weeks	Natural: illness	Mild left ventricular dilatation with mitral and aortic endocardiosis (heart), peracute tracheitis, acute and chronic pulmonary oedema	Mild to moderate cardiomegaly Chronic moderate myocardial fibrosis with mild to moderate lymphohistiocytic infiltrate Chronic moderate aortic stenosis Mitral valve endocardiosis
C28	Male	3	12	Drowned in moat	Accidental	Water and foam in trachea	No abnormalities

Table 6.1 (cont.). Available information and cardiovascular diagnoses on chimpanzee hearts received by the AHP between 2017 and 2020.

Study ID	Sex	Age at death (years)	Body weight (kg)	Recent clinical history/ circumstances of death	Manner/ cause of death	Main reported PM findings	Cardiovascular diagnoses
C29	Female	44	50	Suffered trauma then presented lethargy, anorexia, hepatomegaly, pleural effusion and ascite.	Natural: illness	Subacute to chronic suppurative hepatitis, suppurative interstitial pneumonia, severe diffuse enteritis, gastritis and colitis, chronic glomerulonephritis	Dilated cardiomyopathy Mod to marked interstitial and replacement fibrosis Chronic moderate to marked myofibre atrophy Acute multifocal rhabdomyolysis with contraction bands, mineralisation and marked neutrophilic infiltration. Cartilage and bone formation, atrioventricular node.
C30	Male	22	61	Did not recover from anaesthesia to treat severe wounds	Peri-anaesthetic	Acute pulmonary haemorrhage	Diffuse, mild to moderate, chronic interstitial fibrosis and perivascular fibrosis Multifocal, acute to subacute areas of rhabdomyolysis with contraction bands and mineralisation Multifocal, mild, acute myocardial and epicardial haemorrhages
C31	Female	60 to 65	63	Severe osteoarthritis	Euthanasia	Marked osteoarthritis in several joints	Mild, chronic, diffuse interstitial fibrosis Mild, multifocal replacement fibrosis Multifocal, mild to focally moderate lymphocytic myocardial infiltration Mild to moderate, chronic endocardiosis of the mitral valve
C32	Male	19	69	Died during anaesthesia for tooth extraction	Peri-anaesthetic	Moderate chronic cholangitis with multifocal parasitic hepatic granulomas	Minimal to mild interstitial and replacement fibrosis with scattered, mild lymphocytic infiltrate
C33	Female	47	44	Five day of depression and anorexia due to renal disease	Euthanasia	Moderate chronic active suppurative pyelonephritis, moderate multifocal chronic tubulointerstitial nephritis	Hypertrophic cardiomyopathy Mild interstitial fibrosis Mild to moderate replacement fibrosis with associated fibre disarray and mild mixed leucocytic infiltrate Scattered random intimal and media arterial thickening and arteriolosclerosis
C34	Female	42	48	Sudden loss of hind leg function, no improvement after 10 days	Euthanasia	Subacute extensive occlusive vascular thrombosis (right femoral vessels), focally extensive chronic aortic thrombosis and focal aortic aneurysm (abdominal aorta)	Mild to moderate, chronic, diffuse interstitial fibrosis, perivascular fibrosis Subacute, mild to moderate to focally marked replacement fibrosis with granulation tissue formation and scattered fibre mineralisation Area of cartilage formation around atrioventricular node Mild to moderate chronic mitral valve endocardiosis.

Table 6.1 (cont.). Available information and cardiovascular diagnoses on chimpanzee hearts received by the AHP between 2017 and 2020.

Study ID	Sex	Age at death (years)	Body weight (kg)	Recent clinical history/ circumstances of death	Manner/ cause of death	Main reported PM findings	Cardiovascular diagnoses
C35	Female	40	82	Apnoea and cardiac arrest on anaesthesia induction	Peri-anaesthetic	Moderate pulmonary oedema with inflammatory infiltrate and haemosiderin	Mild to moderate, focally extensive replacement fibrosis Minimal to mild interstitial fibrosis
C36	Female	10	41.5	Suspected encephalitis	Natural: illness	Large abscess near pharynx	Small, focal, acute infarct within interventricular septum
C37	Male	24		Found dead after display	Natural: sudden	Haemorrhage in thoracic and abdominal cavity	Chronic mild to focally moderate replacement fibrosis, mild interstitial fibrosis Multifocal acute to subacute ischemic infarcts with mixed leucocytic infiltrate
C38	Female	40	37.5	Diabetic, euthanised due to weight loss and lethargy.	Euthanasia	Not disclosed	Min to mild interstitial fibrosis Multifocally extensive acute contraction band necrosis Focal epicardial chronic granulation tissue formation
C39	Female	33		Died on anaesthesia induction	Peri-anaesthetic	Renal carcinoma, marked glomerulonephritis.	Chronic, mild to moderate interstitial fibrosis with mild, multifocal replacement fibrosis Chronic, minimal to mild mitral valve degeneration Focal cardiac melanoma metastasis, tricuspid valve
C40	Male	52		Sudden death	Natural: sudden	Acute severe congestion and oedema of right lung lobe	Chronic, multifocal, random, moderate replacement fibrosis Chronic, diffuse, moderate interstitial fibrosis Acute, multifocal, random, cardiomyofibre degeneration
C41	Female	41	43	Loss of function of left arm, lethargy	Euthanasia	Occlusive thrombus of the left axillary artery	Chronic, multifocal, marked replacement fibrosis with interstitial and perivascular fibrosis Acute, multifocal contraction band necrosis, oedema, and multifocal acute myocytolysis Chronic, mild to focally moderate lymphocytic pericarditis and aortic perivasculitis and focal, acute adventitial haemorrhage
C42	Female	41	46.6	Hypotensive shock during anaesthesia to investigate leg paralysis, lethargy and bloody diarrhoea	Peri-anaesthetic / illness	Severe acute transmural necrosuppurative colitis; fibrinoid vascular thrombosis and haemorrhage (left foot), acute and subacute haemorrhages in lung and adrenal gland	Chronic, moderate to marked, multifocal, random replacement fibrosis with occasionally subacute granulation tissue formation Chronic, marked, interstitial fibrosis Subacute venous thrombosis (medium to large vein of left ventricular myocardium) Acute, mild cardiomyofibre degeneration with occasional neutrophilic infiltration

C27, a case of aortic stenosis and cardiomegaly

C27 was a 47-years old male chimpanzee that died suddenly after having suffered several episodes of syncopes during the previous 2 weeks. Although the quality of the received heart was not optimal, an impression of cardiomegaly and thickened ventricular walls were noticed on macroscopical examination, and a large amount of fat was covering most of the epicardium (figure 6.6). Firm small nodules were palpable on the mitral valve leaflet, the posterior leaflet of the tricuspid valve was mildly hardened, and the left coronary cusp of the aortic valve was diffusely thickened and stiffened by moderately increased fibrous tissue, which was diagnosed as chronic, moderate aortic stenosis (figure 6.7). Histologically, the left ventricle showed mild interstitial fibrosis, perivascular fibrosis and mild to moderate, multifocal replacement fibrosis with random mild inflammatory infiltrates and fatty cores in some areas. In the septum and free ventricular walls, myofibres presented mild to moderate nuclear hypertrophy. Focally within the right ventricle, there was an area of acute cardiomyocyte necrosis with mixed cellular infiltrate. Small clusters of lymphocytes were visible in the epicardium and multifocally within the myocardium. The aortic adventitia showed a mild to moderate lymphocytic perivascular infiltrate. The mitral valve was multifocally thickened by increase fibroblastic cells and collagen deposition (mild endocardiosis).

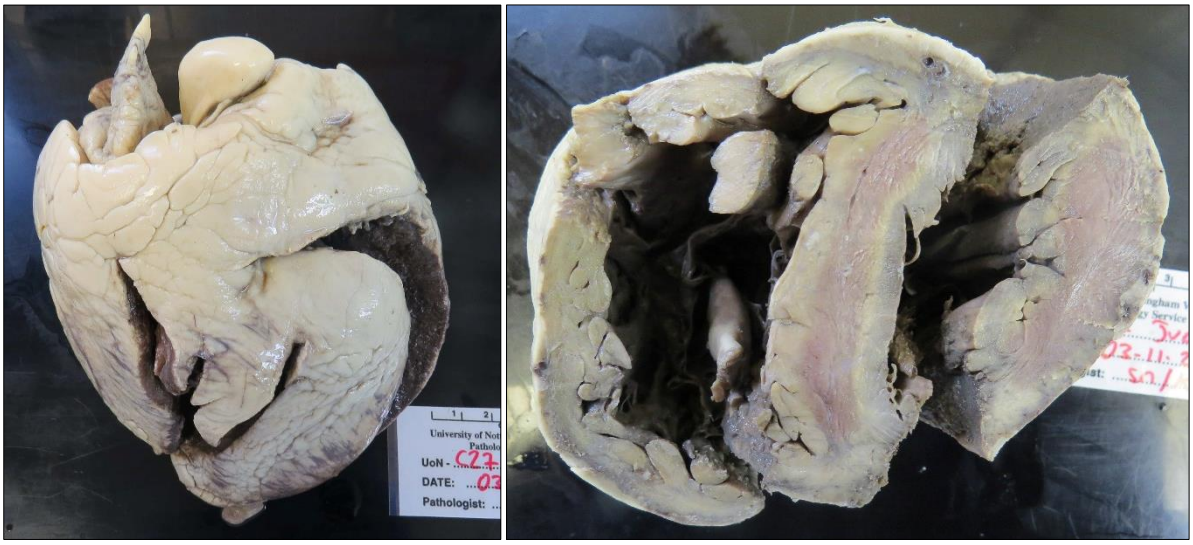

Figure 6.6. Macroscopical aspect of C27 heart. Level of epicardial fat was ranked as 3/3. The heart appeared rounded and ventricular walls appeared thickened.

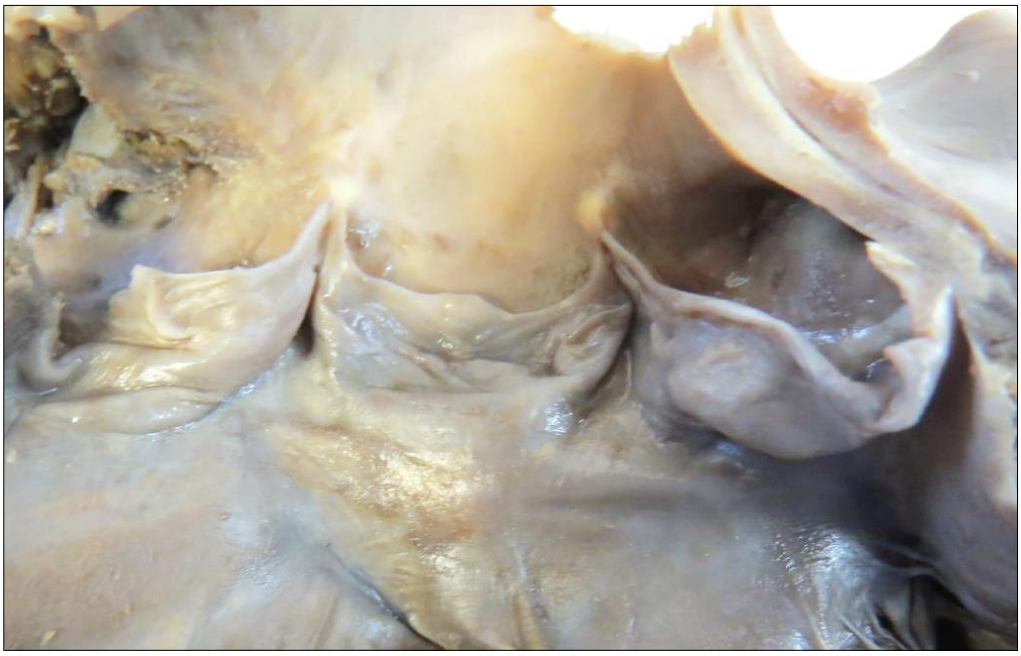

Figure 6.7. Aortic valve of C27 with thickened and stiffened left cusp denoting moderate aortic stenosis.

Aortic stenosis in humans usually develops later in life with potentially serious consequences like syncopes. C27 left ventricular hypertrophy was likely due to the volume overload and the right ventricular hypertrophy a consequence of pulmonary hypertension due to the left elevated end-diastolic pressure. It remains unclear whether C27 myocardial fibrosis could be related to the aortic stenosis leading to diastolic and systolic dysfunction.

C29, a case of dilated cardiomyopathy

C29 was a 44-year-old female chimpanzee that was reported to have died with suppurative interstitial pneumonia, severe subacute to chronic necrotizing and suppurative hepatitis and haemorrhagic gastroenteritis after having suffered traumas inflicted by other chimpanzees.

On macroscopical examination, the left atrium and the left ventricle seemed moderately dilated (see figure 6.8), and the circumferences of the mitral valve and tricuspid valve were on the high end of the usual range noted in our chimpanzee group (10 and 12.5 cm respectively).

Figure 6.8. Myocardial cross section of C29. Note the impression of dilation of the left chamber.

On histological examination, areas of moderate to marked replacement fibrosis were observed multifocally throughout the myocardium together with diffuse, moderate to marked interstitial fibrosis. In the left ventricle and right ventricular outflow tract, there were scattered areas of acute myocytolysis with neutrophilic infiltration and prominent areas of contraction band necroses corroborating acute terminal cardiac failure and damage. Within the left ventricular and septal myocardium were prominent areas of thin, wavy fibres with loss of myofibrils while other areas showed fibre and nuclear hypertrophy indicating a potential end-stage phase of a decompensating previous left ventricular hypertrophy. An area of cartilage and bone formation was present in the vicinity of the atrioventricular node (please see chapter 7 for discussion).

C39, a case of focal cardiac metastasis of melanoma.

C39 was a 33-year-old female chimpanzee that died during induction of anaesthesia. Unfortunately, very little clinical information was made available from the zoo of origin, but a renal carcinoma was reported to have been found on post-mortem examination.

The AHP received a full heart, with a moderate to large amount of fat present in the atrioventricular groove and extending along the course of the coronary arteries. The left ventricular wall appeared mildly thickened and the mitral valve presented mild thickening of the margin of the anterior cusp. The septal cusp of the tricuspid valve presented a nodule of approximate 1cm of greater diameter (figure 6.9).

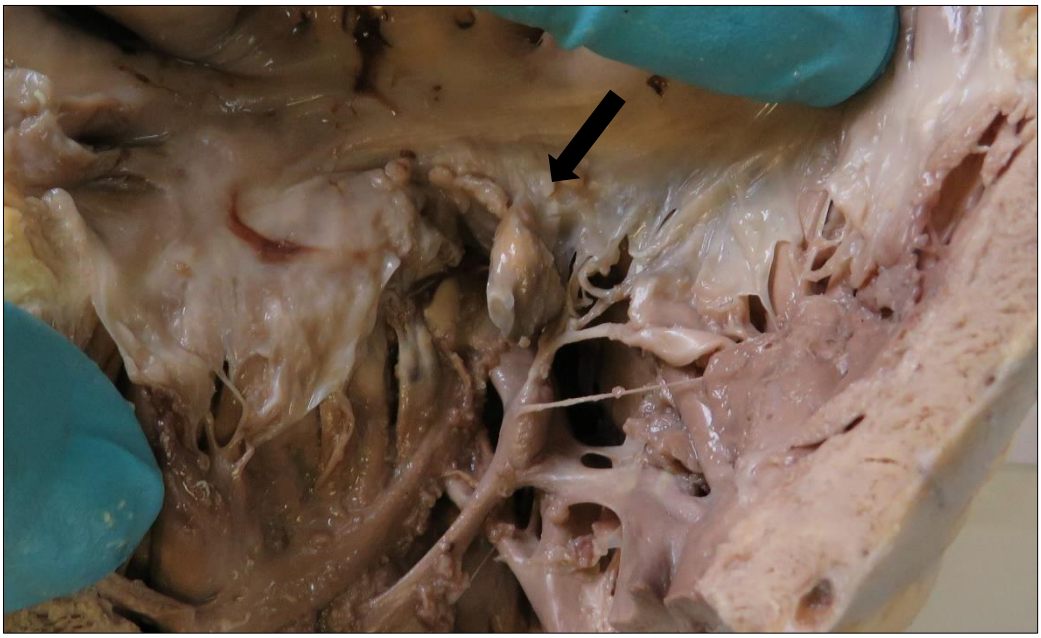

Figure 6.9. Melanoma metastasis on the tricuspid valve of C39 (arrow).

On histopathology, C39 presented chronic, mild to moderate interstitial fibrosis with mild, multifocal replacement fibrosis as well as minimal to mild, nodular myxomatous mitral valve degeneration (endocardiosis). On the tricuspid valve, there was a focal proliferation composed of a dense capillary network, a round cell infiltrate and sheets of black pigment containing polygonal epithelioid cells with distinct cell margins and a round to oval, often large irregular euchromatic nucleus with an eccentric, prominent nucleolus embedded in pre-existing stroma. This focal proliferation expanded markedly the affected leaflet of the tricuspid valve. Mitotic activity was 2 per 10 High Power Fields but likely obscured by the pigment content. An additional Perl's Blue and Masson Fontana stain was performed and was negative for haemosiderin and positive for melanin, thus findings were interpreted as melanoma metastasis.

It is highly likely that this tumour on the tricuspid valve will have markedly hampered cardiac function and contributed to the terminal cardiac failure. In humans, melanomas show a high rate of cardiac metastasis, and interestingly there is a reported strong

association between the diagnoses of renal cell carcinoma and melanomas, but the mechanisms for this association is still unclear (Kim et al. 2018).

6.3.2. Gorillas

General findings

Between 2017 and 2020, 14 formalin-fixed gorilla hearts from European zoos were received and examined (6 males, 8 females). Animal ranged from 1 year to 58 years in age (mean 32 year ±17 years), with a bodyweight ranging from 7.2 to 183 kg (mean 99.44kg ±63.24kg). Results are summarised in table 6.2. Eleven out of fourteen animals were considered adults. Sample quality was very varied, from sampled exactly as per project protocols (n=8) to hearts having suffered extensive previous sectioning, sampling or deformation due to inadequate storage (n=4).

The fat content on the epicardial surface and coronary groove was good for most animals, with five animals having a large amount of fat and only two animal having little fat present (G18 and the newborn gorilla).

Mean adult fixed heart weight was 702.6g ± 268.7g and mean adult fixed heart weight/body weight ratio was 0.61% (SD 0.18%). Adult heart circumference ranged from 27 to 35 cm (mean 33.19 ± 11.15cm). Mean adult wall thicknesses were 1.32 cm (±0.41), 1.29 cm (± 0.35) and 0.28 cm (± 0.11) for the left ventricle, interventricular septum, and right ventricle, respectively.

In adults, mitral valve circumference ranged from 7.5 to 13 cm (mean 9.78, SD 1.64), tricuspid valve circumference ranged from 10 to 15cm (mean 11.85, SD 1.6), aortic valve circumference ranged from 5.5 to 8cm (mean 7.01, SD 0.8), and pulmonary valve circumference ranged from 6.5 to 9 cm (mean 7.36, SD 0.67).

The severity of interstitial and replacement myocardial fibrosis ranged from minimal to mild/moderate, except for one individual, G8, that presented moderate to marked replacement and interstitial fibrosis (see case detailed below).

Levels of interstitial fibrosis did not correlate with age (Pearson r=0.52; P=0.056) but did show a positive correlation with body weight (Pearson r= 0.64; p=0.035). Levels of IF also showed a significant positive correlation with fixed heart weight (Pearson r=0.83; P=0.003), left ventricle thickness (Pearson r=0.64; P=0.013) and interventricular septum thickness (Pearson r=0.58; P=0.029). Levels of replacement

fibrosis did not correlate with age nor body weight. Although levels of replacement fibrosis showed a positive correlation with fixed heart weight (Pearson r=0.66; P=0.037) it did not correlate with other heart measurements.

Inflammatory infiltrations within the myocardium were present in 7/14 hearts. Most infiltrates were low grade, mixed and associated with areas of fibrosis, granulation tissue or areas of rhabdomyolysis. G8 however, presented moderate mixed infiltration (see case detailed below). G17 presented focally prominent clusters of lymphocytes within subendocardial areas of the left ventricle and interventricular septum. The aetiopathogenesis of these lymphocyte infiltrates were ambiguous, as they did not appear to be inflammatory, but no lymphoproliferative disease had been reported elsewhere in this animal.

Two animals suffered from endocarditis: G7, the newborn male with suspected sepsis, presented a focal mild acute neutrophilic endocarditis with focal haemorrhage in the mitral valve and G10, a 52-year-old female that died two days after a tooth extraction, presented a chronic, mild endocardiosis and subacute, moderate, fibrinous endocarditis of the mitral valve.

Small fenestrations in pulmonary and/or aortic valve leaflets were observed in four animals (G11, G14, G16, G18) and are a common change in older hominids (Seki and Fishbein 2016) (figure 6.10).

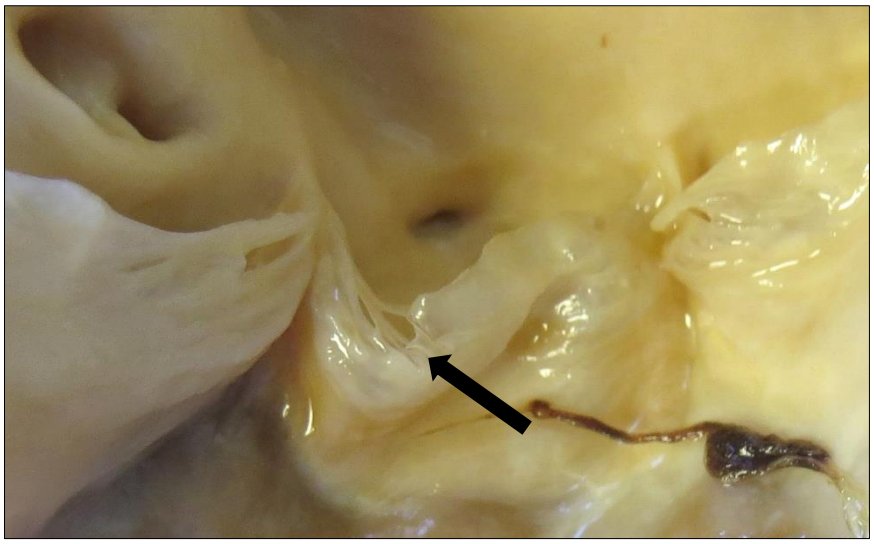

Figure 6.10. Valvular fenestration (arrow), aortic valve.

Vascular changes were observed in seven animals (50%).

Small vessel changes (microangiopathies) were seen in four animals (G6, G8, G11 and G14) and consisted of arteriolosclerosis. Multiple small to middle size arteries within the left ventricular and interventricular myocardium of G6 showed hyaline changes of vascular walls often associated with increased perivascular fibrosis (Figure 6.11); this, together with the findings of marked renal fibrosis and glomerulosclerosis with signs of hyaline and proliferative arteriolosclerosis in the kidneys, pointed towards systemic hypertension in that case.

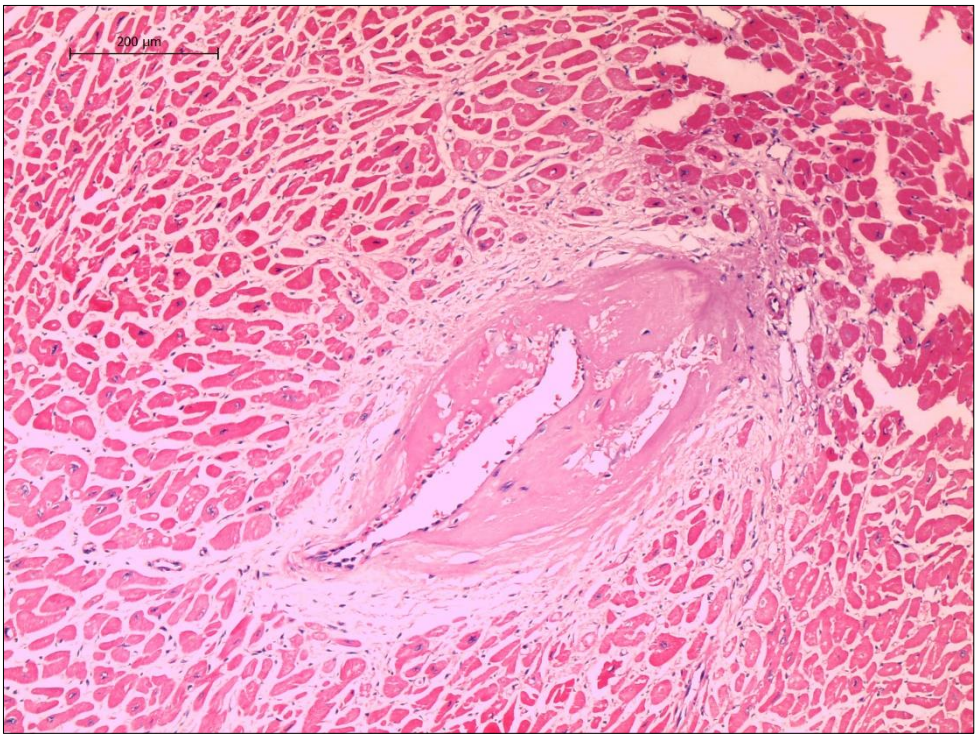

Figure 6.11. Hyaline arteriolosclerosis of a small branch of the coronary of G6. Haematoxylin-eosin x100.

Chronic medium to large vessel changes were also commonly observed. Multifocal intimal thickening was seen in coronary arteries of G10, G14, G15 and G17, and coronary atherosclerosis in G10 and G14. Mild cystic media degeneration was seen affecting the aorta of three animals (G8, G11, G17): focally, elastic fibres were pale, fragmented and disorganised.

Two animals had marked acute changes affecting the ascending aorta: G11 suffered an acute aortic dissection leading to a fatal cardiac tamponade, while G18 presented an isolated aortitis which had never been described before in great apes but in humans (these cases are detailed further below).

Table 6.2. Available information and cardiovascular diagnoses on gorilla hearts received by the AHP between 2017 and 2020.

Study ID	Sex	Age at death (years)	Body weight (kg)	Recent clinical history/ circumstances of death	Manner/ cause of death	Main reported PM findings	Cardiovascular diagnoses
G6	Male	32.93	183	Died on recovery from anaesthesia to suture wound	Peri-anaesthetic	Congestive lungs, large amount of internal fat	Diffuse mild to moderate myocardial interstitial fibrosis Minimal mild multifocal replacement fibrosis Multifocal hyaline changes of vascular walls with increased perivascular fibrosis (small to medium arteries)
G7	Male	0.99	7.2	Sudden onset of lethargy followed by death	Natural: illness	Acute purulent bronchitis and hepatitis, chronic interstitial nephritis	Focal mild acute neutrophilic endocarditis and focal haemorrhage in the mitral valve.
G8	Female	41.30	111	On treatment for heart disease and pulmonary hypertension, suspected CHF	Natural: illness	Generalised oedema, free fluid in thorax, plaques in abdominal aorta.	Multifocal, random, moderate to marked replacement fibrosis associated with fibre and nuclear hypertrophy Moderate perivascular and interstitial fibrosis with mild to moderate mixed leucocytic infiltrates Focal, subacute granulation tissue formation with focal endocarditis (left atrium) Scattered vascular hyalinosis
G9	Female	1.43	8	Severe diarrhoea unresponsive to treatment	Natural: illness	Severe proliferative and ulcerative necrotizing colitis, thoracic effusion	No abnormalities detected
G10	Female	51.82	n/a	Died 2 days after teeth extraction	Natural: illness	Not disclosed	Chronic mild endocardiosis and subacute, moderate, fibrinous endocarditis of the mitral valve Minimal, chronic, interstitial fibrosis with mild to focally moderate replacement fibrosis Coronary intimal thickening and atherosclerosis
G11	Male	34.66	170.6	Sudden death	Natural: sudden	Pulmonary oedema, haemopericardium, haemorrhagic pancreas	Moderate interstitial and replacement fibrosis Acute aortic dissection Scattered media thickening and hyalinisation in small to medium arteries
G12	Male	14.35	146	Acute abdominal pain followed by death within 2 days	Natural: illness	Acute peritonitis	Minimal interstitial fibrosis Multifocal rhabdomyolysis in interventricular septum

Table 6.2 (cont.). Available information and final cardiovascular diagnoses on gorilla hearts received between 2017 and 2020.

Study ID	Sex	Age at death (years)	Body weight (kg)	Recent clinical history/ circumstances of death	Manner/ cause of death	Main reported PM findings	Cardiovascular diagnoses
G13	Female	58.70	78	Increased lethargy in the last 2 weeks before death	Natural: illness	Perforating ulcer in jejunum with fibrinous peritonitis	Minimal to mild, multifocal, perivascular and replacement fibrosis
G14	Female	38.67	81	Weight loss, lethargy and abdominal mass	Euthanasia	Presumptive ovarian tumours	Minimal interstitial and replacement fibrosis Mild scattered media hyaline thickening in small to medium arteries Coronary intimal thickening and atherosclerosis Aortic intimal thickening
G15	Male	32.45	n/a	Chronic enteritis unresponsive to treatment, poor body condition	Euthanasia	Severe chronic segmental granulomatous enteritis	Minimal to mild interstitial fibrosis Aortic intimal thickening
G16	Female	35.96	61.5	Marked weight loss, lesions compatible with herpes simplex, diarrhoea	Euthanasia	Gravid uterus, herpes simplex infection (skin), marked liver steatosis, focal severe bronchopneumonia, chronic enteritis.	Multifocal, chronic minimal to mild replacement fibrosis
G17	Female	46.00	n/a	Died during anaesthesia to investigate chronic GI issues and cachexia.	Peri-anaesthetic	Not disclosed	Chronic, diffuse mild to moderate interstitial fibrosis Mild, multifocal, random replacement fibrosis Mild to moderate, multifocal lymphocyte infiltration Scattered media hyperplasia of medium size arteries Scattered mild to moderate coronary intimal thickening
G18	Female	41.13	72	Weight loss, cough, pleural effusion	Euthanasia	Pulmonary oedema and chronic hepatic congestion related to cardiac insufficiency, aortic arteriosclerosis	Mild interstitial fibrosis and multifocal mild to moderate replacement fibrosis Mild, multifocal chronic-active lymphoplasmacytic epicarditis, pericarditis and epicardial fibrosis Marked, chronic-active, granulomatous aortitis with acute ischaemic degeneration, atheromatous plaques and thrombosis
G19	Male	21.94	175.5	Fibrinosuppurative peritonitis and necrotic bowel	Euthanasia	Rupture of intra-abdominal abscess leading to septic peritonitis	No abnormalities detected

G8, a case of congestive heart failure

G8, a 41-year-old female lowland gorilla, was the only gorilla in this study with known heart disease. She had reportedly been diagnosed with severe pulmonary hypertension and heart disease a few months before death and was treated with angiotensin-converting enzyme (ACE) inhibitor ramipril and beta-blocker carvedilol. Recently, the diuretic furosemide was added to her treatment due to the presence of subcutaneous oedema. Post-mortem examination carried out at the University of Bristol led to a diagnostic of congestive heart failure as it revealed extensive marked subcutaneous oedema affecting the whole carcass, the presence of several litres of fluid in the peritoneal and pleural cavity, and a swollen liver. One area of a firm, white and yellow streak was found in the abdominal aorta, but the heart was reported as grossly normal.

A good quality fixed heart was received by the AHP, showing an overall normal shape with a large amount of adipose tissue covering most of the epicardium. Although the shape of the heart was unremarkable, the fixed heart weight as 991g and was the highest of our gorilla cohort in relation to body weight. Across the myocardium, several paler areas were observed. A large blood clot was present in the left atrium, sticking to the atrial wall and when removed, the endocardium underneath presented with an area of red discolouration compatible with ecchymotic haemorrhages (Figure 6.12).

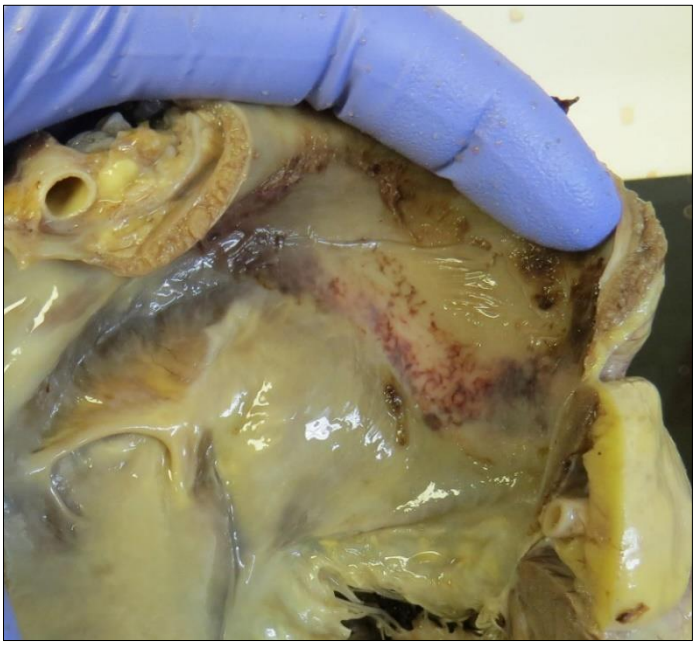

Figure 6.12. Multifocal haemorrhages in G8 left atrial wall.

Microscopically, the left ventricular myocardium and interventricular septum showed multifocal, random, moderate to marked areas of replacement fibrosis, moderate perivascular fibrosis and moderate, diffuse interstitial fibrosis (Figure 6.13). Areas of replacement fibrosis were associated with mild fibre and nuclear hypertrophy and mild to focally moderate, mixed leukocytic infiltrates (lymphocytes, histiocytes, and lesser eosinophils and neutrophils). Focally within the left ventricular wall, an area of replacement fibrosis showed a fatty core indicating a long-standing scar. The right ventricular myocardium showed mild replacement and interstitial fibrosis with a moderate number of mixed infiltrating leucocytes. Multifocal, small acute haemorrhages were visible within the myocardium of the right outflow tract. Focally within the left atrial wall, the subendocardial space was markedly expanded by subacute granulation tissue with prominent neovascularisation, eosinophils, lymphocytes and histiocytes. The endocardium was thickened and infiltrated by neutrophils and lymphocytes, showed multifocal acute haemorrhages and focal prominent fibrin exudation (corresponding to the area of red discolouration seen macroscopically; extensive acute to subacute atrial thrombus with underlying infarction). Although G8 heart's shape appeared normal, findings of the histopathological examination confirmed chronic degenerative heart disease in this animal, as the level of myocardial interstitial and replacement fibrosis likely contributed to a decline in heart function and ultimately congestive heart failure. Changes in the left atrium were focal and some days to few weeks old but suggest previous atrial thrombi formation and focal infarction of the associated left atrial wall.

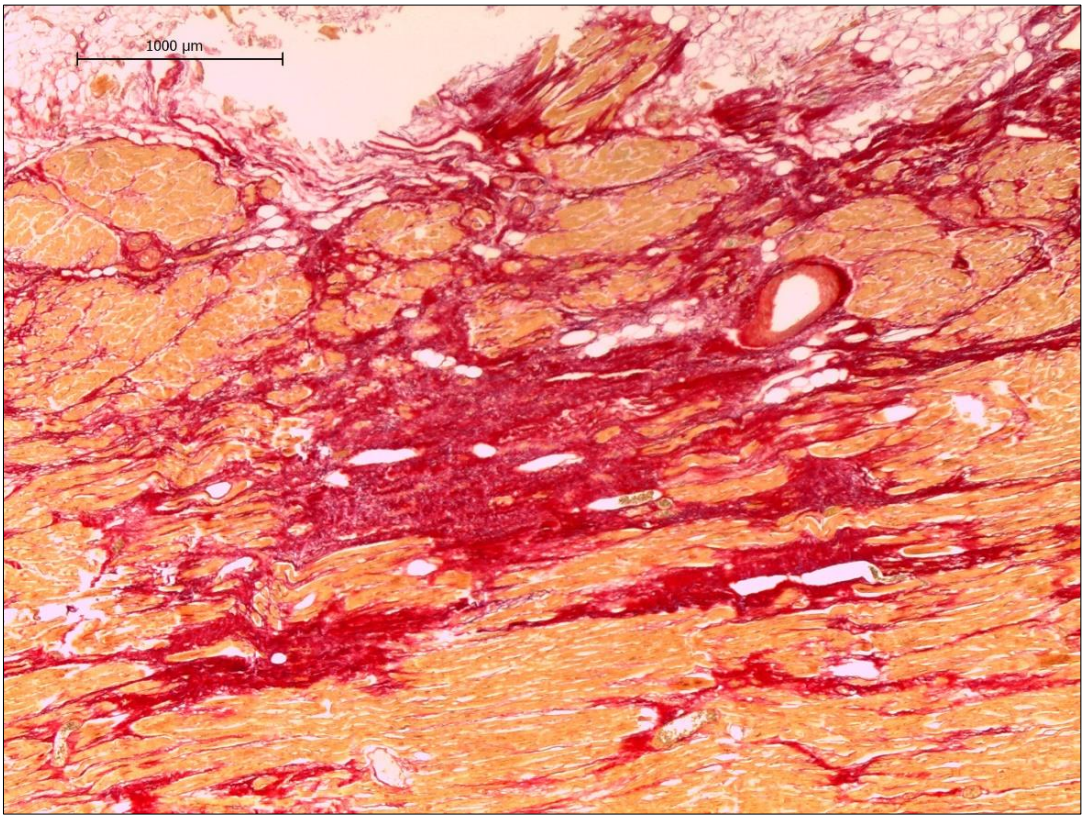

Figure 6.13. Replacement fibrosis in G8 myocardium. Picrosirius red stain, x50.

G11, a case of aortic dissection

The heart of a 34-years old male lowland gorilla that died suddenly was submitted to the AHP. Main reported post-mortem findings were pulmonary oedema, haemopericardium (410ml), severely haemorrhagic pancreas, and multiple antemortem and post-mortem skin wounds. The whole heart cut as per AHP protocol was received. The pericardium, epicardium and vascular adventitia at the base of the heart were dark red and extravasated blood was present underneath these structures. Blood extravasation was visible expanding the adventitial tissue of the ascending aorta, proximal pulmonary artery and epicardial tissue at the base of the heart and an aortic tear was identified (Figure 6.14).

Microscopically, within the left ventricular myocardium, there was mild to focally moderate random replacement fibrosis. Within the anterior left ventricular myocardium, one focally extensive area of replacement fibrosis was associated with reactive fibre disarray and mild to moderate, mixed leucocytic infiltrate was observed. There was diffuse mild to moderate interstitial fibrosis which in the anterior septum was associated with mild fibre disarray and scattered lymphohistiocytic infiltrate. One

area of subendocardial replacement fibrosis was also observed in the posterior septum. Scattered small to medium size arteries showed hyalinisation and thickening of the tunica media. A focally extensive haemorrhage was visible within the atrioventricular node, in the separation between the pulmonary artery and the pericardium and between the pericardium and the base of the great vessels. The aorta presented a moderate disorderly collagen arrangement and blood covering the adventitia. Focally, there was a separation of the media and this area was filled with blood which was likely the source of the observed pericardial bleed and cardiac tamponade.

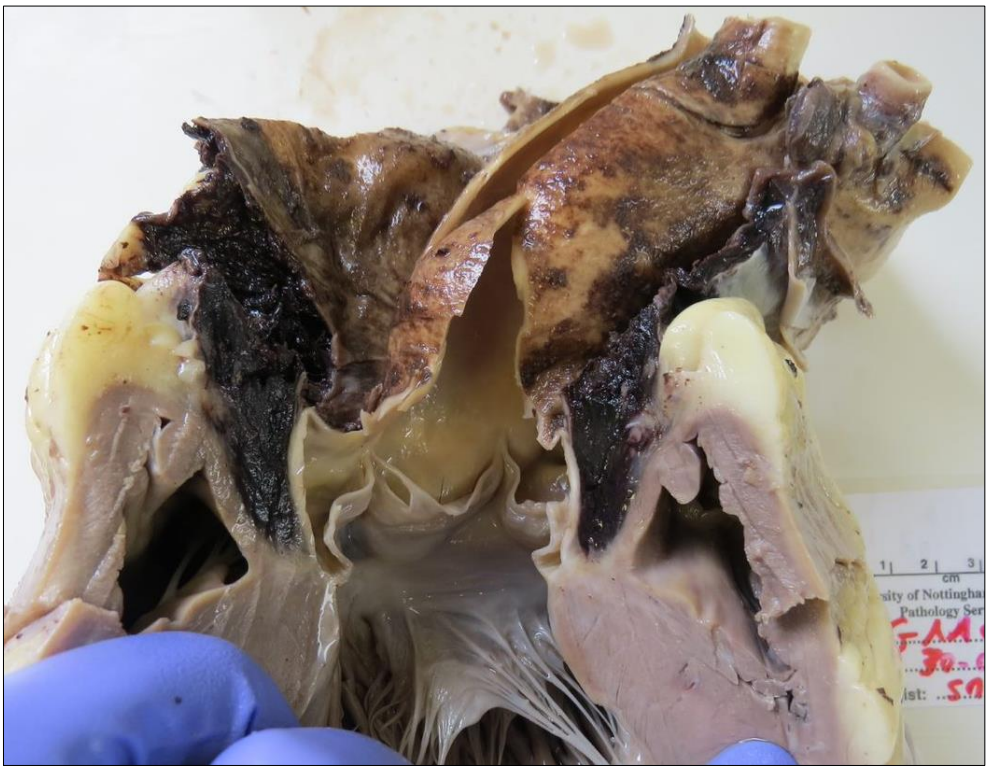

Figure 6.14. G11 heart base showing blood extravasation due to aortic dissection.

G18, a rare case of non-infectious necrotising and granulomatous aortitis

This case was published as a case report in the Journal of Comparative Pathology https://doi.org/10.1016/j.jcpa.2020.09.009 (Moittié et al. 2020c).

G18 belonged to a 41-year-old female Western lowland gorilla (*Gorilla gorilla gorilla*), that was euthanised due to pleural effusion of uncertain origin and continuous weight loss over several months. Reported post-mortem findings included moderate hydrothorax, mild pericardial adhesions, mild left ventricular dilation, moderate, acute pulmonary oedema, and thickened and irregular intima of the ascending aorta.

When received by the AHP, G18's heart had already undergone sectioning and sampling. The aorta appeared opened by several cuts which hampered the macroscopic evaluation of a possible aortic arch aneurysm; however, aortic valve circumference appeared inconspicuous. The ascending aortic wall was thickened and the intima presented a rugged, coarse texture with raised areas (so-called 'tree bark' appearance; Figure 6.15) (Maksimowicz-McKinnon and Hoffman 2012; Stone et al. 2015).

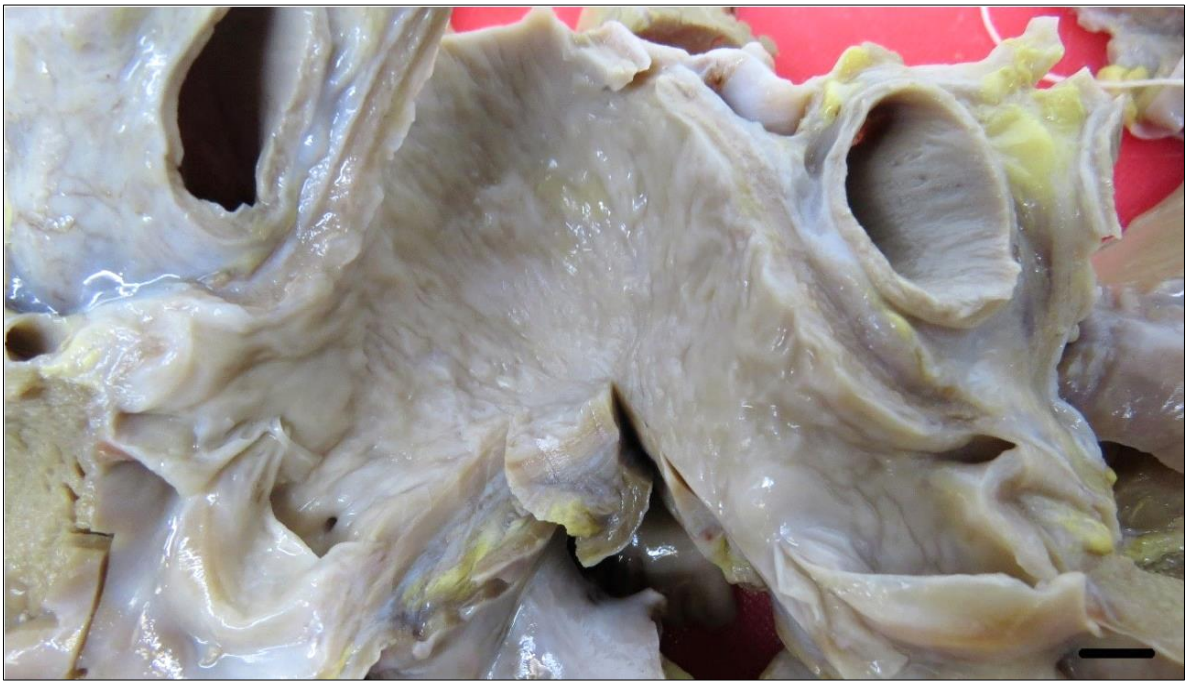

Figure 6.15. Ascending aortic wall is thickened and the intima presents a rugged, coarse texture with raised areas, so called 'tree bark' appearance. Bar, 1cm

Other large and medium-sized vessels such as coronary arteries and the pulmonary artery as well as the heart itself including other valvular structures presented no significant macroscopic abnormalities. Twenty samples were taken for histopathology,

including eight transverse, full-thickness sections from the ascending aorta, periaortic and pericardial tissues. All routinely processed sections were stained with haematoxylin-eosin with four aortic samples also being stained with Elastic Van Gieson, Ziehl-Neelsen, Periodic Acid-Schiff, Gram and Warthin-Starry stains using adequate positive controls and established staining methods (Morris et al. 2018).

Histological examination revealed marked inflammatory changes in the ascending aorta. Multifocally to coalescing, the aortic intima was thickened by proliferating vascular smooth muscle cells with prominent deposition of extracellular matrix, occasional foamy macrophages and patchy infiltrations of viable and often degenerated neutrophils (figure 6.16). Multifocally, and often correlated with the neutrophil infiltration, these intimal thickenings were covered by variably sized amounts of fibrin, consistent with disrupted atherosclerotic inflammatory plaques with acute surface thrombosis.

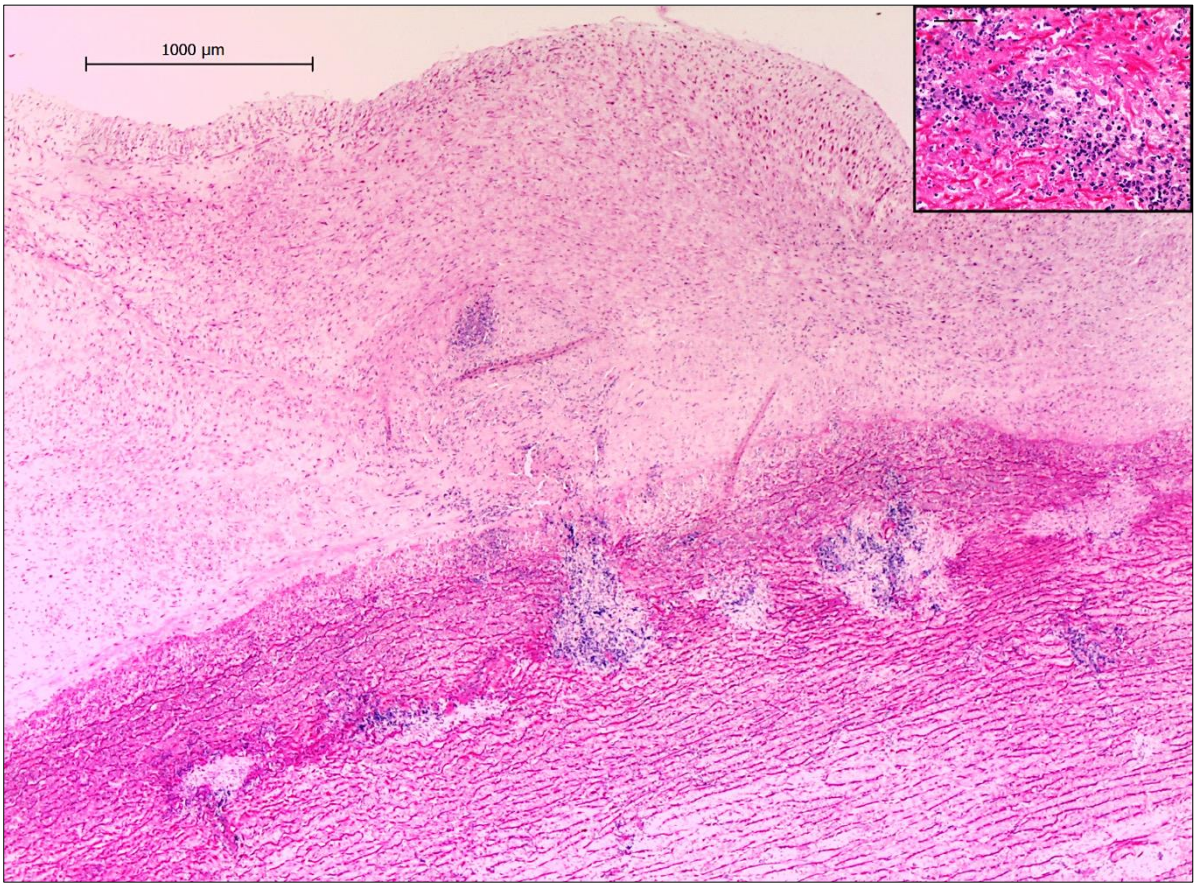

Figure 6.16. Multifocal acute inflammation and necrosis of the inner media with spill over of inflammatory infiltrates into the irregularly thickened intima. HE. Bar, 1000µm. Inset: Large numbers of degenerating neutrophils and lesser epithelioid macrophages are associated with acute necrosis. HE. Inset bar, 50µm.

Predominantly affecting the inner half of the tunica media, elastic fibres and smooth muscle cells were multifocally lost with replacement by dense infiltrates of degenerating neutrophils (acute florid media degeneration and necrosis) (figure 6.16) or mixed clusters of epithelioid macrophages with scattered multinucleated cells, variable lymphoplasmacytic infiltrates and scattered neutrophils (chronic-active granulomatous aortitis) (Figure 6.17). Other medial areas showed deposition of collagen (interpreted as scarring), dark grey bluish, amorphous material (interpreted as dystrophic mineralisation) and revascularisation (extension of vasa vasorum into the media) (Figure 6.18).

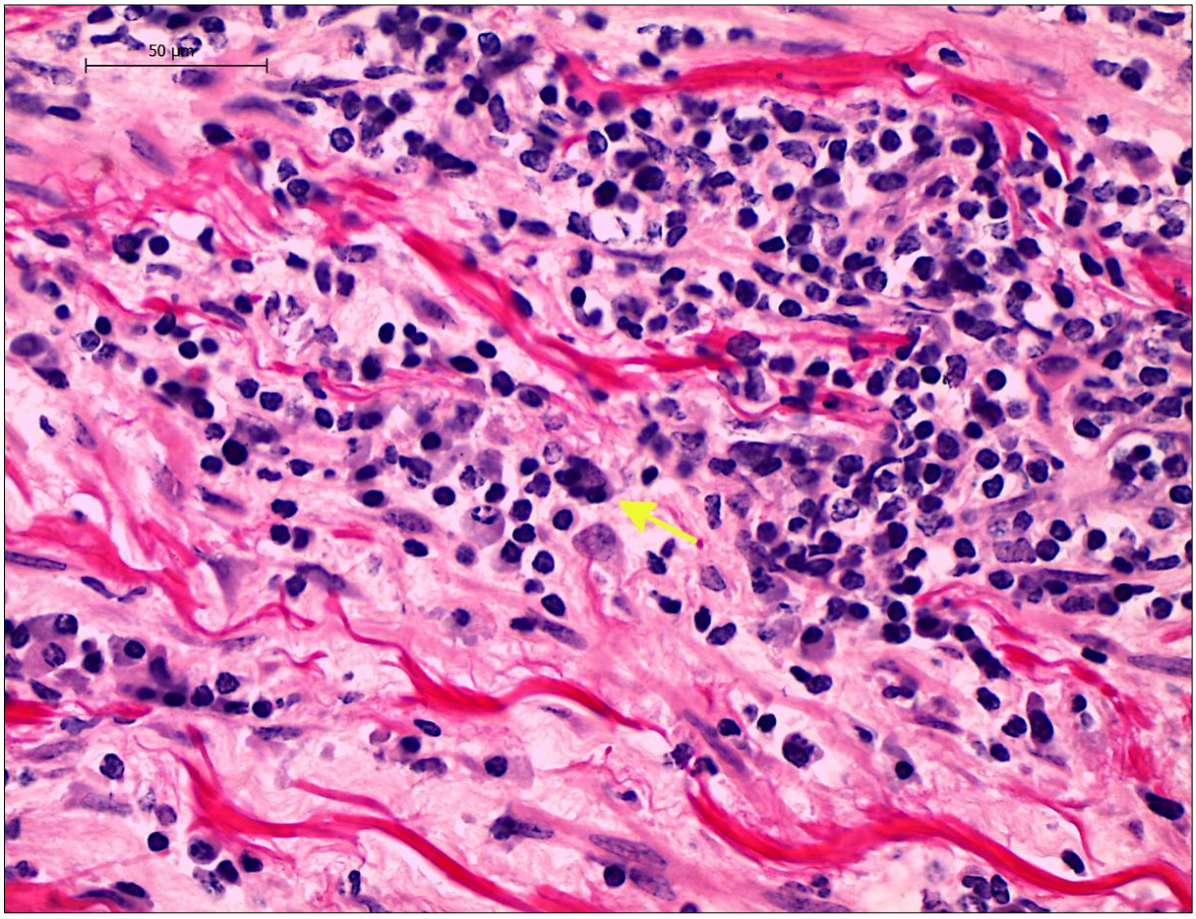

Figure 6.17. Granulomatous aortitis with multinucleated macrophages (yellow arrow) and a lymphoplasmacytic infiltrate. HE. Bar, 50µm.

Within the aortic tunica adventitia, there was mild to moderate perivascular infiltration of mainly lymphocytes and plasma cells with lesser macrophages and neutrophils. The media of vasa vasora was occasionally markedly thickened and the lumina appeared occluded (obliterating endarteritis).

All additional stains of aortic tissue for infectious agents were negative and there was no evidence of vasculitis in any other body organs or any other changes consistent with systemic diseases like rheumatoid arthritis or systemic lupus erythematosus that may involve inflammatory aortic changes (Stone et al. 2015). Sections of the pulmonary artery and coronary arteries showed no inflammatory or degenerative changes.

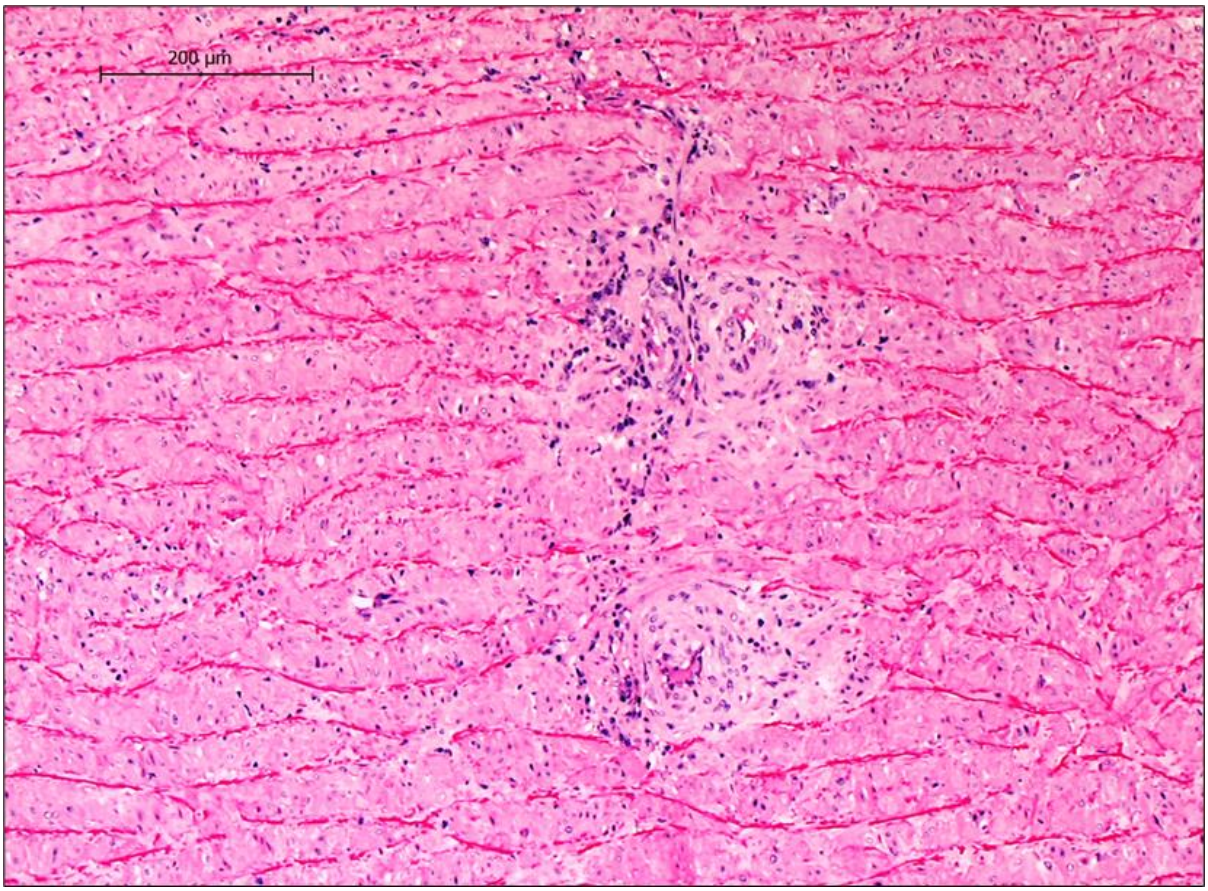

Figure 6.18. Revascularisation with vasa vasorum deeply extending (accompanied by inflammation) into the tunica media of the ascending aorta. HE. Bar, 200µm.

Changes in the heart were mild and mostly associated with the age of the animal (Schulman et al. 1995; Strong et al. 2017) but also likely aggravated by the ongoing inflammatory changes affecting the aorta likely causing cardiovascular functional deficiencies. Within the mid-portion of the left ventricular and septal myocardium, there was mild interstitial fibrosis and mild nuclear hypertrophy in addition to normal variation of cardiomyocyte nuclei in hominids. Multifocal small areas of replacement fibrosis were visible in the lateral and posterior left ventricle with one moderate area of granulation tissue observed in a minor papillary muscle. The right ventricular wall

showed multifocal small areas of acute contraction band necroses often seen in cases of acute cardiac failure and terminal dysrhythmic events (Strong et al. 2020). The epicardium showed patchy mild lymphoplasmacytic infiltration with multifocal activation of fibrocytes and collagen deposition (fibrosis), likely reflective of macroscopically observed pericardial adhesions.

The observed aortic inflammation and its granulomatous cell pattern with multinucleated macrophages of gorilla heart G18 is most consistent with changes described in Giant cell arteritis (GCA) or Takayasu arteritis (TAK) in humans (Maksimowicz-McKinnon and Hoffman 2012; Weyand and Goronzy 2012; Ryan et al. 2015; Stone et al. 2015; Cinar et al. 2017). The necrosis and neutrophils in the media are indicative of active ongoing disease and often assumed to be ischaemia-related (Ryan et al. 2015). GCA and TAK are well-known forms of large vessel vasculitides that affect the aorta and its proximal branches in humans and are still of uncertain aetiology but likely immune-mediated (Saadoun et al. 2015; Koster and Warrington 2017; Kermani 2019). Both, TAK and GCA, show a granulomatous pattern with epithelioid macrophages, occasional multinucleated giant cells and an accompanying lymphoplasmacytic infiltrate. Intimal thickenings combined with disrupted atheromatous plaques and thrombosis can give a “tree bark” appearance to the aortic intima (Gornik and Creager 2008; Stone et al. 2015) as observed in this gorilla. Endothelial cell dysfunction and loss stimulates medial smooth muscle cell recruitment and proliferation with extracellular matrix synthesis resulting in the observed intimal thickenings with further acute inflammatory damage to endothelium leading to acute fibrin-rich surface thrombus formation (Mitchell 2014; Stone et al. 2015). In this case, no evidence of fungal, bacterial, parasitic or viral pathogens were detected, which render an infectious, focal aortitis unlikely but cannot be fully excluded.

There was no evidence of an infectious process anywhere else in the body after full histopathological examination of all major body organs which would be also unusual for a systemic viral infection. Additionally, the animal responded negatively to tuberculin skin testing before euthanasia.

Although granulomatous inflammation of the aorta can occur as part of a more widespread immune-mediated systemic disease and known syndromes in humans, the histopathological findings in this gorilla together with the absence of systemic vasculitis point toward an isolated/idiopathic nature (Ryan et al. 2015; Cinar et al.

2017). However, extra-aortic vascular involvement of arteries not routinely examined, for example the temporal or subclavian artery, may not have been identified. Furthermore, early inflammatory changes that had not progressed yet to other vascular structures which we did examine cannot be ruled out in this case but appear unlikely considering the severity and chronicity of the aortic lesions.

6.3.3. Orangutans

Between 2017 and 2020, 10 orangutan hearts were received and examined. Details on each individual and histological diagnoses are summarised in table 6.3. Hearts were from 7 females and 3 males, from newborn to 59-year-old. All animals were adult except for one newborn male (O8) and one subadult male of 13-year-old (O6). Bodyweight at the time of death was available for 9/10 animals and ranged from 2 to 89 kg. Three animals were euthanised due to disease, 2 died during anaesthetic procedures, and the new-born died of trauma. The other four animals died of disease.

Sample quality was varied with three hearts (O4, O7 and O12) having undergone extensive sectioning and sampling before being received by the AHP, making difficult the assessment of the shape of the heart. One heart, O3, seemed to be well fixed on macroscopical examination but showed marked fragmentation and fixation artefacts hampering histopathological examination. O12 showed freeze and thaw artefacts on histology. Mean adult fixed heart weight (n=7) was 232.9 g (SD 87.56) and mean fixed heart weight/body weight ratio calculated for six adults was 0.4% (SD 0.09%).

Mean adult heart circumference (n=6) was 22.80 cm (SD 3.23) and mean adult heart length (n=6) was 8.25cm (SD=1.91).

Mean adult heart wall thicknesses (n=8) were: Left ventricle 1.06 cm (SD 0.16), interventricular septum 1.01 cm (SD 0.19), right ventricle 0.24 cm (SD 0.05).

Mean adult valve circumferences were: mitral valve 6.76 cm (SD 1.44, n=7), tricuspid valve 9.69 cm (SD 1.73, n=7), Aortic valve 4.99 cm (SD 0.87, n=8), pulmonary valve 6.01 cm (SD 0.98, n=8).

None of the orangutan hearts presented evidence of chamber enlargement nor abnormally thin or thickened walls. Some paler areas were detected on the epicardium of five hearts and interpreted as ‘soldier patches’. O6 presented a 3.5x1.5cm well-demarcated, white area on the epicardium of the anterior right ventricle, this was sampled for histopathology (figure 6.19).

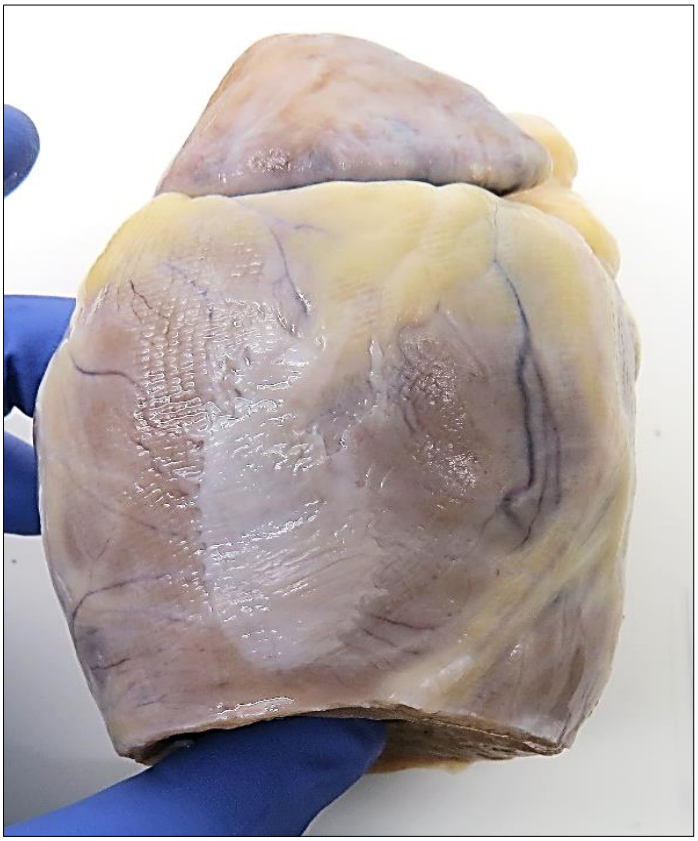

Figure 6.19. White demarcated area on anterior right ventricular epicardium, O6.

When present, mottling of the myocardium was subtle and likely due to a difference in formalin intake or vascular congestion. In O7, however, a distinctive paler area was visible around a small vessel of the left ventricular myocardium. Vessels appeared overall normal, although two individuals (O5 and O17) presented small yellow deposits on the intima of the ascending aorta (figure 6.20), and O12 had several small variably shaped intimal thickenings on the ascending aorta.

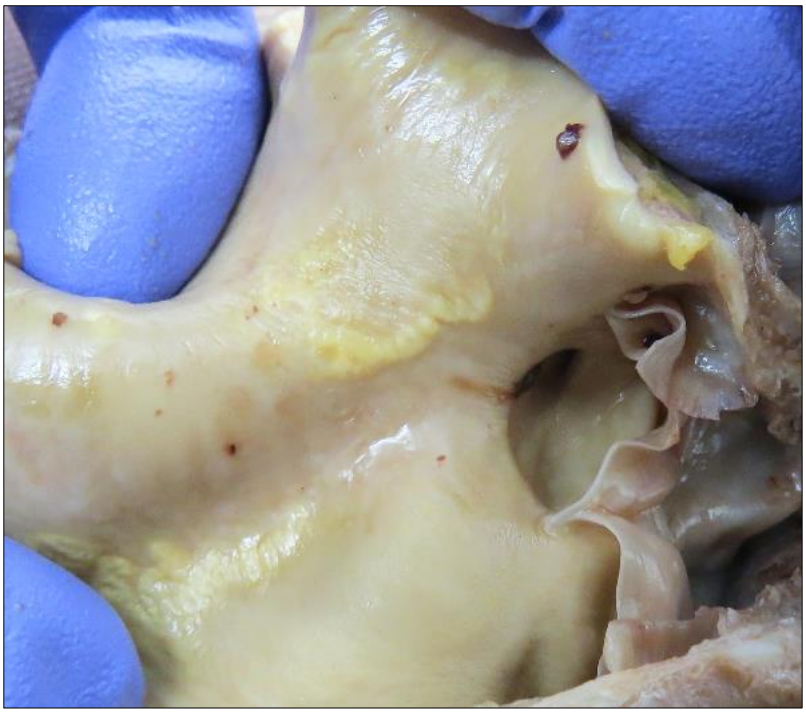

Figure 6.20. Intimal thickenings on the aortic intima of O5.

Histologically, none of the orangutan hearts submitted presented significant lesions, except for O11 that presented multifocal, chronic-active, mild to moderate lymphoplasmacytic and histiocytic myocarditis. Despite no protozoal amastigote was identified in the heart, the observed myocarditis was consistent with changes described with systemic Leishmaniosis (Costagliola et al. 2016). O11 was the only orangutan presenting significant cellular infiltrations.

The well-defined white area of epicardium in O6 revealed an area of mature connective tissue expanding the epicardial space with the impression of scattered infiltrated lymphocytes, degenerated neutrophils, and macrophages (focal epicardial fibrosis or extensive soldier patch). Although only four animals presented scattered areas of replacement fibrosis, all animals except O3 and the newborn O8 presented some degree of interstitial fibrosis. The severity of both interstitial and replacement fibrosis ranged from minimal to mild except for O7 that showed mild to focally moderate interstitial fibrosis and mild to focally moderate, chronic replacement fibrosis with multifocal peracute myofibre contraction band necrosis). Contraction band necrosis was observed in three animals (O4, O7 and O9) and believed to be related to terminal dysrhythmic events. Although the presence of atherosclerotic lesions in large arteries and coronary vessels were reported for O7 and O9 by the submitting zoos, this was not observed in our detailed exams of the fixed heart and coronary vessels. O7 did

present yellow areas on the aortic intima compatible with fatty streaks on macroscopical examination. O12's ascending aorta presented a focal, mild intimal thickening composed of subendothelial smooth muscle cell infiltrations.

O5, the oldest orangutan submitted to the project, presented mild tricuspid valve endocardiosis and two areas of mineralisation within the aortic ring, without associated inflammation. Within the right ventricular outflow tract, there was a focally extensive area of replacement fibrosis with associated fibre hypertrophy and mild lymphohistiocytic infiltrate, but the level of fibrosis was overall mild to moderate and likely age-related.

Table 6.4. Available information and cardiovascular diagnoses for the orangutan hearts received between 2017 and 2020.

Study ID	Sex	Age at death (years)	Body weight (kg)	Recent clinical history/ circumstances of death	Manner/cause of death	Main reported PM findings	Cardiac diagnoses
O3	Female	27	35.0	Chronic airsacculitis, died during anaesthesia for transport	Peri-anaesthesia	Chronic aerosacculitis and high-graded bronchitis/bronchiolitis.	Possible focal, small acute myocardial haemorrhage in interventricular wall Acute congestion
O4	Male	24	89.0	Lethargy, respiratory symptoms	Natural: illness	Pleuropneumonia, nephritis	Mild, focal, chronic interstitial fibrosis in papillary muscle of the left ventricle Acute contraction band necrosis in right ventricular outflow tract
O5	Female	59	n/a	Gastro-intestinal disease	Natural: illness	Not disclosed	Mild diffuse interstitial fibrosis with scattered minimal to mild replacement fibrosis Mineralisation of the aortic ring
O6	Male	13	64.5	Died during anaesthesia to investigate and treat respiratory infection	Peri-anaesthesia	Purulent air sacculitis, pneumonia, pleuritis.	Minimal interstitial fibrosis, left ventricle Minimal replacement fibrosis, septum Mild, focal chronic epicardial fibrosis, right anterior wall
O7	Female	34	54.0	Died overnight after showing acute haematuria	Natural: illness	Atherosclerosis of the aorta and coronary arteries, uterine masses, intestinal serosal adhesions and nodules	Mild to focally moderate interstitial fibrosis with mild to focally moderate, chronic replacement fibrosis Multifocal peracute myofibre contraction band necrosis
O8	Male	0	2.0	Found dead with signs of trauma	Natural: trauma	Thoracic puncture wounds with trauma to the liver and haemoabdomen.	NAD. Patent foramen ovale.
O9	Female	47	70.0	Age-related deterioration	Euthanasia	Renal carcinoma and chronic nephritis. Atherosclerotic plaques in large arteries of heart base.	Multifocal, chronic, minimal to mild interstitial fibrosis Multifocal, acute myofibre contraction band necrosis
O10	Female	30	56.0	Respiratory infection unresponsive to treatment	Euthanasia	Chronic purulent air sacculitis, pneumonia, peritonitis	Mild, multifocal, chronic interstitial fibrosis
O11	Female	35	43.6	Severe chronic leishmania infection	Natural: illness	Visceral leishmaniosis, membrano-proliferative glomerulonephritis.	Multifocal, chronic-active, mild to moderate lymphoplasmacytic and histiocytic myocarditis. Minimal to mild interstitial fibrosis
O12	Female	46	65.4	Broken leg	Euthanasia	Not disclosed	Minimal to mild myocardial interstitial and replacement fibrosis Focal mild aortic intimal thickening

6.3.4. Bonobos

A total of four bonobo hearts were received by the AHP between 2017 and 2020, three males and one female. Results are summarised in table 6.4. Ages ranged from 1 day to 39 years old, with one male newborn and one subadult male of 8 years old.

No abnormalities were detected on macroscopical and microscopical examination of a newborn bonobo heart (B8) except for some small areas of haemorrhage on the epicardium.

The adult male bonobo B6 that was euthanised due to emaciation and a comatose state after a period of diarrhoea unresponsive to treatment showed a heart with no fat visible within the coronary groove and epicardial surface (figure 6.21). In the anterior left ventricle myocardium, close to a major papillary muscle, was a well-circumscribed, 3mm, roughly circular area of pallor. This corresponded histologically with a focally extensive acute myocardial infarction with a large infiltration of viable and degenerated neutrophils associated with multiple acute haemorrhages. This lesion was considered severe enough to cause cardiovascular problems and potential central nervous system hypoxia, but more clinical and histopathological data of other organs would have been necessary to identify its aetiopathogenesis.

Figure 6.21. Fixed heart of bonobo B6, with no fat visible on epicardial surface.

The shape of the heart of the adult female (B7) that died of Yersiniosis was difficult to assess due to previous sectioning. On transverse examination at the level of sectioning, the myocardium of the left ventricle and posterior septum presents numerous white areas compatible with myocardial fibrosis (figure 6.22). This was confirmed during the microscopical examination that showed chronic multifocal, random, marked replacement fibrosis, chronic diffuse moderate interstitial fibrosis and moderate to marked perivascular fibrosis. Moreover, the left ventricular wall and septum appear mildly thickened macroscopically, and multifocal moderate to marked myofibre disarray was observed microscopically which point towards hypertrophic cardiomyopathy. The spillover from the systemic Yersiniosis was seen in the form of acute fibrinous mixed mild to moderate epicarditis with pericardial histiocytosis.

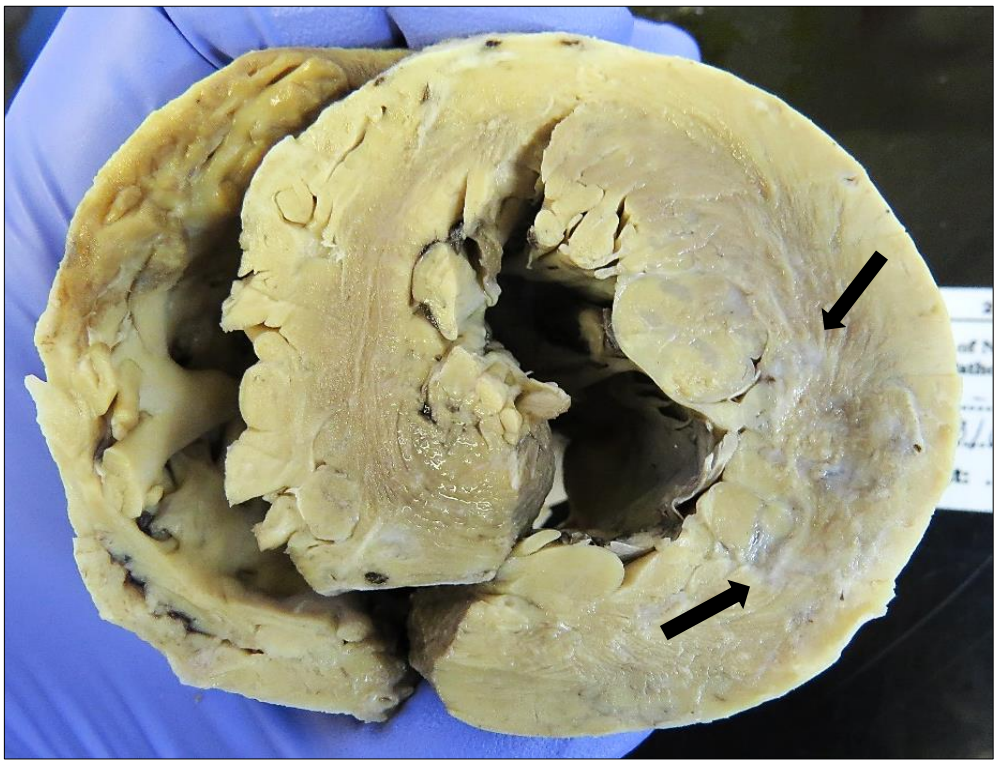

Figure 6.22. B7 myocardial cross section showing areas of replacement fibrosis (arrows) and a mildly hypertrophied left ventricle.

The subadult male bonobo, B9, died at Twycross Zoo of severe, acute to subacute necrosuppurative bronchopneumonia and suspected disseminated intravascular coagulation. His heart showed the most extensive changes with moderate, chronic, concentric left ventricular hypertrophy (figure 6.23) and multifocal, acute and subacute ischaemic infarcts. Infarcts were very likely related to reduced tissue oxygenation due

to the cardiac hypertrophy, severe lung disease and terminal systemic thrombotic events, and were severe enough to have caused the death of the animal.

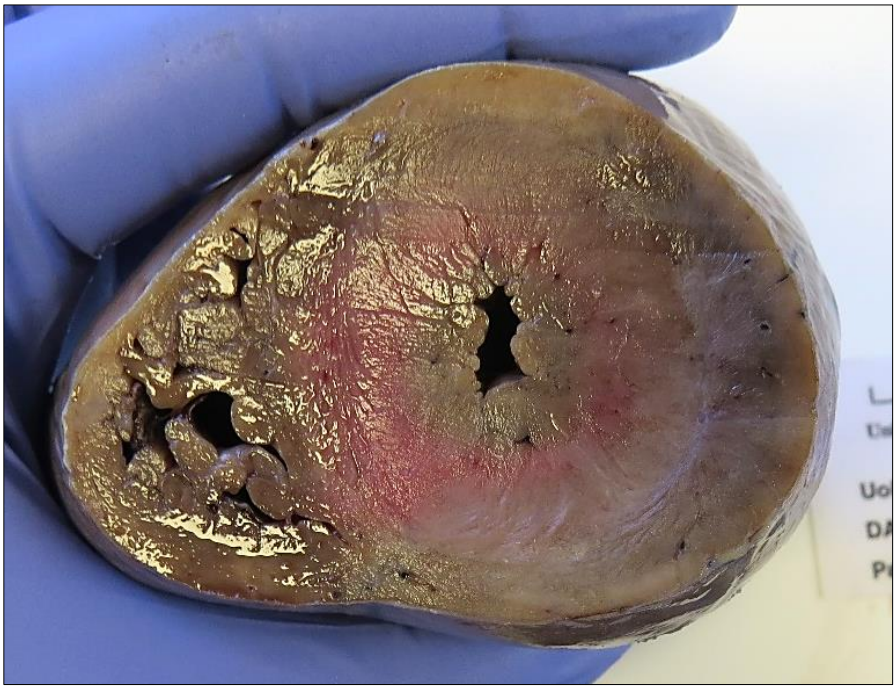

Figure 6.23. B9 myocardial cross section showing the left concentrically hypertrophied ventricle. Note the pink colour of the mid myocardium denoting inadequate fixation.

Table 6.5. Available information and cardiovascular diagnoses for the bonobo hearts received between 2017 and 2020.

Study ID	Sex	Age at death (years)	Body weight (kg)	Recent clinical history/ circumstances of death	Manner/cause of death	Main reported PM findings	Cardiac diagnoses
B6	Male	24	33	Subacute bloody diarrhoea unresponsive to treatment, euthanised after being found in a comatose state	Euthanasia	Emaciation	Mild, chronic diffuse interstitial fibrosis Mild to focally moderate, chronic, random replacement fibrosis Focally extensive acute myocardial infarction with multifocal, acute, small haemorrhages Multifocal, random acute rhabdomyolysis
B7	Female	39	36	Pneumonia	Natural: illness	Systemic *Yersinia pseudotuberculosis* infection	Chronic multifocal, random, marked replacement fibrosis with mild lymphohistiocytic infiltration Chronic, diffuse, moderate interstitial fibrosis and moderate to marked perivascular fibrosis Multifocal moderate to marked myofibre disarray Acute, multifocal, mild cardiomyofibre necrosis with contraction bands Acute fibrinous mixed mild to moderate epicarditis with pericardial histiocytosis
B8	Male	0	1	Neonate found dead	Trauma or stillborn	Fractured skull, poor aeration of alveoli, meconium aspiration	No abnormalities detected
B9	Male	8	32	Found dead when seemingly recovering from respiratory infection	Natural: illness	Necrosuppurative bronchopneumonia, possible intravascular disseminated coagulation	Moderate, chronic, concentric left ventricular hypertrophy Multifocal, acute and subacute ischaemic infarcts

6.4. Discussion

The development and distribution of a comprehensive cardiac post-mortem protocol by the Ape Heart Project has allowed regular reception and examination of high-quality great ape heart samples from dozens of European zoos. Between 2017 and 2020, chimpanzee followed by gorilla samples were most received, while orangutan and bonobo samples were scarcer. This likely reflects the number of individuals of each species kept in European zoos and their proportional mortality rate.

Although some received hearts were of suboptimal quality and not always sampled as per AHP guidelines, taking macroscopical measurements and a minimum of 12 samples from predetermined locations were possible for most hearts. The value of macroscopical measurements is still unclear until more hearts are examined, and it is important to keep in mind that some measurements can vary depending on sample handling and storage. For instance, the degree of formalin penetration or the presence of blood clots in the chambers can affect the fixed heart weight.

Findings were interpreted together with the information on the individual submitted by the zoo, as the clinical history of the animal and post-mortem findings in other organs must be carefully analysed when interpreting cardiac post-mortem changes. The accuracy and completeness of these reports were still highly variable depending on the submitting zoo. Some zoos reported macroscopical or microscopical cardiac changes that were not confirmed following our detailed examination, one example is the common reporting of atherosclerosis of the aorta, that were in fact small intimal thickenings or xanthomatous changes, a common clinically silent, age-related change in hominids and non-hominids that should not be called ‘atherosclerosis’ without the identification of further pathological changes like core necrosis, further inflammation, surface erosion and thrombus material. Atherosclerotic plaques are considered a progression of intimal thickening and fatty streaks due to chronic hypercholesterolemia and appear to be relatively rare in great apes.

Findings in chimpanzees confirm that the presence of interstitial and replacement fibrosis is highly prevalent in this species, and in many cases is severe enough to have contributed to the death of the animal. Many of these affected individuals did not present obvious macroscopic changes that could have been diagnosed premortem or

with diagnostic techniques other than comprehensive histological examination. Although myocardial fibrosis is a known age-related change in humans and animals, the high prevalence in zoo chimpanzees together with the fact that the affection has been identified in several subadult chimpanzees suggests the needs for further investigation into the pathophysiology of myocardial fibrosis to hopefully soon identify antemortem serum biomarkers.

The article on Idiopathic Myocardial Fibrosis in captive chimpanzees published by the AHP expands the description of this entity and investigate possible causes and risk factors, such as the possibility of a relationship between low vitamin D levels and the development of IMF (Strong et al. 2020). Since the publication of this paper, C41 (corresponding to C1 in chapter 3), who was euthanised at Twcyross zoo in early April 2020 due to thrombosis and presented marked cardiac fibrosis on histology, had a serum vitamin D level of only 22.7 nmol/L the day of her death, one of the lowest levels measured in Twycross zoo chimpanzees, which stresses further the importance of investigating hypovitaminosis D as a risk factor for cardiovascular disease in great apes. Although areas of replacement fibrosis were often accompanied by a minimal to mild inflammatory infiltrate, these were considered reactive to the damage remodelling process and no link between IMF and infectious processes has been found (Strong et al. 2020). Apart from chronic changes such as myocardial fibrosis, acute changes such as acute cardiomyofibre necroses and contraction bands were also observed in 45% of the chimpanzee hearts and were especially common in animals that died suddenly. In humans, most sudden cardiac deaths are not associated with acute myocardial infarcts but with the presence of substrates of life-threatening ventricular arrhythmia such as healed infarct (areas of replacement fibrosis) (Saffitz 2005). Although chimpanzees do not commonly suffer from coronary atherosclerotic which is the predominant cause of ischaemic heart disease in humans, their myocardium does present the anatomic substrates of lethal ventricular arrhythmias identified in humans: cardiac myocyte hypertrophy, interstitial and/or replacement fibrosis, and acute cardiac myocyte necrosis (Saffitz 2005). The contribution of local homeostatic perturbations such as myocardial hypoxia, acidosis or ion imbalances to lethal arrhythmias remain to be investigated in chimpanzees.

Although the prevalence of myocardial fibrosis in gorillas was relatively high, the overall degree was far less severe. Also, the occurrence of sudden cardiac death

seems to be much lower than in chimpanzees, and acute myocardial damage such as myocytolysis and contraction band necrosis also appeared to be less prevalent. Our data, however, indicate a higher prevalence of small and large vascular changes which could indicate a different aetiopathogenesis of cardiac fibrotic remodelling in gorillas compared with chimpanzees and bonobos. More than half of the gorilla hearts submitted since 2017 presented some degree of vascular changes such as arteriolosclerosis, intimal thickenings or atherosclerosis of the coronary arteries, preliminary evidence of cystic degeneration of the aorta, aortic dissection, or aortitis. Cystic media degeneration of the aorta is a well-known degenerative change in humans that causes a reduction in arterial elasticity and predisposition to aneurysm, with the most important risk factor being systemic hypertension (Stone et al. 2015). This, together with the other chronic changes identified in small and medium vessels in our case cohort, indicates that hypertension may be an important cardiovascular risk factor in European zoo gorillas. Future work will try and further characterise some identified degenerative vascular changes in gorillas and compare them to changes described in humans. Although the occurrence of aortic dissection in gorillas has never been linked to aortitis (McManamon and Lowenstine 2012; Mussa et al. 2016), the identified aortic inflammation in G18 indicates that inflammatory changes should routinely be ruled out in gorillas diagnosed with aortic aneurysm and intimal changes, as it is known that humans with chronic aortitis often show a significantly higher rate of aortic aneurysm formation and dissections (Wang et al. 2012a; Stone et al. 2015; Russo and Katsicas 2018). Routine sampling and careful examination of small, medium and large vessels is indicated in all post-mortem cases in order to gain knowledge about acute and degenerative vascular diseases in great apes.

Although the number of orangutan hearts examined was relatively low, it seems that the occurrence and grade of myocardial fibrosis is much lower in this species compared with other great apes. Acute changes such as acute cardiomyocyte necrosis were sometimes observed and associated with terminal arrhythmic events. Only in one case were cardiac changes severe enough to have contributed to the death of the animal.

Although only three adult bonobos were submitted to the project since 2017, all of them presented significant cardiac lesions, with both chronic and acute changes being

observed. Further bonobo samples are greatly needed to investigate the nature and aetiopathogenesis of cardiac disease in this species.

7. Microcomputed tomography of the chimpanzee heart

The high prevalence and severity of cardiac changes detected histologically in the hearts of zoo chimpanzees (see previous chapter) justifies the need to investigate the ability of new imaging techniques to detect these changes. Although computed tomography is routinely used in companion animal medicine, its use in zoo animals is not so widespread due to its high cost, restrictions on patient size, and the need for general anaesthesia. Micro-CT scan, a relatively new imaging technique that can achieve a higher resolution than traditional CT, has, to the author´s knowledge, never been used in chimpanzees *in-vivo* or *ex-vivo*. The original goal of this study was to assess the use of the micro-CT scan to detect structural changes (and especially IMF) in formalin-fixed chimpanzee hearts. For this purpose, chimpanzees' hearts that had already undergone full histopathological examination and with different degrees of IMF were chosen. Although IMF could unfortunately not be detected in formalin-fixed heart with the method employed (e.g without the use of contrast agent), the identification of bone and cartilage formation in chimpanzees´ hearts affected by high levels of IMF demonstrated the value of micro-CT scan as an ancillary post-mortem diagnostic technique in the characterisation of chimpanzee cardiac disease. The findings of this study were published in June 2020 in *Scientific Reports* under the title "*Discovery of os cordis in the cardiac skeleton of chimpanzees (Pan troglodytes)*" https://doi.org/10.1038/s41598-020-66345-7.

The original study ID (used in the precedent chapter) were changed for the publication of this manuscript (table 7.1).

Table 7.1. New IDs (from S1 to S16) assigned to the chimpanzee hearts in the published "os cordis" manuscript and their corresponding original IDs used in the previous chapter.

Original study ID	C1	C12	C32	C14	C7	C20	C26	C2	C25	C10	C9	C38	C23	C15	C33	C21
New ID	S1	S2	S3	S4	S5	S6	S7	S8	S9	S10	S11	S12	S13	S14	S15	S16

This study was highly collaborative, and below is a description of the principal authors contribution:

- Sophie Moittie (myself): assisted with the original macro and microscopical examination, selected the hearts for micro-CT scan, dissected the hyperdense areas found on micro-CT scan for histopathology, performed the statistical analysis, wrote the manuscript (except the collagen proportion analysis), participated in the subsequent revisions.
- Dr Catrin Rutland: performed the CT scan and subsequent image analysis/editing together with Craig J Sturrock, performed the staining and histology of hyperdense areas, wrote the collagen proportion analysis for the manuscript and contributed towards subsequent manuscript revisions.
- Kerstin Baiker: performed the original histopathological examination, assisted with the histology of hyperdense areas, contributed towards the writing of the manuscript and its subsequent revisions.

7.1. Introduction

In humans, endomyocardial biopsies can be performed for the investigation of some cardiomyopathies or unexplained arrhythmias. This procedure is not performed in nonhuman hominids due to its invasive nature and the unknown sensitivity and specificity as a diagnostic test in these species. All confirmed cases of IMF in chimpanzees have been diagnosed via post-mortem histopathological examination. Lesions vary from minimal to marked (frequently chronic) and show variable degree of diffuse, reactive interstitial fibrosis and/or focally extensive or multifocal areas of replacement fibrosis.

Cardiac imaging is often performed for the assessment of CVD in animals and humans. Modalities commonly used in human medicine include radiography, echocardiography, computed tomography (CT), and cardiac magnetic resonance imaging (MRI) with or without contrast agents. In zoological medicine, however, most of the advanced techniques are not readily available and radiography and ultrasonography remain the most widely used techniques. Despite being a clinical challenge, echocardiographic parameters of clinically normal but anaesthetised chimpanzees have been published (Sleeper et al. 2014). Anaesthesia is normally required for these animals but makes interpretation more complicated in many cases. Although echocardiography is useful to detect cardiac structural changes and function, myocardial fibrosis can occur with only subtle image variations (Jellis et al. 2010), and the effect of anaesthetic agents complicates the interpretation of echocardiographic findings. With the exception of an anatomical study comparing cardiac innervation and position in orang-utans, chimpanzees, and gorillas, no reports exist on the use of CT scanning to assess cardiac function or structure in great apes(Kawashima and Sato 2012).

X-ray microtomography (microCT), like CT, is a non-destructive X-ray imaging technique that produces three-dimensional images from two-dimensional trans-axial projections. MicroCT generally works on smaller specimens but with a much higher resolution than standard CT producing images and maps with voxels in the micrometre range. MicroCT has been used since the 1980’s in the industrial and biomedical sectors. Its main applications in the latter sector are studies involving bone structure and function, the development of tissue engineering techniques and for the detection

of vascular and soft tissue lesions when combined with the use of contrast agents (Boerckel et al. 2014). Whereas CT is widely used in clinical studies and routine diagnostics and treatment, in veterinary science, microCT has mostly been used in anatomical research studies and for use in cadaver materials (Witkowska et al. 2014; Keane et al. 2017). Its application in published clinical practice in living animals has been restricted due to high radiation doses but the detection of bone fractures and oral diseases in rabbits and the study of diseases mechanisms in laboratory animals have been undertaken (Badea et al. 2008; Sasai et al. 2014, 2015).

As IMF has been linked to the occurrence of cardiac arrhythmias and sudden death in chimpanzees (Lammey et al. 2008a,b), the study of the anatomy and structure of the cardiac conduction system and its surrounding tissues is of utmost importance. In all mammals, the electrical impulse for each cardiac cycle starts in the sino-atrial node, situated in the right atrium. Depolarisation spreads through the atrial muscle cells and reaches the atrio-ventricular (AV) node, located anterior to the coronary sinus ostium and directly superior to the septal leaflet of the tricuspid valve(Kim and Fishman 2012). The Bundle of His passes the electrical impulse to the infranodal conduction system through the cardiac skeleton.

The fibrous skeleton of the heart is a supportive and functional structure formed by fibrous rings of high-density connective tissue (annulus fibrosus) surrounding the two atrioventricular orifices (also called the atrioventricular rings), the aortic orifice (frequently termed the aortic ring) and opening of the pulmonary trunk (pulmonary ring) (Tohno et al. 2007; Drake et al. 2010; du Plessis et al. 2014). Areas connecting these fibrous rings form the central fibrous body and right and left fibrous trigones or trigonum fibrosum dextrum et sinistrum, which in certain species contain fibrocartilage, hyaline cartilage (cartilago cordis) and even bone (os cordis) (Schumer et al. 1981). The cardiac skeleton provides rigidity to prevent dilatation of valves and outflow tracts, gives attachments to the valves leaflets and myocardium, and electrically isolates the atria from the ventricles (Drake et al. 2010). The presence of an os cordis is a regular finding in large ruminants such as cattle, ox, water buffalos and sheep and has also been described in otters and camelids (James 1965; Egerbacher et al. 2000; Mohammadpour 2007; Ghonimi and Balah 2014; Daghash and Farghali 2017), but is not reported in other mammals. In cattle, the os cordis is located near the junction of the interatrial and interventricular septa and extends anteriomedially into the right

atrioventricular ring. Occasionally, a second bone is present within the left atrioventricular ring (James 1965). Although the exact localisation, size and number of the os cordis varies, in all species it lies within the trigonum fiobrosum, adjacent to the AV node and consists of trabecular bone with marrow and fat. Its function is unclear but it is believed to serve as a pivot and anchoring support for the cardiac valves (James 1965; Frink and Merrick 1974). Cartilage (*cartilago cordis*) can also be present within the cardiac skeleton of individuals of other animal species such as horses, pigs, canids, felids, mice, rats, snakes, white rhinoceros and Syrian hamsters (Schumer et al. 1981; Young 1994; Durán et al. 2004; Erdoğan et al. 2014; Ghonimi and Balah 2014). In humans, mineralisation of the cardiac skeleton can occur as mitral and aortic annular calcification and aortic valve sclerosis. They are considered degenerative changes associated with aging and are linked with cardiovascular disease (Barasch et al. 2006).

The aim of this study was to characterise the hyperdense tissue discovered in the chimpanzee heart using microCT and histopathological techniques. In addition, the relation between the presence of os cordis, cartilago cordis or foci of ectopic calcifications and the level of IMF, age and sex of the animals were studied.

7.2. Material and Methods

Formalin fixed whole hearts from chimpanzees that died in European zoos were received for detailed macroscopical and histopathological examination as part of the Ape Heart Project (led by Twycross Zoo and the University of Nottingham). The manner and cause of death were retrieved from the zoos' submission forms and post-mortem records, together with other information such as sex, age and presence of significant comorbidities. Ethical permission was given by The University of Nottingham, School of Veterinary Medicine and Science ethics committee in adherence to institutional and national guidelines (ethics number 1843 160905). Permission from each zoo was given for investigation of every animal and no chimpanzees were euthanised for the purposes of research.

7.2.1. Heart macroscopical examination and histology

Examinations were carried out as per published protocols, similar to those carried out in cases of sudden cardiac death in humans (Basso et al. 2008; Sheppard 2012; Strong et al. 2018c). Hearts were received fixed in neutrally buffered 10% formalin, with an incision made transversally across both ventricles approximately 3 cm from the apex to allow better fixation. Each heart was weighed, measured (length and circumference), the coronary artery sinuses were probed, and coronary arteries were cut at 3 mm intervals to check for dilatation or other vascular changes. The left and right ventricular walls as well as the interventricular septum were measured at the level of the transversal section. The transverse myocardium was assessed for any evidence of mottling or infarction. Major vessels and valves were examined, and valve circumferences were measured. A minimum of 12 samples were taken for histopathology, including three sections from the left ventricle, three sections from the right ventricle, two sections from the interventricular wall, and sections of the right ventricular outflow tract, the sino-atrial node region, the atrioventricular node region, and the aorta. Any abnormalities or lesions identified were also sampled.

Serial sections (7 µm per section) were cut and stained with haematoxylin and eosin and evaluated under the microscope by a diplomate from the European College of Veterinary Pathologists with expertise in great ape cardiovascular pathology. Pathological features such as myocyte degeneration, interstitial myocardial fibrosis, replacement fibrosis, perivascular fibrosis, cellular infiltration, myofibre disarray, myofibre necrosis, myofibre hypertrophy, vascular and valvular changes were assessed. Severity, location, distribution and chronicity of findings were described. Levels of IMF were ranked as follow: no IMF= level 0, minimal IMF= level 1, mild IMF= level 2, mild to moderate IMF= level 3, moderate IMF= level 4, moderate to marked IMF= level 5, marked IMF= level 6. Assigned IMF levels reflected the average levels of replacement, perivascular and interstitial fibrosis of all 12 slides. Every sample totalling eight hearts from female and eight hearts from male chimpanzees, presenting with different levels of IMF, and from individuals that died at different ages underwent microCT analysis (Table 1).

7.2.2. X-ray microtomography

Following pathological examination, each heart was wrapped in thin sheets of X-ray transparent polyethylene packing foam and placed into plastic specimen jars. A cone beam X-ray microCT scanner was used: Phoenix v|tome|x m (GE Sensing and Inspection Technologies GmbH, Wunstorf, Germany), set at 125 kV and 320 µA. The distances between the X-ray source and the sample and the X-ray source and the detector were optimised in order to achieve appropriate magnification and spatial resolution on a sample-by-sample basis. Some of the hearts were larger than others so the resolution was coarser. Each scan acquired over 2160 projection images over a 360° rotation of the sample using a detector exposure time of 333 ms, integrated over three averaged images, resulting in a total scan time of 48 min to 60 min depending on the heart size. Data were reconstructed using an inline median smoothing filter in datos|x software (GE Sensing and Inspection Technologies, Wunstorf, Germany), and exported as a 3D volume file. Higher resolution scans (6 – 10 micron range depending on sample size) were conducted on dissected regions to reveal the microstructure of the dense objects. High resolution scans were acquired at 80 kV, 120 µA, 200 ms detector timing and 2160 projection images with each image being the integration of 5 images to reduce noise. X-ray CT image data was visualised using VGStudioMAX v2.2 Software (Volume Graphics GmbH, Heidelberg, Germany). The high-density objects were digitally segmented from the 3D volumetric data based on their higher X-ray attenuation values in the images (brighter colour) and exported as image stacks. Mean local thickness for each object was measured using the BoneJ plugin for the open source image quantification and analysis software ImageJ 1.44 (Doube et al. 2010; Schneider et al. 2012) following a protocol previously published (Witkowska et al. 2014). Local thickness heat map images were imported and visualised in VGStudioMax.

7.2.3. Hyperdense areas dissection and histology

Following pathology investigations and microCT analysis, areas containing hyperdense structures were dissected out of each heart and prepared for histopathology analysis (n=4 samples containing bone/cartilage, n=4 with no mineralised tissue present, n=2 samples containing foci of ectopic calcifications). In brief, samples were processed through graded ethanol and xylene, prior to being

embedded in paraffin. Serial sections (7 µm per section) were cut throughout each piece of tissue. A minimum of 8 sections per sample were then stained with haematoxylin and eosin. In addition, specimens with either bone, cartilage or foci of ectopic calcifications were stained with Masson-trichrome (100485; Merck KGaA, Germany) and Picrosirius red (ab150681; Abcam, UK) in order to quantitate total collagen levels immediately adjacent to the bone or cartilage. These specimens also underwent Von Kossa staining (ab150687; Abcam, UK) in order to evidence calcium deposition. Manual analysis of photomicrographs taken at 5X, 10X, 20X and 40X magnifications was carried out on all samples alongside the use of Image Pro (Media Cybernetics, USA) colour detection software of 5 images per section using systematic random sampling, both adjacent to the bone, cartilage or foci of ectopic calcification tissue and at 1mm away from these areas in order to calculate the proportions of collagen (Mayhew and Lucocq 2015).

7.2.4. Statistical analysis

Statistical analysis was conducted in IBM SPSS statistics 26. P-values less than 0.05 were considered statistically significant. A Shapiro-Wilk test revealed no significant deviation from normality for age ($p=0.522$), heart weight ($p=0.416$) but significant deviation from normality for IMF levels ($p=0.035$). Thus, non-parametric tests were used when comparing levels of IMF with other variables. Independent samples Mann-Whitney U tests were used to compare levels of IMF with presence of bone/cartilage, ectopic calcifications, and sex. Exact significance levels were used for Mann-Whitney tests because of the small sample size. Spearman's correlations were used to compare levels of IMF with age and heart weight. Independent samples T-tests were used to compare the presence of os cordis with age and heart weight, and to compare presence of vascular calcifications with age. Fisher's exact tests were used to compare sex with presence of os cordis and ectopic calcifications (Fisher's tests were used rather than Chi square tests because the expected values in the contingency tables were <5). Collagen proportions were compared using T-test (n=4/group).

7.3. Results

7.3.1. Initial cardiac examination and interstitial fibrosis histopathology

Three of the 16 investigated hearts, S2, S6 and S9, showed no histological evidence of IMF. Three chimpanzees were affected by marked IMF (IMF level = 6): two males aged 22 and 37 years (S5 and S8 respectively) and one female aged 25 years (S10). The remaining ten animals were affected by minimal to moderate levels of IMF (IMF levels ranging from 1 to 5; Table 1). None of the chimpanzees had known cardiac disease before death. Clinical and pathological results are summarised in Table 1 and chapter 6.

Table 7.2. Chimpanzee sex, age, heart weight, IMF levels and microCT and histological observations presented in age order for each sex. IMF levels are ranked from 0 (no IMF to 6 (marked IMF).

Specimen ID	Sex	Age	Heart weight (g)	IMF level	CT scan findings (confirmed histologically)
S1	Male	10	299	2	-
S2	Male	11	201	0	-
S3	Male	19	396	1	-
S4	Male	20	378	1	-
S5	Male	22	709	6	Trabecular bone within cardiac skeleton
S6	Male	22	362	0	-
S7	Male	28	485	2	-
S8	Male	37	446	6	Cartilage within cardiac skeleton
S9	Female	21	253	0	-
S10	Female	25	455	6	Trabecular bone within cardiac skeleton
S11	Female	32	276	2	-
S12	Female	32	242	1	Multiple foci of ectopic calcification
S13	Female	42	422	5	Multiple foci of ectopic calcification
S14	Female	46	324	5	Endochondral ossification within cardiac skeleton + Multiple foci of ectopic calcification
S15	Female	47	325	3	-
S16	Female	59	551	3	Multiple foci of ectopic calcification

7.3.2. X-ray microtomography

X-ray microCT generated clear images of the structure of the formalin fixed hearts (Figure 1). The dissection cuts made during a detailed macroscopic examination and sampling for histopathology were apparent on the scans. Cardiac chambers appeared as hypodense spaces (corresponding to darker regions on images, Figure 1), whilst cardiac muscle, valves and vascular walls contrasted well at a medium density. Tissue in these areas was homogeneous overall, therefore it was noted that histomorphological changes in the formalin-fixed parenchyma such as myocardial fibrosis could not be observed using the parameters set for microCT scanning.

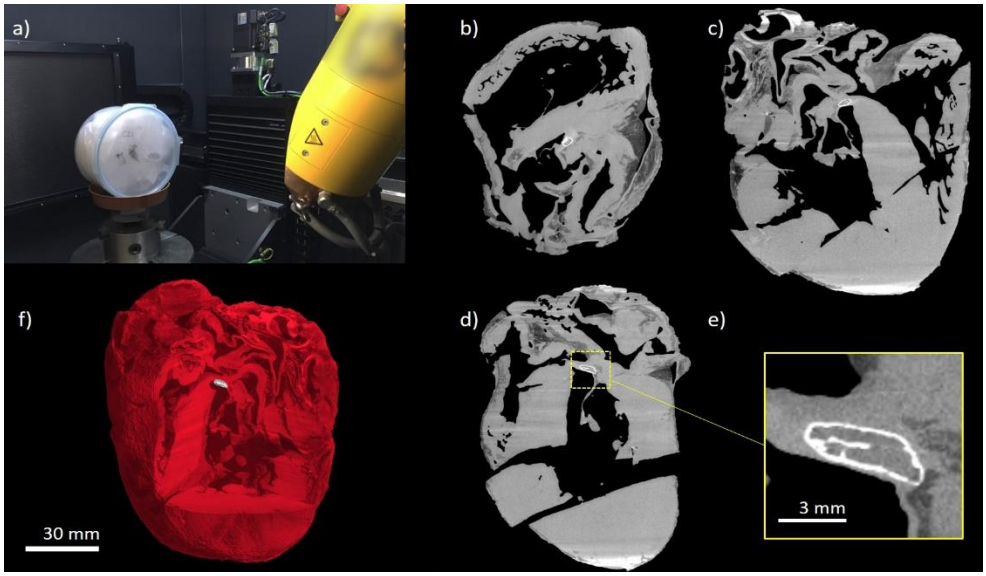

Figure 7.1. MicroCT images of showing hyperdense structures within the cardiac skeleton of S3. Data was visualised using VGStudioMAX v2.2 Software, https://www.volumegraphics.com/en/products/vgstudio-max.

Nine hearts showed no hyperdense areas. These hearts had either IMF levels of 0 (n=3), 1 (n=2), 2 (n=3) or 3 (n=1; Table 7.1). In the remaining seven hearts, hyperdense areas were detected and were compatible with areas of mineralisation or bone formation (shown as very bright regions in the images). These hearts had IMF levels of 1 (n=1), 3 (n=1), 5 (n=2) or 6 (n=3). In four of these specimens (S5, S8, S10, S14, all IMF levels 5 or 6), a hyperdense structure was located within the cardiac skeleton, on the valvular plane between the mitral and tricuspid valve (right fibrous trigone), just above the interventricular septum (Figures 7.2 to 7.4). Higher-resolution images of these structures revealed trabecular bone in S5 (Figure 7.2) and S10 (Figure 7.3), non-trabecular bone in S14 (Figure 7.4 a-c) and a mineralised structure in S8 (Figure 7.4 d-f) later confirmed as cartilage via histological examination. The

measurements of these features were taken following microCT analysis (Table 7.2). S5 was shown to have the largest volume, surface area and tissue thickness compared to the other structures.

In S12, S13, S14 and S16, multiple, well-demarcated areas of increased density were detected mostly within the walls of the great vessels, and for S12 and S16, within the cardiac skeleton as well. These were later confirmed histologically as foci of ectopic calcification.

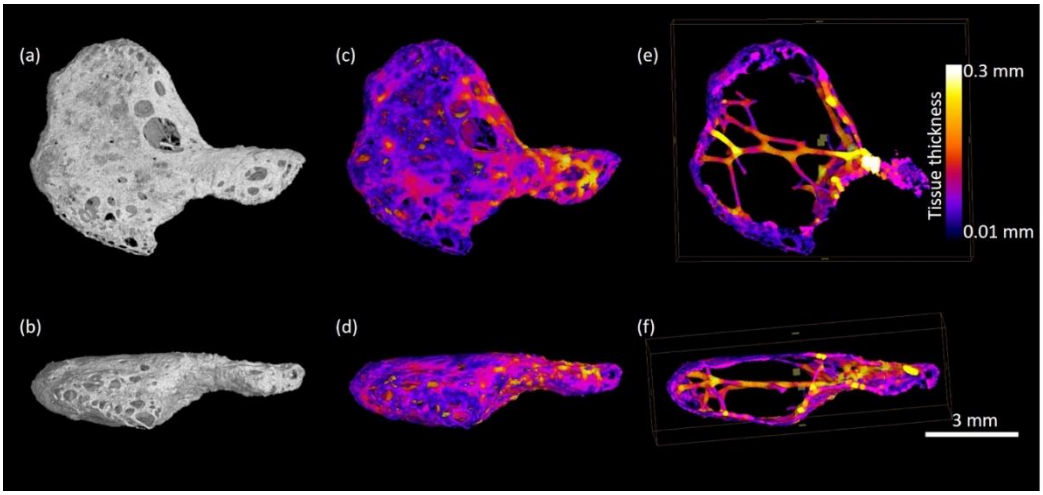

Figure 7.2. High-resolution microCT images of dissected hyperdense structure; os cordis from specimen 5. Figures depict rendered specimens (a+b) and those undergoing local thickness measurement (c-f) from two different angles at different depths. Data was visualised using VGStudioMAX v2.2 Software https://www.volumegraphics.com/en/products/vgstudio-max. BoneJ plugin http://bonej.org/ and ImageJ v1.44 https://imagej.nih.gov/ij/ were used to image and quantify bone thickness.

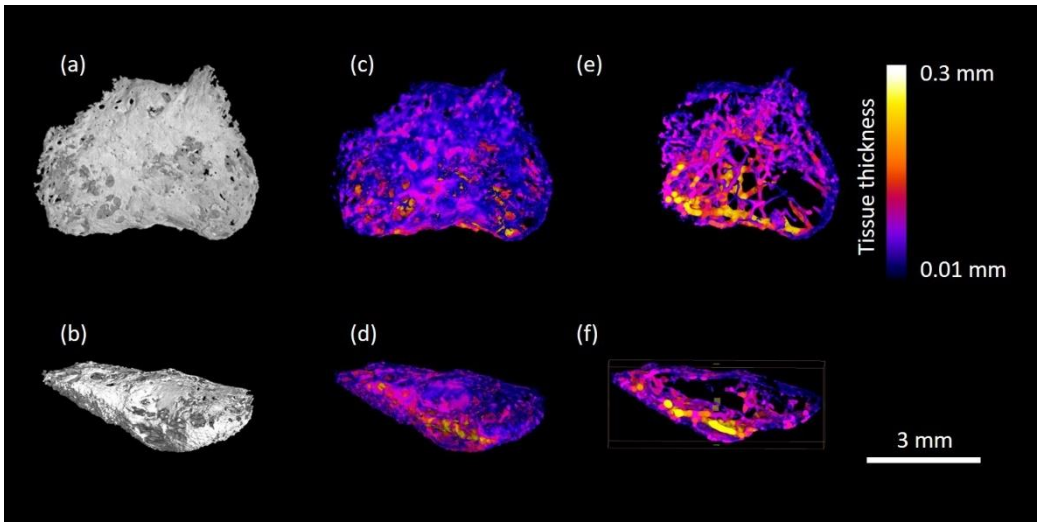

Figure 7.3. High-resolution microCT images of dissected hyperdense structure; os cordis from specimen 10. Figures depict rendered specimens (a+b) and those undergoing local thickness measurement (c-f) from two different angles at different depths. Data was visualised using VGStudioMAX v2.2 Software https://www.volumegraphics.com/en/products/vgstudio-max. BoneJ plugin http://bonej.org/ and ImageJ v1.44 https://imagej.nih.gov/ij/ were used to image and quantify bone thickness.

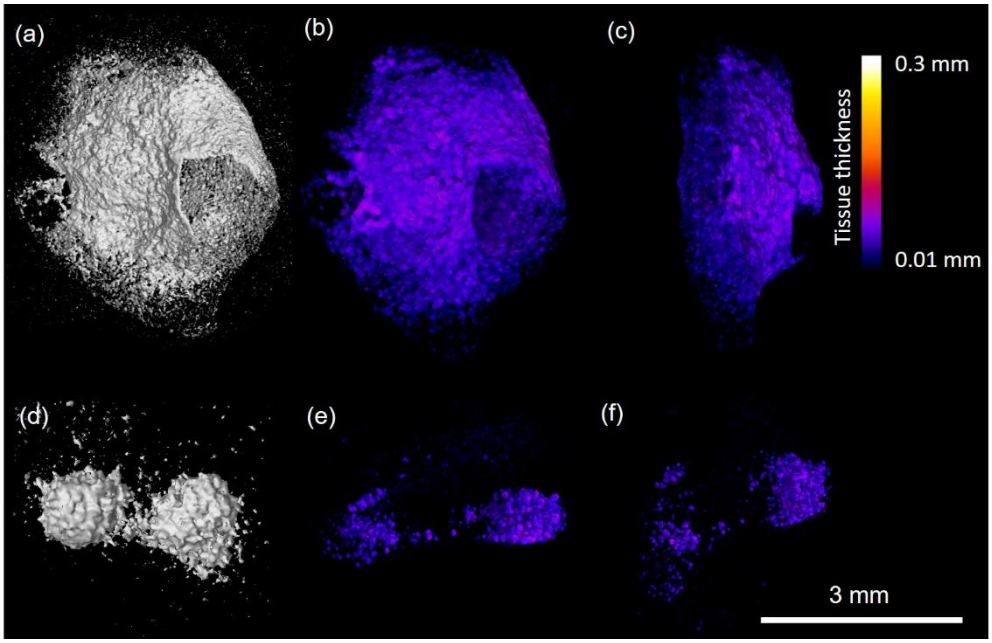

Figure 7.4. High-resolution microCT images of dissected hyperdense structure. a-c) os cordis from specimen S14 and d-f) cartilago cordis from specimen 8. Figures depict rendered specimens (a+d) and those undergoing local thickness measurement (b,c,e,f). Data was visualised using VGStudioMAX v2.2 Software https://www.volumegraphics.com/en/products/vgstudio-max. BoneJ plugin http://bonej.org/ and ImageJ v1.44 https://imagej.nih.gov/ij/ were used to image and quantify bone thickness.

Table 7.3. Dimensions of os cartilago and os cordis features within the hearts. SD=standard deviation.

Specimen ID	Length (mm)	Width (mm)	Depth (mm)	High density material volume (mm^3)	Mean local thickness (mm±SD)	Maximum local tissue thickness (mm)	Surface area (mm^2)
S8 cartilage	1.5	0.944	0.48	0.30	0.058±0.033	0.146	7.659
S5 bone	7.4	7.6	4.2	9.37	0.147±0.064	0.437	218.10
S10 bone	5.5	2.6	5	4.25	0.094±0.047	0.234	162.44
S14 bone	5.5	7.8	5.9	1.73	0.053±0.018	0.101	87.32

7.3.3. Histopathology of os cordis, cartilago cordis and other hyperdense structures.

Histopathological examination was utilised in order to determine the exact nature of the hyperdense structures. Histology of S5 and S10 hyperdense structures revealed focal areas of ectopic bone tissue formation, which contained bone marrow composed of marrow adipose tissue, supportive stromal cells, numerous osteocytes and additionally in the case of S5 large numbers of haematopoietic cells including red and white blood cell precursors (Figure 7.5b-d). In S14, histology of the hyperdense area within the cardiac skeleton revealed a focal area of mineralised cartilaginous metaplasia with endochondral ossification (Figure 7.5a). The other hyperdense areas visible in S14 were foci of ectopic calcifications, no attributes of cartilage or bone were observed within ectopic calcifications. In S8, a focal, a well-demarcated area of hyaline cartilage development with an area of central necrosis and subsequent dystrophic mineralisation (a cartilago cordis) was observed.

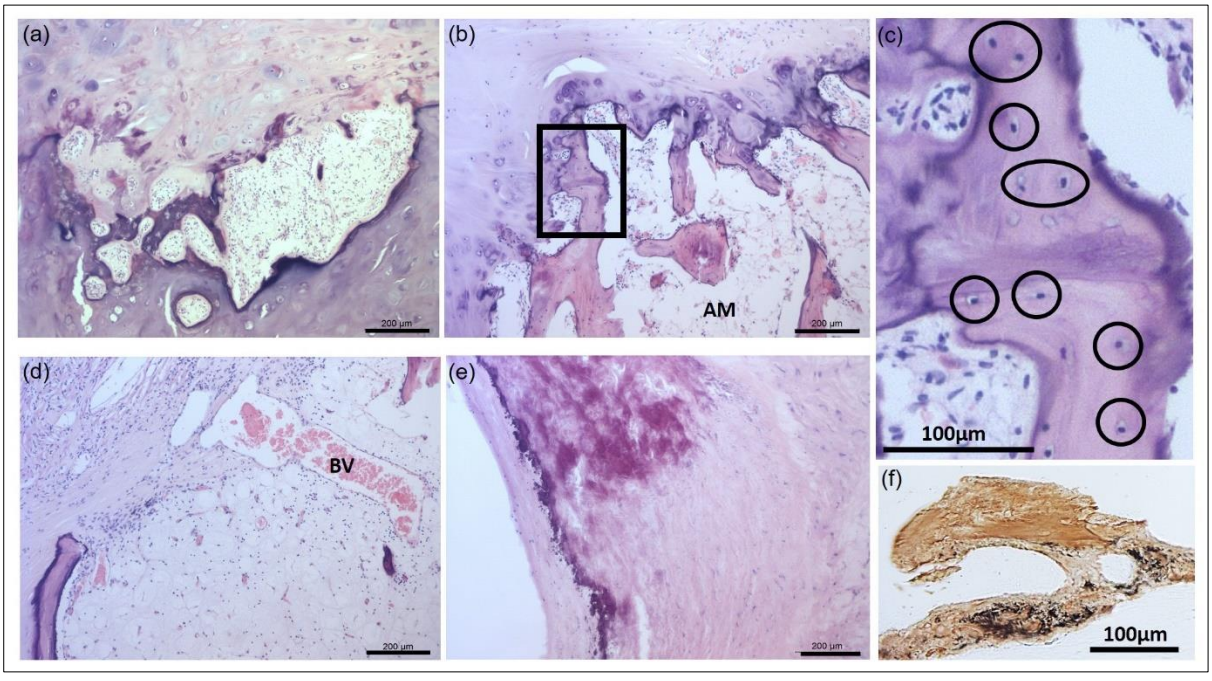

Figure 7.5. Cardiac bone and ectopic calcification histology. Areas of endochondral ossification were evident in photomicrographs of ectopic hyaline cartilage and lamellar bone with adipose marrow (AM), fibrovascular stroma, blood vessels (BV) and small numbers of haematopoietic cells in addition to osteocytes. a) S14 and b-d) S10. The box in b) is shown in a higher magnification in c) to highlight osteocytes. Hyperdense areas on microCT images revealed well-demarcated areas of ectopic calcification in some specimens including which was shown by histology including e) tunica media of the aortic wall S16. f) Photomicrograph of Von Kossa positive staining (brown/silver in colour) showing areas of calcification in S14. Scale bars represent 200µm in a,b,d,e and 100µm in c+f.

In S12, S13, and S16 only areas of ectopic calcification were detected histologically. S12 presented foci of ectopic calcification in the aorta and within the cardiac skeleton.

Both S13 and S16 presented foci of ectopic calcification of the aortic wall (Figure 5e). S16 also presented with well-demarcated foci of ectopic calcification within the cardiac skeleton, between the right and left ventricular outflow tract and the interventricular septum. Von Kossa staining also highlighted calcification within hyperdense material (Figure 5f).

7.3.4. Statistical analysis of os/cartilago cordis formation, interstitial myocardial fibrosis, age and sex.

Hearts presenting with os or cartilago cordis had significantly higher levels of IMF than hearts without os/cartilago cordis (Mann-Whitney U=0.5, p-value=0.001). Although the level of IMF was significantly associated with age (Spearman's rho=0.546, p-value 0.029), it was not associated with sex (Mann-Whitney U=24.00, p-value=0.44). The presence of os/cartilago cordis was not associated with age (t=-0.483, p-value=0.636) nor with sex (Fisher's exact test p-value>0.99). The presence of ectopic calcifications, however, was significantly associated with age (t=-3.308, p-value=0.005), with a mean age of 24.5 years (SD=10.44) for animals without ectopic calcification and a mean age of 44.75 years (SD=11.177) for animals with ectopic calcifications. Although the presence of ectopic calcifications was not significantly associated with sex (Fisher's exact test p-value=0.077), half of the females presented with ectopic calcifications, while none of the males did. Heart weight was significantly associated with the level of IMF (Spearman's rho= 0.642, p-value=0.007) but not with the presence of bone/cartilage cordis (t=-1.960, p-value = 0.07).

7.3.5. Collagen proportions in cardiac skeleton containing os/cartilago cordis or ectopic calcifications.

The percentage of collagen within the cardiac skeleton was increased in areas immediately adjacent to the os cordis or cartilago cordis in comparison to areas of the heart where neither bone, cartilage nor foci of ectopic calcification were present (mean±standard deviation was 64.11±10.61% around bone/cartilage compared to 10.91±5.18% in tissue not immediately adjacent to bone/cartilage; P<0.05; Figure 7.6). A similar feature was observed around foci of ectopic calcification in comparison to tissue not containing hyperdense material but only two samples were present with these features therefore statistical analysis could not be carried out (47.90±2.97%

around foci of calcification compared to 10.91% in tissue not adjacent to hyperdense material; Figure 7.6).

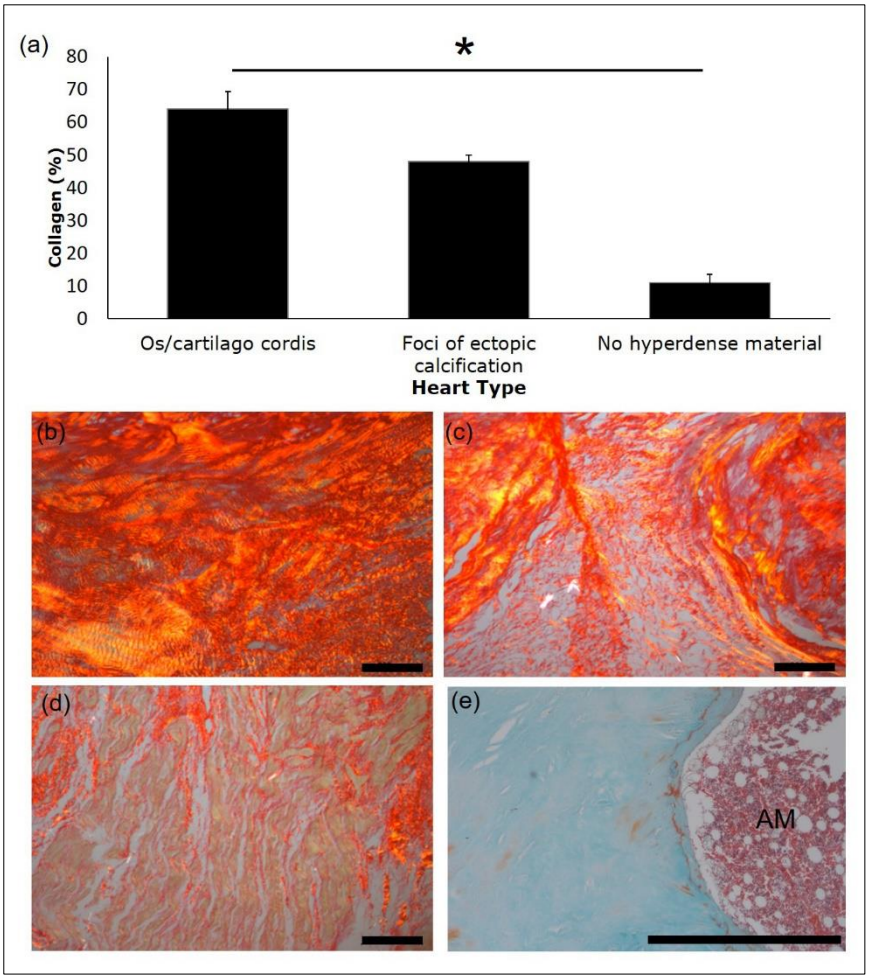

Figure 7.6. Collagen proportions in the cardiac skeleton.
*Graphical and photomicrograph representation of picrosirius stained tissue under polarised light showing the percentage of collagen present in the cardiac skeleton/myocardium tissue for areas surrounding bone/cartilage (n=4; a,b), adjacent to foci of ectopic calcification (n=2; a,c) and in myocardial tissue without hyperdense material (n=4; a,d). Masson-trichrome staining showing tissue adjacent to bone containing adipose marrow (AM). Bars represent mean ± standard error of the mean. * Indicates P<0.05. Scale bars represent 200µm.*

7.4. Discussion

The aim of this study was to characterise the mineralised tissue discovered in the chimpanzee heart using microCT and histopathological techniques. This research has uncovered the presence of cartilage and/or bone formation in the cardiac skeleton of several chimpanzees. The bones and cartilage varied in size and two bones were trabeculated whilst the third was not. This is the first time that an os cordis has been observed in this species and also represents a rare observation in a non-bovid mammal. In addition, the relation between the presence of os cordis, cartilago cordis or ectopic calcifications and the level of IMF, age, sex of the animals and heart weight were studied. The significant association between the presence of an os cordis and high levels of IMF suggests that the presence of an os cordis in this species may be a pathological finding or marker rather than an anatomical feature.

In humans, cardiac CT is performed generally with the use of contrast agents in order to assess the morphology and function of the heart and great vessels, while non-contrast CT is mostly used for the detection and quantification of coronary artery calcification (Rumberger 2010). In this study, the use of microCT without contrast agents did not allow for the detection of IMF probably due to the relatively low differential attenuation of X-rays in biological tissue and potentially due to tissue fixation. It is probable that extra deposition of tissue of the same approximate density (rather than calcified) would be difficult to detect other than by measuring volume increases or thickening of the walls given standards to control against and assuming that the increases were large enough and did not simply replace existing tissues. Iodine staining techniques have been used elsewhere to enhance contrast for post-mortem cardiac tissue computed tomography (Stephenson et al. 2012; Butters et al. 2014). Areas of mineralisation and ossification, however, were easily detected thus demonstrating that post-mortem microCT is a suitable technique for the detection of mineralised areas within the heart.

In humans, the coronary artery calcification score measurable by CT increases as a function of age in both men and women (Rumberger 2010), and deposition of calcium on the aortic cusps and on the fibrous skeleton of the base of the heart (mitral and aortic annuli) is also associated with aging (Barasch et al. 2006). Vascular calcification in humans is localised either in the tunica media or in the tunica intima of the vessel.

Intima calcification, which was not observed in the chimpanzees in this study, is associated with atherosclerosis and formation of atherosclerotic plaques, whereas media calcification of larger vessels is more generalised and often found in the elderly or patients with chronic renal disease, hypertension and osteoporosis (Persy and D'Haese 2009). According to the available clinical history of the animals in the present study, S13, S14 and S16 showed evidence of chronic renal disease and S15 had end stage renal disease on post-mortem examination, which may explain the vascular media calcifications (ectopic calcifications) seen in their hearts. Chimpanzees are not as prone to coronary artery disease as humans (Strong et al. 2018a); however as they age, an increase in media calcifications was evident in our specimens, similar to findings in humans (Giallauria et al. 2013). The microCT scan of the oldest chimpanzee in the present study, a female aged 59 years-old, revealed multiple areas of calcification within the great vessels. Pathological, histological and microCT results showed that she presented with only mild to moderate (level 3) IMF and no ossification nor cartilage in the cardiac skeleton, despite the multiple areas of ectopic calcification and her advanced age.

As three out of 16 examined hearts presented with bone formation within the trigonum fibrosum, it cannot be ruled out that the os cordis could be an anatomical peculiarity in some individuals of this species rather than linked to cardiovascular disease. Similarly, one heart contained cartilage within the trigonum fibrosum, a cartilago cordis. This mineralised cartilage area may be a precursor to bone formation in this animal. The exact function of cartilago or os cordis is unclear in other animal species. In cattle, the os cordis is believed to support normal motion of the valves in a heavy heart (James 1965) and has not been linked to cardiovascular disease. In otters (*lutra lutra)*, a smaller species, the presence of bone within the cardiac skeleton is also considered normal and its prevalence increases with age, as it was found in 11 out of 13 adult otter hearts but not in juveniles (Egerbacher et al. 2000). The presence of hyaline cartilage has also been described in the aorticopulmonary septum of individuals of eleven species of snakes, with a great variation in size, shape and precise location, and seemingly little functional influence (Young 1994). In Syrian hamsters, the cartilaginous foci in the central fibrous body of the heart have been proposed to act as pivots resisting mechanical tensions generated during the cardiac cycle (Durán et al. 2004).

In other species, however, bone and cartilage formation in the heart has been associated with CVD. In large breed dogs, although the presence of cartilage and bone formation in the central fibrous body of the heart has been reported as a normal occurrence at all ages, most of the dogs presenting with it are Doberman Pinschers, that suffer from a very high prevalence of dilated cardiomyopathy (Sandusky et al. 1979; Wess et al. 2010). Moreover, some researchers have linked cardiac bone formation in dogs to sudden death, suggesting that the cartilage and bone formation relates to chronic ischemia, as they observed that the local small coronary arteries were normal in the os cordis area of cattle but were focally narrowed in the Dobermans (James and Drake 1968). A crossbred heavy horse with systemic circulatory disturbance presented with ectopic ossification with haematopoietic bone marrow in the heart valves and cardiac skeleton (Matsuda et al. 2010). Degeneration and fibrosis of the atrioventricular nodal tissue and left bundle branch, associated with cartilage or bone in the central fibrous body, were observed in 63 cats with cardiomyopathy (Liu et al. 1975). Finally, in humans, the presence of cartilage in the central fibrous body of the heart in relation to the conducting system was observed in two children who died suddenly (Ferris and Aherne 1971). Naturally it is still difficult to detach cause and correlation both in the above studies and our present findings linking os cordis and cartilago cordis to increased IMF levels.

Considering that the atrioventricular conducting system (Bundle of His) is the only electrical connection between the atria and the ventricles in a normal heart, it is possible that lesions or anatomical peculiarities affecting this area could result in altered function. One study evaluating the fibrous skeleton of the heart with CT and MRI imaging stated that large calcifications involving the central fibrous body can cause heart block by interfering with the normal function of the His bundle and its branches, and concludes that CT is the preferred technique for showing the extent of calcifications in the fibrous skeleton (Saremi et al. 2017).

In our study, despite the limited number of samples, the significant association between the presence of cartilage and/or bone and the level of IMF supports the theory that endochondral ossification occurs in areas of high mechanical forces and/or ischaemia. In humans, a certain degree of interstitial cardiac fibrosis is an age related-change that can lead to functional decline (Biernacka and Frangogiannis 2011) but is also seen secondary to pressure or volume overload and after myocardial infarction

(Gyongyosi et al. 2017). In chimpanzees, the pathophysiology of IMF is still under debate, as lesions can appear in animals as young as 10 years old (Strong et al. 2020). Mineralised lesions, cartilage and bone formation are usually formed following a dystrophic calcification/mineralisation process, which generally occurs after an insult of the affected area resulting in necrosis. It is known that oxygen tension, pH, micronutrients and mechanical stimuli impacts bone formation. Hypoxic environment and an abnormally heightened or prolonged inflammatory response to injury are believed to be key factors in the developments of heterotopic ossifications in humans (Ranganathan et al. 2015). One possible theory based on our study is that in chimpanzees affected by IMF, chronic strain on the heart (as a result and/or cause of IMF) could also lead to heterotopic ossification of the cardiac skeleton, which is considered the fibrous structural support of the heart and an area exposed to high haemodynamic stress.

A novel finding was that the higher amounts of collagen present in the cardiovascular tissue (cardiac skeleton) surrounding areas of hyperdense material such as bone and cartilage. It is possible that collagen amounts were higher prior to the formation of hyperdense material, and/or could have developed after the hyperdense material formed, but it is difficult to measure in practical terms over time. It has been hypothesised that fibrous tissue is a prerequisite for the formation of cartilage and subsequently bone within the heart skeleton (Egerbacher et al. 2000). Normal foetal endochondral bone formation requires deposition of type I collagen followed by type II collagen at the onset of chondrocyte differentiation (Dessau et al. 1980). The cartilage becomes calcified and is replaced by osteoblasts depositing type I collagen once again (Wulf et al. 1994). This is in accordance with the results obtained in the present study, with evidence of endochondral ossification occurring within areas of mineralised cartilaginous metaplasia and expression of type I collagen surrounding areas of bone and no collagen III present. The bone formation observed in this study can be considered to be heterotopic ossification, in which bone forms in soft tissue structures within the body (Kaplan et al. 2004). Less is understood about the role of collagen in heterotopic ossification, however one human study demonstrated that the collagen expression pattern in heterotopic ossification was largely similar to foetal bone formation (Wulf et al. 1994). As such it would be reasonable to assume that collagen deposition may be an important factor in the endochondral formation of bone in the

cardiac skeleton of the chimpanzee. It has also been suggested that collagen synthesis can be upregulated due to mechanical stress on the heart (Weber et al. 1988; Bishop and Lindahl 1999). This is in accordance with the theory that increased cardiac strain due to IMF is potentially leading to further fibrous tissue deposition and subsequent endochondral ossification.

The clinical and functional implications of the presence of cartilage and bone tissue in the chimpanzee cardiac skeleton remain to be elucidated. The ectopic vascular calcifications found in some chimpanzees appear to correlate well with the media calcifications reported in humans with chronic renal disease, hypertension and age. However, of the animals who presented with focal ossifications or cartilage formation in the cardiac skeleton, one died of sudden cardiac death and another following anaesthesia a few days after an episode of syncope. Myocardial fibrosis is known as a favourable substrate for the generation of re-entrant ventricular arrhythmias (John et al. 2004), but whether the presence of cartilage formation or ossification within the cardiac skeleton of chimpanzees further increases the chances of arrhythmic events is, as yet, unknown.

Both IMF and foci of ectopic calcification and ossification within the heart are difficult to detect using conventional echocardiography and radiography; however, the relative ease of detection of both bone and mineralised cartilage by microCT in our specimens make these structures good candidates as ante-mortem markers of IMF in chimpanzees. However, it should be noted that not all chimpanzees affected with IMF had os/cartilago cordis, therefore it may serve as an indicator rather than diagnosis tool. The possibility of os cordis and cartilago cordis occurring in humans suffering from similar cardiovascular disorders should be considered. In conclusion this new discovery of both os cordis and a cartilago cordis, in the chimpanzee heart highlights the need for further cardiovascular investigations in this and other species including humans using the latest technologies in order to gain valuable clinical and anatomical knowledge.

Conclusion

In 2021, more than 1750 chimpanzees, 952 orangutans, 840 gorillas and 220 bonobos were recorded by Species360 as living in zoological institutions worldwide. The protection of these populations is essential and veterinary research carried out in zoos allows for a better understanding of the environmental needs, physiology and disease mechanisms of each species, which not only benefits the health and welfare of captive individuals but will also help for the conservation of wild populations.

Early work from the Ape Heart Project confirmed that heart disease is a major cause of morbidity and mortality in captive great apes (Strong et al. 2016), and developed protocols and recommendations to improve clinical and post-mortem diagnostic of CVD in these species (Strong et al. 2015, 2018c).

The first chapter of this thesis synthesises and evaluates the literature available on the topic of great ape cardiovascular disease, with some insights into advances made in the human field for comparison purposes. Idiopathic myocardial fibrosis appeared as the CVD type most commonly reported in all ape species, followed by aortic dissection especially in gorillas. Atherosclerosis, valvular disease, infective myocarditis and congenital defects were only sporadically reported. Although cases of IMF in great apes are frequently described in the literature, publications investigating its causes are scarce. Ageing, hypertension, inflammatory processes and deficiencies in nutrition or husbandry such as hypovitaminosis D or stress were identified as likely to play a role in CVD in great apes, thus warrant being thoroughly studied as possible risk factors. Regarding clinical presentation, although symptoms of congestive heart failure are sometimes reported, sudden death without previous symptoms commonly occurs and is believed to be due to arrhythmic events, thus the investigation of arrhythmia in great apes was considered an indispensable part of this thesis.

Hypertension has been proposed as a possible aetiology of heart disease in apes, as changes such as hypertrophic cardiomyopathy and hyaline arteriosclerosis of small intrinsic arteries are sometimes present (Lowenstine et al. 2016). The demonstration of hypertension antemortem in apes is challenging, and the use of accurate blood pressure equipment is essential. Chapter 2 demonstrates that there is a critical need for the validation of oscillometric blood pressure devices in great apes. Results from

studies evaluating the accuracy of blood pressure oscillometric machines in apes should be shared amongst the zoo veterinary community, as although some devices may not meet all the requirements for validation, they may still be useful to monitor trends during anaesthesia and to make clinical decisions as long as the imprecision of the device is known and taken into account. Hypertension needs to be detected to be able to set up a treatment protocol and decrease the risk of cardiac disease, vascular events, kidney disease and other complications. Hypotension during anaesthetic procedures also needs to be quickly identified to decrease the risk of anaesthetic death. In humans, intraoperative hypotension is a major cause of death during anaesthesia (Lonjaret et al. 2014) and it is probable that in great apes already affected with chronic myocardial fibrosis, the occurrence of an acute ischaemic myocardial injury due to a prolonged hypotensive event could have disastrous consequences. Thus, the effects of anaesthetic drugs not only represent a major obstacle to the diagnostic of CVD in great apes but also contribute to the risk of developing a cardiac event. Efforts to investigate novel anaesthetic protocols with fewer negative cardiovascular effects should be made, and zoos need to continue to develop training programmes and equipment for the measurement of blood pressure in conscious great apes.

As cardiac fibrosis may provide a substrate for severe arrhythmic events and increase the risk of sudden cardiac death, in chapter 3 we investigated the use of implantable loop recorders as an integral part of cardiac monitoring in chimpanzees. Thousands of recorded single lead-ECG episodes confirmed that in chimpanzees, ventricular premature complexes (VPCs) are the most common type of arrhythmia, and although the availability of longitudinal clinical and post-mortem data such as echocardiography, serum biomarkers and histopathology made this study unique, it was difficult to judge the significance of the occurrence of arrhythmias due to the low number of animals studied. One chimpanzee that during the years before death presented multimorphic VPCs, couplets, triplets, ventricular bigeminy and trigeminy together with abnormal echocardiographic findings and high levels of cardiac biomarkers was found to have marked chronic and acute cardiac and vascular changes on histopathology, demonstrating that antemortem clinical findings can be significant in animals with high degrees of cardiac changes. Our findings indicate that the implantation of ILR devices is justified in zoo chimpanzees at risk of cardiac disease as the data collected can be

combined with other screening methods to monitor cardiac health. Ideally ILR implantations should be synchronised with routine health-checks in order to avoid unnecessary repetitions of anaesthetic procedures.

Deficiencies in husbandry need to be investigated as possible risk factors in great ape CVD, as some research seems to indicate that zoo apes are more affected with CVD compared with their wild counterparts. All the species of great apes naturally live in tropical areas that receive high amounts of direct sunlight, they are thus likely poorly adapted to restricted UVB exposure and may not synthesise enough cutaneous vitamin D when housed in zoos at Northern or Southern latitudes. It is critical to establish reference intervals in apes living in their natural environment to be able to define hypovitaminosis D in our zoo great apes, this has however not yet been achieved partly due to logistical impediments associated with sample collection and analysis in the field. Thus, the use of the dry blood spot (DBS) method to measure vitamin D in chimpanzees was explored in chapter 4, as this sampling method represents great advantages for field studies. The DBS technique, however, presented a relatively high imprecision compared with the measurement in serum, and results from DBS cannot be directly compared with results from serum samples. Reference intervals specific to the DBS methods could, however, be calculated in the future.

Despite the lack of a “normal” vitamin D range in great apes, the analysis of more than 200 serum samples from European zoo chimpanzees demonstrated that low vitamin D concentrations are commonly encountered in this population year-round, even in Southern Europe. This is a concerning finding and confirms that hypovitaminosis D could be a risk factor for cardiac disease and especially IMF in great apes, as human data shows an inhibitory role of vitamin D in cardiac fibrosis (Meredith et al. 2015b). As the provision of daily outside access in European zoo great apes was associated with higher levels of vitamin D concentrations, zoos need to understand the importance of allowing and stimulating their animals to spend time outdoors when the cutaneous synthesis of vitamin D is possible. Other options for countries where the climate does not allow for sufficient sun exposure would be regular supplementation with oral vitamin D or the provision of artificial full-spectrum light in the indoor enclosures. Detailed recommendations on how to improve the vitamin D status in European zoo great apes are urgently needed.

Histology is still considered the gold-standard technique for a definitive diagnostic of CVD, and particularly IMF, in great apes. Results from the thorough post-mortem examination of 50 hearts of European zoo great apes are detailed in chapter 6 and findings from fifteen of these hearts were published in the AHP paper on chimpanzee myocardial fibrosis (Strong et al. 2020). Our cohort showed that a high percentage of chimpanzees are affected by moderate to marked myocardial fibrosis, while gorillas seem to present with lower degrees of fibrosis and more prevalent vascular changes. Myocardial fibrosis was characterised by the presence of interstitial, perivascular and/or replacement fibrosis, with a few cases showing only minimal to mild diffuse interstitial fibrosis and more chronic and severe cases presenting several prominent areas of replacement fibrosis that were randomly distributed across the myocardium. As only a minimal to mild inflammatory infiltrate was present in most cases and generally associated with areas of cardiac remodelling, an infectious aetiology of IMF is unlikely. Acute myocardial damage in the form of myocardial necrosis and contraction bands was also commonly seen in bonobos and chimpanzees especially in cases of unexpected death. Both myocardial fibrosis and myocardial necrosis are considered the most frequent substrates for abrupt electrical disorders (Thiene et al. 2016), thus terminal arrhythmias due to ischaemic myocardial damage can be considered as the final mechanism of death if other cardiac and extracardiac causes are excluded. The scattered areas of replacement fibrosis and acute necrosis found in chimpanzees resemble the pattern of multifocal microinfarction caused by catecholamine toxicity in humans, where vascular spasm of small intramural vessels, enhanced contractility and increased heart rate lead to a mismatch between demand and supply of oxygen in the myocardium, inducing cardiomyocyte death and progressive multifocal myocardial fibrosis (Liaudet et al. 2014). Chimpanzees and bonobos live in complex social groups, and in the wild, it has been shown that social support with bond partners can decrease urinary glucocorticoid levels in everyday life. In zoo settings, the artificial composition of social groups and a restricted "*fly response*" after stressful events may cause chronic stress and a sustained elevation of endogenous catecholamines. Interestingly, orangutans, who are solitary and often considered as having a much calmer nature than other apes, present a lower occurrence of myocardial fibrosis than other great apes. In gorillas, degenerative and inflammatory vascular changes were commonly seen, which points towards a different

aetiopathogenesis of cardiac disease in these cases. A unique case of granulomatous aortitis in a female gorilla was described (Moittié et al. 2020c). It is interesting to note that several zoos reported atherosclerosis of the aorta in great apes at post-mortem, however, for most of these cases, the detailed examination of cardiac vessels by the AHP could not confirm this finding but did commonly diagnose age-related and non-pathogenic aortic intimal thickenings and fatty streaks that could be confused macroscopically with atherosclerotic lesions. In humans, the abdominal aorta is affected much earlier, more frequently and more severely by atherosclerosis compared to the thoracic aorta (Stone et al. 2015), thus the abdominal aorta should routinely be examined histopathologically to rule out atherosclerosis in great apes.

The last chapter of this thesis described the use of micro computed tomography on fixed chimpanzee hearts and documents the discovery of the first os cordis in chimpanzees (Moittié et al. 2020a). Although it is still unclear if the presence of an os cordis is an anatomical feature or a pathological finding in this species, the formation of bone tissue within the fibrous trigone of chimpanzee hearts affected with moderate to marked degrees of myocardial fibrosis is likely a result of the increased strain that these hearts face to maintain an adequate cardiac output in settings of reduced myocardial oxygenation. In turn, the presence of bone near or within the conduction system of the heart could hinder electrical transmission and lead to arrhythmic events and sudden cardiac death. Ideally, imaging techniques to detect antemortem the presence of an os cordis should be developed for chimpanzees and integrated into the screening protocol for cardiac disease.

Much work is still needed to better understand the aetiopathogenesis and risk factors associated with cardiovascular disease in great apes, and the Ape Heart Project with the greatly appreciated and valued help and support of collaborating zoos throughout Europe will continue investigating this complex issue in the future.

Literature cited

Aarnes, T. K., J. A. E. Hubbell, P. Lerche and R. M. Bednarski. 2012. Comparison of invasive and oscillometric blood pressure measurement techniques in anesthetized camelids. Can. Vet. J. 53: 881. Canadian Veterinary Medical Association.

Abel Nielsen, S. C., T. Mourier, U. Baandrup, T. M. Søland, M. F. Bertelsen, M. T. P. Gilbert and L. P. Nielsen. 2012. Probable transmission of coxsackie B3 virus from human to chimpanzee, Denmark. Emerg. Infect. Dis. 18: 1163–1165. Centers for Disease Control and Prevention.

Agborsangaya, C., A. T. Toriola, K. Grankvist, H. M. Surcel, K. Holl, S. Parkkila, P. Tuohimaa, A. Lukanova and M. Lehtinen. 2010. The effects of storage time and sampling season on the stability of serum 25-hydroxy vitamin D and androstenedione. Nutr. Cancer 62: 51–57.

Åkeson, P. K., T. Lind, O. Hernell, S.-A. Silfverdal and I. Öhlund. 2016. Serum Vitamin D Depends Less on Latitude Than on Skin Color and Dietary Intake During Early Winter in Northern Europe. J. Pediatr. Gastroenterol. Nutr. 62: 643–649. Lippincott Williams and Wilkins.

Al Mheid, I. and A. A. Quyyumi. 2017. Vitamin D and Cardiovascular Disease: Controversy Unresolved. Elsevier USA.

Amoore, J. N., W. B. Geake and D. H. T. Scott. 1997. Oscillometric non-invasive blood pressure measurements: The influence of the make of instrument on readings? Med. Biol. Eng. Comput. 35: 131–134.

Andrade, M. C., P. B. Higgins, V. L. Mattern, M. A. De, L. Garza, K. M. Brasky, V. S. Voruganti and A. G. Comuzzie. 2011. Morphometric Variables Related to Metabolic Profile in Captive Chimpanzees (Pan troglodytes). 61: 457–461.

Artigos. 2014. Sudden cardiac death and obesity. Expert Rev. Cardiovasc. Ther. 12: 1099–1110.

Atencia, R., L. Revuelta, J. D. Somauroo and R. E. Shave. 2015. Electrocardiogram reference intervals for clinically normal wild-born chimpanzees (Pan troglodytes). Am. J. Vet. Res. 76: 688–693.

Babbs, C. F. 2012. Oscillometric measurement of systolic and diastolic blood pressures validated in a physiologic mathematical model. Biomed. Eng. Online 11: 56. BioMed

Central.

Badea, C. T., M. Drangova, D. W. Holdsworth and G. A. Johnson. 2008. In vivo small-animal imaging using micro-CT and digital subtraction angiography. NIH Public Access.

Baitchman, E. J., P. P. Calle, T. L. Clippinger, S. L. Deem, S. B. James, B. L. Raphael and R. a Cook. 2006. Evaluation of blood lipid profiles in captive western lowland gorillas (Gorilla gorilla gorilla). J. Zoo Wildl. Med. 37: 126–129.

Bald, M., R. Westhues and K. E. Bonzel. 1996. Blood pressure monitoring at the wrist: is it reliable in children and adolescents? Z. Kardiol. 85 Suppl 3: 106–8.

Barasch, E., J. S. Gottdiener, E. K. Marino Larsen, P. H. M. Chaves, A. B. Newman and T. A. Manolio. 2006. Clinical significance of calcification of the fibrous skeleton of the heart and aortosclerosis in community dwelling elderly. The Cardiovascular Health Study (CHS). Am. Heart J. 151: 39–47. Mosby.

Bartlett, S. L., T. C. Chen, H. Murphy, M. F. Holick, M. Tlusty and E. Baitchman. 2017. Assessment of serum 25-hydroxyvitamin d concentrations in two collections of captive gorillas (gorilla gorilla gorilla). J. Zoo Wildl. Med. 48: 144–151. American Association of Zoo Veterinarians.

Basso, C., M. Burke, P. Fornes, P. J. Gallagher, R. H. De Gouveia, M. Sheppard, G. Thiene and A. Van Der Wal. 2008. Guidelines for autopsy investigation of sudden cardiac death. Springer-Verlag.

Bermejo, M., J. D. Rodriguez-Teijeiro, G. Illera, A. Barroso, C. Vila and P. D. Walsh. 2006. Ebola Outbreak Killed 5000 Gorillas. Science (80-.). 314: 1564–1564.

Bertelsen, M. F., C. Grøndahl, G. F. Stegmann, C. Sauer, N. H. Secher, J. M. Hasenkam, M. Damkjær, C. Aalkjær and T. Wang. 2017. Accuracy of noninvasive anesthetic monitoring in the anesthetized giraffe (Giraffa camelopardalis). J. Zoo Wildl. Med. 48: 609–615. American Association of Zoo Veterinarians.

Biase, M. Di, A. Chiddo, G. Caruso, M. Tritto, A. Marchese and P. Rizzon. 1992. Ventricular premature beats in young subjects without evidence of cardiac disease: Histological findings. Eur. Heart J. 13: 732–737. Oxford University Press.

Biernacka, A. and N. G. Frangogiannis. 2011. Aging and Cardiac Fibrosis. Aging Dis. 2: 158–173. JKL International LLC.

Binkley, N. and C. T. Sempos. 2014. Standardizing vitamin D assays: The way forward. Wiley-Blackwell.

Bishop, J. E. and G. Lindahl. 1999. Regulation of cardiovascular collagen synthesis by

mechanical load. Cardiovasc. Res. 42: 27–44.

Bjerg, L. N., J. R. Halgreen, S. H. Hansen, H. A. Morris and N. R. Jørgensen. 2019. An evaluation of total 25-hydroxyvitamin D assay standardization: Where are we today? J. Steroid Biochem. Mol. Biol. 190: 224–233. Pergamon.

Black, L. J., D. Anderson, M. W. Clarke, A.-L. Ponsonby and R. M. Lucas. 2015. Analytical Bias in the Measurement of Serum 25-Hydroxyvitamin D Concentrations Impairs Assessment of Vitamin D Status in Clinical and Research Settings. PLoS One 10: e0135478.

Bland, J. M. and D. G. Altman. 2007. Agreement between methods of measurement with multiple observations per individual. J. Biopharm. Stat. 17: 571–582. Taylor & Francis Group .

Blaton, V. and H. Peeters. 1976. The nonhuman primates as models for studying human atherosclerosis: studies on the chimpanzee, the baboon and the rhesus macacus. Adv. Exp. Med. Biol. 67: 33–64.

Boerckel, J. D., D. E. Mason, A. M. McDermott and E. Alsberg. 2014. Microcomputed tomography: approaches and applications in bioengineering. Stem Cell Res. Ther. 5: 144. BioMed Central.

Bommineni, Y. R., E. J. Dick, J. S. Estep, J. L. Van de Berg and G. B. Hubbard. 2009. Fatal acute Chagas disease in a chimpanzee. J. Med. Primatol. 38: 247–251.

Bosiack, A. P., F. A. Mann, J. R. Dodam, C. C. Wagner-Mann and K. R. Branson. 2010. Comparison of ultrasonic Doppler flow monitor, oscillometric, and direct arterial blood pressure measurements in ill dogs. J. Vet. Emerg. Crit. Care 20: 207–215.

Bouillon, R. 2017. Comparative analysis of nutritional guidelines for vitamin D. Nature Publishing Group.

Boyd, R., M. D. Danforth, G. Rapoport, M. M. Sleeper, W. H. Devlin, I. Kutinsky, B. Brainard and H. W. Murphy. 2020. Great Ape Heart Project guidelines for the echocardiographic assessment of great apes. J. Zoo Wildl. Med. 50: 822. American Association of Zoo Veterinarians.

Brown, S., C. Atkins, R. Bagley, A. Carr, L. Cowgill, M. Davidson, B. Egner, J. Elliott, R. Henik, M. Labato, M. Littman, D. Polzin, L. Ross, P. Snyder and R. Stepien. 2007. Guidelines for the Identification, Evaluation, and Management of Systemic Hypertension in Dogs and Cats. J. Vet. Intern. Med. 21: 542–558. John Wiley & Sons, Ltd (10.1111).

Butters, T. D., S. J. Castro, T. Lowe, Y. Zhang, M. Lei, P. J. Withers and H. Zhang. 2014.

Optimal iodine staining of cardiac tissue for X-ray computed tomography. PLoS One 9: e105552. Public Library of Science.

Caccamo, D., S. Ricca, M. Currò and R. Ientile. 2018. Health risks of hypovitaminosis D: A review of new molecular insights. Multidisciplinary Digital Publishing Institute (MDPI).

Caforio, A. L. P., S. Pankuweit, E. Arbustini, C. Basso, J. Gimeno-Blanes, S. B. Felix, M. Fu, T. Heliö, S. Heymans, R. Jahns, K. Klingel, A. Linhart, B. Maisch, W. McKenna, J. Mogensen, Y. M. Pinto, A. Ristic, H. P. Schultheiss, H. Seggewiss, L. Tavazzi, G. Thiene, A. Yilmaz, P. Charron and P. M. Elliott. 2013. Current state of knowledge on aetiology, diagnosis, management, and therapy of myocarditis: A position statement of the European Society of Cardiology Working Group on Myocardial and Pericardial Diseases. Eur. Heart J. 34: 2636–2648. Oxford University Press.

Cardoso, S., A. Santos, R. S. Guerra, A. S. Sousa, P. Padrão, P. Moreira, C. Afonso, T. F. Amaral and N. Borges. 2017. Association between serum 25-hidroxyvitamin D concentrations and ultraviolet index in Portuguese older adults: A cross-sectional study. BMC Geriatr. 17: 256. BioMed Central Ltd.

Carter, G. D., J. Berry, R. Durazo-Arvizu, E. Gunter, G. Jones, J. Jones, H. L. J. Makin, P. Pattni, K. W. Phinney, C. T. Sempos and E. L. Williams. 2017. Quality assessment of vitamin D metabolite assays used by clinical and research laboratories. J. Steroid Biochem. Mol. Biol. 173: 100–104. Pergamon.

Cashman, K. D., K. G. Dowling, Z. Škrabáková, M. Gonzalez-Gross, J. Valtueña, S. De Henauw, L. Moreno, C. T. Damsgaard, K. F. Michaelsen, C. Mølgaard, R. Jorde, G. Grimnes, G. Moschonis, C. Mavrogianni, Y. Manios, M. Thamm, G. B. M. Mensink, M. Rabenberg, M. A. Busch, L. Cox, S. Meadows, G. Goldberg, A. Prentice, J. M. Dekker, G. Nijpels, S. Pilz, K. M. Swart, N. M. Van Schoor, P. Lips, G. Eiriksdottir, V. Gudnason, M. F. Cotch, S. Koskinen, C. Lamberg-Allardt, R. A. Durazo-Arvizu, C. T. Sempos and M. Kiely. 2016. Vitamin D deficiency in Europe: Pandemic? Am. J. Clin. Nutr. 103: 1033–1044. American Society for Nutrition.

Chen, S., C. S. Law, C. L. Grigsby, K. Olsen, T.-T. Hong, Y. Zhang, Y. Yeghiazarians and D. G. Gardner. 2011. Cardiomyocyte-Specific Deletion of the Vitamin D Receptor Gene Results in Cardiac Hypertrophy. Circulation 124: 1838–1847.

Chilton, J., A. Wilcox, M. Lammey and D. Meyer. 2016. Characterization of a Cardiorenal-like Syndrome in Aged Chimpanzees (Pan troglodytes). Vet Pathol 53: 417–424.

Christakos, S., M. Hewison, D. G. Gardner, C. L. Wagner, I. N. Sergeev, E. Rutten, A. G. Pittas, R. Boland, L. Ferrucci and D. D. Bikle. 2013. Vitamin D: Beyond bone. Ann. N. Y.

Acad. Sci. 1287: 45–58.

Cieslik, K. A., G. E. Taffet, S. Carlson, J. Hermosillo, J. Trial and M. L. Entman. 2011. Immune-inflammatory dysregulation modulates the incidence of progressive fibrosis and diastolic stiffness in the aging heart. J. Mol. Cell. Cardiol. 50: 248–256.

Cinar, I., H. Wang and J. R. Stone. 2017. Clinically isolated aortitis: pitfalls, progress, and possibilities. Elsevier Inc.

Clyde, V. L., L. Roth, B. Bell, R. Wallace, D. Slosky and J. Dolan. 2002. Cardiac and gestational ultrasound parameters in non-anesthetized bonobos. P. 365 in 2002 Proceedings AAZV. AAZV.

Cooper, J. E. 2017. Respiratory and Cardiovascular Systems. Pp. 107–118 in Gorilla Pathology and Health: With a Catalogue of Preserved Materials (J. E. Cooper and G. Hull, eds). Elsevier.

Costagliola, A., G. Piegari, I. Otrocka-Domagala, D. Ciccarelli, V. Iovane, G. Oliva, V. Russo, L. Rinaldi, S. Papparella and O. Paciello. 2016. Immunopathological features of canine myocarditis associated with leishmania infantum infection. Biomed Res. Int. 2016. Hindawi Limited.

Cremer, J., A. da Cunha, K. Aulakh, C. C. Liu and M. J. Acierno. 2020. Validation of the oscillometric blood pressure monitor Vet20 SunTech in anesthetized healthy cats. Vet. Anaesth. Analg. 47: 309–314. Association of Veterinary Anaesthetists and American College of Veterinary Anesthesia and Analgesia.

Crissey, S. D., J. E. Barr, K. A. Slifka, P. E. Bowen, M. Stacewicz-Sapuntzakis, C. Langman, A. Ward and K. Ange. 1999. Serum concentrations of lipids, vitamins A and E, vitamin D metabolites, and carotenoids in nine primate species at four zoos. ZOO Biol. 18: 551–564. John Wiley & Sons, Inc.

Cvan Trobec, K., J. Trontelj, J. Springer, M. Lainscak and M. Kerec Kos. 2014. Liquid chromatography-tandem mass spectrometry method for simultaneous quantification of bisoprolol, ramiprilat, propranolol and midazolam in rat dried blood spots. J. Chromatogr. B Anal. Technol. Biomed. Life Sci. 958: 29–35.

D'avolio, A., V. Avataneo, A. Manca, J. Cusato, A. De Nicolò, R. Lucchini, F. Keller and M. Cantù. 2020. 25-hydroxyvitamin D concentrations are lower in patients with positive PCR for SARS-CoV-2. Nutrients 12. MDPI AG.

da Cunha, A. F., S. J. Ramos, M. Domingues, H. Beaufrère, A. Shelby, R. Stout and M. J. Acierno. 2016. Agreement between two oscillometric blood pressure technologies and

invasively measured arterial pressure in the dog. Vet. Anaesth. Analg. 43: 199–203.

Daghash, S. M. and H. A. M. Farghali. 2017. The cardiac skeleton of the Egyptian Water buffalo (Bubalus bubalis). Int. J. Adv. Res. Biol. Sci 4: 1–13.

Datta, P., P. A. Philipsen, P. Olsen, M. K. Bogh, P. Johansen, A. V Schmedes, N. Morling and H. C. Wulf. 2017. The half-life of 25(OH)D after UVB exposure depends on gender and Vitamin D receptor polymorphism but mainly on the start level. Photochem. Photobiol. Sci. 16: 985–995.

De Jong, S., J. J. Zwanenburg, F. Visser, R. van der Nagel, H. V. van Rijen, M. A. Vos, J. M. de Bakker and P. R. Luijten. 2011. Direct detection of myocardial fibrosis by MRI. J. Mol. Cell. Cardiol. 51: 974–979.

de Winter, J. C. F. and D. Dodou. 2010. Five-point likert items: T test versus Mann-Whitney-Wilcoxon. Pract. Assessment, Res. Eval.

DEQAS review 2016/2017. 2016.

Dessau, W., H. von der Mark, K. von der Mark and S. Fischer. 1980. Changes in the patterns of collagens and fibronectin during limb-bud chondrogenesis. J. Embryol. Exp. Morphol. 57: 51–60.

Dick, S. A. and S. Epelman. 2016. Chronic heart failure and inflammation.

Dirks, N. F., M. T. Ackermans, P. Lips, R. T. de Jongh, M. G. Vervloet, R. de Jonge and A. C. Heijboer. 2018. The when, what & how of measuring vitamin D metabolism in clinical medicine. MDPI AG.

Doane, C. J., R. D. Lee and M. M. Sleeper. 2006. Electrocardiogram Abnormalities in Captive Chimpanzees (Pan troglodytes). Comp. Med. 56: 512–518.

Doube, M., M. M. Klosowski, I. Arganda-Carreras, F. P. Cordelières, R. P. Dougherty, J. S. Jackson, B. Schmid, J. R. Hutchinson and S. J. Shefelbine. 2010. BoneJ: Free and extensible bone image analysis in ImageJ. Bone 47: 1076–1079. Europe PMC Funders.

Drake, R. L. (Richard L., W. Vogl, A. W. M. Mitchell, H. Gray and H. Gray. 2010. Gray’s anatomy for students. Churchill Livingstone/Elsevier.

Drane, A. L. A. A. L. A., R. Atencia, S.-M. M. Cooper, P. Rodriguez, C. Sanchez, S. Simcox, Y. Feltrer, B. Peck, J. Eng, S. Moittie, S. Unwin, G. Howatson, D. Oxborough, M. R. Stembridge, R. E. E. Shave, M. R. Stembrirdge and R. E. E. Shave. 2019. Cardiac structure and function characterized across age groups and between sexes in healthy wild-born captive chimpanzees (Pan troglodytes) living in sanctuaries. Am. J. Vet. Res. 80: 547–557.

Drane, A. L., R. Atencia, S. M. Cooper, Y. Feltrer, T. Calvi, T. Strike, C. Palmer, S. Simcox, P. Rodriguez, C. Sanchez, H. van Bolhuis, B. Peck, J. Eng, S. Moittie, S. Unwin, G. Howatson, D. Oxborough, M. R. Stembridge and R. E. Shave. 2020. Evaluation of relationships between results of electrocardiography and echocardiography in 341 chimpanzees (Pan troglodytes). Am. J. Vet. Res. 81: 488–498.

Drynan, E. A. and A. L. Raisis. 2013. Comparison of invasive versus noninvasive blood pressure measurements before and after hemorrhage in anesthetized greyhounds using the Surgivet V9203. J. Vet. Emerg. Crit. Care 23: 523–531.

Drynan, E. A., M. Schier and A. L. Raisis. 2016. Comparison of invasive and noninvasive blood pressure measurements in anaesthetized horses using the Surgivet V9203. Vet. Anaesth. Analg. 43: 301–308.

du Plessis, M., C. Blaak, R. S. Tubbs and M. Loukas. 2014. Unraveling the anatomy of the cardiac skeleton of the heart. Federation of American Societies for Experimental Biology.

Durán, A. C., D. López, A. Guerrero, A. Mendoza, J. M. Arqué and V. Sans-Coma. 2004. Formation of cartilaginous foci in the central fibrous body of the heart in Syrian hamsters (Mesocricetus auratus). J. Anat. 205: 219–227.

Egerbacher, M., H. Weber and S. Hauer. 2000. Bones in the heart skeleton of the otter (Lutra lutra). J. Anat. 196: 485–91. Blackwell Science Ltd.

Eichberg, J. W. and R. E. Shade. 1987. “Normal” blood pressure in chimpanzees. J. Med. Primatol. 16: 317–21.

Ely, J. J., M. A. Bishop, M. L. Lammey, M. M. Sleeper, J. M. Steiner and D. R. Lee. 2010. Use of biomarkers of collagen types I and III fibrosis metabolism to detect cardiovascular and renal disease in chimpanzees (Pan troglodytes). Comp. Med.

Ely, J. J., T. Zavaskis and M. L. Lammey. 2013. Hypertension increases with aging and obesity in chimpanzees (Pan troglodytes). Zoo Biol 32: 79–87.

Ely, J. J., T. Zavaskis, M. L. Lammey and D. Rick Lee. 2011a. Blood pressure reference intervals for healthy adult chimpanzees (Pan troglodytes). J. Med. Primatol. 40: 171–180.

Ely, J. J., T. Zavaskis, M. L. Lammey, M. M. Sleeper and D. R. Lee. 2011b. Association of brain-type natriuretic protein and cardiac troponin I with incipient cardiovascular disease in chimpanzees (Pan troglodytes). Comp. Med. 61: 163–9.

Ercole, A. 2006. Commentary: Attenuation in invasive blood pressure measurement systems. Br. J. Anaesth. 96: 560–562. Oxford University Press.

Erdoğan, S., M. Lima and W. Pérez. 2014. Inner ventricular structures and valves of the heart

in white rhinoceros (Ceratotherium simum). Anat. Sci. Int. 89: 46–52. Springer Japan.

Esper, S. A. and M. R. Pinsky. 2014. Arterial waveform analysis. Best Pract. Res. Clin. Anaesthesiol. 28: 363–380.

Everett, R. J., C. G. Stirrat, S. I. R. Semple, D. E. Newby, M. R. Dweck and S. Mirsadraee. 2016. Assessment of myocardial fibrosis with T1 mapping MRI.

Eyles, D., C. Anderson, P. Ko, A. Jones, A. Thomas, T. Burne, P. B. Mortensen, B. Nørgaard-Pedersen, D. M. Hougaard and J. McGrath. 2009. A sensitive LC/MS/MS assay of 25OH vitamin D3 and 25OH vitamin D2 in dried blood spots. Clin. Chim. Acta 403: 145–151.

Fairey, E. R., N. G. Shuart, M. Busman, P. D. R. Moeller and J. S. Ramsdell. 2001. Biomonitoring brevetoxin exposure in mammals using blood collection. Environ. Health Perspect. 109: 717–720.

Fan, D., A. Takawale, J. Lee and Z. Kassiri. 2012. Cardiac fibroblasts, fibrosis and extracellular matrix remodeling in heart disease. Fibrogenesis Tissue Repair 5: 15.

Feltrer, Y., T. Strike, A. Routh, D. Gaze and R. E. Shave. 2016. Point-of-care cardiac troponin I in non-domestic species: a feasibility study. J. Zoo Aquarium Res. 4: 99–103.

Ferrari, D., G. Lombardi and G. Banfi. 2017. Concerning the vitamin D reference range: Pre-analytical and analytical variability of vitamin D measurement. Croatian Society for Medical Biochemistry and Laboratory Medicine.

Ferris, J. A. J. and W. A. Aherne. 1971. Cartilage in relation to the conducting tissue of the heart in sudden death. Lancet 297: 64–66. Elsevier.

Formenty, P., C. Boesch, M. Wyers, C. Steiner, F. Donati, F. Dind, F. Walker and B. Le Guenno. 1999. Ebola Virus Outbreak among Wild Chimpanzees Living in a Rain Forest of Cote d'Ivoire. J. Infect. Dis. 179: S120–S126.

France, L. K., M. S. Vermillion and C. M. Garrett. 2018. Comparison of Direct and Indirect Methods of Measuring Arterial Blood Pressure in Healthy Male Rhesus Macaques (Macaca mulatta). J. Am. Assoc. Lab. Anim. Sci. 57: 64–69. American Association for Laboratory Animal Science.

Frink, R. J. and B. Merrick. 1974. The sheep heart: Coronary and conduction system anatomy with special reference to the presence of an os cordis. Anat. Rec. 179: 189–199. Wiley Subscription Services, Inc., A Wiley Company.

From, A. M., J. J. Maleszewski and C. S. Rihal. 2011. Current status of endomyocardial biopsy. Mayo Clin. Proc. 86: 1095–1102. Mayo Foundation.

Fung, G., H. Luo, Y. Qiu, D. Yang and B. McManus. 2016. Myocarditis. American Heart Association, Inc.

Furuichi, T., G. Idani, H. Ihobe and S. Kuroda. 1998. Population Dynamics of Wild Bonobos (Pan paniscus) at Wamba. Int. J. Primatol. 19: 1029–1043. Kluwer Academic Publishers-Plenum Publishers.

Furukawa, T., R. Maggi, C. Bertolone, F. Ammirati, M. Santini, R. Ricci, F. Giada and M. Brignole. 2011. Effectiveness of remote monitoring in the management of syncope and palpitations. Europace, doi: 10.1093/europace/euq503.

Gaggin, H. K. and J. L. Januzzi Jr. 2013. Biomarkers and diagnostics in heart failure. Biochim. Biophys. Acta - Mol. Basis Dis. 1832: 2442–2450.

GAHP Recommended Cardiac Trimming Protocol for Pathologists. n.d.

Galior, K., H. Ketha, S. Grebe and R. J. Singh. 2018. 10 years of 25-hydroxyvitamin-D testing by LC-MS/MS-trends in vitamin-D deficiency and sufficiency. Bone Reports 8: 268–273. Elsevier.

Gamble, K. C. 2004. Pathologic Review of the Chimpanzee (Pan troglodytes): 1990-2003. P. 561 in 2004 Proceedings AAZV, AAWV,WDA Joint conference. AAZV.

Gardner, D. G., S. Chen, D. J. Glenn and W. Ni. 2011. Vitamin D and the cardiovascular system. Pp. 541–563 in Vitamin D (D. FELDMAN, J. W. Pike, and J. S. Adams, eds). Elsevier Inc.

Ghonimi, W. and A. Balah. 2014. Os cordis of The Mature Dromedary Camel Heart (Camelus dromedaries) with Special Emphasis to The Cartilago Cordis. J Vet. Sci … 5: 193–200. OMICS International.

Giallauria, F., C. Vigorito, N. Ferrara and L. Ferrucci. 2013. Cardiovascular Calcifications in Old Age: Mechanisms and Clinical Implications. Curr. Transl. Geriatr. Exp. Gerontol. Rep. 2: 255–267. Springer US.

Giavarina, D. 2015. Understanding Bland Altman analysis. Biochem. Medica 25: 141–151. Croatian Society for Medical Biochemistry and Laboratory Medicine.

Golbidi, S., J. C. Frisbee and I. Laher. 2015. Chronic stress impacts the cardiovascular system: animal models and clinical outcomes. Am. J. Physiol. - Hear. Circ. Physiol. 308: H1476–H1498. American Physiological Society.

González-Molero, I., S. Morcillo, S. Valdés, V. Pérez-Valero, P. Botas, E. Delgado, D. Hernández, G. Olveira, G. Rojo, C. Gutierrez-Repiso, E. Rubio-Martín, E. Menéndez and F. Soriguer. 2011. Vitamin D deficiency in Spain: A population-based cohort study. Eur.

J. Clin. Nutr. 65: 321–328. Nature Publishing Group.

Gornik, H. L. and M. A. Creager. 2008. Aortitis. Circulation 117: 3039–3051. Lippincott Williams & Wilkins.

Gourdeau, M., R. Martin, Y. Lamarche and L. Tetreault. 1986. Oscillometry and direct blood pressure: A comparative clinical study during deliberate hypotension. Can. Anaesth. Soc. J. 33: 300–307. Springer.

Grant, W. B., H. Lahore, S. L. McDonnell, C. A. Baggerly, C. B. French, J. L. Aliano and H. P. Bhattoa. 2020. Evidence that vitamin d supplementation could reduce risk of influenza and covid-19 infections and deaths. MDPI AG.

Gray, R., R. O'Neal and F. Jordan. 1981. Sudden death associated with atherosclerosis in a gorilla. J. Am. Vet. … 179: 1306–1307.

Grosenbaugh, D. A. and W. W. Muir. 1998. Accuracy of noninvasive oxyhemoglobin saturation, end-tidal carbon dioxide concentration, and blood pressure monitoring during experimentally induced hypoxemia, hypotension, or hypertension in anesthetized dogs. Am. J. Vet. Res.

Gyongyosi, M., J. Winkler, I. Ramos, Q. T. Do, H. Firat, K. McDonald, A. Gonzalez, T. Thum, J. Diez, F. Jaisser, A. Pizard and F. Zannad. 2017. Myocardial fibrosis: biomedical research from bench to bedside. Eur J Hear. Fail 19: 177–191.

Hamada, Y., T. Udono, M. Teramoto and T. Sugawara. 1996. The growth pattern of chimpanzees: Somatic growth and reproductive maturation in Pan troglodytes. Primates 37: 279–295. Japan Monkey Centre.

Hannah, L., K. Shyamesh, M. A. Owston, R. E. Landford, G. B. Hubbard and E. J. Dick Jr. 2017. Natural mortality and cause of death analysis of the captive chimpanzee (Pan troglodytes): A 35- year review. J. Med. Primatol. 106–115.

Hansen, J. ., P. . Alford and M. . Keeling. 1984. Diffuse myocardial fibrosis and congestive heart failure in an adult male chimpanzee. Vet. Pathol. 21: 529–531.

Heath, A. K., E. J. Williamson, P. R. Ebeling, D. Kvaskoff, D. W. Eyles and D. R. English. 2014. Measurements of 25-hydroxyvitamin D concentrations in archived dried blood spots are reliable and accurately reflect those in Plasma. J. Clin. Endocrinol. Metab. 99: 3319–3324. Elsevier Churchill Livingstone, Edinburgh, UK.

Herrington, W., B. Lacey, P. Sherliker, J. Armitage and S. Lewington. 2016. Epidemiology of Atherosclerosis and the Potential to Reduce the Global Burden of Atherothrombotic Disease. Circ. Res. 118: 535–546.

Hinderer, S. and K. Schenke-Layland. 2019. Cardiac fibrosis – A short review of causes and therapeutic strategies. Elsevier B.V.

Ho, K. M. 2018. Using linear regression to assess dose-dependent bias on a Bland-Altman plot. J. Emerg. Crit. Care Med. 2: 68–68. AME Publishing Company.

Holick, M. F., T. C. Chen, Z. Lu and E. Sauter. 2007. Vitamin D and skin physiology: A D-lightful story. Pp. V28–V33 in Journal of Bone and Mineral Research. John Wiley & Sons, Ltd.

Holmes, E. W., J. Garbincius and K. M. McKenna. 2013. Analytical variability among methods for the measurement of 25-hydroxyvitamin D: Still adding to the noise. Am. J. Clin. Pathol. 140: 550–560.

Hope, K., S. Murray, C. Harris, C. Sanchez, N. Boedeker, S. Rosenthal, D. Kersey, H. W. Murphy, I. B. Kutinsky and L. Padilla. 2008. Brain natriuretic peptide as a novel diagnostic and prognostic indicator of cardiac disease in gorillas: two case reports. P. 157 in 2008 Proceedings AAZV ARAV joint conference.

Hossein-Nezhad, A. and M. F. Holick. 2013. Vitamin D for health: A global perspective. Pp. 720–755 in Mayo Clinic Proceedings. NIH Public Access.

Hubbard, G. B., D. R. Lee and J. W. Eichberg. 1991. Diseases and Pathology of Chimpanzees at the Southwest Foundation for Biomedical-Research. Am. J. Primatol. 24: 273–282.

Huijbregts, B., P. De Wachter, L. S. N. Obiang and M. E. Akou. 2003. Ebola and the decline of gorilla Gorilla gorilla and chimpanzee Pan troglodytes populations in Minkebe Forest, north-eastern Gabon. Oryx 37: 437–443. Cambridge University Press.

Hundae, A. and P. A. McCullough. 2014. Cardiac and renal fibrosis in chronic cardiorenal syndromes. Nephron. Clin. Pract. 127: 106–12. Karger Publishers.

Hyslop, N. P. and W. H. White. 2009. Estimating precision using duplicate measurements. J. Air Waste Manag. Assoc. 59: 1032–1039.

Ianevski, A., E. Zusinaite, N. Shtaida, H. Kallio-Kokko, M. Valkonen, A. Kantele, K. Telling, I. Lutsar, P. Letjuka, N. Metelitsa, V. Oksenych, U. Dumpis, A. Vitkauskiene, K. Stašaitis, C. Öhrmalm, K. Bondeson, A. Bergqvist, R. J. Cox, T. Tenson, A. Merits and D. E. Kainov. 2019. Low temperature and low UV indexes correlated with peaks of influenza virus activity in northern europe during 2010–2018. Viruses 11. MDPI AG.

Ip, J. E. and B. B. Lerman. 2018. Idiopathic malignant premature ventricular contractions. Elsevier Inc.

Istrătoaie, O., A. M. Ofiţeru, G. C. Nicola, R. I. Radu, C. Florescu, L. Mogoantă and C. T.

Streba. 2015. Myocardial interstitial fibrosis – Histological and immunohistochemical aspects. Rom. J. Morphol. Embryol. 56: 1473–1480.

IUCN. 2020. The IUCN Red List of Threatened Species.

Iung, B. and A. Vahanian. 2014. Epidemiology of Acquired Valvular Heart Disease. Can. J. Cardiol. 30: 962–970.

Jablonski, N. G. and G. Chaplin. 2010. Human skin pigmentation as an adaptation to UV radiation. Proc. Natl. Acad. Sci. U. S. A. 107: 8962–8968. National Academy of Sciences.

Jablonski, N. G. and G. Chaplin. 2000. The evolution of human skin coloration. J. Hum. Evol. 39: 57–106. Academic Press.

James, T. N. 1965. Anatomy of the sinus node, AV node and os cordis of the beef heart. Anat. Rec. 153: 361–371. Wiley Subscription Services, Inc., A Wiley Company.

James, T. N. and E. H. Drake. 1968. Sudden death in Doberman pinschers. Ann. Intern. Med. 68: 821–829.

Janssen, D. L. and R. M. Bush. 1990. Review of medical literature of great apes in the 1980s. Zoo Biol. 9: 123–134. Wiley Subscription Services, Inc., A Wiley Company.

Jellis, C., J. Martin, J. Narula and T. H. Marwick. 2010. Assessment of Nonischemic Myocardial Fibrosis. J. Am. Coll. Cardiol. 56: 89–97.

Jensen, A. L. and M. Kjelgaard-Hansen. 2006. Method comparison in the clinical laboratory. Wiley/Blackwell (10.1111).

Jensen, M. E., F. M. Ducharme, Y. Théorêt, A. S. Bélanger and E. Delvin. 2016. Assessing vitamin D nutritional status: Is capillary blood adequate? Clin. Chim. Acta 457: 59–62.

John, B. T., B. K. Tamarappoo, J. L. Titus, W. D. Edwards, W. K. Shen and S. S. Chugh. 2004. Global remodeling of the ventricular interstitium in idiopathic myocardial fibrosis and sudden cardiac death. Hear. Rhythm 1: 141–149.

Jones, P., N. Cordonnier, C. Mahamba, F. J. Burt, F. Rakotovao, R. Swanepoel, C. André, S. Dauger and L. Bakkali Kassimi. 2011. Encephalomyocarditis virus mortality in semi-wild bonobos (Pan panicus). J. Med. Primatol. 40: 157–163.

Jones, P., C. Mahamba, J. Rest and C. André. 2005. Fatal inflammatory heart disease in a bonobo (Pan paniscus). J. Med. Primatol. 34: 45–49.

Junge, R. E., F. H. Gannon, I. Porton, W. H. McAlister and M. P. Whyte. 2000. Management and prevention of vitamin D deficiency rickets in captive-born juvenile chimpanzees (Pan troglodytes). J Zoo Wildl Med 31: 361–369.

Kanamori, T., N. Kuze, H. Bernard, T. P. Malim and S. Kohshima. 2012. Fatality of a wild Bornean orangutan (Pongo pygmaeus morio): Behavior and death of a wounded juvenile in Danum Valley, North Borneo. Primates 53: 221–226. Springer Japan.

Kang, S. C., K. Jampachaisri and C. Pacharinsak. 2019. Doppler and oscillometric mean blood pressure best represent direct blood pressure measurements in anesthetized rhesus macaques (Macaca mulatta). J. Med. Primatol., doi: 10.1111/jmp.12397.

Kania, G., P. Blyszczuk and U. Eriksson. 2009. Mechanisms of cardiac fibrosis in inflammatory heart disease.

Kaplan, F. S., D. L. Glaser, N. Hebela and E. M. Shore. 2004. Heterotopic ossification. J. Am. Acad. Orthop. Surg. 12: 116–125.

Karagueuzian, H. S., T. P. Nguyen, Z. Qu and J. N. Weiss. 2013. Oxidative stress, fibrosis, and early afterdepolarization-mediated cardiac arrhythmias.

Kaur, B., S. Kaur, L. N. Yaddanapudi and N. V. Singh. 2019. Comparison between invasive and noninvasive blood pressure measurements in critically ill patients receiving inotropes. Blood Press. Monit. 24: 24–29.

Kaur, T., J. Singh, S. Tong, C. Humphrey, D. Clevenger, W. Tan, B. Szekely, Y. Wang, Y. Li, E. Alex Muse, M. Kiyono, S. Hanamura, E. Inoue, M. Nakamura, M. A. Huffman, B. Jiang and T. Nishida. 2008. Descriptive epidemiology of fatal respiratory outbreaks and detection of a human-related metapneumovirus in wild chimpanzees (Pan troglodytes) at Mahale Mountains National Park, Western Tanzania. Am. J. Primatol. 70: 755–765.

Kawashima, T. and F. Sato. 2012. Detailed Comparative Anatomy of the Extrinsic Cardiac Nerve Plexus and Postnatal Reorganization of the Cardiac Position and Innervation in the Great Apes: Orangutans, Gorillas, and Chimpanzees. Anat. Rec. 295: 438–453.

Keane, M., E. Paul, C. J. Sturrock, C. Rauch and C. S. Rutland. 2017. Computed Tomography in Veterinary Medicine: Currently Published and Tomorrow’s Vision. Pp. 271–289 in Computed Tomography - Advanced Applications. InTech.

Kenny, D. E., R. C. Cambre, T. P. Alvarado, A. W. Prowten, A. F. Allchurch, S. K. Marks and J. R. Zuba. 1994. Aortic dissection - an important cardiovascular disease in captive gorillas (Gorilla gorilla gorilla). J. Zoo Wildl. Med. 25: 561–568.

Kermani, T. A. 2019. Takayasu arteritis and giant cell arteritis: are they a spectrum of the same disease? Blackwell Publishing.

Kikuya, M., K. Chonan, Y. Imai, E. Goto and M. Ishii. 2002. Accuracy and reliability of wrist-cuff devices for self-measurement of blood pressure. J. Hypertens. 20: 629–638.

Kilbourn, A. M., W. B. Karesh, N. D. Wolfe, E. J. Bosi, R. A. Cook and M. Andau. 2003. HEALTH EVALUATION OF FREE-RANGING AND SEMI-CAPTIVE ORANGUTANS (PONGO PYGMAEUS PYGMAEUS) IN SABAH, MALAYSIA. J. Wildl. Dis. 39: 73–83.

Kim, E. and G. I. Fishman. 2012. The Structural Basis of Arrhythmia. Pp. 571–582 in Muscle : fundamental biology and mechanisms of disease (J. A. Hill and E. N. Olson, eds). Academic Press.

Kim, H. A., A. Perrelli, A. Ragni, F. Retta, T. M. De Silva, C. G. Sobey and S. F. Retta. 2020. Vitamin D deficiency and the risk of cerebrovascular disease. MDPI AG.

Kim, K., T. H. Chung, C. J. Etzel, J. Kim, H. Ryu, D. W. Kim, P. Hwu, W. J. Hwu, S. P. Patel, M. Liu and K. B. Kim. 2018. Association between melanoma and renal-cell carcinoma for sequential diagnoses: A single-center retrospective study. Cancer Epidemiol. 57: 80–84. Elsevier Ltd.

Kleinman, B., S. Powell, P. Kumar and R. M. Gardner. 1992. The fast flush test measures the dynamic response of the entire blood pressure monitoring system. Anesthesiology 77: 1215–1220. Anesthesiology.

Kligfield, P., L. S. Gettes, J. J. Bailey, R. Childers, B. J. Deal, E. W. Hancock, G. van Herpen, J. a Kors, P. Macfarlane, D. M. Mirvis, O. Pahlm, P. Rautaharju, G. S. Wagner, M. Josephson, J. W. Mason, P. Okin, B. Surawicz and H. Wellens. 2007. AHA recommendations for ECG reading: part I. Circulation 115: 1306–24. Lippincott Williams & Wilkins.

Köndgen, S., H. Kühl, P. K. N'Goran, P. D. Walsh, S. Schenk, N. Ernst, R. Biek, P. Formenty, K. Mätz-Rensing, B. Schweiger, S. Junglen, H. Ellerbrok, A. Nitsche, T. Briese, W. I. Lipkin, G. Pauli, C. Boesch and F. H. Leendertz. 2008. Pandemic Human Viruses Cause Decline of Endangered Great Apes. Curr. Biol. 18: 260–264. Cell Press.

Kosmala, W., M. Przewlocka-Kosmala, A. Wojnalowicz, A. Mysiak and T. H. Marwick. 2012. Integrated backscatter as a fibrosis marker in the metabolic syndrome: Association with biochemical evidence of fibrosis and left ventricular dysfunction. Eur. Heart J. Cardiovasc. Imaging 13: 459–467. Eur Heart J Cardiovasc Imaging.

Koster, M. J. and K. J. Warrington. 2017. Giant cell arteritis: Pathogenic mechanisms and new potential therapeutic targets. BioMed Central Ltd.

Kuck, K. and P. D. Baker. 2017. Perioperative noninvasive blood pressure monitoring. Anesth. Analg. 127: 408–411. Lippincott Williams and Wilkins.

Kumar, S., H. Laurence, M. A. Owston, R. M. Sharp, P. Williams, R. E. Lanford, G. B. Hubbard

and E. J. Dick. 2017. Natural pathology of the captive chimpanzee (Pan troglodytes): A 35-year review. J. Med. Primatol., doi: 10.1111/jmp.12277.

Kuriachan, V. P., G. L. Sumner and L. B. Mitchell. 2015. Sudden Cardiac Death. Curr. Probl. Cardiol. 40: 133–200.

Kuwabara, M., K. Harada, Y. Hishiki and K. Kario. 2019. Validation of a wrist-type home nocturnal blood pressure monitor in the sitting and supine position according to the ANSI/AAMI/ISO81060-2:2013 guidelines: Omron HEM-9600T. J. Clin. Hypertens., doi: 10.1111/jch.13464. John Wiley & Sons, Ltd (10.1111).

Kwak, H. B. 2013. Aging, exercise, and extracellular matrix in the heart. J Exerc Rehabil 9: 338–347.

Lammey, M. L., G. B. Baskin, A. P. Gigliotti, D. R. Lee, J. J. Ely and M. M. Sleeper. 2008a. Interstitial Myocardial Fibrosis in a Captive Chimpanzee (Pan troglodytes) Population. Comp. Med. 58: 389–394. American Association for Laboratory Animal Science.

Lammey, M. L., R. Jackson, J. J. Ely, D. R. Lee and M. M. Sleeper. 2011. Use of an implantable loop recorder in the investigation of arrhythmias in adult captive chimpanzees (Pan troglodytes). Comp. Med. 61: 71–75.

Lammey, M. L., D. R. Lee, J. J. Ely and M. M. Sleeper. 2008b. Sudden cardiac death in 13 captive chimpanzees (Pan troglodytes). J Med Primatol 37 Suppl 1: 39–43.

Lavie, C. J., R. Arena, D. L. Swift, N. M. Johannsen, X. Sui, D.-C. Lee, C. P. Earnest, T. S. Church, J. H. O'Keefe, R. V Milani and S. N. Blair. 2015. Exercise and the cardiovascular system: clinical science and cardiovascular outcomes. Circ. Res. 117: 207–19. NIH Public Access.

Leask, A. 2015. Getting to the heart of the matter: New insights into cardiac fibrosis.

Lee, A., T. E. Walters, E. P. Gerstenfeld and H. M. Haqqani. 2019. Frequent Ventricular Ectopy: Implications and Outcomes. Elsevier Ltd.

Leendertz, F. H., F. Lankester, P. Guislain, C. Néel, O. Drori, J. Dupain, S. Speede, P. Reed, N. Wolfe, S. Loul, E. Mpoudi-Ngole, M. Peeters, C. Boesch, G. Pauli, H. Ellerbrok and E. M. Leroy. 2006. Anthrax in western and Central African great apes. Am. J. Primatol. 68: 928–933.

Lehner, A. F., M. Johnson and J. Buchweitz. 2017. Veterinary utility of dried blood spots for analysis of toxic chlorinated hydrocarbons. Toxicol. Mech. Methods 1–9.

Levick, S. P., D. C. Loch, S. M. Taylor and J. S. Janicki. 2007. Arachidonic Acid Metabolism as a Potential Mediator of Cardiac Fibrosis Associated with Inflammation. J. Immunol.

178: 641–646.

Liao, P.-H., D. J.-Y. Hsieh, C.-H. Kuo, C.-H. Day, C.-Y. Shen, C.-H. Lai, R.-J. Chen, V. V. Padma, W.-W. Kuo and C.-Y. Huang. 2015. Moderate exercise training attenuates aging-induced cardiac inflammation, hypertrophy and fibrosis injuries of rat hearts. Oncotarget 6: 35383–94. Impact Journals, LLC.

Liaudet, L., B. Calderari and P. Pacher. 2014. Pathophysiological mechanisms of catecholamine and cocaine-mediated cardiotoxicity. Heart Fail. Rev. 19: 815–824. Kluwer Academic Publishers.

Libon, F., E. Cavalier and A. F. Nikkels. 2013. Skin color is relevant to vitamin D synthesis. Dermatology 227: 250–254.

Liu, J., J. O. Hahn and R. Mukkamala. 2013. Error mechanisms of the oscillometric fixed-ratio blood pressure measurement method. Ann. Biomed. Eng. 41: 587–597. Springer.

Liu, S. K., L. P. Tilley and R. J. Tashjian. 1975. Lesions of the conduction system in the cat with cardiomyopathy. Recent Adv. Stud. Cardiac Struct. Metab. 10: 681–693.

Lonjaret, L., O. Lairez, V. Minville and T. Geeraerts. 2014. Optimal perioperative management of arterial blood pressure. Dove Medical Press Ltd.

Lonsdorf, E. V., D. Travis, A. E. Pusey and J. Goodall. 2006. Using retrospective health data from the Gombe chimpanzee study to inform future monitoring efforts. Am. J. Primatol. 68: 897–908.

López, B., A. González, S. Ravassa, J. Beaumont, M. U. Moreno, G. San José, R. Querejeta and J. Díez. 2015. Circulating Biomarkers of Myocardial Fibrosis: The need for a reappraisal. J. Am. Coll. Cardiol. 65: 2449–2456.

Lowenstine, L. 2003. A Primer of Primate Pathology: Lesions and Nonlesions. Toxicol. Pathol. 31: 92–102.

Lowenstine, L. ., R. McManamon, C. J. Bonar and L. Perkins. 2008a. Preliminary results of a survey of United States and Canadian orangutan mortalities in the North American SSP population from 1980-March 2008. P. 40. in American Association of Zoo Veterinarians.

Lowenstine, L. J., R. McManamon and K. A. Terio. 2016. Comparative Pathology of Aging Great Apes: Bonobos, Chimpanzees, Gorillas, and Orangutans. Vet. Pathol. 53: 250–276.

Lowenstine, L., R. McManamon, C. J. Bonar and L. Perkins. 2008b. Preliminary results of a survey of United States and Canadian Orangutan mortalities in the North American SSP population from 1980 to March, 2008. P. 40 in 2008 Proceedings AAZV ARAV joint

conference. AAZV.

Lumsden, J. H. 2000. Laboratory test method validation. Rev. Méd. Vét. 151: 623–630.

Maceira, A. M., J. Barba, N. Varo, O. Beloqui and J. D??ez. 2002. Ultrasonic backscatter and serum marker of cardiac fibrosis in hypertensives. Hypertension 39: 923–928.

Machado, C., F. G. Mihm and C. Noe. 1989. Diagnosis of a ventricular septal defect in a gorilla using in vivo oximetry. American Association of Zoo Veterinarians.

MacKie, B. A., R. L. Stepien and H. B. Kellihan. 2010. Retrospective analysis of an implantable loop recorder for evaluation of syncope, collapse, or intermittent weakness in 23 dogs (2004-2008). J. Vet. Cardiol. 12: 25–33.

Magden, E. R., M. M. Sleeper, S. J. Buchl, R. A. Jones, E. J. Thiele and G. K. Wilkerson. 2016. Use of an Implantable Loop Recorder in a Chimpanzee (Pan troglodytes) to Monitor Cardiac Arrhythmias and Assess the Effects of Acupuncture and Laser Therapy. Comp. Med. 66: 52–58. American Association for Laboratory Animal Science.

Maines, M., A. Zorzi, G. Tomasi, C. Angheben, D. Catanzariti, L. Piffer and M. Del Greco. 2018. Clinical impact, safety, and accuracy of the remotely monitored implantable loop recorder Medtronic Reveal LINQ TM. Europace 20: 1050–1057.

Maksimowicz-McKinnon, K. and G. S. Hoffman. 2012. Takayasu's Arteritis. Pp. 276–288 in Inflammatory Diseases of Blood Vessels (G. S. Hoffman, C. M. Weyand, C. A. Langford, and J. J. Goronzy, eds). Wiley-Blackwell, Oxford.

Mangin, M., R. Sinha and K. Fincher. 2014. Inflammation and vitamin D: the infection connection. Birkhauser Verlag AG.

Marks, L. A. and A. Groch. 2000. Optimizing cuff width for noninvasive measurement of blood pressure. Blood Press. Monit. 5: 153–158.

Martin, C. A., U. Gowda and A. M. N. Renzaho. 2016. The prevalence of vitamin D deficiency among dark-skinned populations according to their stage of migration and region of birth: A meta-analysis. Nutrition 32: 21–32.

Matsuda, K., S. Tabata, Y. Kawamura, T. Kurosawa, N. Yoshie and H. Taniyama. 2010. Ectopic ossification with haematopoietic bone marrow in the heart valves of a crossbred heavy horse. J. Comp. Pathol. 143: 213–217.

Mayhew, T. M. and J. M. Lucocq. 2015. From gross anatomy to the nanomorphome: Stereological tools provide a paradigm for advancing research in quantitative morphomics. Blackwell Publishing Ltd.

McManamon, R. and L. J. Lowenstine. 2012. Cardiovascular Disease in Great Apes. Pp. 408–415 in Fowler's Zoo and Wild Animal Medicine Vol 7 (R. E. Miller and M. Fowler, eds). Elsevier, Saint Louis.

McNamara, T., E. Dolensek, S.-K. Liu and E. Dierenfeld. 1986. Cardiomyopathy associated with vitamin E deficiency in two montain lowland gorillas.

Meehan, T. P. and L. J. Lowenstine. 1994. Causes of mortality in captive lowland gorillas: a survey of the SSP population. P. 190 in 1994 Proceedings ARAV.

Meng, X., G. Zang, L. Fan, L. Zheng, J. Dai, X. Wang, W. Xia, J. Liu and C. Zhang. 2013. Non-invasive monitoring of blood pressure using the Philips Intellivue MP50 monitor cannot replace invasive blood pressure techniques in surgery patients under general anesthesia. Exp. Ther. Med. 6: 9–14.

Meredith, A., S. Boroomand, J. Carthy, Z. Luo and B. McManus. 2015a. 1,25 Dihydroxyvitamin D(3) Inhibits TGFβ(1)-Mediated Primary Human Cardiac Myofibroblast Activation. PLoS One 10: e0128655. Public Library of Science, San Francisco, CA USA.

Meredith, A., S. Boroomand, J. Carthy, Z. Luo and B. McManus. 2015b. 1,25 Dihydroxyvitamin D3 Inhibits TGFβ1-Mediated Primary Human Cardiac Myofibroblast Activation. PLoS One 10: e0128655.

Miki, T., S. Yuda, H. Kouzu and T. Miura. 2013. Diabetic cardiomyopathy: pathophysiology and clinical features. Heart Fail. Rev. 18: 149–66. Springer.

Milazzo, V., M. De Metrio, N. Cosentino, G. Marenzi and E. Tremoli. 2017. Vitamin D and acute myocardial infarction. World J. Cardiol. 9: 14–20. Baishideng Publishing Group Inc.

Miller, L. M. and A. Gal. 2017. Cardiovascular System and Lymphatic Vessels. Pp. 561–616 in Pathologic Basis of Veterinary Disease (J. F. Zachary, ed). Elsevier, Saint Louis.

Mitchell, R. N. 2014. Blood vessels. Pp. 483–522 in Robbins & Cotran Pathologic Basis of Disease (V. Kumar, A. Abbas, and J. Aster, eds). Elsevier, Philadelphia.

Miyagi, J., K. Tsuhako, T. Kinjo, T. Iwamasa, Y. Kamada, T. Kinju and Y. Koyanagi. 1999. Coxsackievirus B4 Myocarditis in an Orangutan. Vet. Pathol. 36: 452–456. SAGE PublicationsSage CA: Los Angeles, CA.

Mohammadpour, A. 2007. Morphological study of the heart and os cordis in sheep and goat. indian Vet. J. 84: 284–284. The Association.

Moittié, S., K. Baiker, V. Strong, E. Cousins, K. White, M. Liptovszky, S. Redrobe, A. Alibhai, C. J. Sturrock and C. S. Rutland. 2020a. Discovery of os cordis in the cardiac skeleton of chimpanzees (Pan troglodytes). Sci. Rep. 10.

Moittié, S., P. A. P. A. Graham, N. Barlow, P. Dobbs, M. Liptovszky, S. Redrobe and K. White. 2020b. Comparison of 25-hydroxyvitamin D concentration in chimpanzee dried blood spots and serum. Vet. Clin. Pathol. 49. John Wiley & Sons, Ltd.

Moittié, S., M. N Sheppard, T. Thiele and K. Baiker. 2020c. Non-Infectious, Necrotizing and Granulomatous Aortitis in a Female Gorilla. J. Comp. Pathol. 181.

Morgan, D. 1970. Dissecting aneurysm of the aorta in a gorilla. Vet. Rec. 86: 502–505. British Medical Journal Publishing Group.

Morita, N., W. J. Mandel, Y. Kobayashi and H. S. Karagueuzian. 2014. Cardiac fibrosis as a determinant of ventricular tachyarrhythmias. Elsevier.

Morris, G. B., E. J. Ridgway and S. K. Suvarna. 2018. Traditional stains and modern techniques for demonstrating microorganisms in histology. Pp. 254–279 in Bancroft's Theory and Practice of Histological Techniques E-Book (S. K. Suvarna, C. Layton, and J. D. Bancroft, eds). Elsevier, Saint Louis.

Mostafa, M. M. A., A. M. Hasanin, F. Alhamade, B. Abdelhamid, A. G. Safina, S. M. Kasem, O. Hosny, M. Mahmoud, E. Fouad, A. Rady and S. M. Amin. 2020. Accuracy and trending of non-invasive oscillometric blood pressure monitoring at the wrist in obese patients. Anaesth. Crit. Care Pain Med. 39: 221–227. Elsevier Masson SAS.

Mourad, A., A. Gillies and S. Carney. 2005. Inaccuracy of wrist-cuff oscillometric blood pressure devices: An arm position artefact? Blood Press. Monit. 10: 67–71.

Munson, L. and R. J. Montali. 1990. Pathology and diseases of great apes at the National Zoological Park. Zoo Biol. 9: 99–105.

Murphy, H. W., P. Dennis, W. Devlin, T. Meehan and I. Kutinsky. 2011. Echocardiographic parameters of captive western lowland gorillas (Gorilla gorilla gorilla). J. Zoo Wildl. Med. 42: 572–9.

Mussa, F. F., J. D. Horton, R. Moridzadeh, J. Nicholson, S. Trimarchi and K. A. Eagle. 2016. Acute aortic dissection and intramural hematoma a systematic review. JAMA 316: 754–763.

Napier, J. E., I. B. Kutinsky, D. L. Armstrong, C. L. Hicks, J. Waldoch and W. H. Devlin. 2013. Evaluating Echocardiogram and Indirect Blood Pressure Results in Male Western Lowland Gorillas (Gorilla Gorilla Gorilla) During Three Phases of an Anesthetic Protocol. J. Zoo Wildl. Med. 44: 875–881.

Narat, V., J. Guillot, F. Pennec, S. Lafosse, A. C. Grüner, B. Simmen, J. C. Bokika Ngawolo and S. Krief. 2015. Intestinal Helminths of Wild Bonobos in Forest-Savanna Mosaic: Risk

Assessment of Cross-Species Transmission with Local People in the Democratic Republic of the Congo. Ecohealth 12: 621–633.

Natterson-Horowitz, B. and J. Wynne. 2009. Should this gorilla be on Lipitor? Echocardiographic identification of patients at risk for aortic dissection. P. 158 in 2009 Proceeedings AAZV AAWV joint conference. American Association of Zoo Veterinarians, Yulee.

New York State Department of Health, W. C. 2015. Clinical Laboratory Evaluation Program; A Guide to Program Requirements and Services.

Nikitin, N. P. and J. G. F. Cleland. 2002. [Use of myocardial tissue Doppler imaging in cardiology]. Kardiologiia 42: 66–79.

NOTES ON INTERPRETING DEQAS REPORTS (25-OHD) Definitions Target Value. n.d.

O'Brien, E., N. Atkins, G. Stergiou, N. Karpettas, G. Parati, R. Asmar, Y. Imai, J. Wang, T. Mengden and A. Shennan. 2010. European Society of Hypertension International Protocol revision 2010 for the validation of blood pressure measuring devices in adults.

O'Neill, C. M., A. Kazantzidis, M. J. Ryan, N. Barber, C. T. Sempos, R. A. Durazo-Arvizu, R. Jorde, G. Grimnes, G. Eiriksdottir, V. Gudnason, M. F. Cotch, M. Kiely, A. R. Webb and K. D. Cashman. 2016. Seasonal changes in vitamin D-effective UVB availability in Europe and associations with population serum 25-hydroxyvitamin D. Nutrients 8. MDPI AG.

Oyama, M. A. 2015. Using Cardiac Biomarkers in Veterinary Practice.

Oyama, M. A., A. Boswood, D. J. Connolly, S. J. Ettinger, P. R. Fox, S. G. Gordon, J. E. Rush, D. D. Sisson, R. L. Stepien, G. Wess and F. Zannad. 2013. Clinical usefulness of an assay for measurement of circulating N-terminal pro-B-type natriuretic peptide concentration in dogs and cats with heart disease. J. Am. Vet. Med. Assoc. 243: 71–82. American Veterinary Medical Association 1931 North Meacham Road - Suite 100, Schaumburg, IL 60173 USA 847-925-8070 847-925-1329 avmajournals@avma.org.

Oyama, M. A., P. R. Fox, J. E. Rush, E. A. Rozanski and M. Lesser. 2008. Clinical utility of serum N-terminal pro-B-type natriuretic peptide concentration for identifying cardiac disease in dogs and assessing disease severity. J. Am. Vet. Med. Assoc. 232: 1496–1503.

Palacios, G., L. J. Lowenstine, M. R. Cranfield, K. V. K. Gilardi, L. Spelman, M. Lukasik-Braum, J. F. Kinani, A. Mudakikwa, E. Nyirakaragire, A. V. Bussetti, N. Savji, S. Hutchison, M. Egholm and W. Ian Lipkin. 2011. Human metapneumovirus infection in wild mountain

gorillas, Rwanda. Emerg. Infect. Dis. 17: 711–713. Centers for Disease Control and Prevention.

Pannarale, G., G. Bebb, S. Clark, A. Sullivan, C. Foster and A. J. S. Coats. 1993. Bias and variability in blood pressure measurement with ambulatory recorders. Hypertension 22: 591–598.

Parati, G., G. S. Stergiou, R. Asmar, G. Bilo, P. de Leeuw, Y. Imai, K. Kario, E. Lurbe, A. Manolis, T. Mengden, E. O'Brien, T. Ohkubo, P. Padfield, P. Palatini, T. Pickering, J. Redon, M. Revera, L. M. Ruilope, A. Shennan, J. A. Staessen, A. Tisler, B. Waeber, A. Zanchetti, G. Mancia, P. De Leeuw, E. O. Brien and J. Redón. 2013. European Society of Hypertension guidelines for blood pressure monitoring at home : a summary report of the Second International Consensus Conference on Home Blood Pressure Monitoring on behalf of the ESH Working Group on Blood Pressure Monitoring. J. Hypertens. 26: 1505–1530. Wolters Kluwer Health | Lippincott Williams & Wilkins.

Patil, H. R., J. H. O'Keefe, C. J. Lavie, A. Magalski, R. A. Vogel and P. A. McCullough. 2012. Cardiovascular damage resulting from chronic excessive endurance exercise.

Persy, V. and P. D'Haese. 2009. Vascular calcification and bone disease: the calcification paradox. Trends Mol. Med. 15: 405–416. Elsevier Current Trends.

Picano, E., G. Pelosi, M. Marzilli, F. Lattanzi, A. Benassi, L. Landini and A. L'Abbate. 1990. In vivo quantitative ultrasonic evaluation of myocardial fibrosis in humans. Circulation 81: 58–64.

Pickering, T. G., J. E. Hall, L. J. Appel, B. E. Falkner, J. Graves, M. N. Hill, D. W. Jones, T. Kurtz, S. G. Sheps and E. J. Roccella. 2005. Recommendations for Blood Pressure Measurement in Humans and Experimental Animals. Part 1. Hypertension 45: 142–161.

Picone, D. S., R. A. Deshpande, M. G. Schultz, R. Fonseca, N. R. C. Campbell, C. Delles, M. Hecht Olsen, A. E. Schutte, G. Stergiou, R. Padwal, X. H. Zhang and J. E. Sharman. 2020. Nonvalidated Home Blood Pressure Devices Dominate the Online Marketplace in Australia: Major Implications for Cardiovascular Risk Management. Hypertension 1593–1599.

Pilz, S., A. Tomaschitz, W. März, C. Drechsler, E. Ritz, A. Zittermann, E. Cavalier, T. R. Pieber, J. M. Lappe, W. B. Grant, M. F. Holick and J. M. Dekker. 2011. Vitamin D, cardiovascular disease and mortality.

Prabhu, S. D. and N. G. Frangogiannis. 2016. The biological basis for cardiac repair after myocardial infarction.

Prior, D. L., J. B. Somaratne, A. J. Jenkins, M. Yii, A. E. Newcomb, C. G. Schalkwijk, M. J. Black, D. J. Kelly and D. J. Campbell. 2015. Calibrated integrated backscatter and myocardial fibrosis in patients undergoing cardiac surgery. Open Hear. 2: e000278. BMJ Publishing Group.

Prisant, L. M., B. S. Alpert, C. B. Robbins, A. S. Berson, M. Hayes, M. L. Cohen and S. G. Sheps. 1995. American national standard for nonautomated sphygmomanometers summary report. No longer published by Elsevier.

Public Health England. 2016. The Scientific Advisory Committee on Nutrition (SACN) vitamin D and health report.

Querejeta, R., N. Varo, B. López, M. Larman, E. Artiñano, J. C. Etayo, J. L. Martínez Ubago, M. Gutierrez-Stampa, J. I. Emparanza, M. J. Gil, I. Monreal, J. P. Mindán and J. Díez. 2000. Serum carboxy-terminal propeptide of procollagen type I is a marker of myocardial fibrosis in hypertensive heart disease. Circulation 101: 1729–1735.

Ranganathan, K., S. Loder, S. Agarwal, V. W. Wong, J. Forsberg, T. A. Davis, S. Wang, A. W. James and B. Levi. 2015. Heterotopic Ossification. J. Bone Jt. Surg. 97: 1101–1111.

Rijksen, H. D. 1978. A field study on Sumatran oran utans (Pongo pygmaeus abelii Lesson 1827). Ecology, behaviour and conservation. Landbouwhogeschool Wageningen, The Netherlands.

Roberts, W. C. 2005. Pericardial Heart Disease: Its Morphologic Features and Its Causes. Baylor Univ. Med. Cent. Proc. 18: 38–55. Informa UK Limited.

Rodríguez, S. M., N. O. Unanue, L. S. Jiménez, M. A. C. Ferrer and L. T. Alonso. 2019. Study of 25-(OH)-vitamin D serum levels in the northern area of Spain. Clin. Chim. Acta 493: S625. Elsevier BV.

Romagnoli, S., Z. Ricci, D. Quattrone, L. Tofani, O. Tujjar, G. Villa, S. M. Romano and A. R. De Gaudio. 2014. Accuracy of invasive arterial pressure monitoring in cardiovascular patients: An observational study. Crit. Care 18: 644. BioMed Central Ltd.

Ross, S., L. Park Zoo Jennie McNary, L. Angeles Zoo, L. Brent, M. Finnigan, P. Zoo, A. Chimpanzee Coordinator Steve Ross, L. Park Zoo Candice Dorsey, J. C. Barber and C. Dorsey. 2010. Chimpanzee (Pan troglodytes) Care Manual. Association of Zoos and Aquariums.

Rubart, M. and D. P. Zipes. 2005. Genes and cardiac repolarization: The challenge ahead. Circulation 112: 1242–1244. American Heart Association, Inc.

Rumberger, J. A. 2010. Using noncontrast cardiac CT and coronary artery calcification

measurements for cardiovascular risk assessment and management in asymptomatic adults.

Russo, R. A. G. and M. M. Katsicas. 2018. Takayasu Arteritis. Front. Pediatr. 6. Frontiers Media S.A.

Ryan, C., A. Barbour, L. Burke and M. N. Sheppard. 2015. Non-infectious aortitis of the ascending aorta: A histological and clinical correlation of 71 cases including overlap with medial degeneration and atheroma-a challenge for the pathologist. J. Clin. Pathol. 68: 898–904. BMJ Publishing Group.

Saadoun, D., M. Garrido, C. Comarmond, A. C. Desbois, F. Domont, L. Savey, B. Terrier, G. Geri, M. Rosenzwajg, D. Klatzmann, P. Fourret, P. Cluzel, L. Chiche, J. Gaudric, F. Koskas and P. Cacoub. 2015. Th1 and Th17 cytokines drive inflammation in takayasu arteritis. Arthritis Rheumatol. 67: 1353–1360. John Wiley and Sons Inc.

Saffitz, J. E. 2005. The pathology of sudden cardiac death in patients with ischemic heart disease - Arrhythmology for anatomic pathologists. Elsevier.

Sandusky, G. E., K. M. Kerr and C. C. Capen. 1979. Morphologic variations and aging in the atrioventricular conduction system of large breed dogs. Anat. Rec. 193: 883–901. Wiley-Blackwell.

Sant Cassia, E. V., A. Boswood and A. S. W. Tordiffe. 2015. Comparison of high-definition oscillometric and direct arterial blood pressure measurement in anesthetized cheetahs (Acinonyx jubatus). J. Zoo Wildl. Med. 46: 506–516. American Association of Zoo Veterinarians.

Saremi, F., D. Sánchez-Quintana, S. Mori, H. Muresian, D. E. Spicer, C. Hassani and R. H. Anderson. 2017. Fibrous Skeleton of the Heart: Anatomic Overview and Evaluation of Pathologic Conditions with CT and MR Imaging. RadioGraphics 37: 1330–1351.

Sasai, H., D. Fujita, Y. Tagami, E. Seto, Y. Denda, H. Hamakita, T. Ichihashi, K. Okamura, M. Furuya, H. Tani, K. Sasai and J. Yamate. 2015. Characteristics of bone fractures and usefulness of micro–computed tomography for fracture detection in rabbits: 210 cases (2007–2013). J. Am. Vet. Med. Assoc. 246: 1339–1344.

Sasai, H., H. Iwai, D. Fujita, E. Seto and Y. Izumi. 2014. The use of micro-computed tomography in the diagnosis of dental and oral disease in rabbits. BMC Vet. Res. 10: 209. BioMed Central.

Saugel, B., K. Kouz, A. S. Meidert, L. Schulte-Uentrop and S. Romagnoli. 2020. How to measure blood pressure using an arterial catheter: A systematic 5-step approach.

BioMed Central Ltd.

Schmidt, R. E. 1975. Systemic pathology of chimpanzees. J. Med. Primatol. 7: 274–318.

Schneider, C. A., W. S. Rasband and K. W. Eliceiri. 2012. NIH Image to ImageJ: 25 years of image analysis. NIH Public Access.

Schober, P. and L. A. Schwarte. 2018. Correlation coefficients: Appropriate use and interpretation. Anesth. Analg. 126: 1763–1768.

Schulman, F. Y., A. Farb, R. Virmani and R. J. Montali. 1995. Fibrosing Cardiomyopathy in Captive Western Lowland Gorillas (Gorilla-Gorilla-Gorilla) in the United-States - a Retrospective Study. J. Zoo Wildl. Med. 26: 43–51.

Schumer, A., H. Wilkens, B. Vollmerhaus and K. Habermehl. 1981. The Circulatory System, the Skin, and the Cutaneous Organs of the Domestic Mammals. Springer-Verlag.

Scott, R. 1987. A case of spontaneous atherosclerosis in a Captive Orangutan.

Seiler, B. M., E. J. Dick Jr., R. Guardado-Mendoza, J. L. VandeBerg, J. T. Williams, J. N. Mubiru and G. B. Hubbard. 2009. Spontaneous heart disease in the adult chimpanzee (Pan troglodytes). J Med Primatol 38: 51–58.

Seki, A. and M. C. Fishbein. 2016. Age-related Cardiovascular Changes and Diseases. Pp. 57–83 in Cardiovascular Pathology (L. M. Buja and J. Butany, eds). Academic Press, London.

Sempos, C. T., A. C. Heijboer, D. D. Bikle, J. Bollerslev, R. Bouillon, P. M. Brannon, H. F. DeLuca, G. Jones, C. F. Munns, J. P. Bilezikian, A. Giustina and N. Binkley. 2018. Vitamin D assays and the definition of hypovitaminosis D: results from the First International Conference on Controversies in Vitamin D.

Sharman, J. E., A. P. Avolio, J. Baulmann, A. Benetos, J. Blacher, C. L. Blizzard, P. Boutouyrie, C. H. Chen, P. Chowienczyk, J. R. Cockcroft, J. K. Cruickshank, I. Ferreira, L. Ghiadoni, A. Hughes, P. Jankowski, S. Laurent, B. J. McDonnell, C. McEniery, S. C. Millasseau, T. G. Papaioannou, G. Parati, J. B. Park, A. D. Protogerou, M. J. Roman, G. Schillaci, P. Segers, G. S. Stergiou, H. Tomiyama, R. R. Townsend, L. M. Van Bortel, J. Wang, S. Wassertheurer, T. Weber, I. B. Wilkinson and C. Vlachopoulos. 2017. Validation of non-invasive central blood pressure devices: Artery society task force (abridged) consensus statement on protocol standardization. Artery Res. 20: 35–43. Oxford University Press.

Shave, R., A. Baggish, K. George, M. Wood, J. Scharhag, G. Whyte, D. Gaze and P. D. Thompson. 2010. Exercise-induced cardiac troponin elevation: Evidence, mechanisms,

and implications.

Shave, R., D. Oxborough, J. Somauroo, Y. Feltrer, T. Strike, A. Routh, S. Chapman, S. Redrobe, L. Thompson, S. Unwin, G. Sayers, H. Murphy, G. Rapoport and E. Stöhr. 2014. Echocardiographic assessment of cardiac structure and function in great apes: A practical guide. Int. Zoo Yearb. 48: 218–233.

Sheppard, M. N. 2012. Approach to the cardiac autopsy. J. Clin. Pathol. 65: 484–495.

Shimizu, M., K. Umeda, N. Sugihara, H. Yoshio, H. Ino, R. Takeda, Y. Okada and I. Nakanishi. 1993. Collagen remodelling in myocardia of patients with diabetes. J. Clin. Pathol. 46: 32–6. BMJ Publishing Group.

Sleeper, M. M. 2009. Is it acute heart failure or sudden cardiac death in the chimpanzee? J Med Primatol 38: 75; author reply 76.

Sleeper, M. M., C. A. Clifford and L. L. Laster. 2001. Cardiac troponin I in the normal dog and cat. J. Vet. Intern. Med. 15: 501–503. Blackwell Publishing Ltd.

Sleeper, M. M., K. Drobatz, D. R. Lee and M. L. Lammey. 2014. Echocardiographic parameters of clinically normal adult captive chimpanzees (Pan troglodytes). J. Am. Vet. Med. Assoc. 244: 2014.

Spiro, A. and J. L. Buttriss. 2014. Vitamin D: An overview of vitamin D status and intake in Europe. Blackwell Publishing Ltd.

Stephenson, R. S., M. R. Boyett, G. Hart, T. Nikolaidou, X. Cai, A. F. Corno, N. Alphonso, N. Jeffery and J. C. Jarvis. 2012. Contrast enhanced micro-computed tomography resolves the 3-dimensional morphology of the cardiac conduction system in mammalian hearts. PLoS One 7.

Stergiou, G. S., B. Alpert, S. Mieke, R. Asmar, N. Atkins, S. Eckert, G. Frick, B. Friedman, T. Graßl, T. Ichikawa, J. P. Ioannidis, P. Lacy, R. McManus, A. Murray, M. Myers, P. Palatini, G. Parati, D. Quinn, J. Sarkis, A. Shennan, T. Usuda, J. Wang, C. O. Wu and E. O'Brien. 2018. A universal standard for the validation of blood pressure measuring devices: Association for the Advancement of Medical Instrumentation/European Society of Hypertension/International Organization for Standardization (AAMI/ESH/ISO) Collaboration Statement. Hypertension 71: 368–374.

Stone, J. R., P. Bruneval, A. Angelini, G. Bartoloni, C. Basso, L. Batoroeva, L. M. Buja, J. Butany, G. D'Amati, J. T. Fallon, A. C. Gittenberger-de Groot, R. H. Gouveia, M. K. Halushka, K. L. Kelly, I. Kholova, O. Leone, S. H. Litovsky, J. J. Maleszewski, D. V. Miller, R. N. Mitchell, S. D. Preston, A. Pucci, S. J. Radio, E. R. Rodriguez, M. N. Sheppard, S.

K. Suvarna, C. D. Tan, G. Thiene, A. C. van der Wal and J. P. Veinot. 2015. Consensus statement on surgical pathology of the aorta from the Society for Cardiovascular Pathology and the Association for European Cardiovascular Pathology: I. Inflammatory diseases. Cardiovasc. Pathol. 24: 267–278.

Strong, V. J., K. Baiker, M. Brennan, S. Redrobe, F. Rietkerk, M. A. Cobb and K. White. 2017. A retrospective review of western lowland gorilla (Gorilla gorilla gorilla) mortality in European zoologic collections between 2004 and 2014. J. Zoo Wildl. Med. 48: 277–286.

Strong, V. J., D. Grindlay, S. Redrobe, M. Cobb and K. White. 2016. A systematic review of the literature relating to captive great apes morbidity and mortality. J. Zoo Wildl. Med. 47: 697–710.

Strong, V. J., M. Martin, S. Chapman, M. Cobb and S. Redrobe. 2015. A Guide to Performing a Complete Standardised Echocardiographic Examination In Great Apes.

Strong, V. J., M. Martin, S. Redrobe, K. White and K. Baiker. 2018a. A retrospective review of great ape cardiovascular disease epidemiology and pathology. Int. Zoo Yearb. 52: 113–125.

Strong, V. J., S. Moittié, M. N. M. N. Sheppard, M. Liptovszky, K. White, S. Redrobe, M. Cobb and K. Baiker. 2020. Idiopathic Myocardial Fibrosis in Captive Chimpanzees (Pan troglodytes). Vet. Pathol. 57: 183–191.

Strong, V. J., T. Möller, A. S. Tillman, S. Träff, L. Guevara, M. Martin, S. Redrobe and K. White. 2018b. A clinical study to evaluate the cardiopulmonary characteristics of two different anaesthetic protocols for immobilization of healthy chimpanzees (Pan troglodytes). Vet. Anaesth. Analg. 45: 794–801. Elsevier.

Strong, V. J., M. N. Sheppard, S. Redrobe and K. Baiker. 2018c. Guidelines for consistent cardiovascular post-mortem examination, sampling and reporting of lesions in European zoo-housed great apes. Int. Zoo Yearb. 52: 126–136.

Suriyaphol, G., N. Kunnasut, S. Sirisawadi, W. Wanasawaeng and S. Dhitavat. 2014. Evaluation of dried blood spot collection paper blotters for avian sexing by direct PCR. Br. Poult. Sci. 55: 321–8.

Synek, V. 2008. Evaluation of the standard deviation from duplicate results. Accredit. Qual. Assur. 13: 335–337.

Talman, V. and H. Ruskoaho. 2016. Cardiac fibrosis in myocardial infarction—from repair and remodeling to regeneration. Springer.

Terio, K. A., D. Ph, A. C. V. P. Dipl, M. J. Kinsel, A. C. V. P. Dipl, J. Raphael, T. Mlengeya, C.

A. Kirchhoff, D. Ph, B. Gilagiza, L. Michael, D. Ph, S. Kamenya, D. Ph, J. D. Estes, D. Ph, F. Brandon, D. Ph, R. S. Rudicell, W. Liu, S. Patton, D. Ph, A. Collins, D. Ph, B. H. Hahn, D. A. Travis, E. V Lonsdorf and D. Ph. 2011. Pathologic Lesions in Chimpanzees (Pan trogylodytes schweinfurthii) from Gombe National Park , Tanzania , 2004 – 2010. J. Zoo Wildl. Med. 42: 597–607.

Thiene, G., S. Rizzo and C. Basso. 2016. Pathology of Sudden Death, Cardiac Arrhythmias and Conduction System. Pp. 361–433 in Cardiovascular Pathology: Fourth Edition. Elsevier Inc.

Thilo, C., M. Hanley, G. Bastarrika, B. Ruzsics and U. J. Schoepf. 2010. Integrative computed tomographic imaging of cardiac structure, function, perfusion, and viability. Cardiol. Rev. 18: 219–229.

Thomas, G. S., L. S. Wann, A. H. Allam, R. C. Thompson, D. E. Michalik, M. L. Sutherland, J. D. Sutherland, G. P. Lombardi, L. Watson, S. L. Cox, C. M. Valladolid, G. Abd el-Maksoud, M. Al-Tohamy Soliman, I. Badr, A. el-Halim Nur el-din, E. M. Clarke, I. G. Thomas, M. I. Miyamoto, H. S. Kaplan, B. Frohlich, J. Narula, A. F. R. Stewart, A. Zink and C. E. Finch. 2014. Why Did Ancient People Have Atherosclerosis? Glob. Heart 9: 229–237.

Tohno, S., C. Azuma, Y. Tohno, Y. Moriwake, A. Izu, T. Kumai and T. Minami. 2007. Increases of calcium, phosphorus, and magnesium in both the right and left fibrous trigones of human heart with aging. Biol. Trace Elem. Res. 119: 111–119. Humana Press Inc.

Tong, L. J., E. J. Flach, M. N. Sheppard, A. Pocknell, A. A. Banerjee, A. Boswood, T. Bouts, A. Routh and Y. Feltrer. 2014. Fatal arrhythmogenic right ventricular cardiomyopathy in 2 related subadult chimpanzees (Pan troglodytes). Vet Pathol 51: 858–867.

Towler, D. A. 2011. Vitamin D: Cardiovascular effects and vascular calcification. Pp. 1403–1426 in Vitamin D (D. FELDMAN, J. W. Pike, and J. S. Adams, eds). Elsevier Inc.

Travers, J. G., F. A. Kamal, J. Robbins, K. E. Yutzey, C. Burns and B. C. Blaxall. 2016. Cardiac fibrosis: The fibroblast awakens. Circ. Res. 118: 1021–1040.

Trial, J. A., M. L. Entman and K. A. Cieslik. 2016. Mesenchymal stem cell-derived inflammatory fibroblasts mediate interstitial fibrosis in the aging heart. NIH Public Access.

Trim, C. M., E. H. Hofmeister, J. F. Peroni and M. Thoresen. 2013. Evaluation of an oscillometric blood pressure monitor for use in anesthetized sheep. Vet. Anaesth. Analg. 40.

Trupkiewicz, J. G., T. S. Mcnamara, K. M. Weidenheim, R. A. Cook, S. L. Grenell and S. M.

Factor. 1995. Cerebral Infarction Associated with Coarctation of the Aorta in a Lowland Gorilla (Gorilla-Gorilla-Gorilla). J. Zoo Wildl. Med. 26: 123–131. American Association of Zoo Veterinarians.

Tse, G., J. M. Yeo, Y. W. Chan, E. T. Lai and B. P. Yan. 2016. What Is the Arrhythmic Substrate in Viral Myocarditis? Insights from Clinical and Animal Studies. Front Physiol 7: 308.

Tuohy, P. P., A. L. Raisis and E. A. Drynan. 2017. Agreement of invasive and non-invasive blood pressure measurements in anaesthetised pigs using the Surgivet V9203. Res. Vet. Sci. 115: 250–254. Elsevier B.V.

Unwin, S., J. Chatterton and J. Chantrey. 2013. Management of severe respiratory tract disease caused by human respiratory syncytial virus and Streptococcus pneumoniae in captive chimpanzees (Pan troglodytes). J. Zoo Wildl. Med., doi: 10.1638/1042-7260-44.1.105.

van Zijll Langhout, M., M. Wolters, K. M. Horvath, H. Thiesbrummel, P. Smits, H. van Bolhuis, V. van der Hulst and R. Riezebos. 2017. Clinical signs, diagnostics and successful treatment of a myocarditis in an adult chimpanzee (Pan troglodytes). J. Med. Primatol., doi: 10.1111/jmp.12273.

Varki, N., D. Anderson, J. G. Herndon, T. Pham, C. J. Gregg, M. Cheriyan, J. Murphy, E. Strobert, J. Fritz, J. G. Else and A. Varki. 2009. Heart disease is common in humans and chimpanzees, but is caused by different pathological processes. Evol Appl 2: 101–112.

Varki, N. M., E. Strobert, E. J. Dick, K. Benirschke and A. Varki. 2011. Biomedical Differences Between Human and Nonhuman Hominids: Potential Roles for Uniquely Human Aspects of Sialic Acid Biology. Annu. Rev. Pathol. Mech. Dis. 6: 365–393.

Vesper, H. W. and J. Cook Botelho. 2014. Vitamin D Standardization-Certification Program (VDSCP) | CDC.

Videan, E. N., C. B. Heward, J. Fritz, J. Murphy, C. Cortez and Y. Su. 2007. Relationship between Sunlight Exposure, Housing Condition, and Serum Vitamin D and Related Physiologic Biomarker Levels in Captive Chimpanzees (Pan troglodytes). Comp. Med. 57: 402–406.

Vitt, R., G. Laschewski, A. F. Bais, H. Diémoz, I. Fountoulakis, A. M. Siani and A. Matzarakis. 2020. UV-index climatology for europe based on satellite data. Atmosphere (Basel). 11. MDPI AG.

Wang, H., R. N. Smith, A. E. Spooner, E. M. Isselbacher, R. P. Cambria, T. E. MacGillivray,

J. H. Stone and J. R. Stone. 2012a. Giant cell aortitis of the ascending aorta without signs or symptoms of systemic vasculitis is associated with elevated risk of distal aortic events. Arthritis Rheum. 64: 317–319. John Wiley & Sons, Ltd.

Wang, L., Y. Song, J. E. Manson, S. Pilz, W. März, K. Michaëlsson, A. Lundqvist, S. K. Jassal, E. Barrett-Connor, C. Zhang, C. B. Eaton, H. T. May, J. L. Anderson and H. D. Sesso. 2012b. Circulating 25-Hydroxy-Vitamin D and Risk of Cardiovascular Disease. Circ. Cardiovasc. Qual. Outcomes 5: 819–829.

Wang, L., Y. Song, J. E. Manson, S. Pilz, W. März, K. Michaëlsson, A. Lundqvist, S. K. Jassal, E. Barrett-Connor, C. Zhang, C. B. Eaton, H. T. May, J. L. Anderson and H. D. Sesso. 2012c. Circulating Levels of 25Hydroxy-Vitamin D and Risk of Cardiovascular Disease: A Meta-Analysis of Prospective Studies. Circ. Cardiovasc. Qual. Outcomes 5: 819–829.

Wax, D. B., H. M. Lin and A. B. Leibowitz. 2011. Invasive and concomitant noninvasive intraoperative blood pressure monitoring: Observed differences in measurements and associated therapeutic interventions. Anesthesiology 115: 973–978.

Webb, A. R., A. Kazantzidis, R. C. Kift, M. D. Farrar, J. Wilkinson and L. E. Rhodes. 2018. Meeting vitamin D requirements in white caucasians at UK latitudes: Providing a choice. Nutrients 10. MDPI AG.

Weber, K. T., J. S. Janicki, S. G. Shroff, R. Pick, R. M. Chen and R. I. Bashey. 1988. Collagen remodeling of the pressure-overloaded, hypertrophied nonhuman primate myocardium. Circ. Res. 62: 757–65.

Wess, G., A. Schulze, V. Butz, J. Simak, M. Killich, L. J. M. Keller, J. Maeurer and K. Hartmann. 2010. Prevalence of dilated cardiomyopathy in Doberman Pinschers in various age groups. J. Vet. Intern. Med. 24: 533–538. John Wiley & Sons, Ltd.

Weyand, C. M. and J. J. Goronzy. 2012. Giant Cell Arteritis. Pp. 263–275 in Inflammatory Diseases of Blood Vessels (G. S. Hoffman, C. M. Weyand, C. A. Langford, and J. J. Goronzy, eds). Wiley-Blackwell, Oxford, UK.

Wharton, G., R. Steeds, J. Allen, H. Phillips, R. Jones, P. Kanagala, G. Lloyd, N. Masani, T. Mathew, D. Oxborough, B. Rana, J. Sandoval, R. Wheeler, K. O'Gallagher and V. Sharma. 2015. A minimum dataset for a standard adult transthoracic echocardiogram: a guideline protocol from the British Society of Echocardiography. Echo Res Pr. 2: G9–G24. BioScientifica Ltd.

Wielders, J. P. M. and F. A. Wijnberg. 2009. Preanalytical stability of 25(OH)-vitamin D3 in human blood or serum at room temperature: Solid as a rock. Clinical Chemistry.

Williams, J. M., E. V. Lonsdorf, M. L. Wilson, J. Schumacher-Stankey, J. Goodall and A. E. Pusey. 2008. Causes of death in the Kasekela chimpanzees of Gombe National Park, Tanzania. Am. J. Primatol. 70: 766–777. Wiley Subscription Services, Inc., A Wiley Company.

Wimalawansa, S. J. 2018. Vitamin D and cardiovascular diseases: Causality.

Witkowska, A., A. Alibhai, C. Hughes, J. Price, K. Klisch, C. J. Sturrock and C. S. Rutland. 2014. Computed tomography analysis of guinea pig bone: architecture, bone thickness and dimensions throughout development. PeerJ 2: e615. PeerJ Inc.

Wulf, M., A. Bosse, T. Wiethege, B. Voss and K. M. Müller. 1994. Localization of collagen Types I, II, and III mRNAs in human heterotopic ossification by non-radioactive in situ hybridization. Pathol. - Res. Pract. 190: 25–32.

Xu, S., M. Bendeck and A. I. Gotlieb. 2016. Vascular Pathobiology: Atherosclerosis and Large Vessel Disease. Pp. 85–124 in Cardiovascular Pathology (L. M. Buja and J. Butany, eds). Academic Press.

Yamaoka, T. T., D. Flaherty, P. Pawson, M. Scott and A. Auckburally. 2017. Comparison of arterial blood pressure measurements obtained invasively or oscillometrically using a Datex S/5 Compact monitor in anaesthetised adult horses. Vet. Anaesth. Analg. 44: 492–501.

Yoshida, T., H. Takemoto, T. Sakamaki, N. Tokuyama, J. Hart, T. Hart, J. Dupain, A. Cobden, M. Mulavwa, Y. Kawamoto, A. Kaneko, Y. Enomoto, E. Sato, T. Kooriyama, T. Miyabe-Nishiwaki, J. Suzuki, A. Saito, M. Okamoto, M. Tomonaga, T. Matsuzawa, T. Furuichi and H. Akari. 2016. Epidemiological surveillance of lymphocryptovirus infection in wild bonobos. Front. Microbiol. 7: 1262.

Young, B. A. 1994. Cartilago cordis in serpents. Anat. Rec. 240: 243–247.

Zittermann, A. 2017. The Biphasic Effect of Vitamin D on the Musculoskeletal and Cardiovascular System. Hindawi Limited.

Zittermann, A. 2018. Vitamin D Status, Supplementation and Cardiovascular Disease. Anticancer Res. 38: 1179–1186.

Zittermann, A. and S. Prokop. 2014. The role of vitamin D for cardiovascular disease and overall mortality. Adv. Exp. Med. Biol. 810: 106–19.

Appendices

1. Echocardiography reports forms for C1, C2 and C3 (chapter 3).

Date : 8JAN15

Name: ROSIE (C1)

ECHOCARDIOGRAPHIC EXAMINATION

Overall image quality: FINE

2-D / M-MODE ASSESSMENT

LEFT ATRIUM

	mm
Aortic valve diameter	19
LA diameter (2D)	34
Ratio	1.79
Comment?	NORMAL

LEFT VENTRICLE

	2D (mm)	M-Mode (mm)
IVSd	8.3	
LVDd	50.8	
LVPWd	11.2	
IVSs	10.1	
LVDs	42.6	
LVPWs	10.0	
FS%	16	
EF%	34	

A4C volume	ml
LVEDV MOD A4C	96
LVESV MOD A4C	70
LVEF MOD A4C	27
Comment?	There is reduced systolic function, but probably normal for UGA. Chamber is normal.

RIGHT ATRIUM

Comment?	NORMAL

RIGHT VENTRICLE

Comment?	NORMAL

DOPPLER STUDIES

Blood flow

	VALVULAR REGURGITATION		MITRAL INFLOW	
MV	None Trace MildX Mod Sev		E vel: 0.54 m/sec	E/A: 1.32
	Peak vel: 4.1 m/sec	Max grad: 68 mmHg	A vel: 0.41 m/sec	☐ N/A
TV	NoneX Trace Mild Mod Sev		LV OUTFLOW	
	Peak vel: m/sec	Max grad: mmHg	Peak vel: 0.97 m/sec	Laminar flow Turbulent flow
AV	None X Trace Mild Mod Sev		Max grad: mmHg	
	Peak vel: m/sec	Max grad: mmHg	RV OUTFLOW	
PV	NoneX Trace Mild Mod Sev		Peak vel: 0.75 m/sec	Laminar flow
	Peak vel: m/sec	Max grad: mmHg	Max grad: mmHg	Turbulent flow
Comment	MILD MR WITH NO LA DILATION. OTHERWISE UNREMARKABLE.			

Tissue Doppler

Cm/s	S wave	E'	A'
LVFW radial	0.05	0.07	0.04
LVFW long			
IVS long			
RVFW long			
Comment?	Reduced function consistent with GA		

Key findings:

Mild Mitral regurgitation, but no 2D lesion seen and no LA dilation. Otherwise unremarkable.

Conclusion/Summary:

Not too remarkable.

Date : 27 Jan 2017

Name: Rosie (C1)

ECHOCARDIOGRAPHIC EXAMINATION

Overall image quality: Fairly good.

2-D / M-MODE ASSESSMENT

LEFT ATRIUM

	mm
Aortic valve diameter	19.3
LA diameter (2D)	42.4
Ratio	2.0
Comment?	Size normal, mild MR present.

LEFT VENTRICLE

	2D (mm)	M-Mode (mm)
IVSd	9.0	
LVDd	51.5	
LVPWd	9.1	
IVSs	7.2	
LVDs	47.1	
LVPWs	9.5	
FS%	9	
EF%	19	

A4C volume	Ml
LVEDV MOD A4C	93
LVESV MOD A4C	62
LVEF MOD A4C%	34
Comment?	Mildly dilated. Mild endocardial fibrosis. Function looks stiff.

RIGHT ATRIUM

Comment?	Normal. trivial TR.

RIGHT VENTRICLE

Comment?	Normal

DOPPLER STUDIES

Blood flow

	VALVULAR REGURGITATION		MITRAL INFLOW	
MV	None Trace MildX Mod Sev		E vel: 0.8 m/sec	E/A: 1.4
	Peak vel: m/sec	Max grad: mmHg	A vel: 0.57 m/sec	☐ N/A
TV	None TraceX Mild Mod Sev		LV OUTFLOW	
	Peak vel: 1.86 m/sec	Max grad: mmHg	Peak vel: m/sec	Laminar flow Turbulent flow
AV	NoneX Trace Mild Mod Sev		Max grad: mmHg	
	Peak vel: 1.2 m/sec	Max grad: mmHg	RV OUTFLOW	
PV	None TraceX Mild Mod Sev		Peak vel: m/sec	Laminar flow
	Peak vel: 0.83 m/sec	Max grad: mmHg	Max grad: mmHg	Turbulent flow
Comment	Unremarkable.			

Tissue Doppler

Cm/s	S wave	E'	A'
LVFW radial	3	4	3
LVFW long	5	6	4
IVS long	5	6	4
RVFW long	12	9	6
Comment?	LV reduced, systolic and diastolic function. RV normal.		

Key findings: LV is slightly dilated and stiff. Suggestion of mild fibrosis.

Blood pressure at start of echo – 105/73

Blood pressure at end of echo – 127/66

Conclusion/Summary:

Early/mild LV myocardial fibrosis. But comparing to previous echo, there is little significant progression.

Date : 9APR18

Name: ROSIE (C1)

ECHOCARDIOGRAPHIC EXAMINATION

Overall image quality:

2-D / M-MODE ASSESSMENT

LEFT ATRIUM

	mm
Aortic valve diameter	
LA diameter (2D)	
Ratio	
Comment?	Unremarkable

LEFT VENTRICLE

	2D (mm)	M-Mode (mm)
IVSd	8.8	
LVDd	46.1	
LVPWd	9.8	
IVSs	9.0	
LVDs	44.1	
LVPWs	10.3	
FS%	4	
EF%	10	

A4C volume	Ml
LVEDV MOD A4C	104
LVESV MOD A4C	69
LVEF MOD A4C	34
Comment?	Very poor systolic function, poorly contractility and dilated LV

RIGHT ATRIUM

Comment?	Unremarkable

RIGHT VENTRICLE

Comment?	Unremarkable

DOPPLER STUDIES

Blood flow

	VALVULAR REGURGITATION		MITRAL INFLOW	
MV	None Trace Mild Mod Sev		E vel: m/sec	E/A:
	Peak vel: m/sec	Max grad: mmHg	A vel: m/sec	☐ N/A
TV	None Trace Mild Mod Sev		LV OUTFLOW	
	Peak vel: m/sec	Max grad: mmHg	Peak vel: 1.1 m/sec	Laminar flow Turbulent flow
AV	None Trace Mild Mod Sev		Max grad: mmHg	
	Peak vel: m/sec	Max grad: mmHg	RV OUTFLOW	
PV	None Trace Mild Mod Sev		Peak vel: m/sec	Laminar flow
	Peak vel: m/sec	Max grad: mmHg	Max grad: mmHg	Turbulent flow
Comment				

Tissue Doppler

Cm/s	S wave	E’	A’
LVFW radial			
LVFW long	5	7	4
IVS long	4	7	3
RVFW long			
Comment?			

Key findings:

Very poor LV function – chamber dilated and poorly contractile

Conclusion/Summary:

Poor LV function.

Date : 20/9/16

Name: Danny (C2)

ECHOCARDIOGRAPHIC EXAMINATION

Overall image quality: Not best views, limiting best measurements.

2-D / M-MODE ASSESSMENT

LEFT ATRIUM

	mm
Aortic valve diameter	25
LA diameter (2D)	47.7
Ratio	1.9
Comment?	Not best views. Normal diameter, trivial MR

LEFT VENTRICLE

	2D (mm)	M-Mode (mm)
IVSd	11.2	
LVDd	55.8	
LVPWd	11.2	
IVSs	12.2	
LVDs	40.7	
LVPWs	16.6	
FS%	27	
EF%	52	

A4C volume	ml
LVEDV MOD A4C	100
LVESV MOD A4C	55
LVEF MOD A4C	45%
Comment?	Adequate views. Looks normal morphology, good chamber shape, reduced contractility under GA

RIGHT ATRIUM

Comment?	Slightly dilated looking. Trivial TR

	Spontaneous contrast present

RIGHT VENTRICLE

Comment?	RV looks slightly dilated, as seems normal in apes, but tending towards upper limits

DOPPLER STUDIES

Blood flow

	VALVULAR REGURGITATION		MITRAL INFLOW	
MV	None Trace Mild Mod Sev		E vel: 0.64 m/sec	E/A:
	Peak vel: 3.3 m/sec	Max grad: mmHg	A vel: 0.18 m/sec	☐ N/A
TV	None Trace Mild Mod Sev		LV OUTFLOW	
	Peak vel: 2.2 m/sec	Max grad: mmHg	Peak vel: m/sec	Laminar flow Turbulent flow
AV	None Trace Mild Mod Sev		Max grad: mmHg	
	Peak vel: 0.79 m/sec	Max grad: mmHg	RV OUTFLOW	
PV	None Trace Mild Mod Sev		Peak vel: m/sec	Laminar flow
	Peak vel: m/sec	Max grad: mmHg	Max grad: mmHg	Turbulent flow
Comment	Not best views / interrogation so MR underestimated at 3.3m/s			

Tissue Doppler

Cm/s	S wave	E'	A'
LVFW radial	7	12	6
LVFW long	7	13	6
IVS long			
RVFW long	9	13	5
Comment?	Reasonably good systolic and diastolic function, slight depression assumed to be a GA effect		

Key findings:

LV looks normal chamber morphology.

RV slightly dilated.

Date : 16APR18

Name: FLYNN (C3)

ECHOCARDIOGRAPHIC EXAMINATION

Overall image quality: GOOD

2-D / M-MODE ASSESSMENT

LEFT ATRIUM

	mm
Aortic valve diameter	
LA diameter (2D)	
Ratio	
Comment?	Unremarkable

LEFT VENTRICLE

	2D (mm)	M-Mode (mm)
IVSd	10.4	
LVDd	54.3	
LVPWd	9.9	
IVSs	14.2	
LVDs	39.1	
LVPWs	11.3	
FS%	28	
EF%	54	

A4C volume	ml
LVEDV MOD A4C	114
LVESV MOD A4C	76
LVEF MOD A4C	33
Comment?	Mild reduction in LV function

RIGHT ATRIUM

Comment?	Trivial TR

RIGHT VENTRICLE

Comment?	Unremarkable

DOPPLER STUDIES

Blood flow

	VALVULAR REGURGITATION		MITRAL INFLOW	
MV	None Trace Mild Mod Sev		E vel: 0.63 m/sec	E/A:
	Peak vel: m/sec	Max grad: mmHg	A vel: m/sec	☐ N/A
TV	None Trace X Mild Mod Sev		LV OUTFLOW	
	Peak vel: 2.4 m/sec	Max grad: mmHg	Peak vel: 1.17 m/sec	Laminar flow Turbulent flow
AV	None Trace Mild Mod Sev		Max grad: mmHg	
	Peak vel: m/sec	Max grad: mmHg	RV OUTFLOW	
PV	None Trace Mild Mod Sev		Peak vel: 0.8 m/sec	Laminar flow
	Peak vel: m/sec	Max grad: mmHg	Max grad: mmHg	Turbulent flow
Comment				

Tissue Doppler

Cm/s	S wave	E’	A’
LVFW radial			
LVFW long	6	10	5
IVS long	6	7	5
RVFW long			
Comment?			

Key findings:

Trivial TR

Mild reduction in LV function

Conclusion/Summary:

The reduced LV function might be associated with GA effects.

2. Sample submission form

This form was created by The Ape Heart Project in 2014 and modified in 2018. It is to be completed by zoos when submitting samples to the project.

Great Ape TAG endorsed

THE APE HEART PROJECT: Sample Submission Form

*To be completed for all samples being donated to the **EAZA Great Ape TAG endorsed Ape Heart Project Biobank***

General Information	
Zoo/Institution:	
Contact Person:	
Institutional Animal ID e.g. ARKS number, name:	**Studbook Number:**
Taxon (please circle): Gorilla / Chimpanzee / Orangutan / Bonobo	**Subspecies:**
Date of Birth (or approx. age): **Date of death** (if applicable):	**Gender:** ☐ Male ☐ Female
Circumstances of death (if applicable): ☐ Sudden ☐ Disease ☐ Peri-anaesthesia ☐ Euthanasia ☐ Other:	
Brief summary of clinical history (including any medications) – can be provided as an additional document if necessary:	
Other comments:	

Please ensure ALL samples are clearly labelled with the animal's identification, zoo of origin and date. All samples MUST be accompanied by a sample submission form.

Before sending samples please refer to the document entitled "Important Information for the Donation of Research Samples to the Ape Heart Project"

Ape Heart Project (EAZA Great Ape TAG Endorsed)
Twycross Zoo, Burton Road, Atherstone, Warwickshire, UK, CV9 3PX
Email: heartproject@twycrosszoo.org *Website:* www.twycrosszoo.org/ape-heart-project.aspx

Great Ape TAG endorsed

Samples being submitted:			
Sample Type	*Quantity/Volume*	*Sampling date*	*Comments*
Formalin-fixed whole heart ☐			
Post-mortem whole blood ☐			
Serum ☐			
Plasma ☐			
EDTA whole blood ☐			
Urine ☐			
Heart tissue (in RNA later) ☐			
Heart tissue (frozen) ☐			
Histo slides (please specify) ☐			
Other (please specify) ☐			

Post-Mortem Cardiac Examination (if applicable):	
Body weight (kg):	
Body condition score (1-5):	
Weight of the heart (g) after removal of clots/washing:	
Appearance of lungs and pleural cavity:	
Appearance of pericardium:	
Appearance and volume of pericardial fluid present:	
Abnormalities of the great vessels?	
Any evidence of thrombus within the pulmonary trunk?	
Any lesions evident on examination of the epicardium?	
Any other significant findings?	
Pictures sent:	

Ape Heart Project (EAZA Great Ape TAG Endorsed)
Twycross Zoo, Burton Road, Atherstone, Warwickshire, UK, CV9 3PX
Email: heartproject@twycrosszoo.org *Website:* www.twycrosszoo.org/ape-heart-project.aspx